ACS SYMPOSIUM SERIES **337**

Crystallographically Ordered Polymers

Daniel J. Sandman, EDITOR
GTE Laboratories, Inc.

Developed from a symposium sponsored by
the Division of Polymeric Materials: Science and Engineering
at the 191st Meeting
of the American Chemical Society,
New York, New York,
April 13–18, 1986

American Chemical Society, Washington, DC 1987

American Chemical Society
Library
1155 16th St., N.W.
Washington, D.C. 20036

ACS Symposium Series

M. Joan Comstock, *Series Editor*

1987 Advisory Board

Foreword

The ACS SYMPOSIUM SERIES was founded in 1974 to provide a
medium for publishing symposia quickly in book form. The
format of the Series parallels that of the continuing ADVANCES
IN CHEMISTRY SERIES except that, in order to save time, the
papers are not typeset but are reproduced as they are submitted
by the authors in camera-ready form. Papers are reviewed under
the supervision of the Editors with the assistance of the Series
Advisory Board and are selected to maintain the integrity of the
symposia; however, verbatim reproductions of previously pub-
lished papers are not accepted. Both reviews and reports of
research are acceptable, because symposia may embrace both
types of presentation.

Preface

DURING THE PAST 20 YEARS, new polymerization reactions that occur in the ordered lattice of appropriate monomeric compounds were discovered. In favorable cases, macroscopic polymeric single crystals were prepared and characterized, and thus a new vector in polymer science was launched. Moreover, commercialization occurred in at least one case. In the best tradition of the uniqueness of chemistry, physical studies of these newly available materials resulted in the observation of interesting and potentially useful electrical and optical properties. The results of these physical studies call for both new theoretical work as well as further development and extension of the chemistry that initially fueled them. Such considerations motivated the organization of the symposium from which this book was developed.

Although several books devoted to selected topics in solid-state polymerization have appeared in recent years, treatment of this subject and closely related topics in their broadest sense has not been attempted. This book is not a treatise. Yet, it will provide the interested reader with a broad introduction to the range of current activities in the area of crystallographically ordered polymers and their properties.

It is not possible to hold a symposium with the degree of international participation as was obtained in this case without considerable assistance. This assistance was provided by the Petroleum Research Fund; the ACS Division of Polymeric Materials: Science and Engineering; Allied Corporation; Celanese Research Company; GTE Laboratories, Inc.; and the Polaroid Foundation.

I am indebted to the numerous authors and referees for their time and efforts related to the symposium and this book. The support and encouragement of C. David Decker throughout the course of these activities is gratefully acknowledged. Finally, I thank my wife Alma and children for their continued forbearance.

DANIEL J. SANDMAN
GTE Laboratories, Inc.
Waltham, MA 02254

December 10, 1986

Chapter 1

Fully Ordered Macromolecules and Their Properties: Current Propositions

Daniel J. Sandman

GTE Laboratories, Inc., Waltham, MA 02254

The solid-state polymerization of the following classes of monomers is discussed: diacetylenes, monoacetylenes, mono- and dienes, ring-opening cyclic monomers, and transition metal systems. With particular emphasis on open questions and current problems, the chemical, structural, and physical properties of the resultant polymers are summarized. A brief prognosis is offered.

At present there is considerable interest in studying various topics relating to or deriving from solid-state polymerization. This has come about because of interesting and potentially useful properties of several polymers formed by lattice-controlled processes and because of the natural desire to increase the number of systems available for additional study. The experimental results alluded to have been achieved in the last several years, and it is now appropriate to take stock of these activities to understand how and why they have come to their present state and also to see how they might be given greater breadth and depth.

While the gas-solid formaldehyde-trioxane reaction (1) is widely regarded as the beginning of the study of solid-state polymerization, a paper submitted eight weeks earlier in 1930 showed considerable prescience. Stimulated by the observation of solid-state reactivity in the light-sensitive 1,4-dihalodiacetylenes, it was suggested (2) that the reaction was a polymerization and that the study of the solids with x-rays would provide useful information. When high energy radiation sources became available, the study of the reactivity of crystalline monomers rapidly expanded; an early example was the interaction of ethylene glycol dimethacrylate with an electron beam in 1951 (3). With the possible exception of N-vinylcarbazole, (4) attempts at the radiation-induced polymerization of crystalline vinyl monomers commonly led to amorphous polymers (5). In 1964, the condensation polymerization of 6-aminohexanoic acid (6) led to oriented chain growth.

In 1964, G.M.J. Schmidt and collaborators (7,8) enunciated the topochemical principle, a structural concept which notes that groups undergoing reaction in the solid state should be close (≤ 4.0 angstroms) and further emphasized reactivity in the ordered lattice rather than at defects.

Topochemical reactivity and solid-state polymerization strongly merged in the extensive studies of diacetylene (1) polymerization by G. Wegner and collaborators beginning in 1969. There are two recent books devoted to polydiacetylenes (PDA, 2) (9,10), and it is fair to say that the literature of fully ordered macromolecules would be much less voluminous without the extensive research associated with diacetylene polymerization and the chemical, structural, and physical properties of these polymers.

$$RCH_2 — C \equiv C — C \equiv C — CH_2R \longrightarrow \left[\begin{matrix} CH_2R \\ | \\ C — C \equiv C — C \\ | \\ CH_2R \end{matrix} \right]_n$$

$$\underset{\sim}{1} \qquad\qquad\qquad\qquad \underset{\sim}{2}$$

$$X\!-\!\!\!\bigcirc\!\!\!-\!SO_3\!-$$

$$\underset{\sim}{a,} \quad X \ = \ CH_3$$

$$\underset{\sim}{b,} \quad X \ = \ F$$

$$\underset{\sim}{c}$$

$$—(CH_2)_n \ O\overset{O}{\overset{\|}{C}}NHCH_2\overset{O}{\overset{\|}{C}}OnC_4H_9$$

$$\underset{\sim}{d} \quad n \ = \ 2,3$$

The outline of this article is as follows. After general remarks about the solid-state polymerization process, adopting the view that it is important to develop new types of solid-state polymerization, the polymerization of the following classes of monomers will be discussed: diacetylenes, monoacetylenes, vinyl and diene monomers, cyclic systems which ring open, and transition metal systems. It is implicit in the discussion that appropriately substituted forms of the above monomers may be polymerized as mono- layers and multilayers (11-13) as well as in the form of inclusion complexes (14). Emphasis will be placed on topics of current interest.

General Aspects of Solid-State Polymerization

Highly or fully ordered crystals of macromolecules are most conveniently obtained via solid-state polymerization, and several accessible general reviews are available (5,6). The initiation of polymerization in a crystalline lattice is typically stimulated by thermal, radiative, chemical, or mechanical means. Interest in high-pressure methods has developed recently (15). Hence there are numerous fundamental questions associated with initiation, propagation, and termination processes in an ordered lattice. As in any mechanistic study, it is desirable to have a "picture" of the energetics of the intermediates. The crystal structures of the monomer and resultant polymer in an ideal case provide the beginning and end points for what has transpired. Considerable detail concerning the structure and properties of growing oligomeric chains in a crystal is available only for the case of diacetylenes (16), and is largely inferred for other cases where polymerization is observed.

A central problem of general interest in the subject of solid-state polymerization is associated with chain propagation in which the hybridization of the atoms involved in covalent bond formation changes in the course of the reaction, e.g., in vinyl polymerization, sp^2 to sp^3 and sp to sp^2 in diacetylene polymerization. In such reactions, since van der Waals contact distances change to covalent bond distances, it had been argued (5) that formation of crystalline polymers without disruption of the lattice might be out of the question. For vinylic systems, the conversion of crystalline monomer to amorphous polymer is often observed (5). The generality of the above argument was precluded by the formation of fully crystalline PDA; nevertheless it could be widely relevant. For example, it might be argued that the observation of the conversion of a crystalline monomer to an amorphous polymer is a manifestation of the above chain propagation problem. But there is a possible alternative explanation: a propagating chain could have an intermediate which could undergo stereomutation. Examples of this situation might include olefin and acetylene polymerization, where complete crystalline order would be precluded by lack of stereochemical homogeneity.

Recently, the term "design" of a solid-state polymerization was introduced with a view toward discovery and development of new lattice-controlled processes (17). The term implies not easily separable crystallographic and mechanistic issues, and it was suggested (17) that mechanistic aspects of initiation and propagation may hold the key to progress along these lines.

Polydiacetylenes and their Properties

As noted above, two recent books (9,10) summarize much of the experimental and theoretical studies of PDA, and hence provide a useful guide to the original literature. Certain topics, such as spectroscopic monitoring of monomer photopolymerization and crystallographic studies of monomers and polymers are widely judged to be mature and need not be repeated here. This section largely focuses on new and still evolving themes.

While diacetylene polymerization is justifiably regarded (18) as better investigated and understood than any other polymerization reaction, several fundamental uncertainties remain. With respect to initiation and propagation, the lack of thermal reactivity of certain monomers (e.g., urethanes) which require radiation for polymerization contrasts with a monomer such as PTS *(1a)*, which polymerizes both thermally and with radiation. Equally

curious is the retardation of PTS polymerization by cocrystallization of the nearly isomophous *1b* (19). Use of orbital correlation diagrams (20) leads to the conclusion that diacetylene polymerization is photochemically allowed. This approach has not been applied to the intermediates of the growing oligomeric chain. (16).

Solid PDA have not had an extensive reaction chemistry largely due to their van der Waals tight-packed structures which effectively preclude diffusion of potentially reactive liquids and gases (21). Recently (17), reactions of poly-DCH *(2c)* with electrophiles have led to modified materials which are homogeneous on microscopic examination. The reactions are anisotropic. Bromination resulted in a crystal-to-crystal transformation, while chlorination and nitration have led to amorphous solids to date. The scope of such reactivity is clearly of interest.

While PDA solutions have been known for some time (22), interest in their structure and properties has increased markedly in recent years. Solutions of poly-BCMUs *(2d)* undergo a color change as nonsolvent is added to the polymer solution. This behavior has been ascribed to a rod-to-coil transition (23,24) or to an aggregation process (25). Experiments on PDA gels with low-frequency ac fields are beginning to yield information on elastic restoring forces in these materials (26). Differing views on solution structure continue to appear (27,28).

The intense visible absorption of PDA peaking at 600–650 nm has been interpreted using a phenomenological charge-transfer exciton model (29). A more fundamental understanding is desirable, especially as a basis for interpretation of third-order nonlinear optical phenomena, and such research has been initiated.

At present, there is considerable interest in both second- and third-order nonlinear optical phenomena in organic materials in general (30,31) and PDA (32) in particular. It has been speculated that third-order processes in PDA may have subpicosecond response times with potential utility in optical communications (33). PDA single-crystal thin films have been grown (32,34). Third-order coefficients have been measured by degenerate four-wave-mixing experiments using both picosecond (35) and femtosecond (36) pulses. Recent experiments at 720 nm in poly-PTS reveal that the response time is pulse-width limited using 300 femtosecond light pulses (36).

Pulsed photoconductivity studies in poly-PTS and -DCH have yielded carrier mobilities comparable to silicon and gallium arsenide (37,38). The question of hole or electron transport in these experiments is unsettled. Differing views of the magnitude of the mobility and the role of traps in the transport process have been offered (39,40). Further experimental and theoretical studies in this area are needed. The general question of carrier creation in PDA by charge-transfer doping remains open. An interesting apparent electric-field-induced doping of poly-DCH has been reported (40). PDA are converted into conductive materials by ion implantation (42).

The use of PDA and other macromolecular monolayers and liposomes as models for biomembranes has recently been reviewed (43).

The color change associated with diacetylene polymerization is useful as a time-temperature indicator (44), and a system using this technology has recently been commercialized.

Monoacetylenes

To a large extent, current interest in solid-state polymerization of monoacetylenes derives from the observation of interesting electrical, magnetic, and optical phenomena in poly-acetylene, $(CH)_x$ (45), a partially crystalline material unstable to ambient conditions typically synthesized by Ziegler-Natta techniques. The fundamental study of $(CH)_x$ and its electron-transferred ("doped") forms has been retarded by the lack of fully ordered materials. Fully ordered polyacetylenes are also of interest because it is conceivable that their crystal structures could allow significant interchain interactions, a situation precluded in most PDA by side chains.

The preparation of a fully ordered polymer containing both PDA and polyacetylene moieties from the oxidatively coupled dimer of 1,11-dodecadiyne *(3)* has been reported (46). While the polymerization of the acetylene to an ordered polymer is revealed by the reported crystal structure (46), the intrinsic properties of this novel polymer are uncertain at present.

Crystalline metal propiolates *(4)* exhibit a variety of short contact distances among the acetylenic carbons and are converted by gamma radiation to amorphous metal polypropiolates (47). Detailed spectroscopic characterization of the soluble polypropiolates is in progress.

Other classes of monoacetylenes exhibit varying degrees of reactivity. Propargylamine in a tetrachlorocadmate layer complex was reported to be unreactive to ultraviolet light to wavelengths shorter than 200 nm, but turned black on exposure to gamma radiation (48). Product characterization is incomplete at present.

Simple hydrogen-bonded acetylenes such as propiolamide *(5)* and propiolaldehyde semicarbazone *(6)*, whose crystal structures reveal short contacts between acetylenic carbons, are unreactive to gamma radiation when the crystals are grown by vacuum sublimation (21). Polymerization of these compounds proceeds to a low degree of conversion for crystals grown in chlorinated solvents.

There are clearly many open questions in the reported attempted polymerizations of terminal acetylenes. Some are clearly crystallographic. The resultant polymer repeat structure could be critically dependent on the substituent of the terminal acetylene and details of monomer orientation, *inter alia*. Figure 1 displays a sketch, which could be relevant to *(6)*, of a monomer which converts, formally, to the product of a 1,2' addition polymerization. In contrast, Figure 2 exhibits the sketch of a monomer, possibly relevant to *(3)* and other structures (49), which formally converts to the repeat observed in (46), here termed 1,1' 2',2'' addition. It should be understood that the sketches of Figures 1 and 2 are not intended to convey a mechanistic process. As noted previously (21), short crystallographic contacts between potentially reactive acetylenic carbons are not sufficient to guarantee reactivity, and mechanistic issues associated with initiation and propagation, presently unknown, may hold the key to progress in this area.
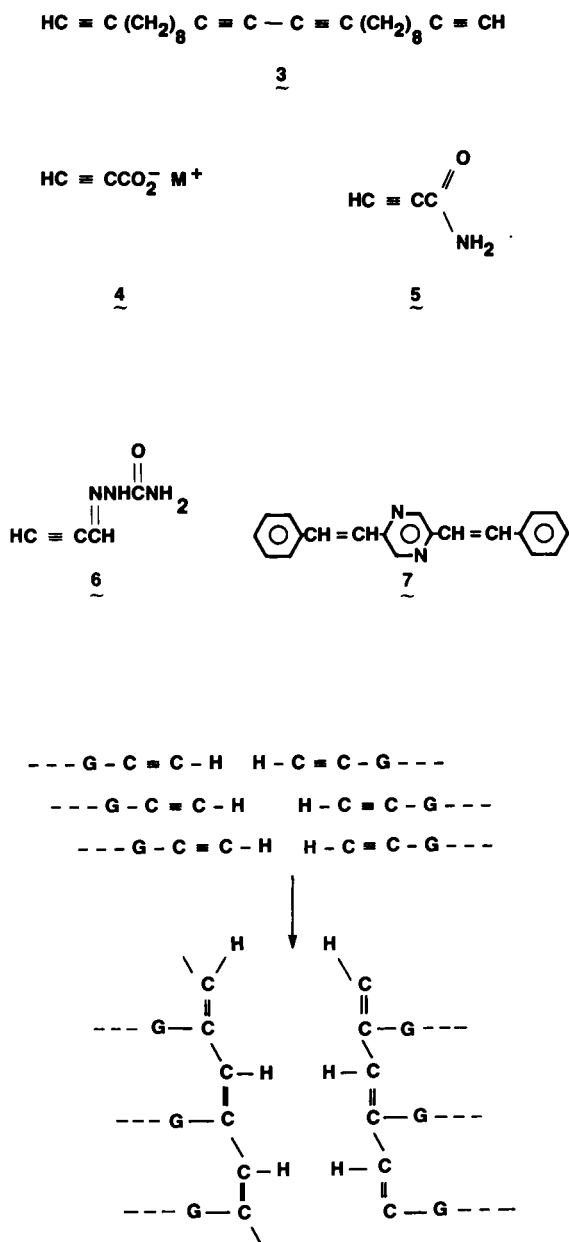
Monoenes and Dienes

Early studies of solid-state polymerization of vinyl derivatives have been reviewed (5). The initial discussions of the topochemical principle (7) were replete with examples from the photocycloaddition of cinnamic acid derivatives.

In 1967, Hasegawa identified the solid-state photochemical transformation of distyrylpyrazine *(7)* as a four center polymerization to a crystalline polymer with cyclobutane rings. Extensive crystallographic and mechanistic studies of this process have been reported (50). This type of four center photopolymerization has been extended to give a quantitative asymmetric induction (51). Laser Raman techniques have been used to study monomer-to-polymer conversion of these photopolymerizations and other processes as well (52).

It has long been known that highly crystalline forms of polybutadiene with melting points higher than conventional crystalline polybutadiene are available via radiation polymerization of thiourea inclusion compounds (14). Crystallographic studies of the polymerization of butadiene derivatives in inclusion complexes have been reported (53). Recently, butadiene derivatives in layer perovskite salts have been polymerized to single-crystal polymers which have been structurally characterized (54).

The solid-state reactivity of acrylate esters and salts and of acrylamide and its derivatives has long been known (5,6). The lack of crystallographic data has retarded understanding of these systems, and this problem has been recently addressed in the case of metal methacrylates (55).

$$HC \equiv C\ (CH_2)_8\ C \equiv C - C \equiv C\ (CH_2)_8\ C \equiv CH$$

3

$$HC \equiv CCO_2^-\ M^+$$

$$HC \equiv CC \overset{\displaystyle O}{\underset{\displaystyle NH_2}{\diagup\hspace{-2pt}\diagdown}}$$

4   **5**

$$HC \equiv CCH \overset{\displaystyle O}{\underset{\displaystyle NNHCNH_2}{}}$$

6   **7**

```
- - - G - C ≡ C - H    H - C ≡ C - G - - -

 - - - G - C ≡ C - H      H - C ≡ C - G - - -

 - - - G - C ≡ C - H    H - C ≡ C - G - - -
```

Figure 1. Schematic representation of a possible mode of polymerization of a terminal acetylene bonded to a group G involved in a nonbonded interaction.
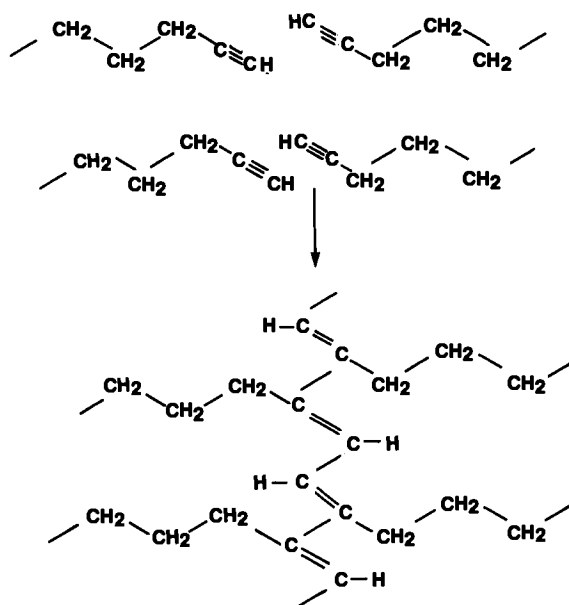
Figure 2. Schematic representation of a possible mode of polymerization of an alkyl-substituted terminal acetylene.

Ring-Opening Polymerization of Cyclic Monomers

The Kohlschutter report of solid-state polymerization (1) involved gas solid reactions of trioxane, and there is continuing interest in reactions of trioxane and other cyclic ethers (13).

Interest in the crystalline polymer derived from S_2N_2, that is poly(sulfur nitride), was stimulated by M.M. Labes and coworkers who have given a comprehensive review (56). This polymer has the electrical properties of a metal and provided the first example of a superconductor which lacked a metal atom.

Polymers of Transition Metal Complexes

B.M. Foxman and collaborators have extensively studied the polymerization of nickel (cyanoetheylphosphine) dihalide complexes and have found the reaction characterized by product specificity, stereospecificity, and crystallographic specificity (57). A detailed review of coordination polymerization has been published (58).

Simultaneous Polymerization and Crystallization

Simultaneous polymerization and crystallization is another approach to macroscopic, defect-free single crystals of macromolecules (59). Recent examples include a preparative method for mixed metal coordination polymers (60), and M. Hanack and coworkers have reacted hemiporphyrazine (61) with iron (II) acetate in nitrobenzene to obtain single crystals of an oxygen-bridged polymer with iron in a +4 oxidation state.

Prognosis

While some of the above discussion is in the general realm of prognostication, some more specific comments are appropriate. It is apparent that an increase in both the number and types of solid-state polymerization is a desirable research objective. Here, the major initial burden lies with the chemist to design (17, 47) new reactive molecular structure *and* appropriately oriented monomer crystal structures. Successful development of new lattice-controlled processes resulting in the availability of well-defined fully ordered macromolecules will readily attract the more physically and theoretically oriented research communities. The PDA and poly (sulfur nitride) cases bear strong witness to this point.

The preparation of the many classes of polymers which are known only as amorphous materials at present in crystallographically ordered forms is clearly a worthy research objective. The existing classes of conducting polymers, whose electrical properties are limited by the structural disorder present in experimental samples, would clearly benefit from such research (62, 63).

Diacetylene monomers with aromatic groups directly bonded to the triple bonds typically do not undergo extensive conversion to polymer (64). More extensive conversions appear to take place in fluorine-substituted diphenyl diacetylenes (65), and this may be an important new vector in PDA research.

Experimental methods likely to have important consequences for the preparation and study of fully ordered macromolecules include high pressure skills (15, 66) and numerous techniques using synchrotron radiation. X-ray topography using a synchrotron source has already been used to study the role of defects in PTS polymerization (67).

Acknowledgment

Literature Cited

1. Kohlschutter, H.W. *J. Liebigs Ann. Chem*. 1930, *482*, 75.

2. Strauss, F.; Kollek, L.; Heyn, W. *Chem. Berichte* 1930, *63*, 1868.

3. Schmitz, J.V.; Lawton, E.J. *Science* 1951, *113*, 718.

4. Tazuka, S.; Okamura, S. "Encyclopedia of Polymer Science Technology"; Interscience Publishers, 1971, *14*, 281.

5. Bamford, C.H.; Eastmond, G.C. *Quart. Rev. Chem. Soc*. 1969, *23*, 271.

6. Morawetz, H. *Science* 1966, *152*, 705.

7. Cohen, M.D.; Schmidt, G.M.J. *J. Chem. Soc*. 1964, 1996.

8. Hirshfeld, F.L.; Schmidt, G.M.J. *J. Polym. Sci. (A)* 1964, *2*, 2181.

9. "Polydiacetylenes," Cantow, H.J. Ed.; "Advances in Polymer Science"; Springer Verlag: Berlin, Heidelberg, 1984; Vol. 63.

10. "Polydiacetylenes," Bloor, D.; Chance, R.R. Eds., NATO ASI *Series*, Martinus Nijhoff: Dordrecht; Boston, 1985.

11. Lando, J.B.; Fort, T., Jr. In "Polymerization in Organized Systems"; Elias, H.G., Ed.; Gordon Breach: New York, 1977; p. 63.

12. Naegele, D.; Ringsdorf, H. *Ibid*., p. 79.

13. Wegner, G. *Faraday Disc. Chem. Soc*. 1979, *68*, 494.

14. Farina, M. "Inclusion Compounds"; Atwood, J.L.; Davies, J.E.D.; MacNicol. D.D., Eds.; Academic Press, 1984; Vol. 3, p. 297.

15. Zharov, A.A. *Russ. Chem. Rev*. 1984, *53,* 140.

16. Sixl, H., in ref. 9, p. 49.

17. Sandman, D.J.; Elman, B.S.; Hamill, G.P.; Velazquez, C.S.; Samuelson, L.A. *Mol. Cryst. Liq. Cryst*. 1986, *134*, 89.

18. Wegner, G. in ref. 9, p. v ff.

19. Enkelmann, V. in ref. 9, p. 91 ff.

20. Burdett, J.K. *J. Am. Chem. Soc*. 1980; *102*, 5458.

21. Sandman, D.J.; Hamill, G.P.; Samuelson, L.A.; Foxman, B.M. *Mol. Cryst. Liq. Cryst*. 1984, *106*, 199.

22. Wegner, G. *Pure Appl. Chem*. 1977, *49*, 443.

23. Patel, G.N.; Chance, R.R.; Witt, J.D. *J. Chem. Phys*. 1979, *70*, 4387.

24. Lim, K.C.; Fincher, C.R.; Heeger, A.J. *Phys. Rev. Lett*. 1983, *50*, 1934.

25. Enkelmann, V.; Wenz, G.; Mueller, M.A.; Schmidt, M.; Wegner, G. *Mol. Cryst. Liq. Cryst*. 1984, *105*, 11.

26. Kapitulnik, A.; Casalnuovo, S.; Lim, K. C.; Heeger, A.J. *Phys. Rev. Lett*. 1984, *53*, 469.

27. Wegner, G.; Schmidt, M. *J. Chem. Phys*. 1986, *84*, 1057.

28. Lim, K.C.; Kapitulnik, A.; Zacher, R.; Heeger, A.J. *J. Chem. Phys. 1986, 84*, 1058.

29. Philpott, M.R. *Annu. Rev. Phys. Chem*. 1980, *31*, 97.

30. Garito, A.F.; Singer, K.D. *Laser Focus*, February 1982, p. 60.

31. Williams, D.J. Ed. "Nonlinear Optical Properties of Organic and Polymeric Materials," ACS *Symposium Series* No. 233, 1983.

32. Sandman, D.J.; Carter, G.M.; Chen, Y.J.; Elman, B.S.; Thakur, M.K.; Tripathy, S.K. in ref. 10, p. 299 ff.

33. Smith, P.W. *The Bell Syst. Techn. J*. 1982, *61*, 1975.

34. Thakur, M.; Meyler, S. *Macromolecules* 1985, *18*, 2341.

35. Carter, G.M.; Thakur, M.; Chen, Y.J.; Hryniewicz, J.V. *Appl. Phys. Lett.* 1985, *47*, 457.

36. Carter, G.M.; Hryniewicz, J.V.; Thakur, M.K.; Chen, Y.J.; Meyler, S.E. *Appl. Phys. Lett.* 1986, *49*, 998.

37. Donovan, K.J.; Wilson, E.G. *Phil. Mag.* 1981, *B44*, 9.

38. Spannring, W.; Baessler, H. *Chem. Phys. Lett.* 1981, *84*, 54.

39. Baessler, H., in ref. 10, p. 137 ff.

40. Donovan, K.J.; Freeman, P.D.; Wilson, E.G. in ref. 10, p. 165 ff.

41. Seiferheld, U.; Baessler, H. *Solid State Commun.* 1983, *47*, 391.

42. Elman, B.S.; Thakur, M.K.; Sandman, D.J.; Newkirk, M.A.; Kennedy, E.F. *J. Appl. Phys.* 1985, *57*, 4996.

43. Bader, H.; Dorn, K.; Hupfer, B.; Ringsdorf, H. In "Polymer Membranes"; Gordon, M., Ed.; Advances in Polymer Science"; Vol. 64; Springer Verlag: Berlin, Heidelberg 1985.

44. Patel, G.N.; Preziosi, A.F.; Baughman, R.H. U.S. Patent 3 999 946, 1976.

45. Etemad, S.; Heeger, A.J.; MacDiarmid, A.G. *Annu. Rev. Phys. Chem.* 1982, *33*, 443.

46. Grasso, R.P.; Thakur, M.K.; Lando, J.B. *Mol. Cryst. Liq. Cryst.* 1985, *118*, 377.

47. Foxman, B.M.; Jaufmann, J.D. *J. Polym. Sci. (C)* 1983, *70*, 31.

48. Tieke, B. *Mol. Cryst. Liq. Cryst.* 1983, *93*, 119.

49. Velazquez, C.S.; Sandman, D.J.; Foxman, B.M. Unpublished experiments, 1986.

50. Hasegawa, M. *Chem. Rev. 1983, 83*, 507.

51. Addadi, L; Lahav, M. *J. Am. Chem. Soc.* 1978, *100*, 2938.

52. Prasad, P.M.; Swiatkiewicz, J.; Eisenhardt, G. *Appl. Spectrosc. Rev. 1982, 18*, 59.

53. Chatani, Y.; Kuwata, S. *Macromolecules* 1975, *8*, 12, and references therein.

54. Tieke, B. In *Adv. Polym. Sci.* 1985, *71*, 79, Springer Verlag: Berlin, Heidelberg.

55. Shepherd, J.W. III; Foxman, B.M. *Mol. Cryst. Liq. Cryst.* 1986, *137*, 87.

56. Labes, M.M; Love, P.; Nichols, L.F. *Chem. Rev.* 1979, *79*, 1.

57. Cheng, K.; Foxman, B.M. *J. Am. Chem. Soc.* 1977, *99*, 8102.

58. Gersten, S.W.; Foxman, B.M. *Encycl. Polym. Sci. and Eng.* John Wiley and Sons, New York, 2nd Ed., 1986, *4*, 175.

59. Wunderlich, B. *Adv. Polym. Sci.* 1968, *5*, 568.

60. Foxman, B.M.; Gersten, S.W. *Inorg, Chim. Acta* 1979, *33*, L 151.

61. Hiller, W.; Strahle, J.; Datz, A.; Hanack, M.; Hatfield, W.E.; terHaar, L.W.; Gutlich, P. *J. Am. Chem. Soc.* 1984, *106*, 329.

62. Sandman, D.J. *J. Electr. Mater.* 1981, *10*, 173.

63. Baughman, R.H.; Bredas, J.L.; Chance, R.R.; Elsenbaumer, R.L.; Schacklette, L.W. *Chem. Rev.* 1982, *82*, 209.

64. Wegner, G. *J. Polym. Sci., Polym. Lett. Ed.* 1971, *9*, 133.

65. Tokura, Y.; Koda, T.; Itsubo, A.; Miyabayshi, M.; Okuhara, K.; Ueda, A. *J. Chem. Phys.* 1986, *85*, 99.

66. Tanaka, Y.; Iijima, S.; Shimizu, T.; Fujikawa, H.; Matsuda, H.; Nakanishi, H.; Kato, M.; Kato, S. *J. Polym. Sci., Polym. Lett. Ed.* 1986, *24*, 177.

67. Sheen, D.B.; Sherwood, J.N. *Chem. in Britain* 1986, *22*, 535.

Chapter 2

Electron Spin Resonance Spectroscopy of Triplet Electron Pairs in Diacetylene Crystals

Hans Sixl[1]

Physikalisches Institut, Pfaffenwaldring 57, D-7000 Stuttgart 80,
Federal Republic of Germany

Recent ESR spectra of linear chain diacety-
lene oligomer and polymer systems are des-
cribed. The electronic properties of the
polymer and of the intermediates are deduced
from the triplet radical pair character of
their ground and excited states. It will be
demonstrated that the polydiacetylenes repre-
sent a unique model system for the study of
the p_z-electron system in conjugated poly-
mers. There is a strong correlation between
the p_z-electron structure of the intermedi-
ate states and that of the polaron and bipo-
laron states. The ground state of the radi-
cal electron pairs is a singlet state with
$S = 0$. The excited states are given by trip-
lets ($S = 1$) and quintets ($S = 2$) as well
as by mixed singlet-quintet states. Recent
time resolved ESR spectra of the polymer
are interpreted to be due to $S = 1$ bipola-
ron states.

In a solid state polymerization reaction monomer crystals
of diacetylene molecules (R-C≡C-C≡C-R) are converted to
polydiacetylene crystals (1,2). The primary photochemical
processes during the low-temperature photopolymerization
reaction have been investigated by ESR (3,4) and optical
absorption spectroscopy (5,6). A review of the spectros-
copy of the intermediate states has been given by Sixl (7).
A simple reaction scheme is shown in Figure 1. The reac-
tion is characterized by the uv-photoinitiation of dira-
dical dimer molecules. Chain propagation is performed by
thermal addition of monomer molecules. Thus trimer, tetra-
mer, pentamer etc.... molecules are obtained.

[1]Current address: Hoechst AG, Angewandte Physik, D-6230 Frankfurt am Main 80,
Federal Republic of Germany

   The electronic structure of the intermediates is
given by a mixture of the mesomeric diradical (DR) and
dicarbene (DC) configurations of Figure 2 (a) and (b).
The energies are non-degenerate. The ground state energy
of the diradical DR_n is given by $n\varepsilon$, where ε is the ener-
gy difference between the butatriene structure and the
acetylene structure per diacetylene unit. This quantity
has been estimated to be 0.4 eV (8,9). The ground state
energy of the dicarbene DC_n is given by ε_π = 2.7 eV, due
to the disruption of an additional π-bond. The energies
of the pure DR_n and DC_n configurations are shown in
Figure 3. As a consequence of the crossing of energies,
intermediates with n > 7 are almost pure dicarbenes (9).
This is consistent with the acetylenic chain structure of
polydiacetylene crystals (10).
   On the other side theoretical work on conjugated
polymers predicts radical pair excitations with singlet,
doublet and triplet character (11). The electronic sing-
let and triplet bipolaron configuration of polydiacety-
lene molecules ($^1BP^0$ and $^3BP^0$, respectively) can be appro-
ximated by the following simplified structures of Figure
4. The BP^0 states are neutral (charge Q = 0) and repre-
sent excited states of the chain. The radical electron
pair is bound, due to the energetically unfavourable
butatriene structure. The singlet radical states there-
fore are expected to recombine at a very short time scale.
However the recombination of the triplets is spin-forbid-
den.
   This paper will be concerned with the ESR-spectros-
copy of S = 1 and S = 2 radical electron pairs. These
pairs are present in the intermediates as well as in the
final long polydiacetylene molecules. Information con-
cerning the ground and excited state radical electron
structures and energies are deduced from the ESR fine
structure and kinetics.

ESR Spectroscopy of the Reaction Intermediates

The radical electron pairs of the diradicals and dicar-
benes can be combined to singlets (S = 0), triplets
(S = 1) and quintets (S = 2). Typical ESR spectra and
energy level diagrams of the reaction intermediates are
shown in Figure 5. The diradicals DR_2 and DR_3 are ob-
tained immediately after a few excimer laser pulses. They
are characterized by a two line spectrum and a small fine
structure splitting. The dicarbenes DC_n are obtained after
thermal reactions. They are characterized by a four line
spectrum and a large fine structure splitting. All spectra
can be described quantitatively by an exact spin hamil-
tonian as shown by the line positions in Figure 5 a and
by the energy level diagram in Figure 5 b. The combination
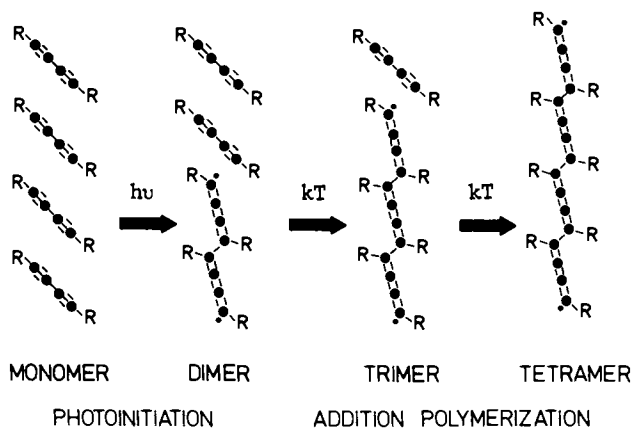of two triplet carbenes leads to mixed singlet-quintets
for the limit of large n (12).

Figure 1.   Reaction scheme of the polymerization reac-
tion in diacetylene crystals. Photoinitiation of the
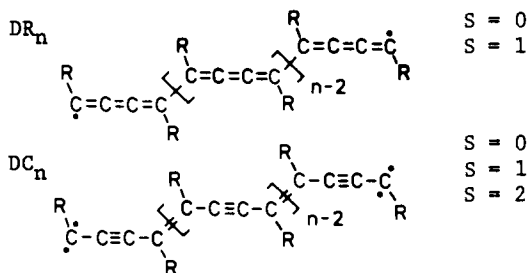dimer molecule and thermal addition reactions to the
trimer etc.

Figure 2.   Diradical DR_n and Dicarbene DC_n ($n \geq 2$)
configurations of the intermediates. The spin multi-
plicities are given by singlets ($S = 0$), triplets
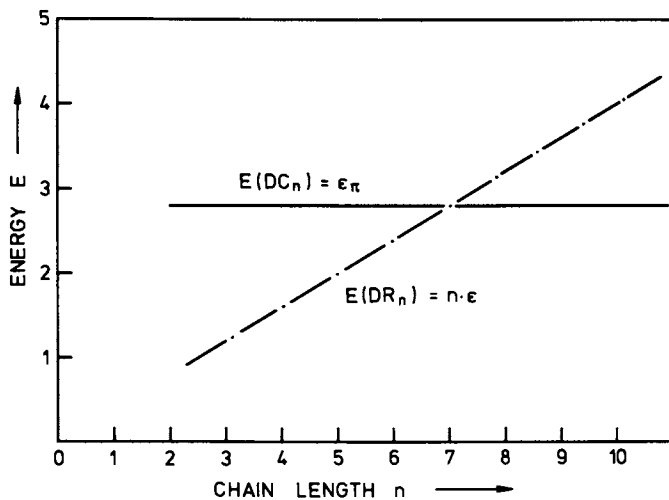($S = 1$) and quintets ($S = 2$).

Figure 3. Energies of the diradical and dicarbene configurations. ε_π is the energy of a π-bond, ε is the energy difference of the butatriene and acetylene configurations per unit cell.
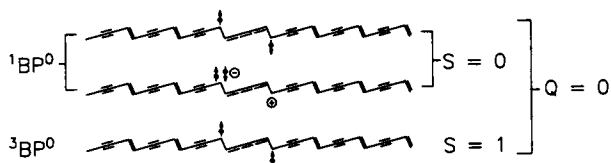
Figure 4. Principal triplet and singlet bipolaron configurations of the polydiacetylene chain.
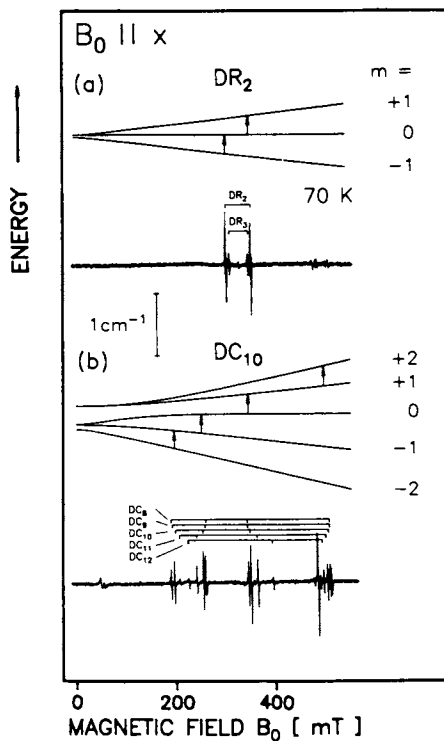
Figure 5. Energy level splitting in a magnetic field B_O and $\Delta m = 1$ ESR-transitions at a microwave frequency of 9.30 GHz. The following parameters are used in the calculation DR_2: $D/hc = 0.0393$ cm^{-1}, $E/hc = -0.0016$ cm^{-1}. DC_{10}: $D/hc = 0.2960$ cm^{-1}, $E/hc = -0.0040$ cm^{-1} and $\varepsilon_{SQ}/hc = 4.5$ cm^{-1}.

The thermal reaction of the diradicals of Figure 5 a
at 90 K is shown in Figure 6. The curves are calculated
using the differential equations of a thermal addition
reaction (intermediate (n) + monomer → intermediate
(n + 1)). The triplets change to quintets at n = 7. Star-
ting from n = 7 triplets and quintets are present simul-
taneously as shown by Neumann and Müller (13).
    The reaction rates of the thermal reaction of the
different intermediates n are strongly temperature depen-
dent and can be described by an Arrhenius law, given by
$k_n = k_0 \exp(-E_a(n)/kT)$. The resulting activation energies
for thermal addition reactions $E_a(n)$ are shown in Figure 7
together with the fine structure parameters D/hc, the
hyperfine structure parameters A_1 and A_2 and the singlet
triplet energy separation $\varepsilon_{ST}(n)$. As seen from Figure 7
the change from diradicals to dicarbenes at n = 6 implies
gross changes in the physical properties of the interme-
diates. Only diradical and dicarbene triplet state proper-
ties are shown in the Figure.
    The combination of the sp^2-radical electron in the di-
radicals leads to a singlet ground state and to a ther-
mally activated triplet state. The sp^2- and p_z-radical
electrons in the carbene form a triplet ground state and a
singlet excited state. Finally, the combination of two
triplet ground state carbenes again leads to a singlet
ground state and to thermally activated triplet and quin-
tet states. The consequence is that all ESR spectra are
thermally activated and therefore disappear at extremely
low temperatures. The singlet-triplet and singlet-quintet
energy separations ε_{ST} and ε_{SQ} can be determined from the
temperature dependence of the ESR intensities. They are
given in Figure 7. Again the diradical properties with
n < 6 are different from those of the dicarbenes for n > 7.

ESR-Spectroscopy of Excitations on the Polymer Chain

The optical absorption and the corresponding prompt fluo-
rescence spectra of diacetylene polymer molecules are
shown in Figure 8. The spectra are typical for almost all
differently substituted polydiacetylene polymer molecules.
They are due to (S = 0) singlet Frenkel excitons of the
quasi one-dimensional system. Upon excitation at much
higher energies a relatively broad delayed emission
appears, which is strongly red shifted as compared to the
exciton emission. The excitation and the corresponding
delayed emission spectra are also shown in Figure 8. The
observed 720 nm-emission and the corresponding high-energy
absorption with maximum at 380 nm are tentatively explained
by electron-hole photoexcitation, lattice-relaxation to
polaron pairs P^+ and P^- and polaron recombination lumines-
cence emission. The resulting triplet bipolarons $^3BP^0$ with
a lifetime of about 80 μs can be detected in a transient
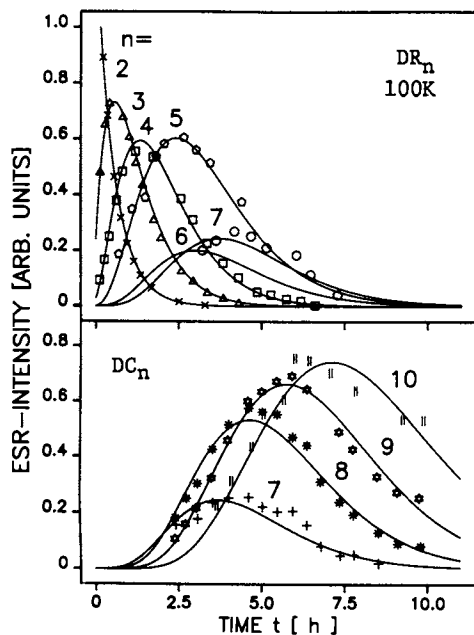absorption experiment described by Orenstein et al (14).

Figure 6. Thermal reaction kinetics of the different reaction intermediates. The upper part shows the triplets (n = 2, 3, 4 and 5 are pure diradicals). The lower part shows the quintets (n > 7 are pure dicarbenes).
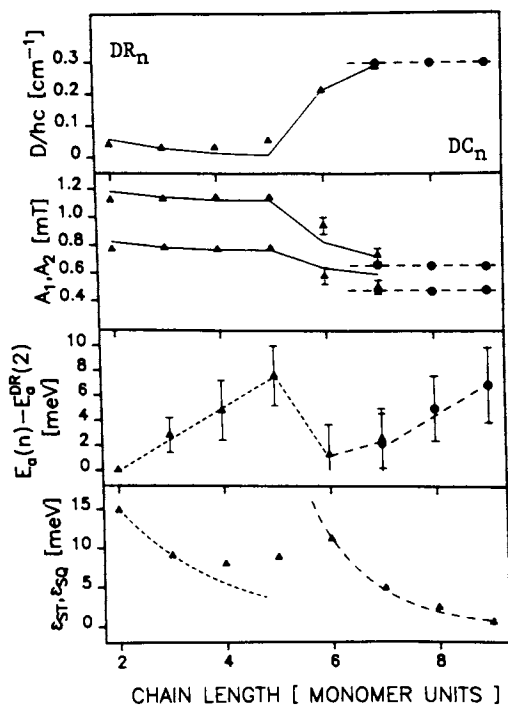
Figure 7. Fine structure constants D, hyperfine struc-
ture constants A, activation energies of the thermal
reaction and singlet triplet energy separation of the
diradical and dicarbene triplet states. There is a
characteristic change of all properties when the
structure changes from diradicals to dicarbenes.
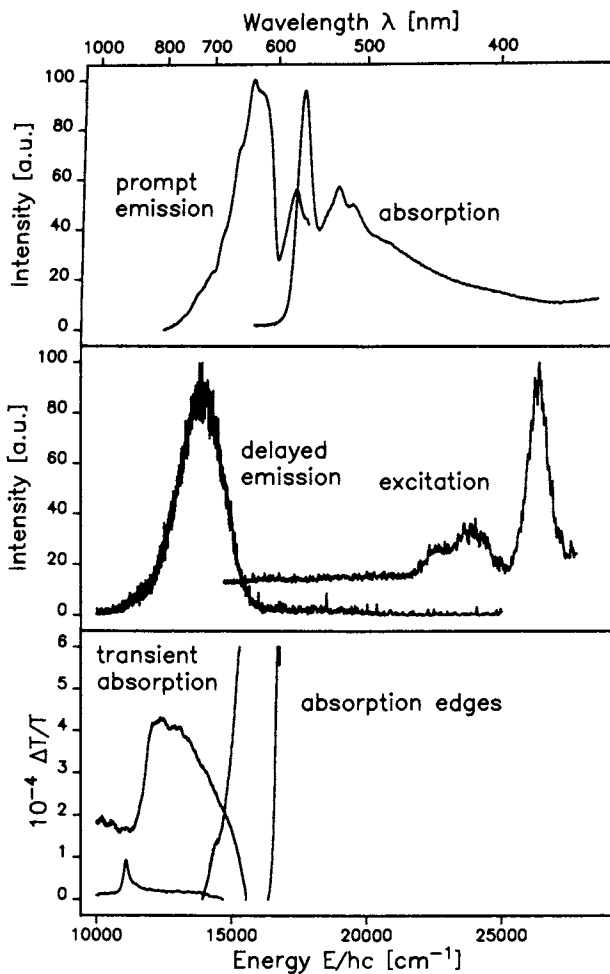
Figure 8. Top, optical absorption and the corresponding prompt
fluorescence spectra of diacetylene polymer molecules; middle,
excitation and the corresponding delayed emission spectra; and
bottom, transient absorption for a partially polymerized (broad
line) and fully polymerized (narrow line) diacetylene crystal.

The transient absorption is also shown in Figure 8 for a
partially polymerized (broad line) and fully polymerized
diacetylene crystal (narrow line).

With recent ODMR experiments Robins et al (15) were
able to correlate the transient absorption to the triplet
state of the polydiacetylene chain. By time resolved ESR
spectroscopy we succeeded in the direct detection of the
triplet state. A spin echo spectrum of the diacetylene
triplet state using N_2-laser excitation is shown in Fi-
gure 9. The individual points of the spectrum are given
by the spin-echo signals every 20 μs after N_2-laser pulse
excitation. From the orientation of the principal axes of
the fine structure tensor it is known that the two radi-
cal electrons are located on the PDA chains. The magni-
tude of the fine structure interaction allows us to esti-
mate that the average distance between the radical elec-
trons is about one unit cell length, as schematically
shown in Figure 4 for the triplet bipolaron.

The emissive and absorptive ESR signals indicate com-
plete spin alignment. From the time dependence of the
signals shown in the insert of Figure 9 it is obvious
that the triplets are formed unselectively. At t = 0 the
ESR signal is zero despite of the fact that the triplet
state is already populated (15). Consequently every zero
field spin component is populated by the same probability
($p_x = p_y = p_z = 1/3$). The kinetics of the ESR-spectra in
all magnetic field orientation is completely described
by two selective decay constants of the triplet sublevels.
In the orientation of B along the chains they are given
by $k_1 = 1.8 \cdot 10^4$ s^{-1} and $k_2 = 5.5 \cdot 10^4$ s^{-1} in a large
temperature regime 10 K < T < 180 K. Consequently the
spin lattice relaxation rate constants are less than ca.
10^4 s^{-1}.

Conclusions

It has been demonstrated by the ESR experiments described
in this contribution that radical pair electrons play an
important role in the physics and chemistry of the solid
state polymerization reaction in diacetylene crystals.
The radical pairs in the diradical and dicarbene reaction
intermediates have been extensively studied spectrosco-
pically and lead to a consistent picture of the reaction
mechanisms and of the π-bond and radical electron struc-
ture of the intermediates. A new field of research has
been opened by time resolved ESR spectroscopy of tran-
sient triplet states on the polymer chains. Spectroscopic
work concerning triplet excited states is just at the
very beginning. The correlation of the optical spectra
(Figure 8), the transient absorption data (14,15) as well
as the very recent spin echo experiments reported in this
paper support the triplet bipolaron character of the
photoexcited polymer chain. The observed unselective popu-
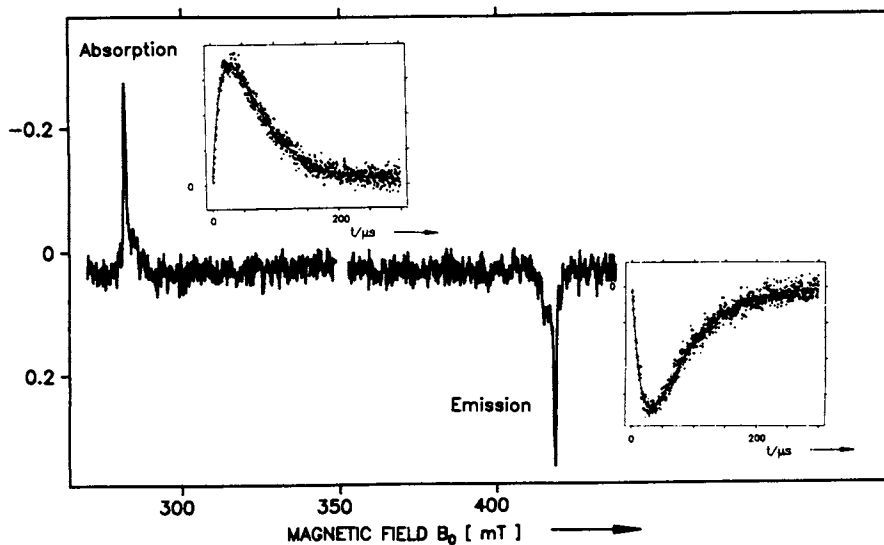lation of the triplet spin sublevels supports a triplet

Figure 9. Electron spin echo ESR spectrum with B_O
parallel to the chain axis. The spectrum is typical
of a triplet state with spin alignment. The kinetics
of the absorption and emission line is shown in the
insert. The microwave freqency is given by 9.24 GHz.
The linewidth is given by $\Delta B_{1/2}$ = 86 independent of
temperature.

formation mechanism via a radical electron pair recombination mechanism. Independent radical pairs are present after the electron-hole photogeneration followed by relaxation to polaron pairs according to the photoexcitation and delayed luminescence spectra of Figure 8. Further details of the transient optical and spin echo experiments will be published in the near future (16,17).

Acknowledgments

Literature Cited

1. Wegner, G., "Molecular Metals"; Hatfield, E., Ed.; Plenum Press; New York, 1979; p. 209, and "Chemistry and Physics of One-Dimensional Metals"; Keller, H.J., Ed.; Plenum Press; New York, 1977; p. 297.
2. Baughman, R.H.; Chance, R.R., "Synthesis and Properties of Low-Dimensional Materials"; Miller, J.S., and Epstein, A., Ed.; Ac. of Science, New York, 1978; p. 795; and Bloor, D., "Developments in Crystalline Polymers"; Basset, D.C., Ed.; Appl. Sci. Publ., London, 1982.
3. Bubeck, C.; Sixl, H.; Wolf, H.C.; Chem. Phys. 1978, 32, 231; Bubeck, C.; Neumann, W.; Sixl, H.; Chem. Phys., 1980, 48, 269; Huber, R.A.; Schwoerer, M.; Benk, H.; Sixl, H.; Chem. Phys. Lett., 1981, 78, 303.
4. Neumann, W.; Sixl, H.; Chem. Phys., 1980, 50, 273; 1981, 58, 303. Mol. Cryst. Liq. Cryst., 1984, 105, 41.
5. Hersel, W.; Sixl, H.; Wegner, G.; Chem. Phys. Lett., 1980, 73, 288. Gross, H.; Sixl, H.; Chem. Phys. Lett., 1982, 91, 262. Gross, H.; Sixl, H.; Mol. Cryst. Liq. Cryst., 1983, 93, 261.
6. Niederwald, H.; Eichele, H.; Schwoerer, M.; Chem. Phys. Lett., 1980, 72, 242. Niederwald, H.; Richter, K.-H.; Güttler, W.; Schwoerer, M.; Mol. Cryst. Liq. Cryst., 1983, 93, 247.
7. Sixl, H.; Adv. Polym. Sci., 1984, 63, 49. Sixl, H.; "Polydiacetylenes", Bloor, D.; Chance, R.R.; Ed.; Martinus Nijhoff, Publ., 1985, p. 41.
8. Karpfen, A.; J. Phys., 1980, C 13, 5673.
9. Sixl, H.; Neumann, W.; Huber, R.; Denner, V.; Sigmund, E.; Phys. Rev., 1985, B 31, 142.
10. Kobelt, D.; Paulus, E.F.; Acta Cryst.; 1974, B 30, 232.
11. Campbell, D.K.; Bishop, A.R.; Phys. Rev., 1981, B 24, 4859; Brédas, J.L.; Chance, R.R.; Silbey, R.; Phys. Rev., 1982, B 26, 5843.
12. Benk, H.; Sixl, H.; Mol. Phys., 1981, 42, 779.

13. Neumann, W.; Ph. D. Thesis, University of Stuttgart,
    1984.
    Müller, K.; Ph. D. Thesis, University of Bayreuth,
    1986.
14. Orenstein, J.; Baker, G.L.; Etemad, S.; J. Phys. C.,
    Solid State Phys., 1984, 17, L 297.; Etemad, S.;
    Baker, G.L.; Orenstein, J.; Lee, K.M.; Mol. Cryst.
    Liq. Cryst., 1985, 118, 389.
15. Robins, L.; Orentstein, J.; Supferfine, R.; Phys. Rev.
    Lett., 1986, 56, 1850.
16. Sixl, H.; Jost, R.; Warta, R., and Orenstein, J.;
    in preparation
17. Grupp, A.; Winter, M.; Mehring, M.; Rühle, W.; Sixl,
    H.; in preparation.

Chapter 3

Structural Studies of Novel Polydiyne Materials

R. J. Butera, R. P. Grasso, Mrinal K. Thakur[1], and J. B. Lando

Department of Macromolecular Science, Case Western Reserve University,
Cleveland, OH 44106

The structure analyses of two special types of
diacetylene "monomers," diyne dimers and polydiyne
macromonomers, are reviewed and preliminary results on
the conversion and chromic behavior of one specific
system, poly(1,8-nonadiyne) (P18N) are presented.
Structure analyses of these materials before and after
solid state polymerization allows a qualitative under-
standing of the diacetylene polymerization. Cross-
polymerized P18N has been shown to display
solvatochromic and thermochromic behavior, even though
this material is insoluble and infusible. Examination
of initial optical spectroscopic data of the chromic
behavior as a function of conversion, as well as
consideration of the chromic behavior of conventional
diacetylenes, leads to a possible explanation of the
chromic behavior of crosspolymerized P18N.

Because of the interest in the optical and electrical properties of
diacetylene polymers, there are many different types of diacetylene
monomers discussed in the literature. Nearly all of these monomers
have only one functionality which is reactive in the solid state —
that being a single diacetylene group. Our work has focused on
diactylene monomers which have more than one group which is
chemically reactive in the solid state. These materials can be
broadly classified into two categories: 1) diyne dimers and 2)
polydiyne "macromonomers" (figure 1).

Most of the work on diyne dimers has focused on
1,11-dodecadiyne dimer (n=8 in figure 1A). When crystals of this
material are irradiated with ultraviolet light or gamma radiation,
both the acetylene and diacetylene groups polymerize to form
sheet-like structures with parallel polyacetylene and
polydiacetylene chains bridged by 8 methylene units. Conductivities
as high as 2×10^{-2} ohm^{-1}-cm^{-1} have been measured for this

[1]Current address: GTE Laboratories, Inc., Waltham, MA 02254

material (1). This high conductivity is thought to be due to the unique packing of the sheet-like structures. The arrangement of the sheets in the unit cell has been determined by comparative structure analysis of 1,11-dodecadiyne dimer before and after polymerization.

The macromonomers also form sheet-like structures upon exposure to high energy radiation, strain, or thermal annealing. The process of diacetylene polymerization in the macromonomers is referred to as "crosspolymerization" (figure 2) (2). This process is very different from the usual random crosslinking that occurs in many polymers. In these macromonomers, the linking reaction takes place predominantly in the crystalline regions and results in a regular structure. It should be stressed that the macromonomers have a typical type of semi-crystalline polymer morphology, and so are very different from conventional diacetylene monomers in terms of morphological order. The crosspolymerized material may be thought of as a composite structure — crystalline domains which have crosspolymerized and, therefore, have a very rigid two dimensional structure, and amorphous (unpolymerized) regions which are soft (14).

The crystal structures of poly(1,11-dodecadiyne) and poly(1,8-nonadiyne), (n=8 and 5 respectively in figure 1B) and their crosspolymerized products have been determined, and a qualitative picture of the crosspolymerization process has been inferred from these structure analyses (2,3). Also, qualitative information about the extent of reaction vs. radiation dose has been obtained on poly(1,8 nonadiyne) (P18N) using differential scanning calorimetry, and optical absorption spectroscopy (4). The information obtained from these experiments will be discussed, along with the problems encountered in trying to monitor the progress of the solid state reaction.

Crosspolymerized poly(1,8-nonadiyne) has been observed to show interesting chromic behavior upon exposure to heat or certain solvents (4). Preliminary results on this chromic behavior have been interpreted in terms of the structure of this material and the observed chromic behavior of other polydiacetylene systems.

The following discussion will briefly review the available information on the synthesis, physical properties, crystal structure, solid state reaction, and chromic behavior of these polyfunctional diacetylenes.

Synthesis of 1,11-dodecadiyne Dimer

Originally, 1,11-dodecadiyne dimer was synthesized using a controlled Glaser coupling polymerization reaction under conditions which would maximize the amount of dimer obtained (3). In this type of reaction, the relative amounts of monomer, dimer, and higher oligomers are determined by the kinetics of the reaction. However, regardless of how carefully the reaction is controlled, small amounts of monomer and oligomeric impurities will be present. To eliminate this contamination, a direct synthesis of 1,11-dodecadiyne dimer was devised. Since the details of this multi-step synthesis have been described elsewhere (11), we will not repeat them here. The important feature of this pathway is that the intermediate which is used in the Glaser coupling reaction is dibromododecyne, which can form only dimer. The coupled product is then dehydrobrominated to yield the dimer. It should be noted that this synthesis is

non-specific and can be applied directly to the production of symmetric dimers with various numbers of methylene groups between the acetylene groups. Work is currently under way to synthesize and characterize other alkyldiacetylene dimers.

Structure Analysis and Polymerization of 1,11-dodecadiyne Dimer (3,21)

A large plate-like crystal (0.5 X 0.05 X 1.5 mm) of polymerized 1,11-dodecadiyne dimer was obtained after cobalt-60 irradiation. The resultant crystal was blue-black in color. This crystal was used for x-ray diffraction data collection from an automated 4 circle diffractometer. The structure was determined using a full matrix least squares refinement program on 926 unique reflections. Results of this analysis show that the final structure has a monoclinic unit cell (space group P2/n, a=26.78 Å, b=8.25 Å, c=4.91 Å, γ=119.6°) and is composed of two-dimensional sheets of trans-polyacetylene and polydiacetylene chains interconnected by eight methylene groups (figure 3). These sheets are staggered by a/2 unit cell lengths. This causes the polyacetylene chain in one sheet to be next to the polydiacetylene chains in the adjacent sheets. As a result, polyacetylene and polydiacetylene chains are about 4 Å apart in the b direction. The bond lengths along the polydiacetylene chain are consistent with the acetylenic form.

For electron diffraction of the unpolymerized dimer, microscopic single crystals were obtained from a dilute hexane solution at 4°C. The structure refinement was carried out using the linked atom least-squares (LALS) program (developed by Arnott and coworkers (12)) on 19 unique reflections. The unit cell is monoclinic (space group $P2_1/b$, a=28.25 Å, b=8.50 Å, c=5.24 Å, α=100.8°).

Comparison of the two structures shows that the diacetylene rod must rotate by an angle of almost 60° and is simultaneously translated by 0.33 Å along the c axis (polydiacetylene chain axis). Also, the two methylene chains swing 7° in order to bring the terminal acetylene groups into position so that they can react to form the trans-polyacetylene chains.

Electrical Conductivity of Polymerized 1,11-dodecadiyne Dimer (3,21)

Since single crystals large enough for a 4 point conductivity measurement of the polymerized dimer could not be obtained, polycrystalline films were used. Samples were prepared by casting a film of the dimer from a 1-2 wt.% acetone solution onto a glass slide at -5°C. The slide was covered with a petri dish to allow slow evaporation of the solvent. The sample was then maintained at 0°C under a nitrogen purge and exposed to ultraviolet light for 45 minutes. The partially polymerized sample was then placed in an airtight aluminum canister and purged with UHP argon. The polymerization vessel was placed into a cobalt-60 gamma radiation source and exposed to 1 Mrad.

The current voltage response was linear at room temperature between 10^{-12} and 10^{-1} amps. Conductivities as high as 2 X 10^{-2} ohm^{-1}-cm^{-1} have been measured for this type of sample. Conductivity did not change over a span of several months indicating

a   H–C≡C–(CH$_2$)$_n$–C≡C–C≡C–(CH$_2$)$_n$–C≡C–H

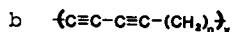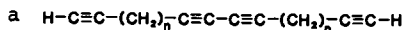
b   —(C≡C–C≡C–(CH$_2$)$_n$)$_x$

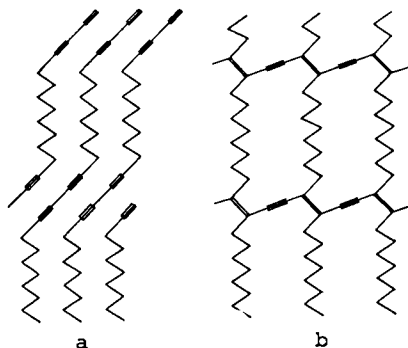Figure 1. General structure of (a) diyne dimers, (b) polydiyne macromonomers.

Figure 2. Schematic of macromonomer crosspolymerization reaction (poly(1,11-dodecadiyne) used as example). (a) macromonomer, (b) crosspolymerized product. Hydrogen atoms omitted for clarity. (Reproduced from reference 2. Copyright 1983 American Chemical Society.)
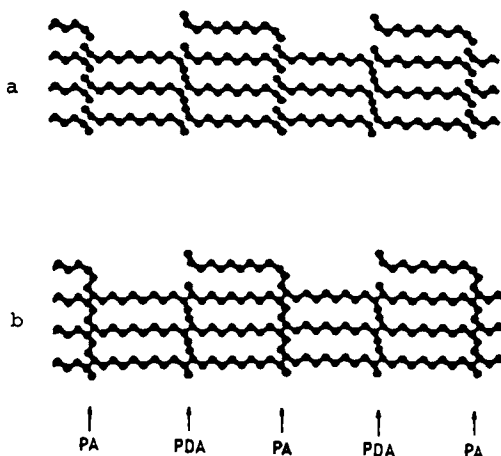

Figure 3. Two dimensional schematic crystal stucture of (a) 1,11-dodecadiyne dimer and (b) the polymer. Hydrogen atoms omitted for clarity.

the polymer is quite stable to atmospheric attack at ambient
temperature (20). A preliminary conductivity-temperature study
showed that the material behaves as a semiconductor.

The observed conductivity is high compared to that of other
organic conducting materials. One possible explanation for this
behavior is based on the fact that the nearest neighbor distance
between a polydiacetylene and polyacetylene chain is 4 Å. This close
approach would allow pi-electron orbital overlap between the chains
and, perhaps, cause enhanced conductivity. Partial charge
calculations indicate a coulombic interaction between polyacetylene
and polydiacetylene chains (13).

Another possible explanation for the high conductivity of the
polymerized dimer is that the material is doped with a small amount
of oxygen due to atmospheric exposure (20). Although exposure to air
for long periods of time (i.e. on the order of 1 year) will decrease
the conductivity, it is possible (though not likely) that small
amounts of oxygen could be present in the "pristine" material (20).
Further experiments are needed to determine if oxygen doping is
indeed the cause for the observed conductivity.

Synthesis of Macromonomers

Originally, a Glaser coupling reaction was used to synthesize the
macromonomers (2,3). However, there are a number of problems with
this synthesis, the most important being low molecular weight and
difficulty in purifying the product. The synthesis now being used is
a catalytic coupling reaction based upon that of White (15). The
synthesis procedure consists of reacting the diyne monomer with
pyridine, N,N,N',N'-tetramethylethylenediamine, and copper (I)
chloride in approximately 60 ml of o-dichlorobenzene at 60°C. The
polymer is then purified by precipitation into methanol (details of
the synthesis will be published elsewhere). Polymer obtained by this
method can reach molecular weights of $Mn= 17,500$ and $Mw= 33,500$ (as
determined by GPC analysis in THF using a polystyrene standard). The
macromonomer is a colorless, thermoplastic material.

Structure and Crosspolymerization of Poly(1,11-dodecadiyne)(2)

Microscopic single crystals of poly(1,11-dodecadiyne) were prepared
by solution crystallization from chloroform solution at 4°C. These
crystals (less than 200 Å thick) were then collected on a carbon
coated copper grid and used for selected area electron diffraction.
Both the macromonomer and crosspolymerized product had monoclinic
unit cells (macromonomer: space group $P2_1/n$, a=13.25 Å, b=14.15 Å,
c=7.63 Å, β=118.50; crosspolymerized product: space group $P2_1/n$,
a=9.17 Å, b=12.25 Å, c=9.92 Å, β=123.50°). Eighteen reflections for
the macromonomer and thirty-six for the crosspolymerized product
were used in the LALS program for the structure determination.
Crosspolymerization was effected using 100 Mrad of cobalt-60 gamma
radiation. Figure 2 shows a schematic of the sheet-like structure
formed upon crosspolymerization.

As shown in figure 4, the diacetylene backbone runs along the c
direction. This is because the neighboring macromonomer chains are
only 4 Å apart along the c axis, whereas the chains in every other
direction have a separation of at least 7 Å. The macromonomer

molcules need only a slight rotation and translation along the c
axis to polymerize, in accordance with the principle of least motion
(10,19). The parallel sheets subsequently slide along the interchain
potential to attain optimum packing. It should be noted that the
bond distances along the polydiacetylene backbone correspond to the
acetylenic structure. Results from solid state C-13 NMR analysis
(14) suggest that reaction in the amorphous regions is minimal, if
present at all. These results also show that the crosspolymerized
material is in the acetylenic form, in agreement with the x-ray
results.

Structure and Crosspolymerization of Poly(1,8-nonadiyne)(22)

The single crystals used for elctron diffraction were prepared in a
manner similar to that described for poly(1,11-dodecadiyne). Both
the macromonomer and crosspolymerized product have monoclinic unit
cells (macromonomer: space group $P2_1$, a=7.88 Å, b=21.00 Å, c=5.67
Å, β=90.8° ; crosspolymerized product: space group $P2_1$/n, a=9.30 Å,
b=17.5 Å, c=4.85 Å, β=101.71°). Eighteen reflections for the
macromonomer and twenty-four reflections for the crosspolymerized
product were used in the LALS structure determination program. The
macromonomer was crosspolymerized using 60 Mrad of cobalt-60 gamma
radiation.
        The diacetylene polymerization takes place along the c axis as
it did in poly(1,11-dodecadiyne). The nearest neighbor distance is
about 5 Å. After reaction, the polydiacetylene backbone (acetylenic
form) has the well known repeat of 4.9 Å. Initially, it appeared
that the reaction could also take place along the diagonal. However,
the angular separation between the diacetylene rods of the
macromonomer chain at the center and in the corner of the unit cell
is too large. A large rotation would be necessary for reaction to
take place. This is not the case along the c axis, so reaction along
the c direction is preferred. This mechanism is consistent with the
principle of least motion (10,19).

Monitoring of Crosspolymerization in Poly(1,8-nonadiyne)

Perhaps the most basic characterization parameter for a diacetylene
material is the extent of conversion of the diacetylene reaction.
The degree of conversion will have a great effect on all physical
properties of the material. For most diacetylenes, conversion can be
determined by extracting the residual monomer from a partially
reacted sample. The weight of extracted monomer can be compared to
the weight of diacetylene polymer to determine a conversion value.
The method works best if the monomer is very soluable in the
extracting solvent, and the polymer is totally insoluble.
        For the macromonomer systems under discussion here, the
extraction method can not be used for a number of reasons. The most
important reason is that different parts of a single macromonomer
chain could possibly be in a reacted region and an unreacted region
at the same time. Since this chain would be rendered insoluble by
inclusion in a reacted region, it would remain with the insoluble
portion of the sample. This would cause a gross overestimation of
the degree of conversion. Another complication is the fact that the
macromonomers contain both crystalline and amorphous regions, unlike

typical diacetylenes. Because of this complication, extraction data would have to be corrected for the degree of crystallinity. The large errors inherent in the determination of the degree of crystallinity, along with the uncertainty in the extraction process itself (5) would rule out the possibility of quantitative results.

From the above discussion, it is clear that quantitative conversion data for the macromonomer systems will be difficult (if not impossible) to obtain. However, there are a number of methods that offer qualitative or semi-quantitative information on the diacetylene reaction. As mentioned earlier, magic-angle C-13 NMR has been used to study the crosspolymerizatin of poly(1,11-doecadiyne) (14). Besides showing that the crosspolymerized material exists in the acetylenic form, results from this study showed that the diacetylene reaction may be qualitatively folowed using solid-state NMR.

We have recently been studying the conversion behavior of macromonomer systems using differential scanning calorimetry (DSC) and optical absorption spectroscopy. The preliminary findings from these studies are described below.

Differential Scanning Calorimetry. As mentioned earlier, crosspolymerized P18N has a two-dimensional sheet-like structure which is both insoluble and infusible. Therefore, when a partially reacted sample is scanned on the DSC, the melting which is observed can be directly related to the amount of non-reacted macromonomer remaining in the sample. As more macromonomer is crosspolymerized, a smaller melting endotherm will be seen in the DSC scan. Relative degrees of conversion can then be determined by comparing normalized endothermic areas for samples with various UV exposures. However, this technique would be expected to be inaccurate at both low and high conversions. At low conversions, before significant network structure has formed, the isolated polydiacetylene chains will probably disorder along with the macromonomer upon heating. This would lead to an underestimation of the degree of conversion. At high conversions, where nearly all the material is crosspolymerized, there will be small pockets of unreacted macromonomer surrounded by crosspolymerized material. The trapped macromonomer may not be able to disorder, and this would lead to an overestimation of the degree of reaction.

Before trying to monitor the extent of reaction using DSC, two questions had to be answered: 1) what is the thermal behavior of the unreacted macromonomer and 2) will the act of heating the macromonomer during the time needed to make a DSC scan cause measurable crosspolymerization?

Figure 5 shows several DSC scans (heating rate 20° /min.) of P18N. The first scan is of P18N film which was solution cast from methylene chloride. No T_g is present and the observed melting point is 363 K. After heating to 430 K, the sample was quick-cooled and run again at 20°/min. to give the scan labeled cycle 1. We see in this scan the appearance of a T_g at 274 K and an exotherm at about 336 K, as well as a diminished endotherm. The sample was again quick-cooled and rescanned a number of times, and on each cycle the exothermic and endothermic areas decreased compared to the previous scan.

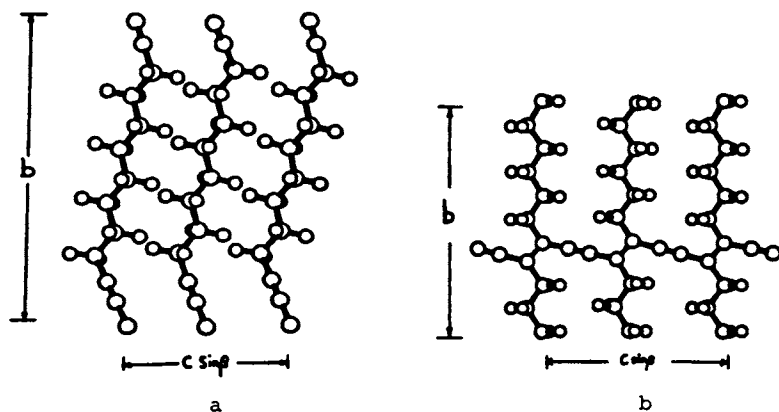Given the type of system we are dealing with, the above thermal

Figure 4. bc projection of (a) poly(1,11-dodecadiyne) and (b) crosspolymerized product. (Reproduced from reference 2. Copyright 1983 American Chemical Society.)
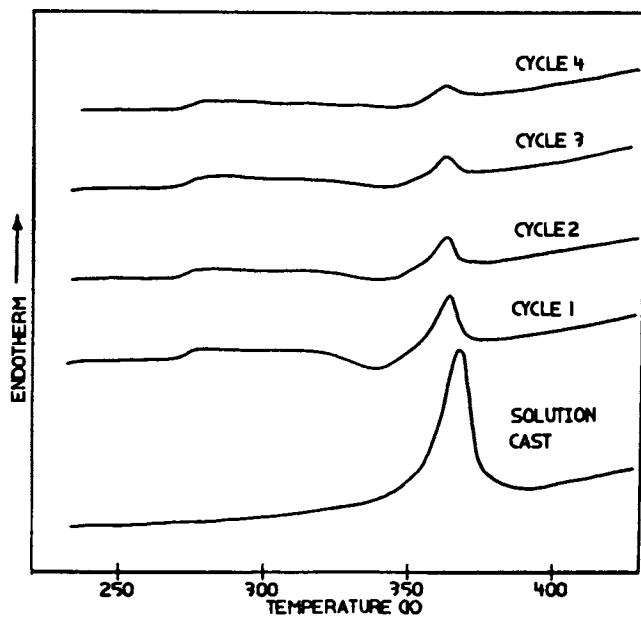

Figure 5. DSC scans of poly(1,8-nonadiyne) at 20°/min.

behavior suggests that the sample is possibly reacting during the heating scans and that the observed exotherm is caused by the solid state reaction. The decrease in exothermic and endothermic areas as the number of scans is increased is consistent with this. The only seeming inconsistency with this explanation would be the lack of an exotherm in the solution cast scan. However, even this could be rationalized if one assumes that the material requires an induction period before the thermal polymerization prodeeds (this is often observed in diacetylene materials (5,6)). Thus, it was important to determine whether this behavior was due to the diacetylene reaction, or just the crystallization behavior of the macromonomer.

To determine the cause of the observed thermal behavior, a solution cast sample was cycled 4 times and then quick-cooled to 336 K and held there for 40 minutes. If the exotherm is due to crystallization, the subsequent heating run should show a recovery of crystallinity (and endothermic area). If the exotherm is due to solid state reaction, the subsequent run should show an even more diminished endotherm. The heating scan performed after the annealing showed an exotherm which had virtually the same area as the original solution cast sample, and therefore, it was concluded that the exotherm is due to crystallization and not reaction (a detailed account of the melting behavior of P18N will be published elsewhere).

Besides showing the origin of the exotherm, the above mentioned study indicates the very slow rate of thermal crosspolymerization of P18N. After 24 hours of annealing at temperatures as low as 25° C, the sample starts to turn blue, which is evidence that some reaction has taken place. However, we have annealed P18N for up to 10 hours in the DSC at various temperatures below the melting point and have found no evidence for autocatalytic behavior. Similarly, we have annealed partially reacted P18N and found no evidence of autocatalytic behavior. It appears that the thermal reaction is so slow as to not to cause significant conversion during the DSC study of conversions.

Figure 6 shows the DSC scans (20° /min. heating rate) of partially polymerized P18N. These scans are normalized so that they can be directly compared. Samples were crosspolymerized using UV radiation (1600 uW/cm^2 at 254 nm) under UHP argon purge. Very thin samples were used so that the light could easily pass through the samples at all conversions. The endothermic area has the expected behavior; it decreases with increasing UV exposure. However, an unexpected event also occured; at about 371 K there is an exotherm. The size of this exotherm also decreases with UV dosage. It was initially thought that the exotherm could be due to crosspolymerization of macromonomer which was surrounded by crosspolymerized material. If small amounts of macromonomer were surrounded by a matrix of crosspolymerized material, it would be more difficult for this macromonomer to lose its order compared to an area which is all macromonomer. Thus, it is conceivable that reaction could occur above the bulk macromonomer melting point. Preliminary experiments show, however, that the exotherm is probably not due to reaction. When a crosspolymerized sample is rescanned in the DSC, the exotherm is not present at all. In fact, if a sample is placed at 120° C for 20 seconds before running a DSC scan, the subsequent heating scan shows no exotherm. It is unlikely that the
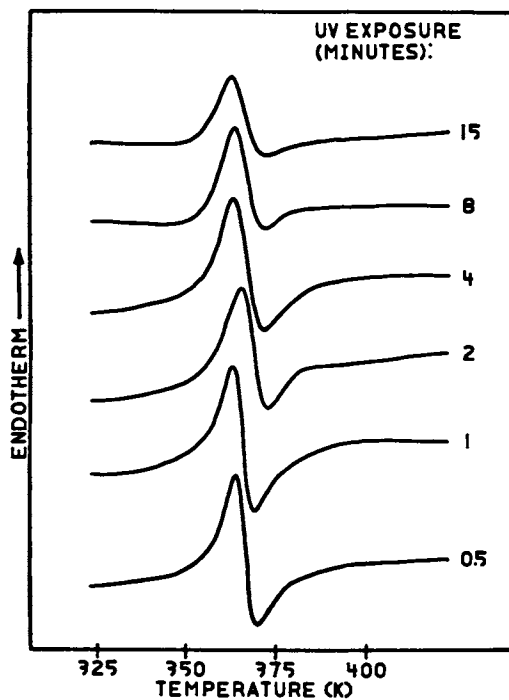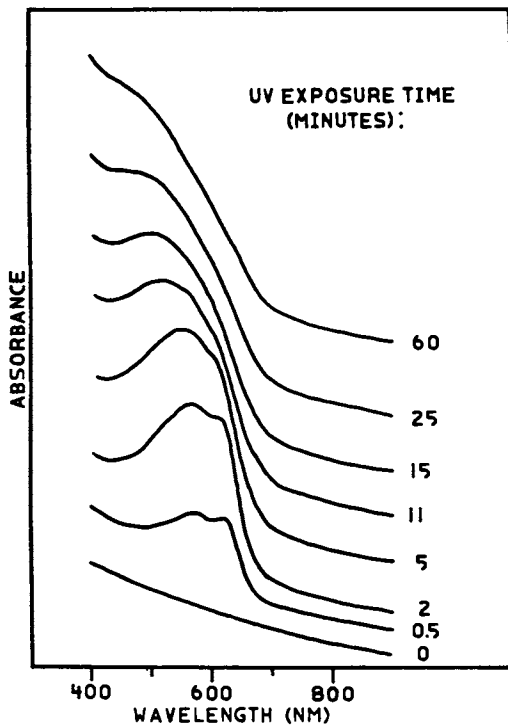
Figure 6. DSC scans (20°/min) of crosspolymerized poly(1,8-nonadiyne) after irradiating with UV light for the indicated time intervals.

diacetylene polymerization is so fast as to be completed in 20 seconds. More experiments will be needed to be sure about this conclusion, and, to discover the actual origin of the exotherm.

To complicate matters further, this exotherm is seen only on scans of samples smaller than about 3 mg. When larger samples are run, the exotherm at 371 K is not observed. This problem is currently under investigation.

Optical Spectroscopy. Figure 7 shows the optical spectra of solution cast (from slowly evaporated methylene chloride solution) poly(1,8-nonadiyne) films which have been exposed to UV light (1600 uW/cm^2 at 254 nm, under UHP argon purge) for various times. The macromonomer has no absorbance maxima in the region shown, whereas, samples with less than about 5 minutes exposure have two discernable maxima— at 575 nm and 630 nm. At low conversions (about 2 to 11 minutes UV exposure), the spectra resemble those from solution cast films of some conventional polydiacetylenes (16). At higher conversions, the spectra are quite broad and similar in shape to those observed for polydiacetylene solutions (7). As the samples are given longer UV exposure, the maximun at 575 nm grows with respect to the one at 630 nm, and the spectrum shows a blue shift. After about 1 hour of UV exposure, a very broad, nearly featureless envelope is obtained.

At low UV exposure (from the start of irradiation to about 1 minute) the samples are greyish-blue. As exposure time increases, the sample color progresses to blue, purple, and then red.

When interpreting spectra such as these, it is important to remember that we are not dealing with a nearly 100% crystalline material (as are most conventional diacetylene monomers), but rather, a relatively poorly ordered semi-crystalline polymeric material (approximately 10% crystalline as solution cast). This means that there will be amorphous regions, some crystalline regions which will have varying degrees of defect density, and some nearly perfectly ordered crystalline regions.

When a growing diacetylene chain encounters a defect, the growth may stop. So, in the case of chain growth in the vicinity of the defect, the chain length and, therefore, maximum conjugation length of the chain, will be dictated by how far the chain can grow before having growth interrupted. It is possible that chains growing in the less perfect crystalline regions contribute to the low wavelength absorption seen in figure 7. Also, the general broadness of the spectra is probably caused by the range of conjugation lengths that will be found in a poorly ordered system. This is probably why the shape of these spectra resemble those of polydiacetylene solutions and solution cast films. The main difference between the P18N spectra and the solution spectra (7) is that the solution spectra generally show maxima at shorter wavelengths than P18N films. This would be expected since the molecules in solution will have shorter conjugation lengths.

The increasing broadness of the spectra with increased exposure time could be due to a number of effects. One possible explanation is that as the polymerization proceeds, lattice strain accumulates, causing disruption of the crystalline regions (9). A unit cell contraction has been observed for this material during crosspolymerization (3). Also, it must be remembered that the

Figure 7. Optical spectra of crosspolymerized poly(1,8-nonadiyne) after irradiating with UV light for the indicated time intervals.

diacetylene units along the b direction are directly connected via
the aliphatic chain (figure 2). When one set of diacetylene groups
polymerizes, any movement of the aliphatic segment will acutely
affect the next set of diacetylene groups along the macromonomer
chains (this type of mechanism has been suggested for some
amphiphilic diacetylene monomers containing two diacetylene groups
per monomer (18)). This could introduce more defects, or place
strain on already existing diacetylene chains. Both of these effects
would tend to decrease the conjugation length of chains formed later
in the reaction, and therefore, cause the observed blue shift and
broadening.

Although this explanation appears reasonable, it seems to
contradict the electron diffraction results for P18N (22). The
diffraction analysis, performed on microscopic single crystals,
shows that the final crosspolymerized product is as ordered as the
initial macromonomer crystals. It is possible that this discrepancy
is related to the differences in the samples used in the two studies
(i.e. single crystals for the diffraction and solution cast films
for the optical spectroscopy). This inconsistency is currently being
investigated.

Another process which could be contributing to the spectral
observations at high conversions is UV degradation of the
diacetylene chains via chain scission. This effect has been
documented for polydiacetylene solutions (8), and it seems likely
that it could also happen in solid polydiacetylenes. Chain scission
would also have the effect of decreasing the conjugation length as
the irradiation time is increased.

It is difficult to know which, if any, of the above
explanations are correct solely on the basis of optical
spectroscopy. We are currently collecting Raman data to correlate
with our optical spetroscopic findings, so that the actual processes
occuring during the polymerization can be more accurately specified.

Chromic Behavior of Crosspolymerized Poly(1,8-nonadiyne)

Polydiacetylenes are typically highly colored materials, and,
consequently, there is considerable interest in their chromic
behavior. In the case of poly(1,8-nonadiyne), chromic transitions
can be induced with heat or solvent treatment. The films used were
cast from slowly evaporated methylene chloride solution. All UV
exposures were performed as described earlier.

Solvatochromism of XP18N. Even though the two-dimensional network of
crosspolymerized P18N (XP18N) is insoluble, solvents that dissolve
the macromonomer can induce a color change in the crosspolymerized
material. The color change is dependent upon the degree of
crosspolymerization and is somewhat reversible. For example, P18N
which has been exposed to 30 seconds of UV irradiation is grey-blue
in color. Upon exposure to methylene chloride, the sample
immediately turns yellow and remains yellow after drying. A sample
which has been given a 1 minute UV dose is blue, and after solvent
treatment it also turns yellow. However, unlike the 30 second
sample, the 1 minute sample takes on a slight purple cast after
drying. As UV exposure continues, the original sample goes from blue
to purple. When soaked in methylene chloride, the purple samples

will still turn yellow, but it is a darker color of yellow than seen in the samples with less UV exposure, and some of the original purple color returns upon drying.

This behavior continues until about 5 - 6 minutes of UV exposure, at which point the sample turns crimson upon solvent treatment. The longer the samples are exposed to UV light, the longer they need to be immersed in solvent to cause any color change (for example, a sample which was exposed to UV light for 14 minutes had to be exposed to solvent overnight to achieve even a minimal color change).

Solvent treated samples were examined using optical spectroscopy. The samples were prepared by exposing the P18N films to UV light (under argon purge) and then immersing the films in methylene chloride for 5 minutes. The films were then dried prior to running the spectra.

Solvent treated samples with 30 seconds of UV exposure showed absorptions which were broadened and blue shifted compared to a similar sample without solvent treatment (figure 8). Solvatochromic samples with longer UV exposure times show less blue shift and less broadening as compared to the untreated samples; this is consistent with the visual observations. These spectra also show that as conversion is increased, more of the 630 nm band is retained in the spectrum of the solvent treated samples. This behavior is most notable in the 3 minute spectrum, where both bands are still somewhat distinct.

Thermochromism of XP18N. Upon exposure to temperatures above approximately 92°C, crosspolymerized P18N will change from blue (or purple, depending upon degree of conversion) to yellow. The thermochromic behavior is dependent upon UV dosage, but not as much as is the solvatochromic behavior. Samples with low UV exposure (i.e. up to about 10 minutes of exposure) turn yellow upon exposure to temperatures above 92°C. At UV dosages between about 10 - 20 minutes the samples (which are purple before heating) turn yellow when exposed to heat, but return to a reddish-yellow color upon cooling to room temperature. At higher conversions, the samples turn crimson color upon exposure to heat, and revert to purple after about a minute at room temperature.

These heat treated samples have also been examined using optical spectroscopy. After exposing the samples to UV light for various times, they were placed in an oven at 115°C for 4 minutes under vacuum. The films were then taken from the oven and allowed to cool to room temperature before recording the spectra.

The spectra of the thermochromic samples (figure 9) show the same type of behavior as the spectra of the solvatochromic samples. However, there is more of a blue shift for the thermochromic samples than for the solvent treated ones with equal UV exposure.

Looking back at the previously mentioned DSC data, it seems possible that the high temperature exotherm (at 100°C) is related to the thermochromic transition. However, if the transition is an order-disorder type (i. e. disruption of the polydiacetylene backbone, leading to decreased conjugation length) it would be expected to be endothermic. Also, the size of the exotherm decreases with increasing exposure time. This suggests that the exotherm is related to the unreacted macromonomer. We are continuing investigation of this exothermic behavior.
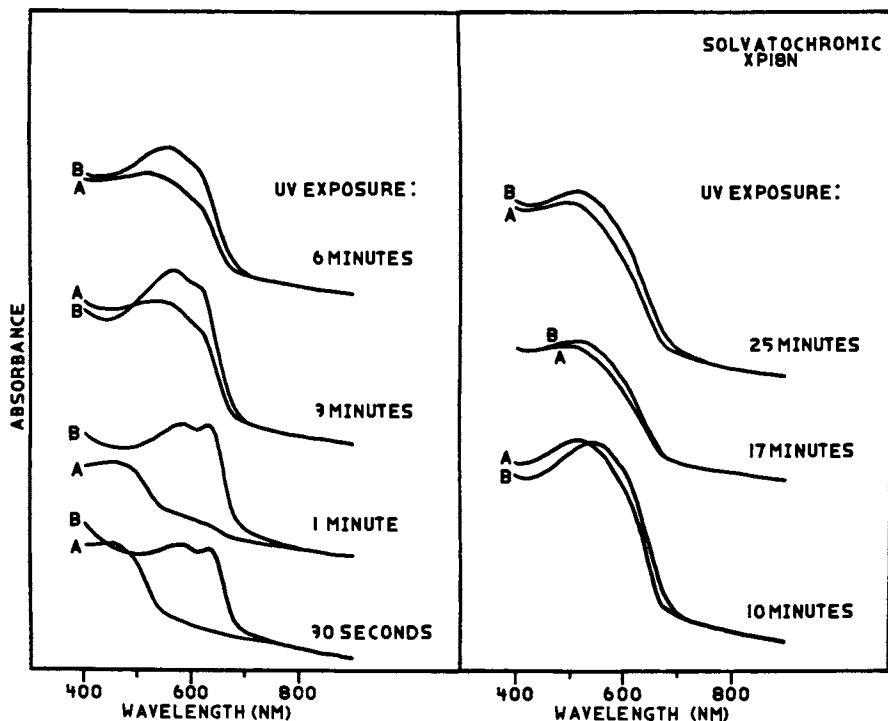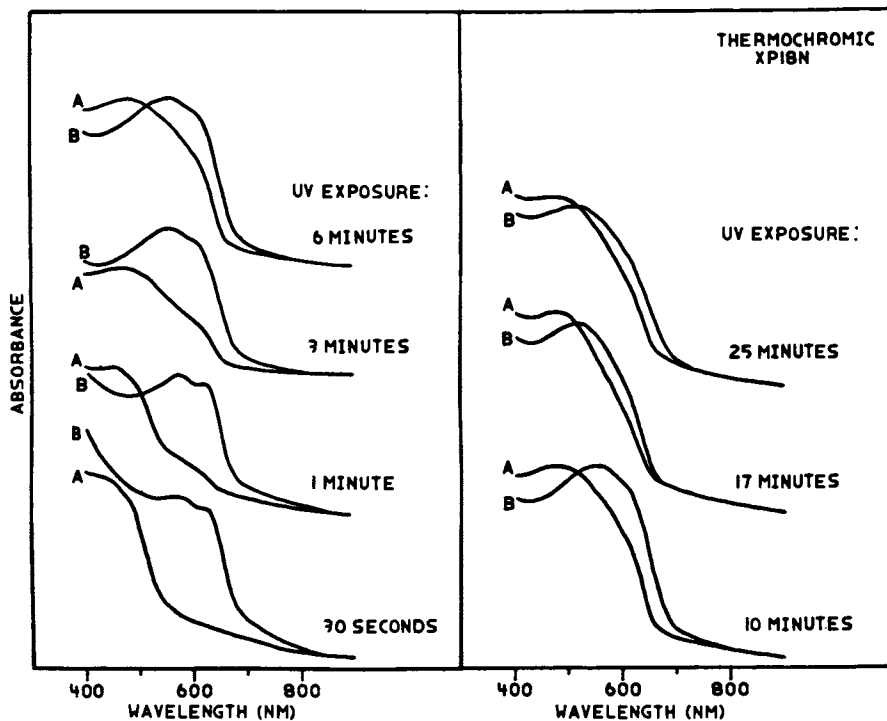
Figure 8. Optical spectra of crosspolymerized poly(1,8-nonadiyne). Spectra labeled A were run after the solvent treatment described in the text. Spectra labeled B were run before solvent treatment.

Discussion of Chromic Behavior. As discussed in the section on solvatochromic behavior, the degree of conversion to polydiacetylene has a pronounced effect on the solvatochromic behavior. At low conversion, the small areas of crosspolymerized material are interspersed in a matrix of macromonomer. Since diacetylene reactions are generally homogeneous (17), it is possible that there will be many regions where there are isolated polydiacetylene chains. When the film is exposed to solvent, the macromonomer will dissolve allowing solvation of these isolated polydiacetylene chains, thereby disrupting the conjugation. The unreacted portion of the macromonomer chain, in this instance, acts like the solubilizing side groups found in polymers such as poly3BCMU. As the films dry, the unreacted macromonomer will either recrystallize or become part of the amorphous regions. In either case, it is unlikely that the original structure will be exactly reformed, so the conformation of the polydiacetylene chain will remain disrupted. This effect will cause the low conversion samples to have virtually no reversibility in the chromic transition. The disruption in conformation (and hence, conjugation) is responsible for the observed blue shift in the dried films.

As more macromonomer is crosspolymerized, any one crosspolymerized region is more likely to be surrounded by reacted material than by macromonomer. In other words, the distance between polydiacetylene chains along the macromonomer chain will decrease. It will be harder for the solvent to diffuse throughout the crosspolymerized material and solvate the network. As network formation continues, the structure will be more constrained as to the possible conformations that will be possible; the structure will be essentially locked-in. Also, if the solvated network is surrounded by other crosspolymerized material, it will have less mobility than is the case at lower conversions, where much of the area surrounding the crosspolymerized material is macromonomer (which can be dissolved by the solvent). So, with increased conversion there is less mobility in the system, and, therefore, less potential for distortion in the crosspolymerized structure. This translates to less severe blue shifting in the optical spectra.

At the higher conversions, we have the case where the sample is composed of a matrix of crosspolymerized material with small pockets of macromonomer. This would further decrease the ability of the solvent to permeate the sample and make it more difficult for the polydiacetylene chain to distort since it will be locked into a network structure (distortions would likely be limited to small changes such as slight torsions and bond angle deformations). This would explain why it takes hours to see only a slight change of color for samples with higher conversion, and why the spectra of the treated and untreated samples with 25 minutes UV exposure are very similar.

The thermochromic behavior seems to be fundamentally similar to the solvatochromic behavior. The major difference between them is that the thermochromic changes are greater at higher conversions than are the solvatochromic changes at similar conversions. Figure 10 illustrates this point. The two curves show how the peak shift between treated and untreated samples compares for thermochromism

Figure 9.   Optical   spectra   of   crosspolymerized poly(1,8-nonadiyne). Spectra labeled A were run after the thermal treatment described in the text. Spectra labeled B were run before thermal treatment.
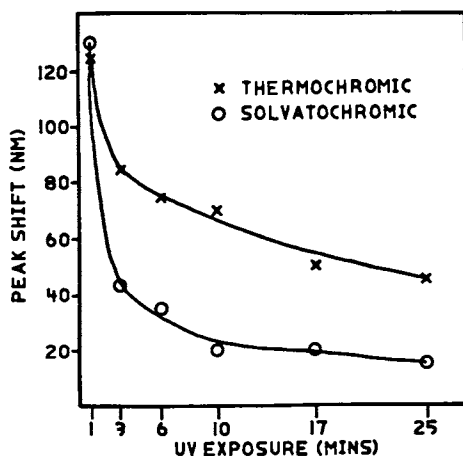
Figure 10. Change in peak maximum position after chromic treatment, as a function of UV exposure.

and solvatochromism. A large difference between the spectra of solvatochromic and thermochromic material is seen for samples with 3 or more minutes of radiation. This is probably due to the fact that solvent can not easily permeate the crosspolymerized regions at these conversions, whereas no such effect would exist for heat.

It was mentioned earlier that unreacted macromonomer appears to play a part in the solvatochromic behavior. Since the thermochromic transition occurs approximately at the melting point of the macromonomer, it is likely that the macromonomer plays a part in the thermochromic response. This is further supported by the fact that the chromic behavior is less drastic at higher conversions. We are currently trying to precisely define the function of residual macromonomer in the thermochromic transition, but an explanation similar to the one given for the solvatochromic response suggests itself. Small, isolated crosspolymerized regions have more conformational mobility when surrounded by molten macromonomer than when they are surrounded by the more rigid crosspolymerized material. At higher conversions,less distortion of the diacetylene chain would be allowed and, therefore, a change to red instead of yellow would occur.

The possible explanations offered above for the chromic transitions deal only with changes in the polydiacetylene backbone. An alternative explanation would be that a crystallographic phase transition takes place. This phase change would affect the environment of the polydiacetylene chain and, therefore, change the electronic energy levels of the backbone, which could lead to chromic changes. Electron diffraction studies are currently being performed to determine whether a unit cell transformation occurs upon heat or solvent treatment. If a unit cell transformation does not take place, and the chromic changes are due only to distortions in the diacetylene backbone, an increase in disorder would be observed in the diffraction pattern. Considering our preliminary evidence from optical spectroscopy and the behavior of diacetylene systems documented in the literature, it seems more likely that the observed chromic behavior is due to disordering of the diacetylene backbone, rather than to a crystallographic phase transition.

Because the optical spectroscopic results alone are not conclusive, the above explanation of the chromic behavior of XP18N must be regarded as speculative. However, these results do give an indication of the molecular mechanism for the behavior, and certainly give a foundation on which to base further experiments.

Acknowledgments

Literature Cited

1. Lando, J. B.; Thakur, M. Synth. Met. 1984, 9, 317.
2. Thakur, M.; Lando, J. B. Macromolecules 1983, 16, 143.
3. Thakur, M. Ph. D. Thesis, Case Western Reserve University, Cleveland, Ohio, 1983.

4. Butera, R. J.; Lando, J. B. to be published.
5. Chance, R. R.; Patel, G. N. J. Polym. Sci.: Polym. Phys. Ed. 1978, 16, 859.
6. Barrall, E. M.; Clarke, T. C.; Gregges, A. R. J. Polym. Sci.: Polym. Phys. Ed. 1978, 16, 1355.
7. Bloor, D.; Batchelder, D. N.; Ando, D. J. J. Polym. Sci.: Polym. Phys. Ed. 1981, 19, 321.
8. Wenz, G.; Wegner, G. Makromol. Chem. Rapid. Commun. 1982, 13, 231.
9. Bloor, D.; Hubble, C. L. Chem. Phys. Lett. 1978, 56, 89.
10. Baughman, R. H. J. Polym. Sci.: Polym. Phys. Ed. 1974, 12, 1511.
11. Grasso, R. P. Ph.D. Thesis, Case Western Reserve University, Cleveland, Ohio.
12. Arnott, S.; Campbell Smith, P. J. Acta. Cryst. 1978, A34, 3.
13. Thakur, M.; Lando, J. B. Is. J. Chem. 1985, 25, 293.
14. Havens, J. R.; Thakur, M.; Lando, J. B.;Koenig, J. L. Macromolecules 1984, 17, 1071.
15. White, D. M. Polym. Prepr., Amer. Chem. Soc., Div. Polym. Chem. 1971, 12(1), 155.
16. Chance, R. R.; Patel, G. N.; Witt, J. D. J. Chem. Phys. 1979, 71, 206.
17. Enkelmann, V. Advances in Polymer Science 1984, 63, 91.
18. Tieke, B.; Lieser, G. Macromolecules 1985, 18, 327.
19. Hine, J. J. Org. Chem. 1966, 31, 1236.
20. Thakur, M. K.; Lando, J. B. accepted for publication in Polymer.
21. Grasso, R. P.; Thakur, M. K.; Lando, J. B. Mol. Cryst. Liq. Cryst. 1985, 118, 337.
22. Thakur, M.; Lando, J. B. J. Appl. Phys. 1983, 54, 5554.
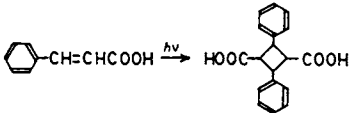
Chapter 4

Four-Center-Type Photopolymerization of Unsymmetrically Substituted Diolefin Crystals
Characteristic Features

M. Hasegawa, K. Saigo, S. Kato, and H. Harashina

Department of Synthetic Chemistry, Faculty of Engineering, The University of Tokyo, Hongo, Bunkyo-ku, Tokyo 113, Japan

The first example of crystalline state [2+2] photocycloaddition polymerization was the reaction of 2,5-distyrylpyradine (DSP) crystal, discovered in 1967. This polymerization proceeds under the strict control of the reacting crystal lattice throughout the course of reaction; it was named the "four-center type photopolymerization" (2). The polymerization of DSP crystal was the first example of photopolymerization by a step-by-step mechanism as well as of topochemical polymerization.

The reactivity of the DSP crystal was thoroughly interpreted in terms of the topochemical concept proposed by Schmidt, in which potentially reactive double bonds are oriented parallel to each other and separated by approximately 3.5-4.2 Å. The reaction proceeds with a minimum of atomic and molecular motion (3). The reactive double bonds in most of the topochemically polymeric crystals thus far found are related to the center of symmetry (centrosymmetric α-type crystal) and dimerize to give highly crystalline polymers containing cyclobutanes with a 1,3-trans configuration in the main chain.

A preparative study of four-center type photopolymerization has established the empirical rule that the crystalline state [2+2] photodimerization of olefins can be widely extended to the crystalline state photopolymerization of diolefins with a rigid linear structure containing conjugated double bonds separated by the 1,4-position of an aromatic ring, such as stilbazol to DSP, or cinnamic derivatives to 1,4-phenylenediacrylic (p-PDA) derivatives (4). During the past eighteen years, a great number of photopolymeric diolefin crystals have been found by the use of this empirical rule (see Table I).

Furthermore, the crystallographic correlation between the starting substance and the final product has been demonstrated in a chemical reaction on DSP - poly-DSP for the first time (5); monomer and polymer crystals are closely related on the level of unit cell dimensions, with a retention of the crystal symmetry during the reaction.

Crystallographic data of DSP* and Poly-DSP

	Space group	a, Å	b, Å	c, Å	Z	Dx	C-C distance
DSP	Pbca	20.638	9.599	7.655	4	1.244	3.939 Å
Poly-DSP	Pbca	18.36	10.88	7.52	4	1.257	

* After our first reports on the crystal structure
correlations between the monomer and the polymer
crystals (5 and 6), a different crystallographic
result was reported on the poly-DSP crystal (7).
We reconfirmed, however, that our first structural
analysis was correct, reporting this in 1979 (8).

The topochemical photopolymerizations of these diolefin crystals
have been reviewed in several reports (9,10).
    Recent studies of the topochemical [2+2] photodimerization have
shown several examples which deviate from the accepted concept of the
topochemical reactions enunciated by Schmidt. This anomalous behavior
has been reviewed in a recent publication (11).
    In the present article the present authors will describe their
results on the four-center type photopolymerization of
unsymmetrically substituted diolefin crystals with the general
formula represented by (I) - (V).
    For the photopolymerization of unsymmetric diolefin crystals
with an α-type crystal structure, we can expect two types of
repeating structures, hetero- and homo-adducts, as shown
in Scheme I.
    Lahav et al. applied the empirical rule of a topochemically
photopolymeric structure (4) to the unsymmetric diolefin crystals,
thus succeeding in obtaining optically active dimers and oligomers
through the crystallization of an achiral monomer into a chiral
crystal, followed by the four-center type photopolymerization (12).
    All the crystals in Groups (I) - (V) were newly prepared on the
basis of the empirical rule for the photopolymeric chemical
structures; with a few exceptions, these crystals showed high
photoreactivities.

Study of the Four-Center Type Photopolymerization of Unsymmetric Diolefin Crystals
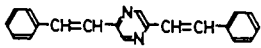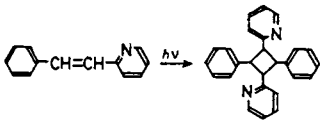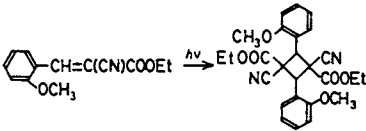
Diolefin crystals (I) were prepared through half-ester intermediates
and, for the (II) - (V) crystals, by two-step aldol condensations.
Further details of the preparation of these monomers have been
described in recent papers (13).
    To check the photoreactivity of these crystals, fine crystals
were dispersed in water and irradiated by a 100 W or 500 W high
pressure mercury lamp for periods ranging from a few to 24 h.
    Most of the crystals showed a high reactivity, with a great
variety of behavior depending on the crystal structure.
    The photochemical behavior is illustrated for several crystals
in Groups (I) - (V) in Tables II, III, and IV.

TABLE I.   Topochemically Photopolymeric Diolefins and Topo-
           chemical [2+2] Photodimerizations (Model Reactions)

Topochemically Photopolymeric Diolefins	Topochemical [2+2] Photodimerizations (Model Reactions)
DSP series	stilbazol
p-PDA series	cinnamic acid
p-CPA series	α-cyanocinnamic derivative
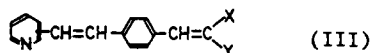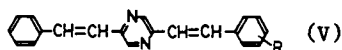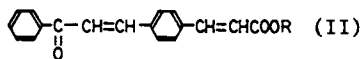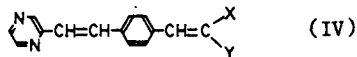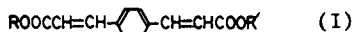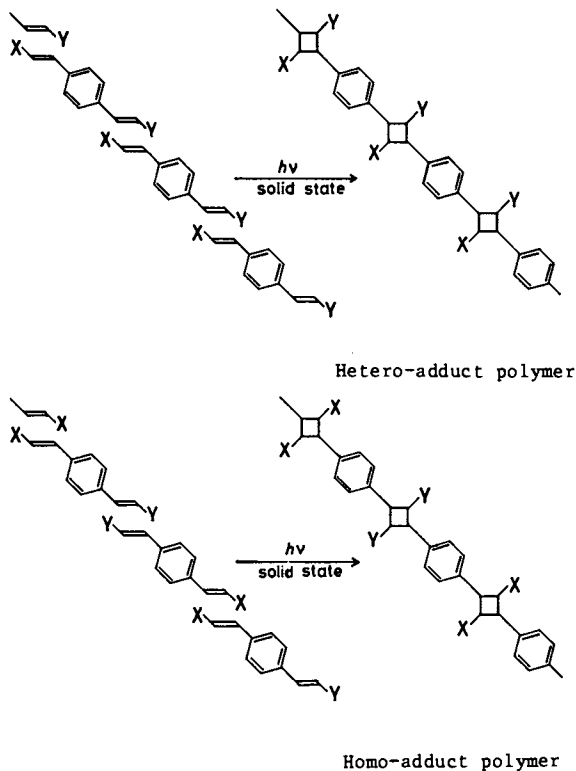
 (I)

 (II)

 (III)

 (IV)

 (V)

Hetero-adduct polymer

Homo-adduct polymer

Scheme I.

TABLE II. Photochemical Behavior of Unsymmetric Diolefin
Crystals in Groups (I) and (II)

	R	R'	Recrystd. solvent	Mp/°C	Reactivity[*1]
Diolefin (I)	Me	H	MeOH	250-252	Very high
	Me	Et	MeOH	91-92	Very high[*2]
	Me	Ph	MeOH	135-136	Very high
	Et	H	Benzene	215-216	Very high
Diolefin (II)	H		MeOH	260-264	None
	Me		MeOH	133-134	None
	Et		EtOH	111-112	Medium[*3]
			Cyclohexane	114-116	Medium
	2-Pr		2-PrOH	137-138	Low
			EtOH	134-135	Medium
	Ph		EtOH	153-154	High

*1 The reactivity was estimated roughly without any quantitative
measurement.
*2 The η inh of the acetone-isoluble portion of the photoproduct
is 3.1 (0.24 g/dL in m-cresol, 30 °C).
*3 The molecular weight of the final polymer is > 24,000.

TABLE III. Photochemical Behavior of Unsymmetric Diolefin
Crystals in Group(III)

Diolefin (III)			Recrystd. solvent	Mp/°C	Irradiation[*] conditions	Product (ηinh)
	X	Y				
2-pyridyl	CN	COOMe	MeOH	179-181	500W/2h	Dimer
4-pyridyl	H	COOMe	MeOH	148-150	500W/13h	Polymer (0.47)
4-pyridyl	CN	COOMe	MeOH	195-196.5	500W/26h	Polymer (0.13)
4-pyridyl	CN	COOEt	EtOH	172-173.5	500W/20h	Polymer (0.36)
4-pyridyl	CN	COOnPr	nPrOH	146-150	Sunlight/5h	Dimer

* By a 500 W high pressure Hg lamp or sunlight at room temperature.

TABLE IV. Photochemical Behavior of Unsymmetric Diolefin
Crystals in Groups (IV) and (V)

		Recrystd. solvent	Mp/°C	Irradiation conditions	Product (ηinh)
Diolefin (IV)					
X	Y				
CN	COOMe	MeOH	192.5-193.5	100W/24hr	Polymer (0.24)
CN	COOEt	EtOH	179.0-180.0	100W/24hr	Oligomer (0.03)
H	COOMe	MeOH	170.0-171.0	500W/5hr	Polymer (3.93)
H	COOEt	EtOH	156.5-157.0	500W/5hr	Polymer (8.19)
H	COPh	H_2O/CH_3CN	159.0	500W/24hr	Dimer
Diolefin (V)					
R					
COOMe		Benzene	241.0-243.0	Sunlight	Polymer (1.27)
Cl		By column		Sunlight	Polymer

In these photoreactive crystals, the crystals of, for example, IV (X : H, Y : COOEt) and V (R : COOMe) are extremely photoreactive; they are converted to the high molecular weight polymers in quantitative yields even under sunlight for a few hours. The crystal of III (2-pyridyl, X : CN, Y : COOMe) is also highly reactive, but, on photoirradiation, it gives a photostable dimer quantitatively. At an early stage of the photopolymerization, an unusually large amount of the photoreactive intermediate dimer is accumulated in the reacting crystal phase, for example, in the reaction of the crystals of I (R : Me and R' : Et) or III (4-pyridyl, X : CN and Y : COOnPr).

The structures of the photoproducts were confirmed by various spectroscopic measurements, with reference to the cyclobutane polymers in the literature (14,15).

Although the final products are amorphous in some cases, it is obvious that the photoreactions of the crystals (I) - (V) proceed under topochemical control, for only a single configuration of the cyclobutane is formed in all cases.

Examples of the Topochemical [2+2] Photoreaction of Unsymmetric Diolefin Crystals

Several examples of the photochemical behavior of unsymmetric diolefin crystals will be described in detail and discussed, in correlation with their crystallographic results.

Photopolymerization of the Ethyl Methyl 1,4-Phenylenediacrylate I (R : Me, R' : Et) Crystal (13a).

Finely powdered crystals of I (R : Me, R' : Et) were dispersed in 500 ml of H_2O containing a few drops of a surfactant (NIKKOL TL-10FF) and then, under rigorous agitation, irradiated for 27 h by means of a light source set in the center of the flask (500 mL) under a nitrogen atmosphere at room temperature (15-25 °C). A 500W high pressure mercury lamp within an uranium glass filter was used as the light source. The high polymers (ηinh 3.1, 0.24 g/dL in m-cresol, 30 °C) were obtained as the acetone insoluble

portion (yield, 50%), and a transparent and flexible film could be cast from a trifluoroacetic acid solution of the same sample. From the study of the NMR spectral change in the course of photopolymerization, an exclusive photocyclodimerization between two olefins at the methyl cinnamate unit was confirmed, whereas none of the other dimers was detected throughout the course of photopolymerization. In addition, a large amount of the dimer was accumulated at an early stage of the reaction and easily isolated (yield, 30%).

The α-type cyclobutane structure of the dimer was determined by NMR and Mass spectroscopies. The NMR spectra of the monomer, dimer, and polymer are shown in Figure 1. The dimer, recrystallized from methanol, shows essentially the same X-ray diffraction pattern as that of the dimer as-prepared, and is also photoreactive to give the polymer. The resulting polymer is highly crystalline. As a result, it is concluded that the polymerization of the I crystal (R : Me, R' : Et) proceeds through one type of intermediate dimer to give the homo-adduct polymer.

Fairly high yields of the oligomers were reported in the early literatures (16,17) from DSP and from diethyl 1,4-phenylenediacrylate crystals on photoirradiation, by controlling the wavelength and/or the reaction temperatures. However, it is of great significance in the present study that only one type of dimer is accumulated in a high yield during the reaction, without any specified photoirradiation conditions. Such a reactivity difference can originate only in different topochemical environments at the two groups in the crystal, since there must be little difference in the intrinsic reactivities of these two olefins under nontopochemical conditions. Such anomalous behavior can be thoroughly explained by the crystallographic analysis of I (R : Me, R' : Et) (Figure 2) (18).

In the crystals, two double bonds of the same ester group are intermolecularly aligned parallel to each other, indicating the formation of a homo-adduct polymer through a topochemical process. The distances between the two pairs of facing double bonds are 3.891(6) Å for methyl cinnamates (A in Figure 2) and 4.917(6) Å for ethyl cinnamates (B in Figure 2); only the former is within the reactive distance postulated by Schmidt (3). Therefore, the preferred photocyclodimerezation of methyl cinnamate units can be quite reasonably interpreted in terms of the crystallographic results. The intermolecular distance of ethyl cinnamate units in the dimer has not yet been determined, but it may be assumed to be smaller than the distance in the monomer (4.917(6) Å). It should be noticed, however, that 4-formylcinnamic acid crystal where the center-center distance is 4.825 Å, photodimerizes quantitatively (11,19).

The intermolecular distance between ethyl and methyl cinnamate units is approximately 6 Å (C in Figure 2); it can, therefore, doubtlessly be excluded for the topochemical cycloaddition.

By means of GPC analysis, a small but definite amount of the trimer was detected as an intermediate of the photopolymerization. This result indicates the occurrence of a small portion of an elementary process between the monomer and the dimer.

Photopolymerization of the Methyl 4-[2-(4-pyridyl)ethenyl]cinnamate III (4-pyridyl, X : H, Y : COOMe) Crystal (13b). The monomer
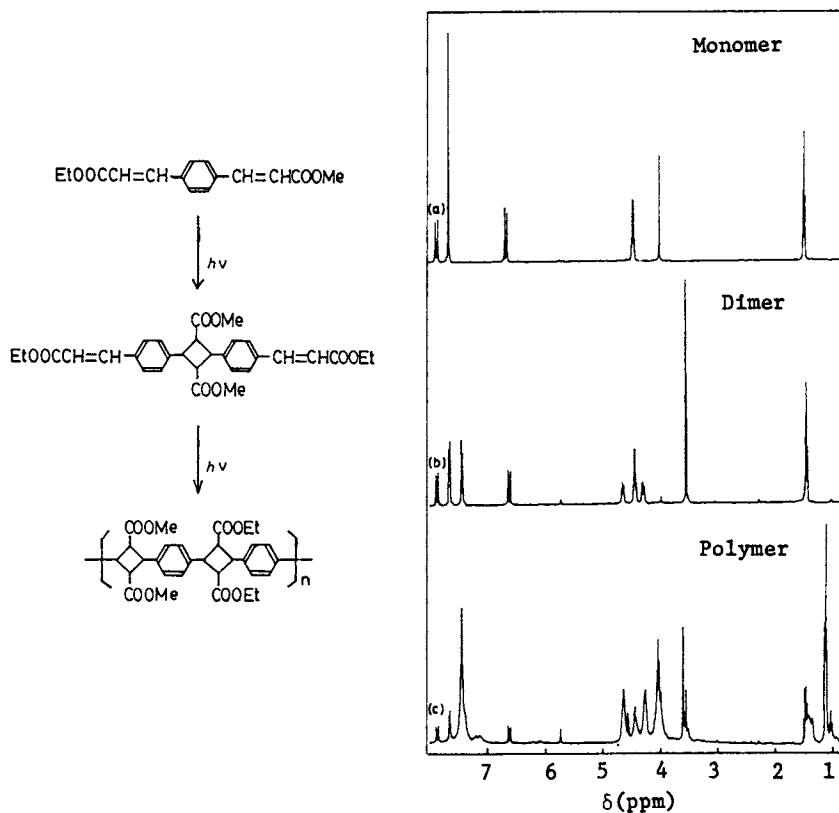
Figure 1. 400 MHz ^{1}H-NMR spectra (CF_3COOD) of (a) I (R : Me, R' : Et), (b) its dimer, and (c) its polymer.

crystal III (4-pyridyl, X = H, Y = COOMe) was gradually transformed
into an nearly amorphous polymer. The cyclobutane structure of the
polymer was confirmed by spectroscopic analysis analogously to the
assignment before. Although the final product is amorphous, only a
single configuration of the cyclobutane is formed, indicating the
topochemical control throughout the course of the
photopolymerization. The polymer (ηinh 0.47, at 0.30 g/dL in m-
cresol, 30 °C) was soluble in N,N-dimethylformamide,
dimethylsulfoxide, and such strong acids as concentrated HCl.
    The crystal structure viewed along the a axis is shown in Figure
3 (20).
    From the crystal structure it is concluded that, on irradiation,
two different double bonds in the crystal react to give a linear
hetero-adduct racemic polymer, in which a cyclobutane ring is in the
1,3-trans configuration (see Scheme II).
    The intermolecular reactive bonds, separated by 4.023(9) Å for
C(7)···C(14) and by 4.097(10) Å for C(8)···C(13), are nonparallel,
while these distances are within those of normal reactive bonds. The
topochemical [2+2] photodimerization of the double bonds oriented
nonparallel has been reported for several olefinic crystals in recent
papers (11,13b,21a-d).

Photodimerization of the Methyl α-cyano-4-[2-(2-pyridyl)ethenyl]-
cinnamate III (2-pyridyl, X : CN, Y : COOMe) Crystal (13c). In the
course of the photoreaction of the crystal of III (2-pyridyl, X : CN,
Y : COOMe), the UV absorption band at 365 nm decreased and a new
absorption peak appeared at 313 nm. In addition, clear isosbestic
points were seen in the spectra at 258 and 329 nm. The photoreaction
was fast, and, finally, the TLC of the photoproduct showed a single
spot.   These spectral data and the results of TLC analysis indicate
the progress of a single reaction on photoirradiation of the crystal.
    After irradiation for 2 h, the product was isolated and purified
by column chromatography on aluminium oxide, followed by
recrystallization from benzene/hexane (yield, 90 %). The IR spectrum
of the photoproduct showed a decrease in the carbon-carbon double
bond (1600 and 980 cm^{-1}) and a shift of the carbonyl and cyano groups
to higher wave numbers (from 1720 to 1740, and from 2210 to 2220
cm^{-1}, respectively), indicating the formation of a saturated ester.
These spectral results coincide with the exclusive progression of
[2+2] cycloaddition between a pair of double bonds. The mass
spectrum shows peaks at m/e 188 and 392 due to an asymmetric cleavage
of the cyclobutane ring, in addition to the peaks originating in the
symmetric cleavage at m/e 290 (M$^+$/2) and 580 (M$^+$). All these
spectral results (22) correspond to the structure of the hetero head-
to-head dimer, namely, methyl 1-cyano-3-[4-[2-(2-cyano-2-methoxy-
carbonylethenyl)phenyl]-2-(2-pyridyl)-4-[4-[2-(2-pyridyl)ethenyl]-
phenyl]cyclobutanecarboxylate (see Scheme III).
    The quantitative formation of a single structural dimer
indicates that the photoreaction is strictly controlled by the
crystal lattice although the final photoproduct is amorphous.
    The crystal structure of the monomer (23) viewed along the c
axis is shown in Figure 4.
    The reactive double bonds, separated by 3.886(7) Å for
C(7)···C(15') and by 3.807(7) Å for C(8)···C(16'), are non-parallel,
while these distances are within the range of those of normal
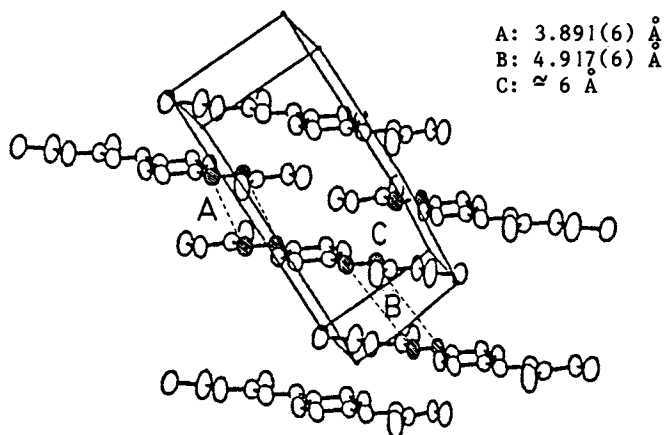
A: 3.891(6) Å
B: 4.917(6) Å
C: ≃ 6 Å

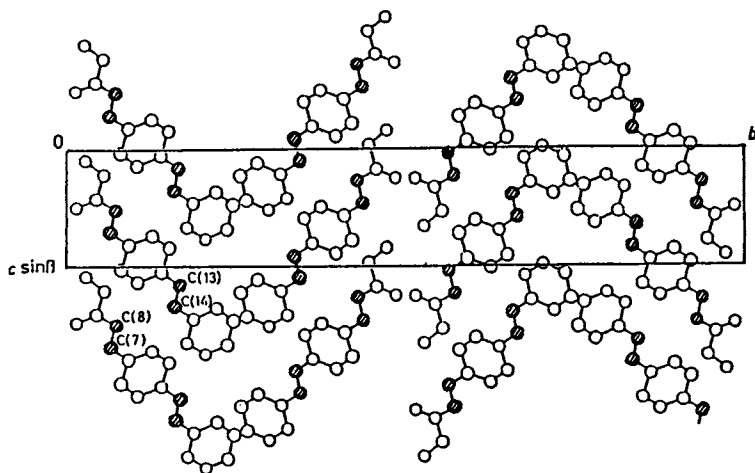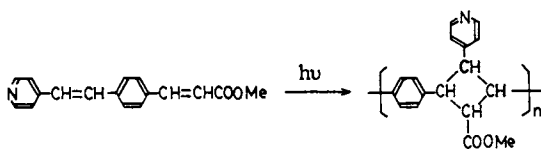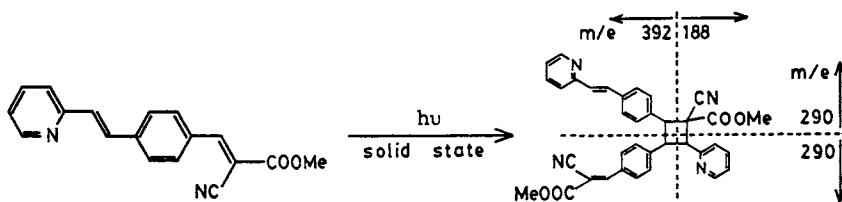Figure 2. Crystal structure of I (R : Me, R' : Et).

Figure 3. Crystal structure of III (4-pyridyl, X : H, Y : COOMe)
viewed along the a axis. The atoms comprising the ethylenic
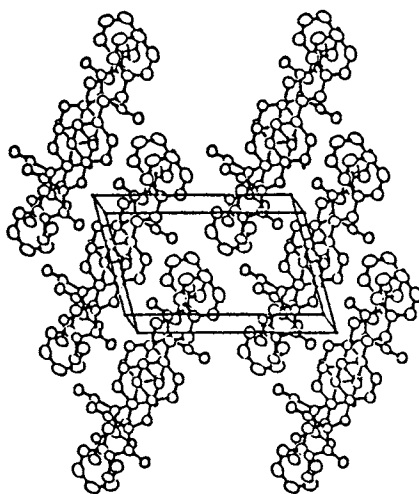groups are hatched for clarity.

Scheme II.

Scheme III.

**Figure 4. Crystal structure of III (2-pyridyl, X : CN, Y : COOMe)
viewed along the c axis.**

reactive bonds. Other distances of the intermolecular olefin double bonds are 4.926(7) Å for C(8)···C(16"), 4.906(7) Å for C(7)···C(15"), and 4.719(6) Å for C(7) ···C(8"). These distances are too long for the limits of ordinary photoreactive double bonds (3). The other short distances between carbon atoms, 4.141(6) Å for C(7)···C(7") and 4.281(6) Å for C(8)···C(15"), are also out of the question because these carbon atoms are not in the disposition of the reactive olefinic double bonds on neighboring molecules.

   Although the dimer has asymmetric carbon atoms, the photoproduct from a large single crystal of the monomer does not show any detectable values of optical rotation and circular dichroism.   Both enantiomers are formed equivalently from the monomer crystal, for the center of symmetry exists between two molecules arranged in the β-form and the two pairs of double bonds should be equivalent in reactivity, as is illustrated in Figure 5.

   Only a few examples are related to the photoreactions of unsymmetrically substituted diolefins arranged in the β-form (12,24a,b).

   The crystal structure of the monomer sufficiently supports the structure of the photodimer expected from the spectral studies if the topochemical process is assumed in this photoreaction. The highly photostable behavior of the dimer is quite reasonable because, after one pair of double bond reacts, then the residual pair will be rearranged far outside of the photoreactive arrangement in the crystal.

   In contrast to the methyl ester crystal, the ethyl ester crystal III (2-pyridyl, X : CN, Y : COOEt) is converted to an amorphous oligomer upon prolonged photoirradiation, although the corresponding dimer is accumulated at the intermediate stage.

<u>Photo-polymerization and -dimerization of the Alkyl α-cyano-4-[2-(4-pyridyl)ethenyl]cinnamate III (4-pyridyl, X : CN, Y : COOR, where R : Me, Et, and n-Pr) Crystals</u> (13b,25). On photoirradiation in the same manner as before, the crystal with a cyano group of III (4-pyridyl, X : CN, Y : COOEt) was found to be highly reactive in the crystalline state; in contrast with the crystal of III (4-pyridyl, X : H, Y : COOMe), the cyano ethyl ester crystal gives a linear homo-adduct polymer.   The polymer shows an inherent viscosity of 0.36 at 0.30g/dL in chloroform at 30 °C and is soluble in ordinary organic solvents and aqueous acidic solutions, e.g., aqueous HCl and H_2SO_4 solutions. At the early stage of the photoreaction, again only one type of dimer is isolated in a fairly high yield (54.2%). From the results of the IR, NMR, and mass spectroscopies, the dimer was confirmed to be the T-dimer, of which the cyano ester side olefins photodimerized, diethyl 1,3-dicyano-2,4-bis[4-[2-(4-pyridyl)ethenyl]-phenyl]-1,3-cyclobutanedicarboxylate (26). No trace of another dimer was detected at any of the reaction stages, as was the case with the I crystal (R : Me, R' : Et). In addition, no growing species with an odd-numbered degree of polymerization has been detected by means of GPC analysis throughout the course of the polymerization. The GPC curve of the photoproduct derived from the III crystal (4-pyridyl, X : CN, Y : COOEt) at an early stage is shown in Figure 6.

   From the GPC curve in Figure 6 it may be concluded that, in the crystal of III (4-pyridyl, X : CN, Y : COOEt), the monomer reacts only with the monomer, followed by the photodimerization between two
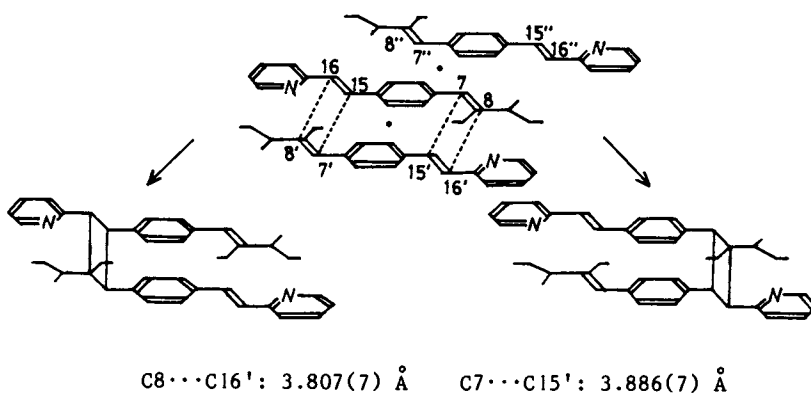
C8···C16': 3.807(7) Å   C7···C15': 3.886(7) Å

Figure 5. Schematic illustration of the formation of the racemic dimer from the crystal of III (2-pyridyl, X : CN, Y : COOMe).
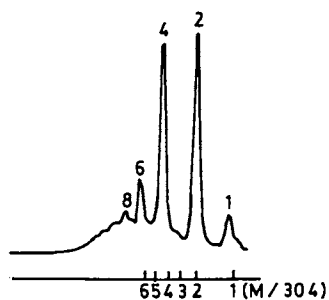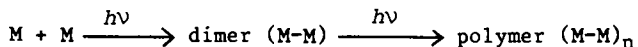

Figure 6. GPC curve of the photoproducts at the intermediate stage of the topochemical reaction of III (4-pyridyl, X : CN, Y : COOEt).

dimers and so on, to result in the "Even-numbered Polymerization Mechanism" shown below.

$$M + M \xrightarrow{\quad h\nu \quad} \text{dimer (M-M)} \xrightarrow{\quad h\nu \quad} \text{polymer (M-M)}_n$$

In addition to the Even-numbered Polymerization Mechanism, the growing terminal olefin group should always consist of the double bonds at the pyridyl side during the reaction.

The dimer crystal, recrystallized from ethanol, shows essentially the same crystal diffraction pattern as the crystal as-prepared, but upon photoirradiation it gives a higher molecular weight polymer (ηinh = 0.36 dL/g → η inh = 0.64 dL/g). According to X-ray diffraction analysis, the photoproduct at the inital stage (after the irradiation for 5 h) is crystalline and then becomes progressively amorphous upon further polymerization.

The crystal structure of the monomer is shown in Figure 7 (27).

In the monomer crystal of the cyano ethyl ester, every molecule is related to its neighboring molecules by two different centers of inversion along the stack direction. The two pairs of equivalent double bonds are separated by distances of 3.758(8) and 4.878(10) Å respectively. As the former distance is within the conventional reactive distance while the later is much longer than the reactive one, the initial dimerization must occur between the double bonds with the distance of 3.758(8) Å. After the dimerization, the facing double bonds between the two dimer molecules become photoreactive; these dimers grow into the higher molecular weight species, and so on. Consequently, under topochemical control the monomer crystal of the cyano ethyl ester gives a linear homo-adduct polymer via the Even-numbered Polymerization Mechanism.

The analogous n-propyl ester crystal III (4-pyridyl, X : CN, Y : COOnPr) is also highly photosensitive, but gives the photostable crystalline dimer quantitatively. The dimer, recrystallized from ethyl acetate, shows essentially the same X-ray diffraction pattern as that of the dimer cryatal as-prepared and is photostable. Furthermore, the same dimer, under recrystallized from l-propanol, is highly photoreactive and gives a high polymer (ηinh 0.87 dL/g, CHCl₃ 30 °C).

The overall reaction scheme of the III (4-pyridyl, X : CN, Y : COOR, where R : Et and n-Pr) crystals is presented in Scheme IV.

Contrary to the ethyl and propyl ester crystals, the same methyl ester crystal III (4-pyridyl, X : CN, Y : COOMe) photodimerizes between two double bonds exclusively at pyridyl side olefins, and, on further irradiation, the dimer is converted to the polymer.

Conclusions

Several new hetero- and homo-adduct polymers were prepared photochemically from the unsymmetrically substituted diolefin crystals. In almost all of the topochemical [2+2] photopolymerizations where the homo-adduct polymers were produced, a single type of dimer was formed, followed by further polymerization. The photoreaction was completed at the dimer in some crystals. Such remarkable differences in the photochemical behavior in these crystals with similar chemical structures, can be explained not by their intrinsic chemical reactivity, but by the difference in the molecular arrangement in the crystals.
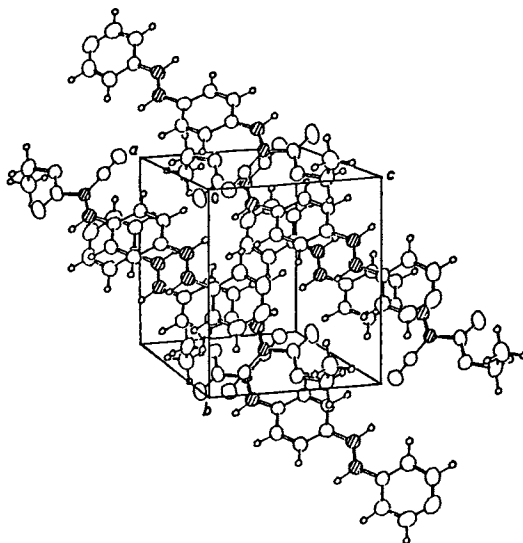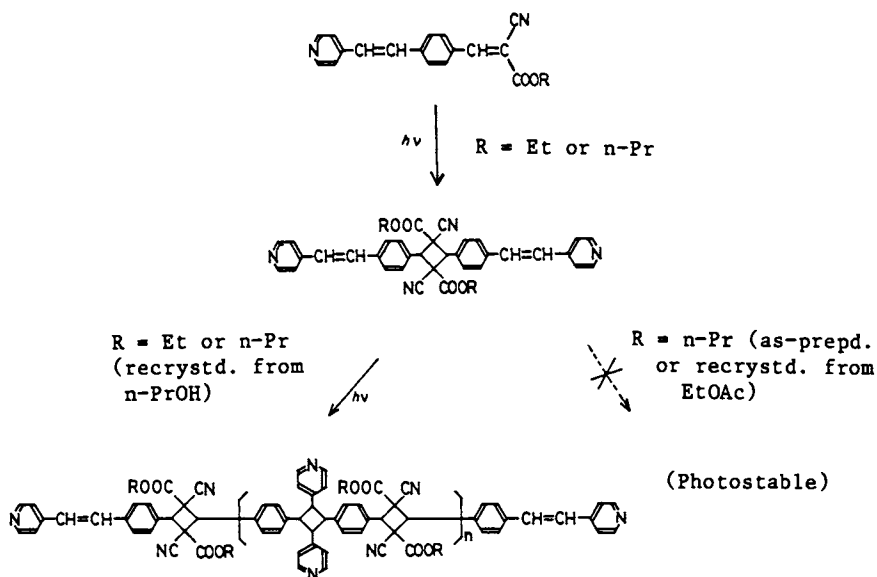
Figure 7.   Crystal structure of III (4-pyridyl, X : CN, Y : COOEt).
The atoms comprising the ethylenic groups are hatched for clarity.

Scheme IV.

In addition to the electrolyte property of the crystals in Groups III and IV, it is of further interest that one side of the rigid hetero-adduct polymer chain as-prepared is hydrophilic, while the other is hydrophobic, under the restricted rotation of the σ-bond in the main chain. On the other hand, the homo-adduct polymer consists of an alternating hydrophilic and hydrophobic structure in the polymer chain (Fig. 8).
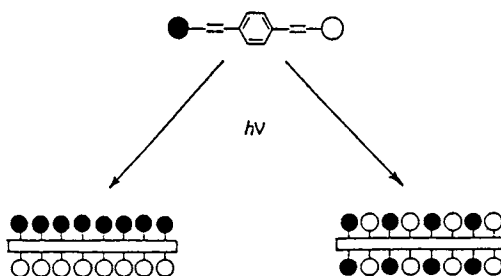
Figure 8. Schematic illustration of the hetero- and homo-adduct types of polymers in groups III and IV. Key: ●, hydrophobic; o, hydrophilic.

Literature Cited

1. Present address: Polyplastics Co., Ltd., 973 Miyajima, Fuji, Shizuoka 416.
2. Hasegawa, M.; Suzuki, Y. Polym. Letts. 1967, 5, 813.
3. Cohen, M. D.; Schmidt, G. M. J. J. Chem. Soc. 1964, 1969; for a review see Schmidt, G. M. J. Pure Appl. Chem. 1971, 27, 647.
4. Nakanishi, F.; Hasegawa, M. J. Polym. Sci., Polym. Chem. Ed. 1970, 8, 2150.
5. (a) Sasada, Y.; Nakanishi, H.; Hasegawa, M. Bull. Chem. Soc. Jpn. 1971, 44, 1262. (b) Nakanishi, H.; Hasegawa, M.; Sasada, Y. J. Polym. Sci., Part A-2 1972, 10, 1537.
6. Nakanishi, H.; Hasegawa, M.; Sasada, Y. J. Polym. Sci., Polym. Phys. Ed. 1977, 15, 173.
7. Meyer, W.; Lieser, G.; Wegner, G. J. Polym. Sci., Polym. Phys. Ed. 1978, 16, 1365.
8. Nakanishi, H.; Sasada, Y.; Hasegawa, M. Polym. Lett. 1979, 17, 459.
9. Dilling, W. L. Chem. Rev. 1983, 83, 507.
10. (a) Hasegawa, M.; Suzuki, Y.; Nakanishi, F.; Nakanishi, H. Progr. Polym. Sci., Jpn. 1973, 5, 143. (b) Hasegawa, M. Adv. Polym. Sci. 1982, 42, 1; Chem. Rev. 1983, 83, 507.
11. Hasegawa, M.; Saigo, K.; Mori, T. ACS Symposium Series 1984, 266, 255.
12. van Mil, J.; Addadi, L.; Gat, E.; Lahav, M. J. Am. Chem. Soc. 1982, 104, 3429 and the references cited therein.

13. (a) Hasegawa, M.; Kato, S.; Yonezawa, N.; Saigo, K. J. Polym.
     Sci. Part C, Polym. Letts. 1986, 24, 513. (b) Hasegawa, M.;
     Harashina, H.; Kato, S.; Saigo, K. Macromolecules 1986, 19,
     1276. (c) Kato, S.; Nakatani,M.; Harashina, H.; Saigo, K.;
     Hasegawa, M.; Sato, S. Chem. Lett. 1986, 847.
14. Anet, R. Can. J. Chem. 1962, 40, 1249;
15. Montaudo, G.; Scamporrino, E. "Developments in Polymer
     Degradation-5," Chap. 4, "Photolytic Behavior of Polyamides
     containing Truxillic and Truxinic Units"; Grassie, N. Ed.; Appl.
     Sci. Publishers Ltd.; London, 1983; p. 121.
16. Tamaki, T.; Suzuki, Y.; Hasegawa, M. Bull. Chem. Soc. Jpn. 1972,
     45, 1988.
17. Nakanishi, H.; Nakanishi, F.; Suzuki, Y.; Hasegawa, M. J. Polym.
     Sci., Polym. Chem, 1973, 11, 2501.
18. Crystal data of I (R : Me, R' : Et): PT, a = 12.460 (1) Å, b =
     9.713(1) Å, c = 5.958(1) Å, α = 77.43(1)°, β = 87.09(1)°, γ =
     80.75(1)°, Z = 2, V = 694.5 Å^3, R = 0.069. The analysis was
     carried out by Dr. S. Sato
19. Nakanishi, H.; Hasegaswa, M.; Mori, T. Acta Cryst., C-41, 1985,
     70.
20. Crystal data of III (4-pyridyl, X : H, Y : COOMe): P2$_1$/a, a =
     7.107(1) Å, b = 35.869(4) Å, c = 5.948(1) Å, β = 114.62(1)°, Z =
     4, V = 1378.4 Å^3, R = 0.069.
21. (a) Ramasubbu, N.; Guru Row, T. N.; Venkatesan, K.; Ramamurthy,
     V.; Rao, C. N. R. J. Chem. Soc., Chem. Commun. 1982, 178.
     (b) Theocharis, C. R.; Jones, W.; Thomas, J. M.; Motevalli, M.;
     Hursthouse, M. B. J. Chem. Soc. Perkin Trans. II, 1984, 71.
     (c) Gnanaguru, K.; Ramasubbu, N.; Venkatesan, K.; Ramamurthy, V.
     J. Photochem. 1984, 27, 355; J. Org. Chem. 1985, 50, 2337.
     (d) Hasegawa, M.; Saigo, K.; Mori, T.; Uno, H.; Nohara, M.;
     Nakanishi, H. J. Am. Chem. Soc. 1985, 107, 2788.
22. Dimer : mp 186-189 °C; ^{1}H NHR (CDCl$_3$) δ3.54 (3H, s), 3.88 (3H,
     s), 4.76 (1H, d), 4.98 (1H, d),5.23 (1H,t), 7.02-7.84 (16H, m),
     8.12 (1H, s), 8.58(1H d), 8.64 (1H, d) ppm; MS m/e 580 (M$^+$), 392
     (asymmetric cleavage of the cyclobutane ring), 290(M$^+$/2
     symmetric cleavage), 188(asymmetric cleavage).
23. Crystal data of Methyl α-cyano-4-[2-(2-pyridyl)ethenyl]-
     cinnamate: C$_{18}$H$_{14}$N$_2$O$_2$ = 290.3, PT, triclinic, a = 12.269(2) Å, b
     = 7.489(1) Å, c = 8.486(2) Å, α = 97.74(1)°, β = 92.42(1)°, γ =
     74.41(1)°, V = 743.8 Å^3, Z = 2, D$_X$ = 1.30 g·cm^{-3}, R = 0.080,
     (Cu Kα) = 0.7 mm^{-1}.
24. (a) Cohen, M. D.; Elgavi, A.; Green, B. S.; Ludmer, Z.; Schmidt,
     G. M. J. J. Am. Chem. Soc. 1972, 94, 6776. (b) Nakanishi, F.;
     Tanaka, T.; Miyagawa, F.; Nakanishi, H. Nippon Kagaku Kaishi
     1981, 412.
25. Hasegawa, M. Pure and Appl. Chem. 1986, 58, 1179.
26. Dimer: mp 189.5-192.0 °C; ^{1}H-NMR (CDCl$_3$, 90MHz) δ0.95 (t, 6H),
     4.03 (q, 4H), 5.13 (s, 2H), 6.9-7.7 (m, 16H), 8.55 (d, 2H); mass
     spectrum, m/e 608 (M$^+$), 304 (M$^+$/2; symmetric cleavage of the
     cyclobutane ring), but no trace of an asymmetric cleavage of the
     cyclobutane ring.
27. Crystal data of III (4-pyridyl, X : CN, Y : COOEt): triclinic,
     PT, a = 11.664(4) Å, b = 9.151(3) Å, c = 7.814(2) Å, α =
     85.84(3)°, β = 104.44(4)°, γ = 80.05(2)°, V = 789.7 Å^3, Z = 2,
     and R = 0.082.

Chapter 5

Solid-State Polymerization of 1,4-Disubstituted Butadienes in Layered Structures

B. Tieke[1,3] and G. Chapuis[2]

[1]Institut für Makromolekulare Chemie, Universität Freiburg, 7800 Freiburg, Federal Republic of Germany
[2]Institut de Cristallographie, Université de Lausanne, 1015 Lausanne, Switzerland

This article describes the solid state polymerization of 1,4-disubstituted butadiene derivatives in perovskite-type layer structures, in layered structures of organic ammonium halide salts, and in lipid layer structures. Recent investigations by spectroscopic methods and x-ray structure analyses are described. The studies clearly indicate that the photolysis in the crystalline state leads to the formation of 1,4-trans-polymers exclusively. Crystal structure analyses of monomeric and polymeric layer perovskites demonstrate that upon γ-irradiation a stereoregular polymer is obtained in a lattice controlled polymerization.

The solid state reactivity of butadiene derivatives has first been investigated by G.M.J. Schmidt and coworkers (1-3). They observed for a number of 1,4-disubstituted compounds that exposure to UV light leads to the formation of dimers according to a [2+2]-cycloaddition reaction. The structure of the dimers was found to be strictly related to the monomer arrangement in the crystal lattice. Oligomers or polymers could only be obtained as side products.

More recently, long chain butadienes were reported to polymerize in monomolecular layers (4) and Langmuir-Blodgett-multilayers (5). As the structure of the polymer either a 1,4-adduct (4) or [2+2] cycloadduct (5) was proposed.

However, the most interesting products could be obtained upon the radiolysis of butadiene derivatives included in a host matrix (6-8). For a number of monomers with a non-centrosymmetric molecular structure it could be demonstrated that γ-irradiation leads to stereoregular, optically active polymers in a direct asymmetric induction. Especially these studies indicate that apart from polymerization in solution using optically active catalyst systems (9), the solid state polymerization represents a suitable method to obtain stereoregular polybutadienes.

[3]Current address: Ciba-Geigy AG, Forschungszentrum KA, 1701 Fribourg, Switzerland

Since polymerization in inclusion compounds is restricted to only a few monomers with small substituent groups, it seemed worthwhile to search for other systems where butadiene derivatives are able to polymerize exclusively according to a 1,4-addition mechanism. In the following, our recent investigations (10-14) on the polymerization behavior of 1,4-disubstituted butadienes in various layered structures will be reviewed. Polymerization has been investigated

(i)   in organic-inorganic complex salts of the general formula ($R-CH=CH-CH=CH-CH_2NH_3$)$_2$MtX$_4$ (for R, Mt and X see Tab. I)

(ii)   in native halide salts ($R-CH=CH-CH=CH-CH_2NH_3$) X (for R and X see Tab. III), and

(iii) in lipid layer structures formed by butadiene derivatives which carry long aliphatic tails either in the 1-position or in the 1- and 4-position.

It will be demonstrated by spectroscopic methods that exposure of some of the compounds to UV-light or γ-irradiation exclusively leads to the formation of 1,4-trans-polymers according to

$$n \quad R_1 \diagdown\!\!\!\diagup\!\!\!\diagdown\!\!\!\diagup R_2 \quad \xrightarrow[\text{crystal}]{h\nu} \quad \left[\begin{array}{c} R_1 \\ \diagup\!\!\!\diagdown\!\!\!\diagup\!\!\!\diagdown \\ R_2 \end{array} \right]_n$$
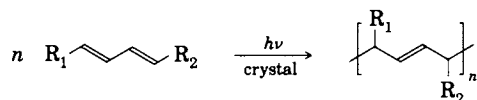
Moreover, it will be shown by x-ray structure analyses of layer perovskites in the monomeric and polymeric states that γ-irradiation leads to the formation of a stereoregular polymer in a lattice controlled polymerization. The properties of the polymers will be discussed briefly.

Experimental

The synthesis of the monomers as well as of the complex salts has been described previously (10,11,13). For polymerization the crystals were either exposed to UV light using a 240 W medium high pressure mercury lamp, or irradiated by high energy radiation using a ^{60}Co-γ-source. In all irradiation experiments care was taken that the temperature never exceeded 25°C. Details of the x-ray structure analyses were given previously (12), or will appear in a forthcoming publication (15).

Organic-inorganic complex salts

Primary amines R-NH$_2$ with R representing an unbranched alkyl chain are able to form complex salts with divalent transition metal halides MtX$_2$. The complex salts of the general formula (R-NH$_3$)$_2$MtX$_4$ are often called "layer perovskites" or "perovskite-type layer structures" and exhibit a structure as schematically shown in Figure 1 (16). As indicated by the Figure, a corresponding complex is also formed by α, ω-substituted diamines.

In recent years interest in these materials has grown mainly for physical reasons. The layer perovskites are looked at as model compounds for the study of magnetic properties in two-dimensional systems (17), and as models for the study of structural phase transitions in lipid bilayer-type arrays (18). The use of layer perovskites as a matrix for organic solid state reactions represents a fairly new research topic. First experiments were carried out studying the photolysis of butadiyne (diacetylene) derivatives (19-20). For a corresponding study of the butadiene derivatives the compounds listed in Table I were synthesized.

Table I. Butadiene derivatives and their photoreactivity in layer
perovskites $(R-CH=CH-CH=CH-CH_2NH_3)_2MtX_4$

No.	R	Mt	X	photoreactivity upon UV- and γ-irradiation	
1	H	Cd	Cl	-	+
2	CH_3	Cd	Cl	-	+
3	COOH	Cd	Cl	+	+
4	COOH	Cu	Cl	-	-
5	COOH	Fe	Cl	+	+
6	COOH	Mn	Cl	+	+
7	COOH	Cd	Br	-	-
8	$COOCH_3$	Cd	Cl	+	+
9	$COOCH_3$	Cu	Cl	-	-
10	$COOCH(CH_3)_2$	Cd	Cl	+	+
11	$COOCH_2CH(CH_3)_2$	Cd	Cl	+	+
12	$COO(CH_2)_3CH_3$	Cd	Cl	+	+

Photoreactivity. The photoreactivity of the complex salts has been investigated by exposing the crystals either to UV-light of a medium high pressure mercury lamp, or to ^{60}Co-γ irradiation. Experiments using vacuum-UV have not been carried out as yet. Upon γ-irradiation the complex salts with cadmium chloride all exhibit a chemical reaction. On the other hand, only the sorbic acid derivatives are reactive upon UV-irradiation. This may simply arise from the fact that these compounds exhibit a chromophore extended by the C=O unit and thus being red-shifted in the optical absorption to about 260 nm. Thermal reactions except for decomposition at high temperatures could not be detected for any of the compounds.

The polymerization is very sensitive to variations of the substituent R or the inorganic matrix MtX_2. The cadmium chloride complex 1 with R=H is highly reactive, whereas the corresponding complex of the acid derivative 3 or the methyl ester 8 are much less reactive. Among the complex salts of the acid derivative, complex 6 with Mt^{2+} being manganese polymerizes more rapidly than complex 3 with cadmium ions. The complex salt 4 with Cu^{2+} is completely photoinactive. A variation of the halide ions also influences the photoreactivity. In contrast to the chloride salt 3 the corresponding

bromide salt $\underline{1}$ is completely photoinactive. Despite the differences in polymerization rate the photoreactive complexes all exhibit a nearly complete conversion to polymer at high radiation doses. The different photoreactivities originate from a topochemical control of the reaction by the inorganic matrix.

Spectroscopic Studies. The photoproducts were characterized by spectroscopic methods. In Figure 2 the infrared spectra of $\underline{3}$ as monomer and after exposure to various γ-ray doses are shown. With increasing radiation dose the intensities of the C=C-stretching (1635 and 1620 cm^{-1}) and wagging (1000 cm^{-1}) modes decrease. Simultaneously a new mode appears at 960 cm^{-1}, which can be ascribed to an isolated trans-C=C-unit as it typically occurs in 1,4-trans-polybutadienes.

After polymerization the complex salts are usually insoluble in all common solvents. Polymerized crystals of $\underline{3}$ represent an exception, as they are easily attacked by aqueous alkaline media. The presence of S^{2-} ions in the aqueous solution causes a simultaneous precipitation of the cadmium ions as insoluble CdS. In this way, the photoproducts can easily be separated from the inorganic matrix and can be analyzed in solution by means of ^{13}C-NMR-spectroscopy, for example. In Figure 3 ^{13}C-NMR-spectra of the monomer and photoproducts are shown. The formation of a 1,4-trans-polymer backbone is indicated by the two signals of the unsaturated carbon atoms at δ = 135.4 and 134.2 ppm, and the saturated carbon atoms at δ = 49.8 and 45.2 ppm. The two signals of the aminomethyl and carboxylic acid substituent groups appear at 184.5 and 59.2 ppm, respectively. Additional signals occuring in the product spectrum can be attributed to small amounts of residual monomer still present in the sample. From the ^{13}C-NMR-spectrum the formation of dimers containing cyclobutane rings can be ruled out. The chemical reaction as derived from the spectroscopic investigation is schematically represented by Figure 4.

Analysis of the Structures. In the following, questions concerning the stereoregularity of the polymer and the origin of the photoinactivity of the copper salts will be answered. For this purpose, the crystal structures of the reactive cadmium chloride complex salt $\underline{3}$ as monomer and polymer, and of the corresponding copper salt $\underline{4}$ have been solved by x-ray diffraction.

The complex salts usually crystallize as platelets of a size up to 1 x 2 x 0.5 mm. They exhibit a layered structure and a characteristic twinning. Microscopic studies indicate that the morphology of the crystals essentially remains unchanged during polymerization ($\underline{11}$). However, occasionally crystals can be found that exhibit a splitting or crack formation subsequent to γ-irradiation. The good quality of the crystals of $\underline{3}$ allowed to determine their structure by single crystal x-ray diffraction. The crystal data are listed in Table II.

Crystals of $\underline{3}$ consist of two types of layers that alternate in the third dimension. One type of layers consists of corner-sharing CdCl$_6$ octahedra, whereas the other type contains the organic monomer (Figure 5a) or polymer (Figure 5b).

The chessboard-like pattern of the octahedra leaves empty channels which are occupied by the ammonium end of the organic residues. The monomer form $\underline{3}$ contains four crystallographically
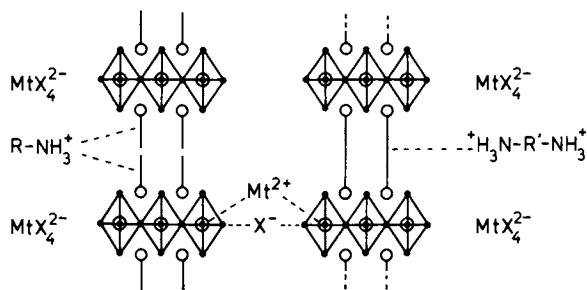
Figure 1.   Schematic   representation   of   the   structure of layer perovskites of mono- and diammonium salts.
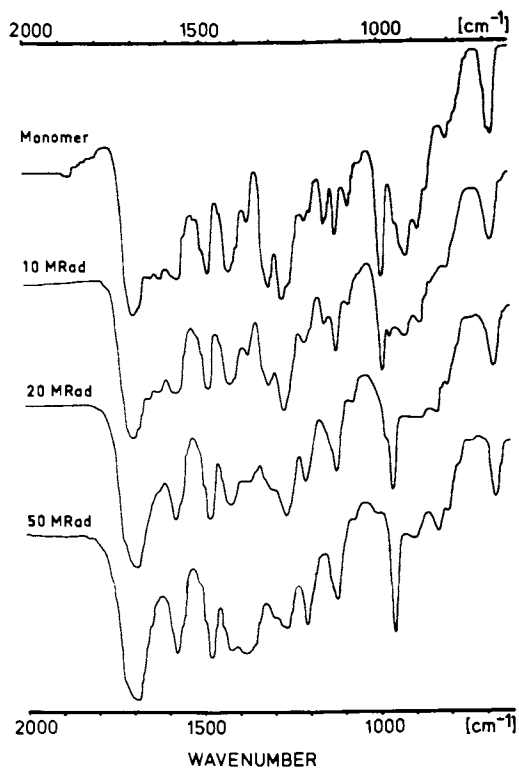

WAVENUMBER

Figure 2.   Section   of   IR-spectra   of   the   layer   perovskite compound 3 as monomer and after various γ-ray doses (Reproduced with permission from Ref. 11, Copyright 1984, John Wiley & Sons, Inc.)

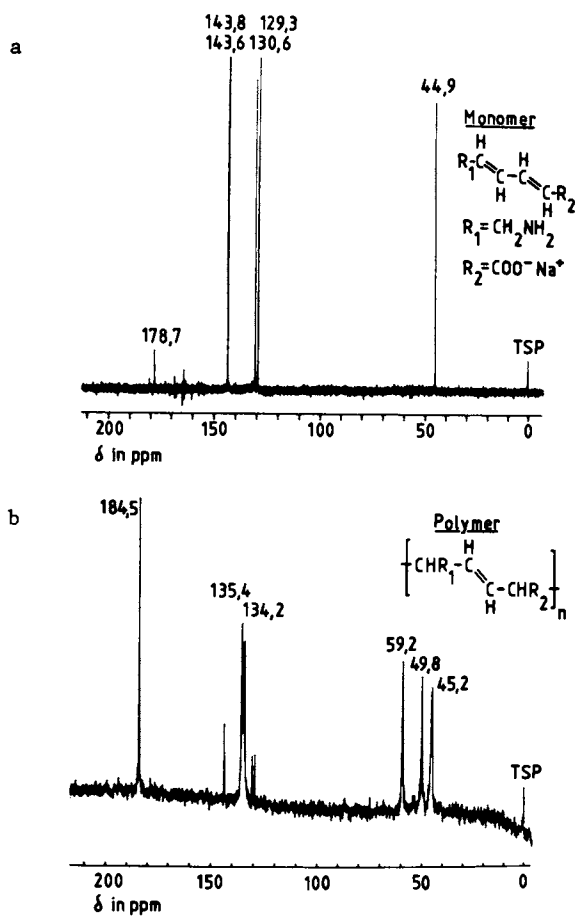Figure 3.   22.7-MHz-^{13}C-NMR-spectrum of **3** a) as a monomer and
b) after exposure to a γ-ray dose of 30Mrad. Subsequent to γ-
irradiation the crystals were disolved in 1 N aqueous KOD. The
cadmium ions were precipitated as CdS and separated. (Reproduced
with permission from Ref. 10, Copyright 1981, Hüthig und Wepf
Verlag, Basel)
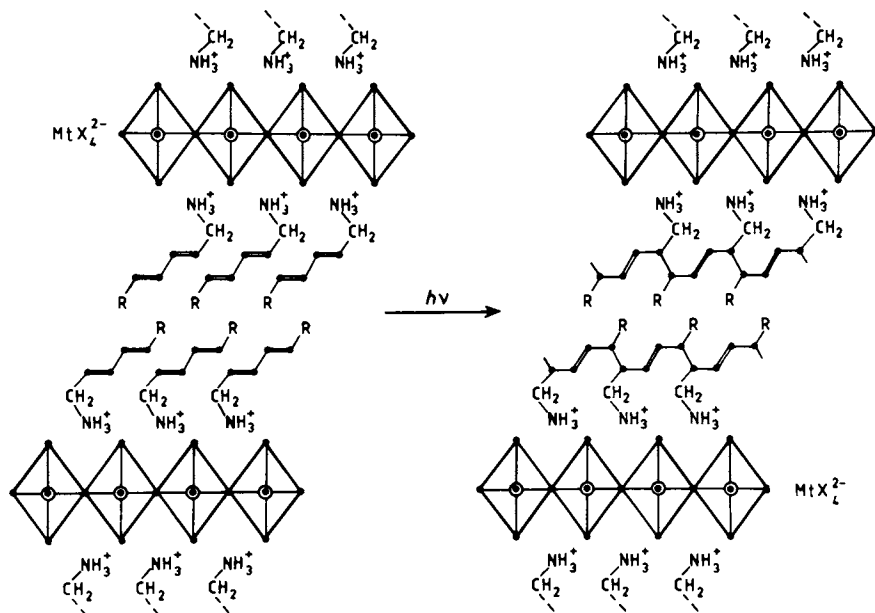
Figure 4. Schematic representation of the butadiene polymerization in layer perovskites. Model of the [010] projection (for R, Mt and X see Tab. 1). (Reproduced with permission from Ref. 10, Copyright 1981, Hüthig und Wepf Verlag, Basel)

Table II.   Crystal data of complex salts 3 and 4

	3 (monomer)	3 (polymer)	4 (monomer)
crystal system	triclinic	triclinic	triclinic
space group	P$\bar{1}$	P$\bar{1}$	P$\bar{1}$
a(Å)	10.43(2)	7.2144(4)	10.422(1)
b	10.806(7)	7.2447(5)	10.736(1)
c	17.78(3)	18.5936(14)	17.340(2)
α(°)	91.4(1)	104.488(5)	87.95(1)
β	109.2(2)	96.631(5)	74.20(1)
γ	92.8(1)	95.706(5)	87.67(1)
Z	4	2	4
d(calc.)	1.78	1.83	1.64
T (K)	170	293	293

independent units which are hydrogen bonded to the inorganic layer by
N-H...Cl bonds (Figure 6). The carboxylic acid ends are also H-bonded
to their centrosymmetric equivalent with O-H...O bonds varying
between 2.5 and 2.6 Å. In the four independent monomers, the
structure analysis reveals the trans form of the dienes. However, the
ammonium ends of each monomer differ by their N-C-C-C torsion angles.
As each monomer tends to align in a unique direction for packing
optimization, this can be achieved by adapting the corresponding
torsion angle of each monomer unit to accommodate for the various
orientations of the four Cl-cavities. In two of them, the ammonium
hydrogen atoms are directed towards two axial Cl- and one equatorial
C-atoms (aae) whereas in the other, the scheme is of the (aee) type.
     Polymerization of 3 induces a complete reorganization of the
structure, the unit cell of which is reported in Table II. The
density of the crystal has increased by 3 % after polymerization.
     In the present centrosymmetric refinement, there are two
crystallographically independent monomer units linked together by C-C
single bonds, C(11)-C(22) and C(5)-C(8). The two entities are
globally quite similar, but the corresponding bond distances and
angles as well as the torsion angles vary quite significantly. The
polymer chains exhibit a 1,4-trans-structure with an erythro-
diisotactic arrangement of the substituents (Figure 7). Individual
polymer chains are chiral, but due to the centrosymmetric crystal
structure, a racemate is obtained. Each polymer chain is linked to
its centrosymmetrical equivalent by hydrogen bonds (indicated by the
open bonds).
     The polymerization induces also a distortion of the Cl-octahedra
packing. The deviation from an ideal chessboard-like arrangement can
be approximated by a rotation of 30° about the layer normal. This
rotation is much less important in the monomer form as can be
observed on Figure 6. The displacement of the Cl-octahedra also
affects the environment of the two ammonium groups (Figure 8). N(1)
has four Cl-atoms within a radius of 3.4 Å, whereas N(2) has five Cl-
atoms within the same radius. N(1) is hydrogen bonded with two axial
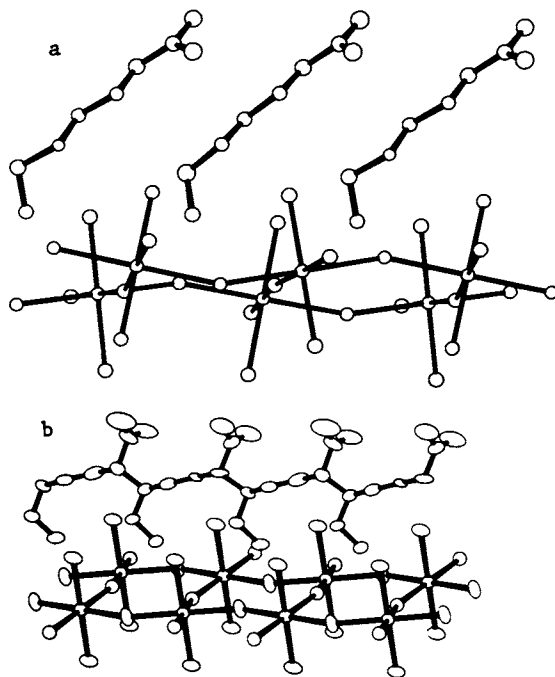
Figure 5. Crystal structure of the layer perovskite compound 3 a) as monomer and b) polymer. Perspective view of the organic and inorganic layers. For clarity, only two independent molecules are represented in the monomer structure.
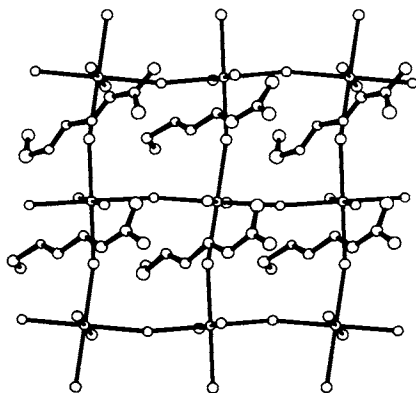

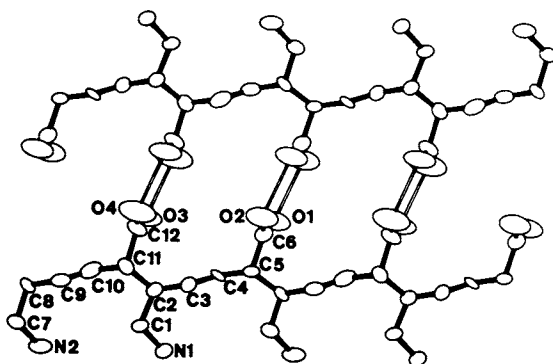Figure 6. Projection of the crystal structure of 3 as monomer onto the layer plane.

Figure 7. Representation of the polymer layer with H-bonded oxygen atoms linked by open bonds. The atoms of the two independent monomer units are identified on the figure. (Reproduced with permission from Ref. 11, Copyright 1984, John Wiley & Sons, Inc.)
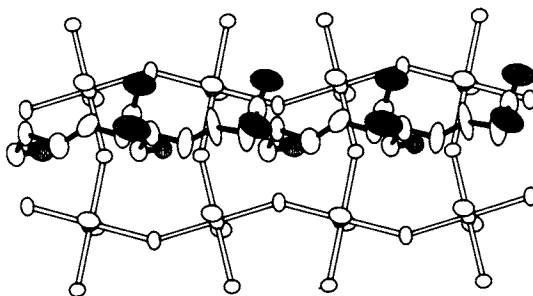
Figure 8. Projection of the crystal structure of 3 in the polymerized state onto the layer plane (the inorganic part is represented by open bonds). (Reproduced with permission from Ref. 14, Copyright 1986, Gordon and Breach, Science Publishers, Inc.)

and one equatorial Cl atoms (aae), whereas for N(2), no clear scheme of the H-bonds can be inferred from the neighboring Cl-atoms.

Crystal data of the photoinactive copper complex salt $\underline{4}$ are given in Table II. This structure also consists of an alternating sequence of organic and inorganic layers. The Cu atoms are coordinated by four Cl-atoms with distances varying between 2.26 and 2.32 Å. There are two additional Cl-atoms separated by 2.99 Å. Thus, the copper atom is coordinated by the Cl-atoms in the form of an elongated tetragonal bipyramid. The axis of the bipyramid lies parallel to the layer plane (Figure 9).

The organic part consists also of four independent monomer units similar to the monomer structure of $\underline{3}$. The main differences in the chains can also be observed on the N-C-C-C torsion angles. The four independent monomers tend to align in a unique direction for packing optimization.

A comparison of the structures of the organic layers for the monomer forms of $\underline{3}$ and $\underline{4}$ shows a nearly perfect match of distances, angles and torsion angles. A one to one correspondence of the four cristallographically independent units can be established without ambiguity between the two structures. In the monomer form of $\underline{3}$, the distances of the C-atoms which are covalently bonded only in the polymer structure, vary between 3.5 and 3.9 Å. In $\underline{4}$, the same distances vary between 3.5 and 4.0 Å. Thus the reason for the various reactivities upon irradiation must be found in the part of the structures which differs most from each other, i.e. the metallic layers. The differenciation originates in the ability of the Cl-octahedra (Cd) or the Cl-bipyramids (Cu) to adapt to the new structural environment imposed by the polymerization of the organic residues. This point is of particular importance for the control of polymerization by a periodic matrix.

Native Halide Salts

In addition to the layer perovskite halide salts, the photoreactivity upon UV and γ-irradiation of the native halide salts of the butadiene derivatives was also studied ($\underline{11}$). Individual salts and their reactivities are listed in Table III.

Table III. Butadiene derivatives and their photoreactivities in native ammonium halide salts (R-CH=CH-CH=CH-CH$_2$NH$_3$) X

No.	R	X	photoreactivity upon UV- and γ-irradiation	
$\underline{13}$	H	Cl	-	◆
$\underline{14}$	CH$_3$	Cl	-	-
$\underline{15}$	COOH	Cl	◆	◆
$\underline{16}$	COOH	Br	-	-
$\underline{17}$	COOCH$_3$	Cl	-	-
$\underline{18}$	COO(CH$_2$)$_3$CH$_3$	Cl	-	-

Photoreactivity and Characterization of the Photoproducts

It is noticed that only compounds 13 and 15 are photoreactive. Figure 10 shows infrared spectra of compound 15 as monomer and after subjecting the crystals to various γ-ray doses. The spectral changes are very similar to those observed in layer peroskites (compare Figure 2) and indicate the formation of a 1,4-trans-polymer as well. The reaction of the butadiene unit is indicated by the disappearance of the C=C stretching and wagging modes at 1620-1650 and 1020 cm⁻¹, and the simultaneous appearance of the wagging mode of an isolated trans-C=C-unit at 970 cm⁻¹, as it typically occurs in polybutadienes. ¹³C-NMR-spectra of the photoproducts are essentially identical with those shown in Figure 3 and confirm the exclusive formation of a 1,4-adduct.

Structure Studies. Compound 15 can be grown as hexagonal platelets of a size up to 6 × 3 × 0.5 mm, whereas 13 only forms a microcrystalline powder. As already pointed out (11), the single crystals of 15 are not preserved during polymerization. Figure 11 shows a crystal after exposure to a γ-ray dose of 30Mrad. The crystal exhibits numerous cracks running parallel to a distinct axis which appears to be consistent with the polymer chain direction. Despite the macroscopic defects the crystallinity is retained in microscopic regions. Cracks and dislocations most likely originate from a phase transition during polymerization. From x-ray powder diffractograms reported earlier (11) it is evident that the phase transition occurs once the crystals have received a γ-ray dose of 15Mrad, i.e., at a conversion to polymer of about thirty percent. The original reflections disappear and new ones appear simultaneously. For example, the (001) reflection changes its d-value from 14.4 to 12.0 Å. This indicates a decrease of the crystal thickness during polymerization by about 17 percent.

Long chain butadiene derivatives

As a third system, the photoreactivity of long chain butadienes forming lipid layer-type structures was studied (13-14). Investigations were carried out in the crystalline state, in monomolecular layers and in LB-type multilayers. The individual compounds and their photoreactivities are listed in Table IV.

Photoreactivity. It is noticed from the Table that only the sorbic acid derivatives are reactive upon UV- and γ-irradiation. From spectroscopic studies of the reaction products a 1,4-addition reaction of the unsaturated units is evident. For example, spectral changes of 19 in the infrared are essentially identical with those observed in layer perovskites (compare Figures 12 and 2). ¹³C-NMR-spectra of 19 are also consistent with a 1,4-trans-adduct (Figure 13). Especially the signal of carbon atom (a) exhibits a splitting, which could indicate the presence of configurational isomers. Further studies are necessary to analyze the stereoregularity of the polymer of 19.
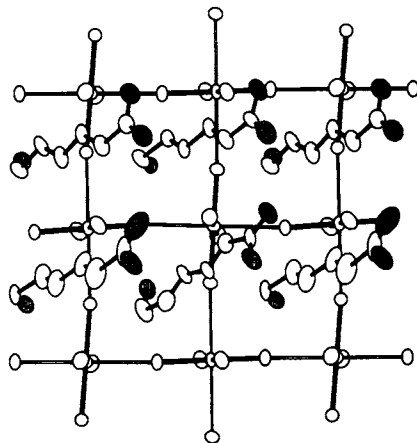
Figure 9. Projection of **4** perpendicular to the layer plane. (Reproduced with permission from Ref. 14, Copyright 1986, Gordon and Breach, Science Publishers, Inc.)
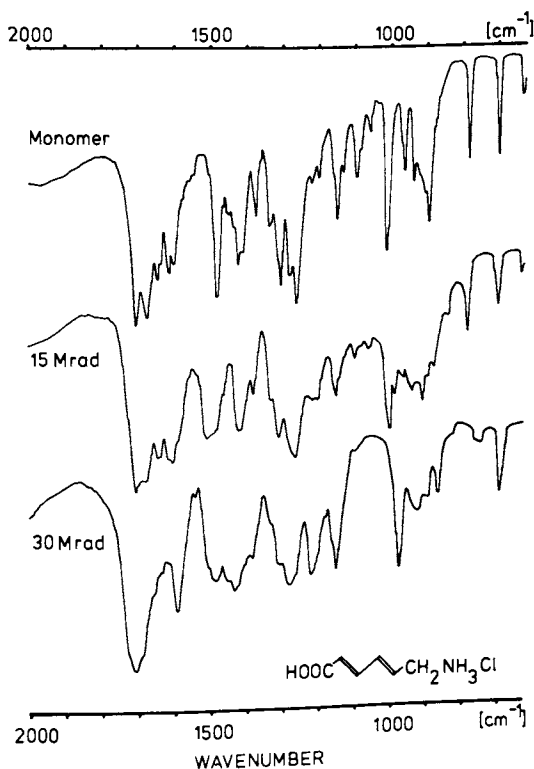
Figure 10. Section of IR spectra of the hydrochloride **15** as monomer and after various γ-ray doses. (Reproduced with permission from Ref. 11, Copyright 1984, John Wiley & Sons)
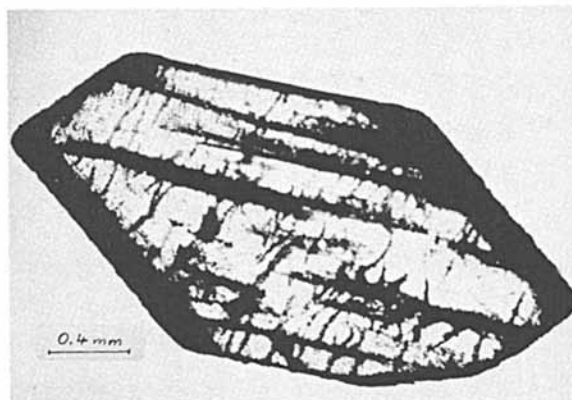
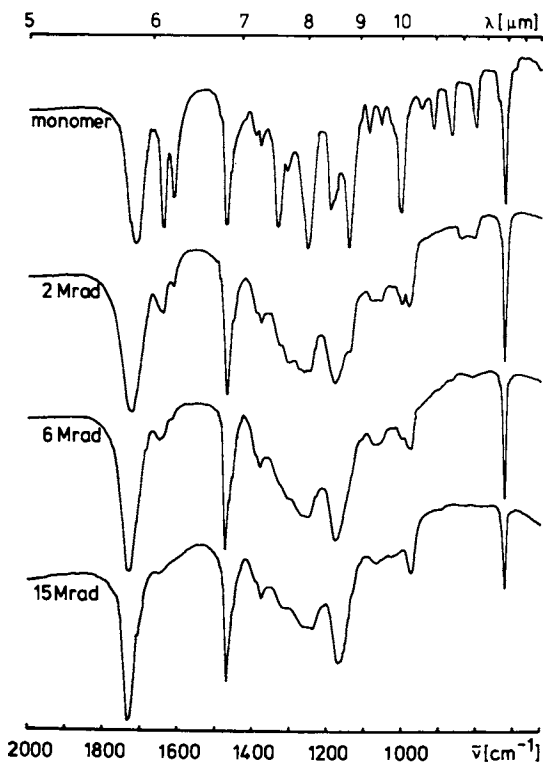Figure 11.   Polymeric crystal of **15** after exposure to a γ-ray dose
of 30 Mrad.

Figure 12.   Section of IR spectra of **19** monitored after various
γ-ray doses received by the crystals. Spectral changes at about
1620 and 1000 cm^{-1} indicate the photoreaction of the butadiene
units. (Reproduced with permission from Ref. 13, Or. Dietrich
Steinkopff Verlag, Darmstadt.)

Table IV. Long chain butadiene derivatives R_1-CH=CH-CH=CH-R_2 and their photoreactivities in the crystalline state

No.	R_1	R_2	m.p. ($^\circ$C)	photoreactivity upon UV- and γ-irradiation	
<u>19</u>	$CH_3(CH_2)_{17}O\overset{O}{C}-$	$-CH_3$	45	+	+
<u>20</u>	$CH_3(CH_2)_{17}\underset{H}{N}\overset{O}{C}-$	$-CH_3$	99	+	+
<u>21</u>	$CH_3(CH_2)_{16}\overset{O}{C}\underset{H}{N}CH_2-$	$-COOH$	145	+	+
<u>22</u>	$CH_3(CH_2)_{17}O\overset{O}{C}-$	$-\overset{O}{C}O(CH_2)_{17}CH_3$	88-89	-	-
<u>23</u>	$CH_3(CH_2)_{17}\underset{H}{N}\overset{O}{C}-$	$-\overset{O}{C}\underset{H}{N}(CH_2)_{17}CH_3$	185-188	-	-

Monomolecular layers and LB-multilayers. Compound <u>21</u> exhibits amphiphilic properties. Spreading at the air-water interface leads to the formation of oriented monomolecular layers. The monolayer forms a solid condensed phase at 20°C with a collapse pressure near 50mN/m. It can easily be transferred onto various hydrophobic substrates such as CaF$_2$, ZnS, AgCl, Si, Ge or metal surfaces, and Langmuir-Blodgett-type multilayers (<u>21</u>) of variable thickness can be built up. These multilayers also exhibit a rapid reaction if exposed to UV- or γ-irradiation. From an infrared spectroscopic study described recently (<u>13</u>-<u>14</u>) a 1,4-addition reaction is evident, as it also occurs in microcrystalline powders of <u>21</u>. The solid state polymerization of <u>21</u> is schematically represented by Figure 14.

Properties of the Polymer

The polybutadienes obtained in the layered structures exhibit interesting properties as recently described (<u>11</u>-<u>12</u>). The polymeric complex crystals represent extremely tough, high temperature stable materials with thermal decomposition starting only at temperatures above 600 K. The polymerized native halide salts are somewhat less stable, but still decompose only at about 600 K without melting. The solution properties of poly(aminosorbic acid) have also been investigated (<u>12</u>). According to viscosity measurements and gel-permeation chromatography, a polymer with an average molecular weight of about 4×10^4 is obtained. The polymer represents an amphoteric polyelectrolyte which is soluble in strong acids and bases, but insoluble in water and organic solvents. The polymer is highly capable of forming complexes with heavy metal ions. The complex formation can be utilized for the separation of heavy metal ions from aqueous solution, especially in the view of a high selectivity for divalent ions.
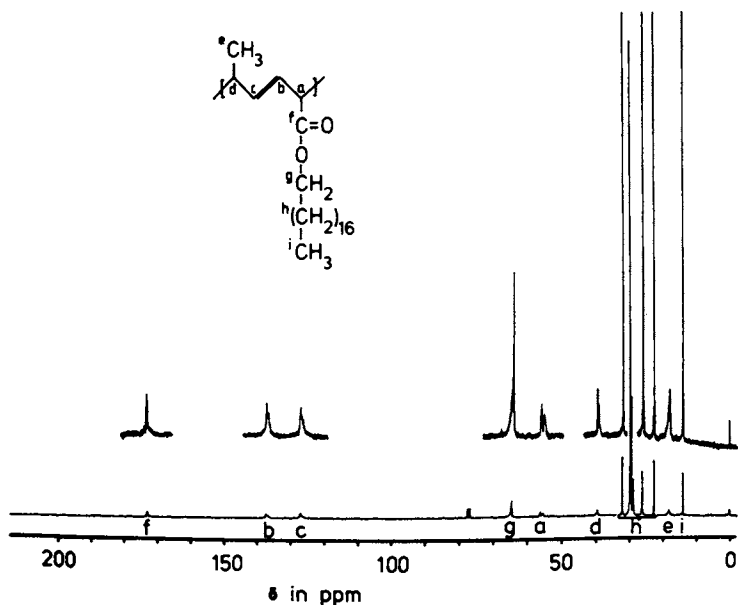
Figure 13. 90.556 MHz-^{13}C-NMR-spectrum of 19 after exposure of the crystals to a γ-ray dose of 15 Mrad and dissolution in CDCl$_3$. The signals ^{a}C - ^{d}C of the 1,4-trans-polybutadiene appear at δ = 137.1, 126.8, 56.0 and 39.4 ppm, respectively (standard : TMS). (Reproduced with permission from Ref. 13, Dr. Dietrich Steinkopff Verlag, Darmstadt.)
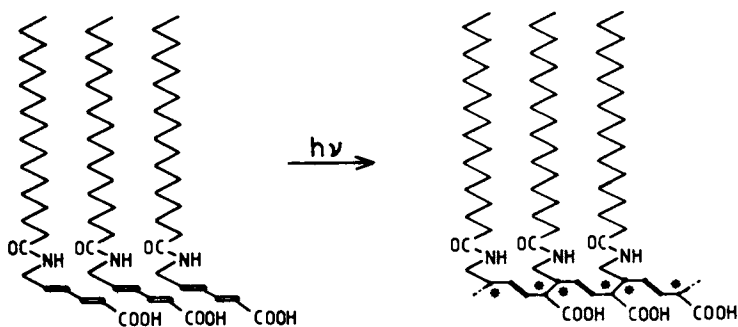

Figure 14. Schematic representation of the solid state polymeri- zation of 21. Provided that polymerization proceeds under lattice control a chiral backbone is obtained. (Reproduced with permission from Ref. 13, Dr. Dietrich Steinkopff Verlag, Darmstadt.)

Conclusions

Our investigations show that 1,4-disubsituted butadiene derivatives react in layered structures under exclusive formation of 1,4-trans-polymers. A stereoregular polymer is obtained. The structure analyses of the monomer and polymer crystals of 3 show that a lattice-controlled reaction takes place. It is certainly worthwhile studying the course of the reaction more in detail, and to compare the reaction mechanism and kinetics with those of other lattice-controlled reactions, as, for example, the polymerization reactions of diolefin (22) and butadiyne derivatives (23).

The exclusive formation of the 1,4-trans-polymer is a consequence of the layer-type arrangement. In a layer structure, photoreactivity is restricted to only two dimensions and the competing [2+2] cycloaddition is less likely to occur. Moreover, in the salt structures the lateral distances between the monomers are determined by the packing mode of the inorganic ions, causing the shortest distance to be about 5 Å. The same is true for the long chain butadienes, where the paraffin packing acts as a matrix also keeping the neighbouring monomers about 5 Å apart from each other. Consequently, the intermolecular distances are favourable to allow the 1,4-addition reaction, but are too large for the competing [2+2] cycloaddition reaction. It may be recalled that the latter reaction requires intermolecular distances of about 4 Å between the reactive units (1-3).

Literature Cited

1. Lahav, M.; Schmidt, G.M.J. J. Chem. Soc. B. 1967, 312-317.
2. Green, B.S.; Lahav, M.; Schmidt, G.M.J. J. Chem. Soc. B. 1971, 1552-1564.
3. For a review see Schmidt, G.M.J. et al.; Solid State Photochemistry, D. Ginsburg ed., Verlag Chemie, Weinheim 1976
4. Ringsdorf, H.; Schupp, H. J. Macromol. Sci.-Chem. 1981, A15, 1015-1026.
5. Barraud, A.; Rosilio, C.; Ruaudel-Teixier, A. Polym. Prepr. 1978, 19, 179-182.
6. Takemoto, K.; Miyata, M. J. Macromol. Sci. Rev. Macromol. Chem. C. 1980, 18, 83-107.
7. Farina, M.; Makromol. Chem. Suppl. 1981, 4, 21-35.
8. Farina, M.; Audisio, G.; Natta, G. J. Am. Chem. Soc. 1967, 89, 5071.
9. Natta, G.; Farina, M.; Donati, M. Makromol. Chem. 1961, 43, 251-254.
10. Tieke, B.; Wegner, G. Makromol. Chem. Rapid Commun. 1981, 2, 543-549.
11. Tieke, B. J. Polym. Sci. Polym. Chem. Ed. 1984, 22, 391-406.
12. Tieke, B.; Chapuis, G. J. Polym. Sci. Polym. Chem. Ed. 1984, 22, 2895-2921.
13. Tieke, B. Coll. & Polym. Sci. 1985, 263, 965-972.
14. Tieke, B.; Chapuis, G. Mol. Cryst. Liq. Cryst. 1986 (in press)
15. Chapuis, G.; Tieke, B., to be published.
16. Arend, H.; Huber, W.; Mischgofsky, F.H.; Richter-van Leeuwen, G.K. J. Cryst. Growth. 1978, 43, 213-223.
17. Arend, H.; Känel, H.v.; Wachter, P. phys. stat. sol. (b) 1976, 74, 151-157.

18. Needham, G.F.; Willet, R.D.; Franzen, H.F. J. Phys. Chem. 1984, 88, 674-680.
19. Wenz, G. Diplomarbeit, Universität Freiburg 1979
20. Ledsham, R.D.; Day, P. J.C.S. Chem. Commun. 1981, 921-922.
21. Kuhn, H.; Möbius, D.; Bücher, H. in "Physical Methods of Organic Chemistry", A. Weissberger, P. Rossiter, eds., Vol. 1, part 3B, Wiley Interscience 1972, pp. 577-702.
22. Hasegawa, M. Chem. Rev. 1983, 83, 507-518.
23. For recent reviews see "Polydiacetylenes", H.J. Cantow ed., Adv. Polym. Sci. Ser. No. 63, Springer-Verlag, Berlin 1984.

Chapter 6

Polymerization in Crystalline Inclusion Compounds

Mario Farina, Giuseppe Di Silvestro, and Piero Sozzani

Dipartimento di Chimica Organica e Industriale, Università di Milano,
Via Venezian 21-I 20133 Milano, Italy

The polymerization of monomers included as guests in
the crystal structure of channel-like inclusion
compounds extends the fields of application of solid
state polymerization far beyond the melting point of
pure monomers. Depending on the nature of both host
and guest compounds, polymers can be obtained having a
wide variety of structural features: regio- and
stereospecificity can reach very high values; optical
activity is induced by using chiral crystal lattices;
extended-chain macroconformations are observed under
specific working conditions. Inclusion polymerization
proceeds by a radical mechanism and its living
character has been demonstrated in some cases. Recent
results concern the production of block and stati-
stical copolymers and a new synthesis of polyethylene
and polypropylene by high-pressure inclusion
polymerization.

Crystalline inclusion compounds containing unsaturated monomers are
effective reactive systems for the production of linear polymers
(1-6). This process belongs to the wider class of solid state
polymerization, but possesses some specific features which make it
worthy of a separate description. Throughout this article, the
polymerization in inclusion compounds will be referred to as "in-
clusion polymerization" (other names currently used in the
scientific literature are channel, canal or tunnel polymerization),
and the terms "clathrate" will be used as synonymous with
"inclusion compound". When there is no risk of confusion, the more
general term of "adduct" will be used for clathrate: in principle a

distinction ought to be made between true adducts in which specific
chemical interactions exist (hydrogen bonding, ion-dipol and other
medium-strength interactions related to the chemical nature of the
host and guest molecules) and clathrates where the host-guest
interactions are essentially steric in origin (7).

Different classes of clathrates exist, depending on the
geometry of the cavities in which guest molecules are confined. As
regards inclusion polymerization, channel-like (or tubulate)
clathrates are particularly suited as the constraints in space
exerted by the host molecules induce the formation of polymers with
no branching or crosslinking. Channels are 10-15 A apart and, at
least when in perfect crystals, are not connected. As a consequence
they behave as independent reaction vessels, each giving rise to an
isolated macromolecule. Some of the features existing in the
included macromolecules can be retained in the "native" polymer.

Distinctive Features of Inclusion Polymerization

In inclusion polymerization a monomeric clathrate is transformed
into a polymeric one (where monomeric and polymeric refer to the
nature of the guest molecules)(Fig. 1) or into a mixture of polymer
and host when the polymer does not possess the steric requirements
for inclusion.

The real occurrence of polymerization inside the channels was
demonstrated in several ways. It does not occur, at least for a
number of monomers, when there is a simple mixture of host and
monomer without the formation of a clathrate or when the monomer is
placed in the presence of solid substances unable to form inclusion
compounds. Even in cases when polymerization does take place the
structure of the polymer formed outside the channels differs from
that obtained in proper conditions. The reaction rate is very
temperature and pressure dependent and has a sharp drop-off point
beyond which reaction ceases. The boundary conditions for
polymerization correspond to those which delimit the field of
thermodynamic stability of the monomeric clathrate, determined by
vapor pressure measurements or by DSC. This coincidence enables us
to state that the two phenomena, monomer inclusion and
polymerization, are strictly related. In addition, in some typical
cases a structural change from monomer to polymer was directly
observed inside the channels by X-ray analysis.

A discussion of inclusion polymerization within the frame of
solid state polymerization requires the specification of the points
which distinguish the two processes. In inclusion polymerization
the solid phase consists of two components, host and guest. The
former is a crystalline substance which possesses a strong tendency
to polymorphism. Generally hosts are able to crystallize in

different forms, some of which retain a definite amount of solvent or other substances.

The role of the host in inclusion polymerization is manifold: it stabilizes the solid phase far beyond the melting point of the monomeric guest, it selects in a more or less specific way the guests according to their shape and dimensions, it imposes on them a regular arrangement inside the channels and keeps the growing chains in well separate channels thus preventing the formation of branched or crosslinked structures. Moreover, it can produce the initiating species for polymerization and stabilize the growing chain-ends. These last points were clearly demonstrated in a specific case, however it is probable that they are generally valid.

The most common hosts for inclusion polymerization are: urea, thiourea, perhydrotriphenylene (PHTP), deoxycholic acid (DCA), apocholic acid (ACA) and tris(o-phenylenedioxy)cyclotriphosphazene (TPP)(Fig. 2). They have the common feature of forming channel-like clathrates, but differ in many specific properties. For instance, urea and thiourea have a rigid structure in which the host molecules are connected by hydrogen bonds and possess a high selectivity towards the guests. In urea channels are rather narrow whereas in thiourea they are wider; as a consequence, linear molecules include only in urea and branched or cyclic molecules in thiourea. On the contrary, channels existing in PHTP clathrates are very flexible and can accomodate linear, branched and cyclic molecules.

The ability of a molecule to act as a guest depends primarily on how it fills the clathrate cavities. In this respect the chemical nature of the guest and host is only of limited importance: polar hosts, such as urea and thiourea, and apolar ones, such as PHTP, can include hydrocarbons, alcohols and ethers, carboxylic acids and esters, etc., i.e. a number of molecules of very different polarity.

Knowing the thermal stability of clathrates permits the prediction of experimental conditions for polymerization (8). A detailed analysis of this problem requires the examination of all the involved phases, particularly the solid and liquid phases. Equations for phase equilibria were derived from within the framework of the regular solution theory; they contain an interaction parameter W, (whose value is always positive or zero for ideal solutions), which measures the tendency of host and guest to segregate in the liquid phase. The melting or decomposition point is very sensitive to the value of W, especially when it exceeds 2 RT, i.e. when a miscibility gap is observed in the liquid phase. For this reason the PHTP-hydrocarbon clathrates melt congruently between 115 and 180°C, whereas the urea-hydrocarbon
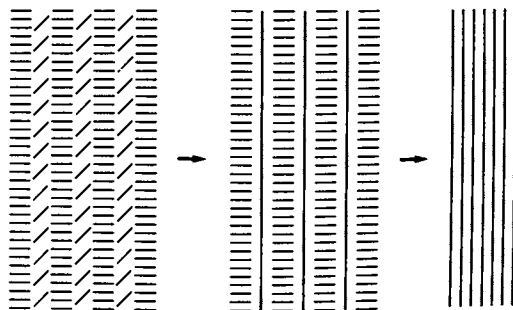
Figure 1. Schematic drawing of inclusion polymerization.
(Reproduced with permission from reference 12. Copyright
1982 Huthig and Wepf Verlag, Basel.)

Urea NH_2-CO-NH_2 Thiourea NH_2-CO-NH_2
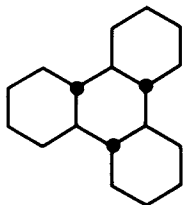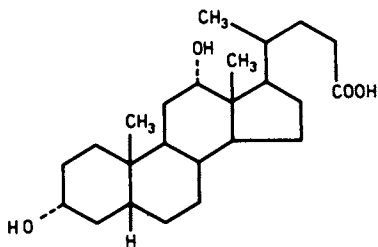
Perhydrotriphenylene PHTP   Deoxycholic acid DCA
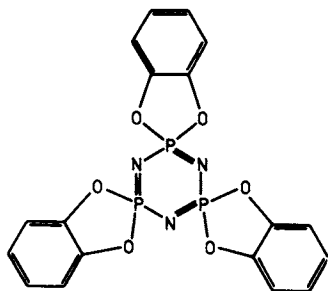
Tris-(o-phenylendioxy)-   Apocholic acid ACA
cyclotriphosphazene TPP
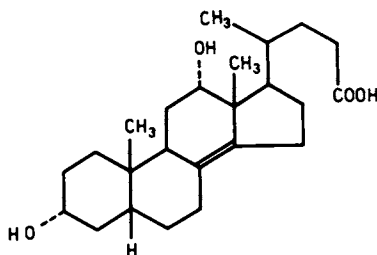
Figure 2. Hosts used in inclusion polymerization.

adducts show incongruent decomposition points at lower temperatures (9). In any case the temperature at which a crystalline clathrate containing the monomer still exists is far higher than the melting temperature of the pure guest. As a consequence, inclusion polymerization offers two definite advantages over common solid state polymerizations: it permits the use of simple monomers, widely used in other fields of polymer chemistry, and extends the range of experimental conditions 100 - 200 K above the temperature used for the polymerization of a given monomer in the solid state.

A topochemical condition for polymerization is the proper approach of successive monomers at the growing chain-end within the channels. In this respect, conjugated dienes like butadiene, isoprene, etc. possessing reactive atoms in terminal positions, are very suited to inclusion polymerization. However, even bulkier monomers such as substituted styrenes or methyl methacrylate can polymerize if the space available inside the channels permits a favorable orientation and/or conformation of the monomer. The most studied examples are: butadiene, vinyl chloride, bromide and fluoride, and acrylonitrile in urea; 2,3-dimethylbutadiene and 2,3-dichlorobutadiene in thiourea; butadiene, isoprene, cis- and trans-pentadiene, trans-2-methylpentadiene, ethylene and propylene in PHTP; butadiene, cis- and trans-pentadiene, cis- and trans-2-methylpentadiene in DCA and ACA; butadiene, vinyl chloride, 4-bromostyrene, divinylbenzene, acrylonitrile and methyl methacrylate in TPP.

The common method for inducing polymerization in clathrates is their exposure to high-energy radiation. Generally, when a preformed clathrate is irradiated, radicals deriving from both host and guest are produced. In the case of PHTP a different process can be used, that of irradiating the pure host and the subsequent inclusion of the monomeric guest; in this way, at the start only radicals derived from the host are present. As we shall see later, polymerization proceeds by a living radical mechanism, thus permitting the formation of block copolymers by subsequent inclusion of two monomers in the same host.

The most notable feature of inclusion polymerization is the high degree of constitutional and steric control found for many host-guest systems. This is particularly true for urea, thiourea, PHTP and TPP on one side, and diene monomers on the other. For instance, butadiene, 2,3-dimethylbutadiene, trans-pentadiene, trans-2-methylpentadiene give 1,4-trans crystalline polymers; polypentadiene and poly-2-methylpentadiene, which possess an asymmetric carbon atom in every monomeric unit, are highly isotactic. A notable exception, which will be discussed later, concerns isoprene. For other hosts, like DCA and ACA, structural control is lower and strongly dependent on the bulkiness of the monomer and on the presence of additives.

PHTP is a chiral host which can be resolved into enantiomers; DCA and ACA are (or derive from) naturally occurring optically active compounds. Using these hosts inclusion polymerization can be performed in a chiral environment and can be used for the synthesis of optically active polymers. This line of research has been very fruitful, both on the synthetic and on the theoretical plane. It has been ascertained that asymmetric inclusion polymerization occurs by a "through space" and not by a "through bond" induction: only steric host-guest interactions (physical in nature) and not conventional chemical bonds are responsible for the transmission of chirality (10).

Stereochemical control extends to conformational aspects too. SAXS and DSC results are consistent with the presence of an extended chain macroconformation in some "native" polymers, i.e. in polymers extracted from the clathrate without dissolving or swelling (11,12).

All the important aspects of inclusion polymerization have been reviewed several times in recent years (3-6). Interested readers can refer to the literature cited in order to have a more complete knowledge of the specific examples. In the next pages, we shall discuss some points which have been recently developed in our laboratory.

An Electron Spin Resonance Study

The mechanistic study of a polymerization process generally requires the combined use of different methods. Among them we recall the determination of the chemical and stereochemical relationships between polymer and monomer structures, the detection of reactive intermediates and the kinetic approach. The first method has a wide application due to the quantity and quality of the possible information; it generally involves an NMR (or X-ray) analysis of products and reagents. Kinetics can hardly be applied to inclusion polymerization due to the high dispersion of experimental data. In the few cases where the detection of reactive intermediates can be successfully realized, a unique and deep knowledge of the intimate reaction mechanism has been obtained. ESR spectroscopy has sometimes been used for the study of radical polymerization in the crystalline solid state or in frozen solutions (13). In the field of inclusion polymerization an ESR study of the urea-butadiene system was reported a long time ago (14). PHTP offers two definite advantages over other hosts: the large number of monomers which can polymerize in its clathrates (a property related to the high flexibility of the crystal structure) and the possibility to perform polymerizations using a

preirradiated matrix and without subjecting the monomer itself to irradiation. The results we obtained can be summarized as follows (15):

1) the nature of radicals was determined at various stages of polymerization and under different conditions;

2) the living character of inclusion polymerization was definitely confirmed;

3) the way of insertion of unsymmetric monomers was established;

4) an indication on the conformational mobility of the chain end was obtained.

Irradiation of pure PHTP produces saturated hydrocarbon radicals which are stable for weeks and months; the spectral complexity is probably due to the presence of a mixture of different radicals. After monomer inclusion, the spectrum changes in a few minutes and converts to that of an allyl type radical. As an example, in the case of butadiene the spectrum recorded at room temperature consists of six lines, spaced 14 gauss, with the intensity ratio 1:5:10:10:5:1, in agreement with structure 1):

$$\underset{C1}{-CH_2}\overset{\alpha_1}{\underset{C2}{-CH}}=\overset{\alpha_2}{\underset{C3}{CH}}-\overset{\alpha_1}{\underset{C4}{CH_2}}\overset{\cdot}{} \qquad\qquad 1)$$

It is assumed that the five α_1 and β hydrogens are coupled with the unpaired electron by the same constant and that the α_2 hydrogen has a much smaller coupling constant owing to its lower spin density. The spectrum is temperature dependent: at $-150°C$ it appears as an ill-resolved curve, but reverts rapidly to the original shape at room temperature. This fact indicates a notable conformational mobility around the C1-C2 bond.

Isoprene, pentadiene, 2,3-dimethylbutadiene and 2-methylpentadiene give spectra corresponding to the following radicals (from 2 to 5) respectively) (Fig. 3):

$$\underset{C1}{-CH_2}-\underset{C2}{C}(CH_3)=\underset{C3}{CH}-\underset{C4}{CH_2}\overset{\cdot}{} \qquad 2) \qquad\qquad \underset{C1}{-CH_2}-\underset{C2}{CH}=\underset{C3}{CH}-\underset{C4}{CH}\overset{\cdot}{}(CH_3) \qquad 3)$$

$$\underset{C1}{-CH_2}-\underset{C2}{C}(CH_3)=\underset{C3}{C}(CH_3)-\underset{C4}{CH_2}\overset{\cdot}{} \qquad 4) \qquad\qquad \underset{C1}{-CH_2}-\underset{C2}{C}(CH_3)=\underset{C3}{CH}-\underset{C4}{CH}\overset{\cdot}{}(CH_3) \qquad 5)$$
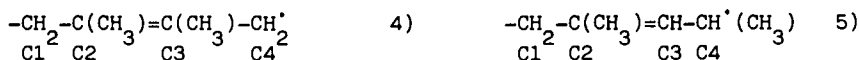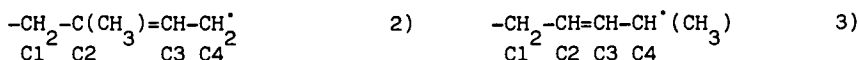
In all cases the spectrum does not change with temperature and

its multiplicity is one degree lower than expected. This fact is interpreted as evidence of restricted rotation around the C1-C2 bond inside the channel: in the frozen conformation one of the hydrogens, that marked by an asterisk in Fig. 4, is roughly perpendicular to the p orbital of the allyl system and does not give a significant coupling. Under this hypothesis, substitution of this hydrogen by a methyl group should not change the spectral multiplicity: this is exactly what happens during the polymerization of 2-cis,4-trans-hexadiene whose spectrum is indistinguishable from that of trans-pentadiene.

The stability of the radicals and the ease of formation of PHTP clathrates permits the realization of an unusual experiment. After recording the spectrum in the presence of a given monomer, the ESR tube is degassed and a second monomer is introduced. A fast transformation of the spectrum is observed and the new radical corresponds to that predicted for the second monomer. When this experiment is performed on a preparative scale, it leads to the formation of a block copolymer. This point is of crucial importance for an understanding of the reaction mechanism because it unequivocally proves the living radical nature of this polymerization. Radicals are not simply side-products formed during irradiation but are the true active chain-ends; they change with the change of the included monomer and are stable indefinitely.

ESR spectra of unsymmetric monomers like isoprene, pentadiene and 2-methylpentadiene indicate, within the limits of the method, the presence of only one (or of prevailingly one) of the two possible radicals, that originated by the 1,4 and not by the 4,1 insertion. As a rule, we can state that those radicals are preferentially formed which allow for extensive coupling with the hydrogens of the methyl groups, in other words those radicals that contain methyl groups bonded to C2 or C4 and not to C1 or C3. This finding has a direct implication on polymerization. In the case of pentadiene and of 2-methylpentadiene, both electronic and topochemical factors are in favor of a highly regular 1,4 insertion: the reactive chain-end consists of a secondary carbon (C4) and the monomer approaches with its less hindered side (C1). For isoprene, where the topochemical factors are less active, 1,4 insertion prevails, but a significant amount of the opposite 4,1 insertion is present, as revealed by NMR spectra.

Regioselectivity in Isoprene Polymerization

When isoprene was polymerized for the first time in PHTP clathrates, a 1,4-trans structure was assigned to the polymer on the basis of its IR spectrum (16). In spite of its high steric

purity and in contrast with samples obtained by other methods, it does not appear to be crystalline. This discrepancy was solved several years ago by examining the ^{13}C NMR spectrum (10,17): the presence of four signals in the saturated methylene region indicates the presence of head-to-head, tail-to-tail besides head-to-tail sequences. The two adjacent methylene carbons are anisochronous in head-to-tail sequences (they correspond to carbons C1 and C4) and isochronous (at least at the dyad level) for head-to-head (C1 and C1) and tail-to-tail (C4 and C4).

-CH$_2$-C(CH$_3$)=CH-CH$_2$-CH$_2$-C(CH$_3$)=CH-CH$_2$- DD dyad
$\quad\quad\quad\quad\quad\quad$ C4$\quad$ C1

$\quad\quad\quad\quad\quad\quad\quad\quad\quad\quad\quad\quad\quad$ head-to-tail
$\quad\quad\quad\quad\quad\quad\quad\quad\quad\quad\quad\quad\quad\quad$ junctions

-CH$_2$-CH=C(CH$_3$)-CH$_2$-CH$_2$-CH=C(CH$_3$)-CH$_2$- II dyad
$\quad\quad\quad\quad\quad\quad\quad$ C1$\quad$ C4

-CH$_2$-CH=C(CH$_3$)-CH$_2$-CH$_2$-C(CH$_3$)=CH-CH$_2$- ID dyad $\quad$ head-to-head
$\quad\quad\quad\quad\quad\quad\quad$ C1$\quad$ C1 $\quad\quad\quad\quad\quad\quad\quad\quad\quad$ junction

-CH$_2$-C(CH$_3$)=CH-CH$_2$-CH$_2$-CH=C(CH$_3$)-CH$_2$- DI dyad $\quad$ tail-to-tail
$\quad\quad\quad\quad\quad\quad$ C4$\quad$ C4 $\quad\quad\quad\quad\quad\quad\quad\quad\quad\quad$ junction
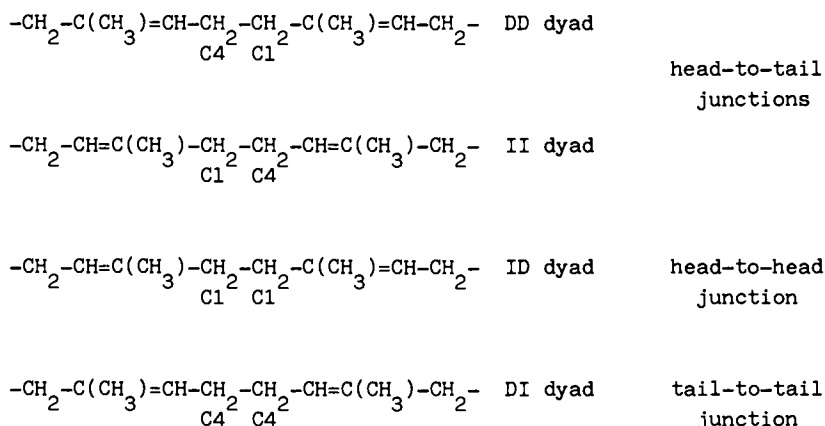
A quantitative determination of regioselectivity is carried out on this basis by using the experimental signal intensities. Nothing, however, could be inferred regarding the distribution of sequences from the analysis of the spectrum run at 25.2 MHz.

The improvement of resolution obtained at 50.3 MHz enabled us to investigate the polymer microstructure in greater detail (18) (Fig. 5). As was shown in our study on ^{13}C NMR spectra of 1,4-trans methylsubstituted polybutadienes, unsaturated carbons are in a more favorable position for examining sequences of three monomeric units. As a matter of fact, the signal of the olefinic C2 carbon of polyisoprene splits into four signals, falling between 134.9 and 135.2 ppm, thus indicating a triad sensitivity. The main peak, which is placed upfield, is clearly related to head-to-tail, head-to-tail sequences (ht,ht); the smallest, placed downfield, is unequivocally assigned to head-to-head, tail-to-tail (hh,tt) sequences. The two peaks of equal intensity placed in the middle belong to tt,ht and ht,hh sequences.
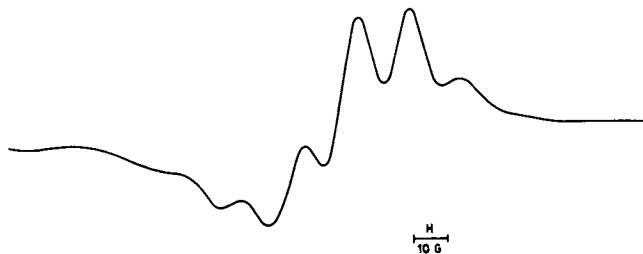
Figure 3. ESR spectrum of polypentadienyl radical included in PHTP.
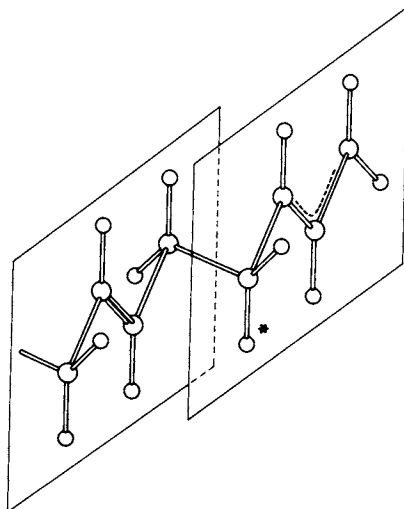
Figure 4. Structure of the growing radical.
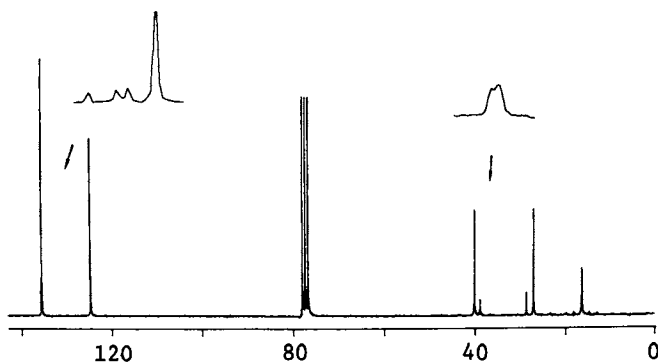
Figure 5. 50.3 MHz ^{13}C NMR spectrum of polyisoprene obtained in PHTP. Expanded spectra correspond to C2 (left, triad sensitivity) and C1 (right, tetrad sensitivity).

$$-CH_2-C(CH_3)=CH-CH_2-CH_2-C(CH_3)=CH-CH_2-CH_2-C(CH_3)=CH-CH_2-\quad\text{DDD triad}$$
$$thth$$

$$-CH_2-CH=C(CH_3)-CH_2-CH_2-C(CH_3)=CH-CH_2-CH_2-C(CH_3)=CH-CH_2-\quad\text{IDD triad}$$
$$hhth$$

$$-CH_2-C(CH_3)=CH-CH_2-CH_2-C(CH_3)=CH-CH_2-CH_2-CH=C(CH_3)-CH_2-\quad\text{DDI triad}$$
$$thtt$$

$$-CH_2-CH=C(CH_3)-CH_2-CH_2-C(CH_3)=CH-CH_2-CH_2-CH=C(CH_3)-CH_2-\quad\text{IDI triad}$$
$$hhtt$$
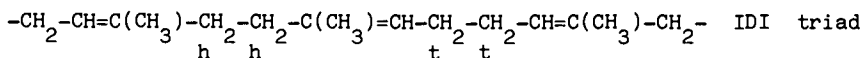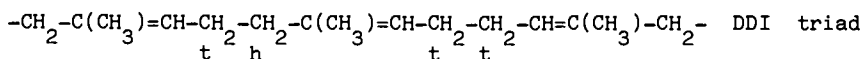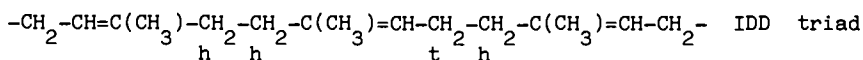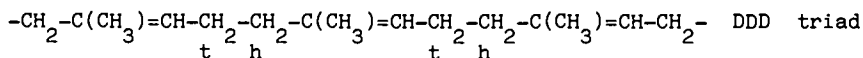
A statistical analysis of the sequence distribution can be performed in terms of direct and inverted units (D and I), i.e. of units written with carbon C1 at the left or at the right, respectively. Dyads DD and II, which differ in the sense of observation, correspond to head-to-tail, ID to head-to-head and DI to tail-to-tail junctions respectively. In the same way triads of D or I units are related to longer sequences. Remember that DDD and III, IDD and IID, DDI and DII, IDI and DID cannot be distinguished from each other. An interpretation according to a first-order Markov chain requires the use of two conditional probabilities, p_{ID} and p_{DI}; this scheme reduces to a simple Bernoulli distribution when $p_{ID} + p_{DI} = 1$. Equations giving the relative frequency of the various sequences are reported in Table 1. It should be pointed out that two solutions, in which the values of p_{ID} and p_{DI} are exchanged, are possible for this system. The choice of the correct value is not possible on statistical grounds only, but requires independent experimental data obtained, for example, from ESR analysis. The ESR spectrum of the growing chain-end in isoprene polymerization consists, as already explained, in an allyl radical with the unpaired electron delocalized on C2 and C4: $-CH_2-C(CH_3)=CH-CH_2^{\bullet}$, corresponding to a prevailing insertion of D (or 1,4) units. As a consequence, for our discussion we shall use a p_{ID} value greater than p_{DI}.

In the specific case of a polymerization carried out at $-40°C$ values of p_{ID} and p_{DI} are 0.806 and 0.103 respectively. As a first approximation, insertion of direct and inverted units follows a Bernoulli process ($p_{ID} + p_{DI} = 0.909$). Similar results were also obtained for the statistical analysis of inversion in poly-2-chloro butadiene (19) and in fluorinated polymers (20). However in our case a slight bias towards the formation of pairs of I units is systematically observed over the entire temperature range.

Table I. Probabilistic Relationships in Polyisoprene

$(ht) = DD + II = 1 - 2 \, p_{ID} \, p_{DI}/(p_{ID} + p_{DI})$

$(hh) = ID = (tt) = DI = p_{ID} \, p_{DI}/(p_{ID} + p_{DI})$

$(ht,ht) = DDD + III = 1 + p_{ID} \, p_{DI} - 4 \, p_{ID} \, p_{DI}/(p_{ID} + p_{DI})$

$(ht,hh) = IDD + IID = (tt,ht) = DDI + DII =$
$$= 2 \, p_{ID} \, p_{DI}/(p_{ID} + p_{DI}) - p_{ID} \, p_{DI}$$

$(hh,tt) = IDI + DID = p_{ID} \, p_{DI}$

$$p_{ID} = \frac{(hh,tt) + ((hh,tt)^2 - ((hh,tt) + (ht,hh))^2 (hh,tt))^{1/2}}{(hh,tt) + (ht,hh)}$$

$p_{DI} = (hh,tt)/p_{ID}$

A careful examination of the CH_2 region shows other elements useful for a structural investigation. When observed in well resolved spectra the head-to-head signal at 38.51 ppm splits into two peaks, which can be assigned to sequences of four monomeric units (see Fig. 5). Only three tetrads centered on a head-to-head (or ID) junction exist for polyisoprene: DIDD (or its equivalent IIDI), DIDI and IIDD. The last two are centrosymmetric (in their zig-zag planar representation) and each gives rise to a single signal for the central C1 carbons. The first is not symmetric and presents two heterotopic carbons. As a consequence, we can expect four signals at most. However, differences in structure are so far from the observed nucleus that some of the resonances are not resolved at 50.3 MHz. If we take into account only α', β and ε' contributions (in the sense indicated in a previous paper of ours) (17) we predict the existence of two signals only, one formed by the C1 carbon of the inverted unit (I) of tetrad DIDD and by the two equivalent carbons in the middle of DIDI tetrad, the other by the C1 carbon of the D central unit of DIDD and the two central carbons of IIDD.

The temperature dependence of the regioselectivity observed in isoprene inclusion polymerization was investigated between –60 and +70°C.   As expected, the number of defects increases with increasing temperature and ranges from 8 to 26%, expressed as fraction of inverted units. If we plot log p_{DI}/p_{DD} and log p_{II}/p_{ID}

vs. $1/T$ the difference in activation energy can be calculated for the insertion of an inverted unit with respect to a direct one, either when the growing radical is $D^{\bullet}$ or $I^{\bullet}$; E_a amounts to 4.5 and 3.9 kJ mol^{-1} respectively. The closeness of these values is again in favor of a roughly Bernoullian distribution of monomeric units.

The detailed analysis reported for polyisoprene was made possible by the extreme selectivity of polymerization in PHTP clathrates which inhibits the presence of any other structure, both at the constitutional (1,2 or cyclic units vs. 1,4) and at the steric level (cis vs. trans).

Copolymerization

Inclusion compounds allow the realization of copolymerization in the crystal state (1-6). This is a further difference with respect to typical solid state reactions. Both block- and statistical copolymers can be obtained: the former involves a two-step process, with subsequent inclusion and polymerization of two different monomers (21); the latter requires the simultaneous inclusion of two guests. This phenomenon has a much wider occurrence than thought at first, especially when a not very selective host such as PHTP is used. Research with this host started with mixtures of 2-methylpentadiene and 4-methylpentadiene, two almost exactly superimposable molecules (22), but was successfully extended to very dissimilar monomers, such as butadiene and 2,3-dimethylbutadiene.

When ternary clathrates form, the structural problem concerning the arrangement of guests in the channel remains undefined. From this point of view useful information can be derived just from copolymerization, which acts as an unconventional probe for structural analysis. If we admit that interchange between included monomers is slow, the sequence of monomer units in the copolymer corresponds to that of the guests in the channel before polymerization. The polymer chain behaves as a recording tape or a permanent copy of an otherwise elusive intermolecular arrangement (23).

The investigation carried out on homopolymerization and copolymerization of diene monomers included in PHTP allowed us to make evident that the same stereochemical control exists for the two processes (17,24). In both cases 1,4-trans units only are produced, thus permitting a straightforward sequential analysis. The only difference concerns regioselectivity, which is somewhat lower in copolymerization. For instance, poly(butadiene-co-pentadiene) contains 1 - 3% of head-to-head pentadiene-pentadiene dyads with adjacent tertiary carbons,

$-CH(CH_3)-CH(CH_3)-$, which are not detectable in the corresponding homopolymer. The disorder existing among the guests probably extends to the host lattice thus making it possible to generate small amounts of usually forbidden sequences.

The ^{13}C NMR spectra of diene homopolymers and copolymers were interpreted on the basis of a fully consistent set of additive parameters (17,24). The presence of methyl groups influences the chemical shift of the chain carbon atoms even when they are four or five bonds aways (δ and ϵ parameters). As a consequence the spectrum generally responds to the structure of triads of monomeric units, the unsaturated carbons often being more sensitive to the polymer microstructure than the saturated ones. The methyl spectrum is comparatively less detailed, in contrast with what happens in other known cases (polypropylene). As an example, poly(2-methylpentadiene-co-4-methylpentadiene) presents 16 signals at low field, corresponding to the eight triads observed on the C2 and C3 carbons (Fig. 6).

Quantitative spectra can give an estimate of the probability parameters according to the copolymerization theory. Poly-(2-methylpentadiene-co-4-methylpentadiene) possesses a Bernoullian distribution of monomer units, moreover polymer composition is the same as that of the monomer mixture used for the formation of the inclusion compound. It can therefore be considered as an ideal azeotropic copolymer. In other instances, we observed that $p_{AB} + p_{BA}$ is often lower than 1, (or that the product $r_A \cdot r_B$ is greater than 1). This fact indicates a tendency toward the formation of blocks of like units.

A single example of terpolymerization is known. It was performed using a PHTP clathrate containing pentadiene, 2-methylpentadiene and 4-methylpentadiene (24). Its actual formation was demonstrated by ^{13}C NMR: the spectrum can in the main be interpreted on the basis of the three known copolymers, but there are four signals that should be assigned to mixed triads. No indication of steric disorder has been observed in spite of the presence of three different guests in the same channel.

High Pressure Inclusion Polymerization

Finally, we wish to comment briefly on a recent development in inclusion polymerization. As already discussed, this reaction can be carried out on the pure clathrate or in the presence of an excess monomer. Consequently, the vapor pressure of a volatile monomer during polymerization ranges from the decomposition pressure of the clathrate to the vapor pressure of the saturated solution of the host in the guest, which is generally very close to that of the pure liquid monomer. For example, the vapor pressure

of pure butadiene, one of the most volatile guests, is 14 torr at -75°C, the temperature at which polymerization in urea is usually carried out, and 2520 torr at +25°C, as is more often used with PHTP. In these conditions decomposition pressure is only 605 torr and polymerization still occurs below the atmospheric pressure.

A different problem arises when simple monomers like ethylene and propylene are subjected to polymerization. All efforts made so far have been unsuccessful, mainly because the correct conditions for inclusion were not known and for the widely diffused erroneous opinion that these molecules cannot act as guests for structural reasons. We directed our work to a knowledge of the decomposition curve of their PHTP clathrates by assuming that the inclusion compound exists in the temperature range in which the equilibrium pressure of the solid phase is lower than that of the pure monomer.

For both guests the adduct has a definite existence and so conditions for polymerization could be determined (25).

We succeeded in polymerizing ethylene in PHTP in a steel tube at 20°C and 50 atm and propylene at 20°C and 10 atm. As far as we know these are the first examples of inclusion polymerization performed under high pressure.

Polypropylene obtained in PHTP is predominantly syndiotactic (26). Its microstructure was studied at the pentad level by NMR: stereosequence distribution agrees with a first-order Markov chain with the following parameters: p_{rm} = 0.238; p_{mr} = 0.437. ESR experiments combined with the synthesis of an isoprene-b-propylene copolymer indicates that even in the case of olefinic compounds inclusion polymerization proceeds by a radical mechanism. In the case of propylene this conclusion appears to be very peculiar, especially if compared with all the other polymerization methods known for this monomer.
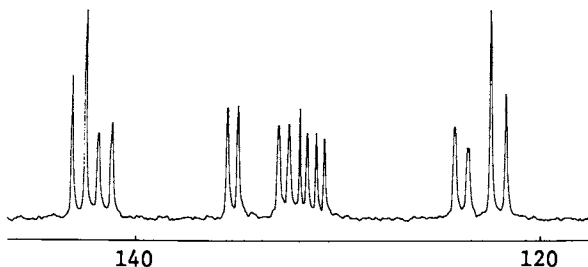
Figure 6.   25.2 MHz ^{13}C NMR spectrum of the unsaturated region of 50:50 poly(2-methylpentadiene-co-4-methylpentadiene) prepared in PHTP.

Acknowledgments

Literature Cited

1. Brown, J. F.; White, D. M. J. Am. Chem. Soc. 1960, 82, 5671.
2. White, D. M. J. Am. Chem. Soc. 1960, 82, 5678.
3. Chatani, Y. Progr. Polym. Sci. Japan 1974, 7, 149.
4. Takemoto, K.; Miyata, M. J. Macromol. Sci., Rev. Macromol. Chem. 1980, C18, 83.
5. Farina, M. Makromol. Chem. Suppl. 1981, 4, 21.
6. Farina, M.; Di Silvestro, G. "Polymerization in Clathrates" in "Encyclopedia of Polymer Science and Engineering" Wiley, J., New York, in press.
7. Weber, E.; Josel, H. P. J. Inclusion Phenomena 1983, 1, 79.
8. Farina, M.; Di Silvestro, G. Gazz. Chim. Ital. 1982, 112, 91.
9. Farina, M.; Di Silvestro, G.; Colombo, A. Mol. Cryst. Liq. Cryst. in press.
10. Sozzani, P.; Di Silvestro, G.; Farina, M. Makromol. Chem., Rapid Commun. 1981, 2, 51.
11. Chatani, Y.; Kuwata, S. Macromolecules 1975, 8, 12.
12. Farina, M.; Di Silvestro, G. Makromol. Chem. 1982, 183, 241.
13. Ranby, B.; Rabek, J. F. "ESR Spectroscopy in Polymer Research" Springer Verlag, Berlin, 1977.
14. Ohmori, T.; Ichikawa, T.; Iwasaki, M. Bull. Chem. Soc. Japan 1973, 46, 1383.
15. Sozzani, P.; Di Silvestro, G.; Gervasini, A. J. Polym. Sci. Polym. Chem. Ed. 1986, 24, 815.
16. Farina, M.; Natta, G.; Allegra, G.; Löffelholz, M. J. Polym. Sci. 1967, C16, 2517.
17. Sozzani, P.; Di Silvestro, G.; Grassi, M.; Farina, M. Macromolecules 1984, 17, 2532.
18. Di Silvestro, G.; Sozzani, P.; Farina, M. to be published.
19. Coleman, M. M.; Tabb, D. L.; Brame, E.G. Rubber Chem. Technol. 1977, 50, 49.
20. Cais, R. E.; Sloane, N. J. A. Polymer 1983, 24, 179.
21. Farina, M.; Di Silvestro, G. J. Chem. Soc., Chem. Commun. 1976, 816.
22. Farina, M.; Audisio, G.; Gramegna, M. T. Macromolecules 1972, 5, 617.
23. Farina, M.; Di Silvestro, G.; Sozzani, P. Mol. Cryst. Liq. Cryst. 1983, 93, 169.
24. Sozzani, P.; Di Silvestro, G.; Grassi, M.; Farina, M. Macromolecules 1984, 17, 2538.
25. Di Silvestro, G.; Sozzani, P. unpublished results.
26. Di Silvestro, G.; Sozzani, P.; Farina, M. A. C. S. Polymer Preprints, 1986, 21, 92.

Chapter 7

Design of a Solid-State Reaction

Crystal Structure and Solid-State Polymerization of Bis(propiolato)tetraaquozinc(II)

C. A. Booth, Bruce M. Foxman, and J. D. Jaufmann

Department of Chemistry, Brandeis University, Waltham, MA 02254

The structural literature may be used as a predictive database for the design of solid state polymerization reactions. Consideration of (a) the packing of molecules in the crystal structure of bis(acetato)-traaquonickel(II) and (b) a proposed similarity in the packing requirements of acetate and propiolate moieties suggested the synthesis of a set of phases $M(H_2O)_4(HC{\equiv}CCOO)_2$, (M=Zn, Ni, Co). The crystal structure of one of these phases (M=Zn) was determined by single crystal x-ray diffraction techniques. It contains an infinite chain of relatively short acetylene-acetylene contacts. Upon x- or γ-irradiation, the Zn salt undergoes a solid phase polymerization to the analogous polypropiolate.

In an extensive study of the preparation and solid-state reactivity of square-planar NiX_2L_2 complexes (X=Cl,Br,I,NCS; L=P(CH_2CH_2CN)_3) it was found that nearest-neighbor interactions, nucleation, temperature, doping, polymorphism and crystal symmetry greatly influence the course of the observed thermal solid state polymerization reactions (1-5). Recently we have begun to examine other materials which undergo solid state polymerization, in particular metal salts and complexes of α,β-unsaturated carboxylic acids. In these latter materials we have sought, first through an examination of the structural literature, and then by planned syntheses and crystal growth, to "design" phases which might exhibit solid state reactivity. Further goals, once the "design" experiment has been successful, are to establish the structure-reactivity relationships (within single crystals) for a broad class of compounds, and ultimately to illustrate to what degree the reactant lattice influences the chemical and/or crystallographic nature of the product.

Although the solid state reactivity of one class of metal-carboxylic acid complexes--those of acrylic acid and methacrylic acid--has been known for some time (6), little convincing information exists as to whether the structural basis for reactivity can be

developed along lines analogous (or identical) to those stated in the topochemical postulate (7). The simple existence of short contacts is clearly an insufficient criterion for the onset of solid state reactivity (8,9). However, a definitive predictive rationale for the reactivity of these phases has not yet appeared. It is likely that such factors as the relative orientations of potentially reactive acrylate and methacrylate planes must also be taken into account. Progress in this area has been slow owing to the unavailabilty of structural data and to the poor crystallinity of many of the monomer phases.

We began the present work with the desire to obtain knowledge on the reactions of acetylenes in solids. Presumably, in many cases such reactions would lead to the production of the analogous poly-acetylenes, although this is by no means always the case. The present report is a detailed experimental account of the synthesis and solid state reactivity of one member of a growing family of metal salts and complexes of propiolic acid, $HC \equiv CCOOH$. We began this work with a knowledge that such salts exhibited solid state reactivity (10), but also with the knowledge that there was no structural rationale for this reactivity. At the outset we sought a method for producing a phase which might have parallel acetylene moieties as well as short (approx. 4.0 Å) contacts between the acetylenes. This simple, straightforward methodology depended, however, on our finding a suitable model phase in the structural literature upon which to base the probable packing of (at least a limited set of) metal propiolates. Inspection of the literature did not reveal the existence of a suitable molecule isosteric to propiolic acid. We thus hypothesized that acetate and propiolate might have similar (though not identical) packing requirements, and a literature search and analysis suggested that bis(acetato)-tetraaquonickel(II) would meet our requirements (see Figures 1-3). Here we review the process by which that phase was selected, so that such principles might be used in other examples.

Finally, since the methodology outlined above led to the straightforward production of a reactive crystalline phase, it seemed possible that many propiolate materials would form high quality single crystals. Access to such phases would allow the determination of a number of crystal structures of the reactive materials. From the thus-generated structural information, a set of criteria for the reactivity of monoacetylenes in solids might be expected to emerge. Before we began this work, no such criteria existed; herein we describe the structural basis for the reactivity of solid bis(propiolato)- tetraaquozinc(II). The complete characterization of the products of this reaction as well as those of reactions of other metal propiolates is underway at the present time, and will be described in detail elsewhere.

<u>Experimental</u>

The title complex was prepared by adding ZnO (1.0 g., 12 mmol) to a solution of propiolic acid (1.72 g., 25 mmol, Aldrich) in 20 mL water. The solution was stirred for 30 minutes, and then filtered through celite to remove any unreacted oxide. The solution was allowed to evaporate in the hood over a two-day period, and the crystalline product was then collected and dried in air. The
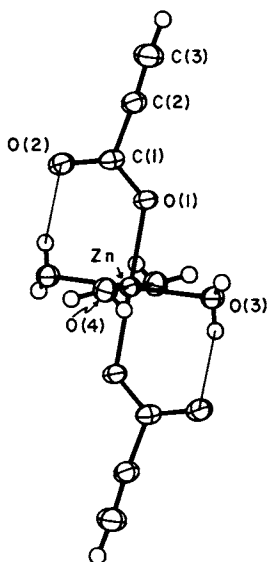
Figure 1. Molecular structure of bis(propiolato)tetra-
aquozinc(II)   (60% probability ellipsoids are shown for atoms
refined using anisotropic temperature factors; H atoms have been
assigned arbitrary temperature factors).
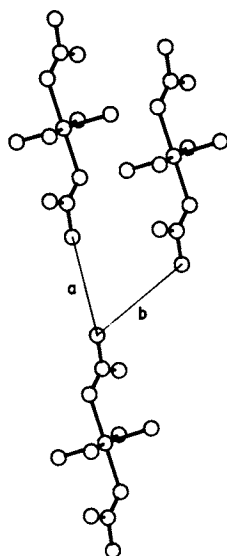
Figure 2. Three molecules of bis(acetato)tetraaquonickel(II),
showing important intermolecular contacts.
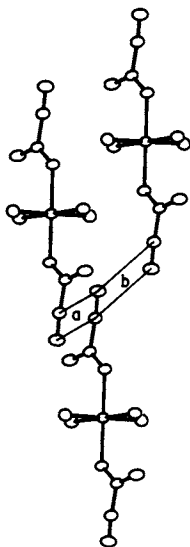
Figure 3. Three molecules of bis(propiolato)tetraaquozinc(II),
showing important pairs of 1,2-acetylene-acetylene contacts.

material was protected from unnecessary exposure to light. Growth
of large single crystals was facilitated if a smaller amount (5-10
mL) of water was used in the above preparation.

A preliminary x-ray photographic examination of a crystal of the
zinc complex showed it to be of excellent quality, and Weissenberg
photographs (0kl, 1kl; 0k0 absent for k=2n+1, h0l absent for
h+l=2n+1) led to a unique choice of $P2_1/n$ as the space group. It
was also noted at this time that the nickel and cobalt complexes,
prepared in a similar manner, were isomorphous to the zinc complex.
Strict isomorphism (11) was confirmed later by both x-ray powder and
single crystal measurements.

The crystal was then transferred to a Supper No. 455 goniometer
and optically centered on a Syntex $P2_1$ diffractometer. Most
operations on the diffractometer were carried out as described
previously (12); other operations are described below. The
analytical scattering factors of Cromer and Waber were used; real
and imaginary components of anomalous scattering were included in
the calculations for the Zn atom (13). Time-dependent decay was
observed in the standard reflections during data collection.
However, no correction for decomposition was applied to the data
since recollection of a small number of intensity data well-
dispersed in reciprocal space indicated that decomposition was not
isotropic, and hence a simple correction could not be made (14).
Further, even more complex forms of decomposition corrections could
not explain the observed intensity changes. It thus seemed best to
allow this systematic error to remain in the data, rather than to
introduce additional errors. In this crystal the maximum decay was
small but nevertheless significant; however, there were no unusual
features in either the final electron density difference map or the
thermal parameters (see Tables I and III). During exposure to x-
rays it was noted that the crystal became gradually darker, changing
from an initially colorless prism to yellow, brown, and finally a
deep brown-black. While this particular crystal was not subjected
to further analysis, other crystals of this material behaved
similarly under x-, γ- or UV irradiation. Product isolation was
carried out as described below. Details of the structure analysis,
in outline form, are given in Table I. Atomic coordinates appear in
Table II, while temperature factors appear in Table III.

Solid-state reactivity of bulk samples was monitored using 1-2
gram samples sealed in Pyrex ampoules at reduced pressure. The
ampoules were placed in an aluminum canister and lowered into a ^{60}Co
γ-irradiation source (Gammacell 220 Sealed Source Irradiator--Atomic
Energy of Canada Limited). Irradiation was carried out at room
temperature and at a nominal (uncalibrated) intensity of 1.32 x 10^5
R·min^{-1}. Samples were irradiated for periods of up to four weeks,
with portions being removed at various intervals. Partially
polymerized samples were extracted repeatedly with 10 mL (per gram
of sample) aliquots of absolute methanol; the methanol-insoluble
polymeric product remained behind, and was dried in air, weighed and
stored. Monomer recovered in this manner could be recrystallized,
and was shown to be chemically and crystallographically identical to
the original material. X-ray diffraction studies of the polymeric
product showed it to be amorphous. Proton and ^{13}C nmr spectra were
obtained on a Varian 300 Mhz nmr spectrometer.

Table I.   Data for the X-ray Diffraction Study of
$Zn(H_2O)_4(HC\equiv CCOO)_2$

(A) Crystal Data at $21(1)°C$.

Crystal system: monoclinic   Z = 2
Space group: $P2_1/n$ [C_{2h}^5 ; no.14]   Crystal Size: 0.80 x 0.20
a = 5.139(2) Å   x 0.20 mm.
b = 11.347(3) Å   Formula Wt : 275.4
c = 8.713(3) Å ρ_{obs} = 1.84(2)[b] $g \cdot cm^{-3}$
$\beta = 101.95(3)°$ ρ_{calc} = 1.84 $g \cdot cm^{-3}$
$V = 497.1 Å^3$ μ = 25.6 cm^{-1} ($Mo\bar{K}\alpha$)

Cell constant determination : 12 pairs of $\pm$(hkl) and refined 2θ, ω,
χ values in the range $30 \leq |2\theta| \leq 32°$ ($\lambda(Mo\bar{K}\alpha)$= .71073 Å)

(B) Measurement of Intensity Data

Radiation : $Mo\bar{K}\alpha$, graphite monochromator
Reflections measured: h, k, $\pm$l (to 2θ = 60°)
Scan type, speed : θ-2θ, 2.44-6.51°/min
Background measurement: stationary, for one-quarter of scan time at
                        each of scan limits
Scan range : symmetrical, $[1.6+\Delta(\alpha_2-\alpha_1)]°$
No. of reflections measured : 1621; 1460 in unique set
Standard reflections : 080, 013, 600 measd after each 55 reflcns;
                       decay 1.33, 1.04, 2.59% respectively
Absorption correction : empirical, using 200, 400, 600 reflections,
                        normalized transmission factors 0.709-1.000
Statistical information : R_s = 0.008; R_{av} = 0.019 (0kl reflections)

 (C) Solution and Refinement, with 1258 Data for which $F>3.92\sigma(F)$

Weighting of reflections : as before[c], p = 0.030
Solution : Patterson, difference-Fourier, routine
Refinement[d] : full-matrix least-squares, with
               anisotropic temperature factors for Zn, O, C atoms;
               isotropic temperature factors for H atoms;
               secondary extinction parameter, g = 1.75(7) x 10^{-7}
               R = 0.026 ; R_w = 0.036 ; SDU = 1.08
               R (structure factor calcn w/all 1460 reflcns) = 0.038
Final difference map : 1 peak, 0.60 $e^-/Å^3$ near Zn; other peaks
                       random and $\leq 0.34 e^-/Å^3$

---

[a] Equivalent positions : $\pm$ (x, y, z); $\pm$ (1/2+x, 1/2-y, 1/2+z); this
 is a nonstandard setting of space group $P2_1/c$.
[b] Measured by neutral buoyancy in CCl_4-$BrCHCl_2$.
[c] Foxman, B. M.; Mazurek H. Inorg. Chem., 1979, <u>18</u>, 113 and
 references therein.
[d] R_s = $\Sigma(\sigma(|F_o|)/\Sigma|F_o|$; R_{av} = $\Sigma|I-I_{av}|/\Sigma I$ R = $\Sigma||F_o|-|F_c||/\Sigma|F_o|$;
 R_w = $\{\Sigma w[|F_o|-|F_c|]^2/\Sigma w|F_o|^2\}^{1/2}$
 SDU = $\{\Sigma w[|F_o|-|F_c|]^2/(m-n)\}^{1/2}$ where m (=1258) is the number of
 observations and n (=91) is the number of parameters.

Table II. Atomic Coordinates for Zn(H$_2$O)$_4$(HC≡CCOO)$_2$[a]

Atom	x	y	z
Zn	0	0	0
O(1)	0.3245(2)	0.03101(12)	0.18667(13)
O(2)	0.2058(2)	0.20093(11)	0.28442(13)
O(3)	0.1883(2)	-0.15454(10)	-0.03685(14)
O(4)	0.2202(3)	0.09010(11)	-0.15299(14)
C(1)	0.3608(3)	0.11656(13)	0.2825(2)
C(2)	0.6070(3)	0.11620(14)	0.4020(2)
C(3)	0.7955(4)	0.1183(2)	0.5049(2)
H(C3)	0.949(5)	0.116(2)	0.583(3)
H(O3a)	0.092(6)	-0.177(3)	-0.116(4)
H(O3b)	0.223(5)	-0.197(2)	0.037(3)
H(O4a)	0.244(5)	0.147(3)	-0.118(3)
H(O4b)	0.364(6)	0.056(3)	-0.162(3)

[a]Numbers in parentheses in this and subsequent tables indicate estimated standard deviations in the least significant digit.

Results and Discussion

The molecular structure of the title complex is shown in Figure 1. The unidentate arrangement of carboxylate ligands found here is quite similar, as expected, to that found for bis(acetato)tetraaquo-nickel(II) and -cobalt(II) (15,16). As is observed in the latter complexes, the metal atom occupies a crystallographic center of symmetry. Important bond lengths and angles are presented in Table IV. The Zn-O bond lengths lie in the range observed for such distances in zinc acetate monohydrate (17) and dihydrate (18). The unbound carboxylate oxygen atom, O(2), participates in an intra- and intermolecular hydrogen bond (Table IV and Figures 1 and 4). The crystal structure thus consists of isolated octahedral zinc complexes interconnected by one weak C-H•••O and two strong O-H•••O hydrogen bonds.
    The particular aspect of the molecular packing to be considered here is that which is suggested to be of interest from the crystal structure of bis-(acetato)tetraaquonickel(II), shown in Figure 2. The a contact, 4.07 Å, is between centrosymmetrically related methyl groups, while the b contact, 4.55 Å, is between translation-related groups. If a propiolate complex of identical stoichiometry were to pack in a similar manner, we would expect to see these contacts occurring in pairs, and shorter contacts might be expected owing to the longer, more compact acetylene moiety replacing the methyl group. Admittedly, these arguments are far from rigorous, but as shown in Figure 3, they do have some validity. Here the a and b contacts are 3.57 and 4.02 Å, respectively, well within the criteria put forth by Schmidt. A reaction pathway of 1,2-additions can be imagined, with alternate a and b contacts being important. We note further that the center of symmetry-related pairs of a and b vectors are all rigorously parallel to one another. A view of these contacts projected down the crystallographic b axis, as well as a complete view of the hydrogen bonds which help to orient the molecules in the ac plane, are shown in Figure 4.

Table III. Thermal parameters for $Zn(H_2O)_4(HC{\equiv}CCOO)_2$ [a]

Atom	U_{11}	U_{22}	U_{33}	U_{12}	U_{13}	U_{23}
Zn	0.0239(2)	0.0177(2)	0.0207(2)	0.00082(8)	-0.00131(10)	-0.00130(7)
O(1)	0.0276(6)	0.0253(5)	0.0231(5)	-0.0005(5)	-0.0031(4)	-0.0056(4)
O(2)	0.0389(3)	0.0284(6)	0.0307(6)	0.0049(5)	-0.0068(5)	-0.0081(5)
O(3)	0.0297(5)	0.0188(5)	0.0265(5)	0.0020(4)	-0.0014(4)	-0.0006(4)
O(4)	0.0294(6)	0.0250(6)	0.0297(6)	0.0004(5)	0.0035(4)	-0.0004(5)
C(1)	0.0284(7)	0.0221(6)	0.0184(6)	-0.0041(5)	-0.0002(5)	0.0004(5)
C(2)	0.0321(8)	0.0243(7)	0.0259(7)	-0.0017(6)	-0.0004(6)	-0.0038(5)
C(3)	0.0358(9)	0.0356(9)	0.0336(8)	-0.0005(7)	-0.0061(7)	-0.0019(6)
H(C3)	0.064(8)					
H(O3a)	0.076(9)					
H(O3b)	0.055(7)					
H(O4a)	0.048(8)					
H(O4b)	0.063(8)					

[a]Anisotropic thermal parameters are of the form:
Exp$[-2\pi^2\{(a^*)^2 \cdot U_{11} \cdot h^2 + \ldots + 2b^*c^* \cdot U_{23} \cdot kl)]$
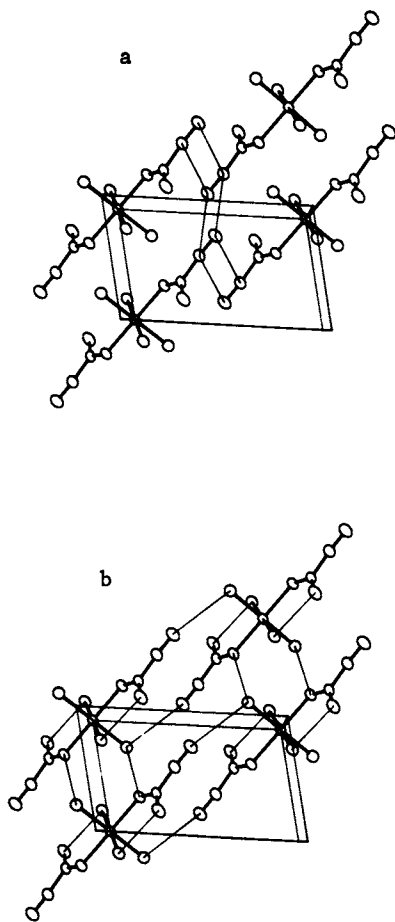
Figure 4. Two views of the crystal structure of bis(propiolato)-tetraaquozinc(II), showing (a) 1,2-acetylene-acetylene contacts; (b) inter- and intramolecular hydrogen bonding in the ac plane.

Table IV. Selected Bond Lengths (Å) and Angles (deg) in
$Zn(H_2O)_4(HC{\equiv}CCOO)_2$[a]

Zn-O(1)	2.104(1)		C(2)-C(3)	1.176(3)
Zn-O(3)	2.060(1)		C(3)-H(C3)	0.93(3)
Zn-O(4)	2.174(1)		O(3)-H(O3a)	0.80(3)
O(1)-C(1)	1.269(2)		O(3)-H(O3b)	0.79(3)
O(2)-C(1)	1.248(2)		O(4)-H(O4a)	0.72(3)
C(1)-C(2)	1.463(2)		O(4)-H(O4b)	0.85(3)
O(1)-Zn-O(3)	86.57(5)		O(2)-C(1)-C(2)	116.9(1)
O(1)-Zn-O(4)	88.01(5)		C(1)-C(2)-C(3)	175.7(2)
O(3)-Zn-O(4)	89.08(5)		C(2)-C(3)-H(C3)	176(2)
Zn-O(1)-C(1)	128.4(1)		H(O3a)-O(3)-H(O3b)	119(3)
O(1)-C(1)-O(2)	126.1(1)		H(O4a)-O(4)-H(O4b)	112(3)
O(1)-C(1)-C(2)	117.0(1)			

O(3)-H(O3a)$\cdots$O(2)[i]	2.687 Å	163.6°
O(3)-H(O3b)$\cdots$O(2)[ii]	2.707 Å	177.7°
O(4)-H(O4b)$\cdots$O(1)[iii]	2.781 Å	176.1°
C(3)-H(C3)$\cdots$O(4)[iv]	3.325 Å	157.7°

i $(\bar{x}, \bar{y}, \bar{z})$ iii $(1-x, \bar{y}, \bar{z})$
ii $(1/2-x, y-1/2, 1/2-z)$ iv $(1+x, y, 1+z)$

With increasing γ-irradiation, the IR spectrum of the monomer loses definition, and the C$\equiv$C absorption at 2090 cm^{-1} decreases in intensity; the IR spectrum becomes increasingly diffuse during the irradiation period. The visible spectrum consists of a broad absorption band from 340-520 nm, with $\lambda_{max} = 455$ nm. Owing to the low solubility of the irradiation product in water, it was necessary to dissolve the product in aqueous formic acid. It was thus difficult to obtain useful nmr spectra of the putative zinc poly-propiolate. The main feature in the spectrum of zinc polypropiolate is a broad signal at 130-139 ppm, which is in the region where α- and β-carbon resonances have been observed for poly(5-X-1-pentyne) (19). These values are also consistent with those reported by us for barium and strontium polypropiolates (20). It is expected that solid state ^{13}C nmr would yield improved spectra for the zinc phase, and plans to obtain such spectra are underway. Work on this and other solid-state polyacetylene syntheses is continuing in our laboratory.

Acknowledgments

Literature Cited

1. Cheng, K.; Foxman, B. M. J. Am. Chem. Soc., 1977, 99, 8102.

2. Cheng, K.; Foxman, B. M.; Gersten, S. W. Mol. Cryst. Liq. Cryst., 1979, 52, 77.
3. Foxman, B. M.; Gersten, S. W. Inorg. Chim. Acta, 1979, 33, L151.
4. Foxman, B. M.; Goldberg, P. L.; Mazurek, H. Inorg. Chem., 1981, 20, 4381.
5. Foxman, B. M.; Jaufmann, J. D. J. Polym. Sci., Polym. Symp., 1983, 70, 33.
6. Restaino, A. J.; Mesrobian, R. B.; Morawetz, H.; Ballantine, D. S.; Dienes, G. J.; Metz, D. J. J. Am. Chem. Soc., 1956, 78, 2939.
7. Cohen, M. D.; Schmidt, G. M. J. J. Chem. Soc., 1964, 1996; Hirshfeld, F. L.; Schmidt, G. M. J. J. Polym. Sci., Sect A, 1964, 2, 2181.
8. Shepherd III, J. W.; Foxman, B. M. Mol. Cryst. Liq. Cryst., 1986, 137, 87.
9. Kennard, C. H. L.; Smith, G.; Greaney, T. M.; White, A. H. J. Chem. Soc., Perkin Trans. 2, 1976, 302.
10. Davidov, B. E.; Krentsel, B. A.; Kchutareva, G. V. J. Polym. Sci., Sect C, 1967, 16, 1365.
11. Megaw, H. D. "Crystal Structures: A Working Approach"; Saunders: New York, 1973; p. 13.
12. Foxman, B. M. Inorg. Chem., 1978, 17, 1932; Foxman, B. M.; Mazurek, H. Inorg. Chem., 1979, 18, 113.
13. "International Tables for X-ray Crystallography" ; Kynoch Press: Birmingham, England, 1974; Vol. IV: (a) pp. 99-101; (b) pp.148-150.
14. Buckingham, D. A.; Clark, C. R.; Foxman, B. M.; Gainsford, G. J.; Sargeson, A. M.; Wein, M.; Zanella, A. Inorg. Chem., 1982, 21, 1986.
15. Van Niekerk, J. N.; Schoening, F. R. L. Acta Crystallogr., 1953, 6, 609.
16. Cramer, R. E.; Van Doorne, W.; Dubois, R. Inorg. Chem., 1975, 14, 2462.
17. Capilla, A. V.; Aranda, R. A. Cryst. Struct. Commun., 1979, 8, 795.
18. Van Niekerk, J. N.; Schoening, F. R. L.; Talbot, J. H. Acta Crystallogr., 1953, 6, 720.
19. Katz, T. J.; Ho, T. H.; Shih, N. Y.; Ying, Y.-C.; Stuart, V. I. W. J. Am. Chem. Soc., 1984, 106, 2659.
20. Booth, C. A.; Jaufmann, J. D.; Foxman, B. M. Polym. Prepr. (Am. Chem. Soc. Div. Polym. Chem.), 1986, 54, 206.

Chapter 8

Dynamics of Solid-State Polymerization

Paras N. Prasad

Department of Chemistry, State University of New York at Buffalo, Buffalo, NY 14214

This paper presents studies of solid state
polymerization aimed towards formulating a dynamic
model of reactivity in the condensed phase. Phonon
spectroscopy is successfully used to elucidate the
mechanism of lattice control of the reaction. Novel
concepts of phonon-assisted thermal and photochemical
reactions are introduced, supported by experimental
data. Non-linear laser spectroscopy is used to find
the importance of biexcitonic processes in
photopolymerization. Also, spectroscopic studies of
reactions in Langmuir-Blodgett films and at gas-solid
interface which produce ordered polymers are presented.

Polymerization in the solid state holds promise for making highly
ordered polymers by highly selective reaction pathways. In these
polymerization processes, the molecular rearrangement within the
constraints of the monomer crystal lattice plays an important role.
In many polymerization reactions, these molecular rearrangements
produce sufficient strain in the lattice to disrupt the crystal.
The result is a polycrystalline polymeric sample. An understanding
of the molecular mechanism of these arrangements in the solid phase
can be valuable in formulating conditions under which this strain
can be minimized or released for producing a defect-free ordered
polymer.
     The molecular rearrangements encountered in a solid state
reaction are governed not only by the static properties
(topochemical) of the lattice but also by the dynamical features of
the lattice. The molecular motions, also called lattice phonon
motions, describe the dynamical response of the lattice and can be
expected to play an important role in determining the reaction
course.
     The objective of our research is to incorporate the effect of
nature of molecular organization together with that of molecular
motions and develop a dynamic model of reactivity in the solid
phase. For this purpose, a comprehensive study of solid state

polymerization using various spectroscopic techniques, non-linear
laser spectroscopy as well as x-ray diffraction methods has been
conducted.

   To obtain information on the role of dynamics of molecular
motions in the reactive systems, the approach of phonon spectroscopy
is used. Phonons are low-frequency cooperative lattice vibrations
of a solid and, therefore, probe the lattice interactions and
dynamics directly. Phonons can be observed as optical transitions
in the Raman spectra and in the electronic spectra (in the latter as
a phonon side band). Some information regarding averaged
librational and translational phonon motions can also be obtained
from the rigid-motion analysis of the thermal parameters of x-ray
diffraction studies.

   In this paper, we show that phonon spectra can conveniently be
used to understand the mechanism of the lattice control of the
reaction. Phonon spectral study as a function of the reaction can
be used to identify any lattice intermediates as well as deduce the
mechanism of polymerization. Furthermore, it can also be used to
derive information on the extent of order in the polymer product.

   Next, we discuss the concept of phonon-assisted reactions. In
relation to thermal reactions, they can be assisted by phonon-mode
softening leading to large-amplitude overdamped oscillations. In
the case of a photochemical reaction, a strong electron-phonon
coupling can assist in polymerization. Then some non-linear
spectroscopic studies are discussed which illuminate on the
dynamics of photopolymerization process. Then follows a discussion
of results on reaction in a different kind of molecular assembly,
the Langmuir-Blodgett films. Finally, some gas-solid interface
reactions which produce polymers in a doped state are discussed.

Mechanism of the Lattice Control

A major thrust of this paper is the use of phonon spectroscopy to
investigate the dynamics of reactions in solids (1-3). The
information on optical phonon spectra is obtained by laser Raman
investigation in the low frequency region (10-200 cm^{-1}). We find
the phonon spectra very useful in investigating the nature of
lattice rearrangement during the reaction course. A clear example
of the application of Raman phonon spectra in understanding the
lattice rearrangement is provided by the photopolymerization of 2,
5-distyryl pyrazine in the solid state α-form (3). This is an
example of a "four-center type" polymerization of diolefins and can
be represented as (4)

2, 5-Distyryl pyrazine   Poly-2, 5-distyryl pyrazine
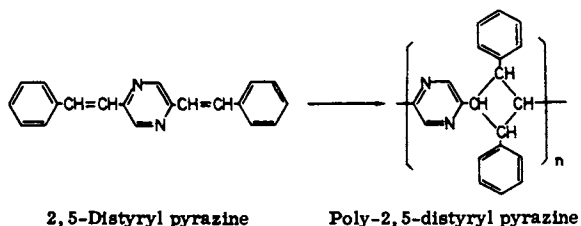
This reaction is ideally suited for the investigation of the mechanism of lattice control of reaction because a stepwise photoreaction can be used to stabilize the intermediate oligomer structures. The photoreaction can be started by using a long-wave length such as 476.5 nm from an argon ion laser. At this wavelength, the monomer absorbs but as the oligomers form, they do not absorb at this wavelength. Consequently, photoexcitation by 476.5 nm produces only finite chain oligomers. Then further photoreaction of the oligomers to produce the polymer was carried out with the 355 or 417 nm laser line from a Nd:Yag laser system.

    A comparison of the phonon spectra of the monomer, the oligomer, and the polymer under identical experimental conditions (temperature, laser power, spectrometer slits, etc.) is shown in Figure 1. It reveals that the phonon bands observed in the oligomer are considerably broader than those observed for both the monomer and the polymer. This result indicates the presence of a considerable amount of disorder in the oligomer lattice caused, possibly, by the lattice strain due to a substitutional disorder (presence of dimer, trimer, etc.). The phonon spectra show a continuous change in the frequency and the intensity of various bands as the oligomerization proceeds. As the oligomerization proceeds, the bands broaden and shift to lower values. These changes in the phonon spectra are representative of formation of a random solid-solution, and, thereby, of a homogeneous reaction mechanism. Our result also shows that at the start of this reaction, although the intramolecular vibration spectra show only a mild change, the phonon spectra change drastically. Since the intramolecular modes are more sensitive to chemical changes, our result suggests that there is an initial period in which a small amount of the product formed produces a substantial lattice rearrangement to facilitate further formation of the product. Hence, we find that the phonon spectrum is a sensitive probe for the molecular mechanism of reaction in the condensed phase. The Raman phonon spectra, monitored during the conversion of the oligomer to the polymer, show that initially the process starts homogeneously, with considerable lattice rearrangement. Then it turns heterogeneous, with a phase separation accompanied by a gradual ordering of the polymer product lattice.

    In our phonon spectral study of solid state reactions, both photochemical and thermal, we find (1,2) that many of them start as homogeneous process with random distribution of the product. However, as the product accumulates and creates strain, a phase separation occurs. The process then turns heterogeneous.

Concept of Phonon Assisted Reactions

Recently, we have introduced a new concept of phonon-assisted reaction (2). In other words, a reaction in the solid state can be assisted by these low frequency cooperative molecular motions. The concept of the phonon-assisted chemical transformation bears a direct analogy to that of a phonon-assisted physical transformation in solid. Important phonon interactions can be divided into two categories: (i) Anharmonic phonon-phonon interactions and (ii) electron-phonon interactions.
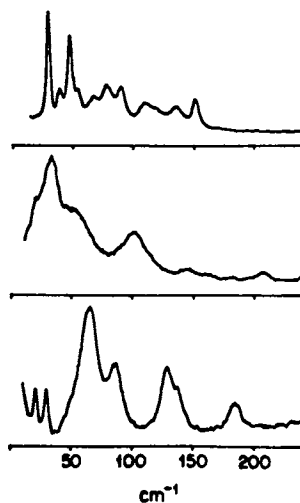
Figure 1. Raman phonon spectra of α-DSP monomer (top), oligomer
(middle), and polymer (bottom) at room temperature. The spectral
resolution is ca.1cm^{-1}.

One manifestation of the anharmonicity is the shift of phonon frequencies to lower values at higher temperatures. This shift is also accompanied by a broadening (or damping) of the phonon transitions at higher temperatures. In some cases the shift behavior, called mode softening, leads to an overdamped oscillation where the amplitude of the motion along the soft-mode coordinate is large. In a reactive system, large amplitude displacements, owing to mode-softening, are analogs of molecular collisions in a gas phase. Thus the mode-softening can be expected to assist in reactivity. The role of phonon mode-softening in a thermal reaction can easily be investigated by Raman spectroscopy if the soft mode is a Raman-active optical mode. The mode softening can be observed as a gradual shift of the phonon frequency to the zero value accompanied by a rapid broadening of the transition with the increase of temperature. Some information about the co-ordinate of the soft mode can be derived from the thermal motion anisotropy observed in the thermal parameters of the x-ray diffraction studies.

The electron-phonon interaction arises because the electronic potential is a function of intermolecular separation (2). Therefore, it is modulated by the intermolecular displacement occurring in a phonon motion. Photochemical aggregation reactions, such as dimerization or polymerization reactions, can be assisted by the occurrence of strong electron-phonon interaction in the reactive electronic state. This strong electron-phonon interaction creates a local lattice-deformation in the reactive (excited) electronic state. The deformation traps the electronic excitation and, at the same time, it may provide a local preformation of the product lattice if the distortion is along the reaction co-ordinate. Both these features assist a photochemical aggregation reaction. Depending on the strength of the electron-phonon coupling, one may observe the formation of a polaron or an excimer. The formation of a polaron does not lead to the loss of the identity of the monomer in the excited state, but simply the excitation is localized by local lattice-deformation. The excimer formation requires a severe distortion of the local structure which leads to an excited state dimer. It may also be pointed out that the polaron mechanism is a purely dynamic effect which can occur even in a defect-free lattice. In contrast, the excimer formation can occur either by a dynamic effect due to strong electron-phonon coupling or by a static effect due to sites deformed by the presence of defects.

The information on the formation of a polaron or an excimer is derived from the low temperature electronic absorption and emission spectra of the reactive crystals. The strong electron-phonon coupling in the reactive state manifests itself as a very strong phonon-side band in the liquid helium temperature spectra.

An example of the phonon assisted thermal reaction is the solid state thermal rearrangement of methyl-p-dimethyl aminobenzene sulfonate (MSE) which can be illustrated as follows (1):

$$(CH_3)_2 N - \!\!\bigcirc\!\! - SO_3-CH_3 \longrightarrow (CH_3)_3 \overset{+}{N} - \!\!\bigcirc\!\! - SO_3^-$$
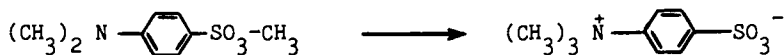
It involves an intermolecular rearrangement by migration of an ester methyl group from the oxygen atom of a MSE molecule to the nitrogen atom of the neighboring molecule in the b crystallographic direction along which the molecules are stacked. The reaction is greatly accelerated when temperature is raised above the room temperature. This thermal reaction requires a co-operative intermolecular transformation. Both the thermal nature and the co-operative behavior make this reaction suitable for testing the applicability of the model of a phonon-assisted reaction which involves an over-damped (soft-mode) oscillation. To investigate this possibility, a temperature dependence study of the phonon spectra was conducted. The 27 cm^{-1} (100k value) phonon revealed a mode-softening behavior (5).

For further confirmation of the mode-softening and a possible identification of the molecular nature of the over-damped mode, we used the rigid-body motion analysis of the thermal parameters of the room temperature x-ray diffraction study. A thermal-motion analysis (TMA) program was used to calculate the components of the librational (L) and the translational (T) tensors with a least-square fit of the published thermal parameters (6) of all non-hydrogen atoms of the molecule. The librational frequencies were calculated by the method of Cruickshank (7), using the appropriate eigenvalues of the L-tensor and the corresponding moments of inertia.

Using Cruickshank's formula, the calculated frequency of the largest amplitude libration is 23.5 cm^{-1} which compares favorably with the observed Raman frequency of 18 cm^{-1} soft mode at room temperature. Furthermore, the librational axis for the soft mode is perpendicular to the b-axis. Therefore, during this large amplitude libration, the reactive methyl sulfonate group and the neighboring dimethyl amino group come close together. As a result, softening of this libration would assist the rearrangement reaction. Our analysis of the x-ray diffraction thermal parameters along with the Raman phonon spectra, therefore, indicate this reaction to be phonon-assisted.

An example of phonon-assisted photochemical reaction is provided by the photodimerization of 2,6-dimethyl benzoquinone in the solid state. Our infrared spectral study of the reactant and the product dimer suggests that the following reaction occurs(8):
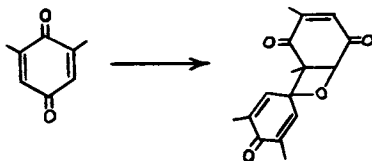
In order to investigate the phonon-assistance of the
photodimerization process, the electron-phonon coupling in the
photoreactive state ($^1n\pi^*$) was studied ($\underline{8}$). The electronic
absorption spectra of the monomer crystal were obtained ($\underline{8}$) at
cryogenic termperatures. At 6 K, a sharp zero-phonon transition at
19952 cm^{-1} is accompanied by a strong phonon side band which appears
to fit into a progression of a 65 cm^{-1} phonon. This study is
interpreted in terms of a selective and strong electron-phonon
coupling with a specific phonon mode which gives rise to the
formation of a polaron. Another example is provided by the four-
center type photopolymerization which in the crystalline state
describes the reaction of a group of compounds containing a
conjugated diolefinic group. By photopolymerization, the crystal
of the monomer is converted into crystals of linear polymer
containing cyclobutane rings. This reaction in case of 2,5-distyryl
pyrazine (DSP) has been discussed above. Another compound of this
class is 1,4-bis(β-pyridyl-2-vinyl)benzene (abbreviated as P2VB).
Two crystalline modifications of DSP are known, of which only the α-
form is photoreactive. Both α-DSP and P2VB are isomorphic. The
distance between the reactive double bonds of the neighboring
molecules in α-DSP is 3.939 A. This value for P2VB is shorter
(3.910 A). Therefore, one would expect P2VB to be more reactive
than α-DSP. Comparing the quantum yields listed by Hasegawa ($\underline{4}$),
the contrary is observed. This failure may be because the dynamic
nature of the lattice is not considered. Due to strong electron-
phonon coupling the excited state may have a different geometry
which may favor reaction in the case of α-DSP.
     The emphasis of our study was to examine if the differences in
their reactivities could be related to the differences in the
electron-phonon interaction in the excited states. A comparison of
the electronic absorption spectra of α-DSP and P2VB revealed that
the spectra of α-DSP consist of considerably broad bands (FWHH> 100
cm^{-1}) compared to those of the P2VB. This width is not due to
disorder, because the phonon spectra of α-DSP, at this temperature,
reveal a highly ordered lattice. We, therefore, conclude that this
large width is due to a strong electron-phonon coupling in α-DSP.
Hence, the photopolymerization in α-DSP is assisted by a strong
electron-phonon coupling. In contrast, the electron-phonon coupling
in the reactive excited state of P2VB is not so strong.

Non-Linear Laser Spectroscopic Studies

The dynamics of the photoreactive systems were investigated by two-
photon absorption processes. The photopolymerizable α-DSP system
was investigated by two-photon absorption process. For this process
a dye-laser pumped by the second harmonic of a Nd-Yag laser was used
to provide a tunable wavelength range from 600 to 700 nm. Even at

room temperature, a considerable amount of α-DSP fluorescence at the
blue shifted wavelength was observed indicating significant two-
photon absorption. However, no photoreaction was observed to take
place even for a long irradiation time of several hours. This
result in conjunction with the observation that the
photopolymerization of α-DSP is greatly reduced at lower temperature
leads us to propose that the reaction is biexcitonic. In other
words, the initial step is started by deformed excitations hopping
and coming next to each other. The kinetic scheme will be

$$A + h\nu \longrightarrow A^*$$
$$A^* + A^* \longrightarrow \text{photoreaction}$$
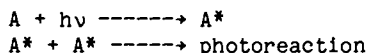
Such a mechanism would be consistent with the absence of reaction by
a two-photon absorption process, because such a process does not
produce excitons in high concentration and, therefore, reduce
biexcitonic process. The temperature effect is simply a
manifestation of reduced exciton hopping at lower temperature.

Polymerization in the Langmuir-Blodgett Films

Photopolymerization in the Langmuir-Blodgett films provides a method
to produce highly oriented monolayer films of polymers for
application in integrated optical and electronic devices. We have
studied the photopolymerization of several diacetylenes in the
Langmuir-Blodgett films (9,10); Here results from two such studies
will be presented.
     The amphiphillic diacetylenes of general formula
$C_mH_{2m+1}-C\equiv C-C\equiv C-(CH_2)_n-COOH$ form traditional mono and multilayer
Langmuir-Blodgett (L-B) films. Photopolymerization have been
observed in these L-B films to produce highly oriented polymer
films. Polymers formed in the L-B films are initially in a blue
form which is non-fluorescing. But subsequently they transform (by
heating) to a red form which is highly fluorescent (11,12).
     In our work, the technique of Raman optical wave guide was used
to study the structure of mono and multilayer L-B films of a
specific amphiphillic diacetylene with m=12 and n=8 in the above
general formula. The films were characterized by traditional force
area isotherms while on water subphase. Then molecular organization
in both mono and multilayer (successively dipped) films were
investigated by the resonance Raman optical wave guide method. For
these studies, we found it very convenient to use a cover glass
(average thickness 90-100μ) as a wave guide. The L-B films were
deposited on the cover glass and the light was coupled through the
use of a prism. In monolayer and successively dipped multilayer
studies, the resonance Raman spectra revealed only the
polydiacetylene transitions due to the C=C stretch at 1456 cm^{-1} and
that due to the C≡C stretch at 2081 cm^{-1}. We compared spectra of
the monolayer of polydiacetylenes formed in two different ways. In
the first case, the monolayer was photo-polymerized on the water
subphase and then transferred to the substrate. In the second case,
it was transferred first and then photopolymerized. In both cases,
we obtained identical resonance Raman spectra indicating same
molecular organization for the polymer. A comparison of the

spectra of a monolayer with that of a successively built multilayer
film revealed identical features with no shift in vibrational
frequencies. We, therefore, conclude that the molecular
organization in both the monolayer and multilayer films are the
same.

    The initially formed polymer film in both the monolayer and
multilayer cases is in the blue form. By heat treatment (or even
local heating by laser), the blue form transforms into the red form
which has reduced π-electron conjugation. In accordance with this,
the vibrational frequencies of both the -C=C- and -C≡C stretches
shift to high values at 1517 cm⁻¹ and 2119 cm⁻¹. The spectral
changes monitored as a function of the extent of conversion from the
blue to the red form reveal that as conversion proceeds the peaks
due to the blue form decrease in intensity while those due to the
red form grow in intensity. No frequency changes of the bands due
to the blue or red forms are observed in the intermediate conversion
range. Therefore, the process of the blue-to-red transformation in
the polymer is a heterogeneous two-phase process.

    Another system studied is a soluble polydiacetylene, poly -5,
7 dodecadiyn-1,12-bis(4-butoxycarbonylmethylurethane), commonly
known as poly-4-BCMU. Poly-4-BCMU has been a subject of
considerable recent interest because of its phase transition
behavior involving a transformation from the room temperature red
form to a high temperature yellow form both in the solution cast
film and in a toulene solution. The polymer formed by the solid
state polymerization is in the blue form.

    We have characterized both the monomer and the polymer
monolayer films by the force-area isotherm (13). The monomer (4-
BCMU) isotherm is found to be featureless, characteristic of an
expanded state of high compressibility. The film collapses at about
10 dynes/cm and 110Å²/molecule, in accordance with the Corey-
Pauling-Kaltung (CPK) space-filling molecular model. The
photopolymerization of the monomer yields a blue polymer film. In
contrast, the polymer film shows an unusual behavior. At a very low
surface pressure, it is in the yellow form, as characterized by its
visible absorption spectrum. As the film is compressed, the surface
pressure (π) vs. area per residue (Å²) isotherm of poly-4-BCMU shows
a distinct horizontal plateau characteristic of a two-phase, first-
order transition. During this plateau, the film starts turning red.
Films transferred to the substrate at the end of the plateau are in
the red form as confirmed by its visible absorption spectra. This
yellow-to-red transition we assigned as a monolayer to bilayer
transition. Using the Langmuir-Blodgett technique, therefore, we
have been able to prepare the polymer, poly-4-BCMU, films in all
three forms, blue, yellow and red.

Gas-Solid Interface Reactions

Gas-solid interface reaction can provide a simple method of
producing ordered polymers. In our laboratory, we have used
reactions with AsF₅ to produce polymers. The advantage of this
method is that it produces electroactive polymers (enhanced
electrical conductivity) in a doped state. The polymer formed,
however, generally contains disorder as revealed by their x-ray

powder diffraction (14). We have so far polymerized furil (14), azulene, and several diacetylenes. Polyazulene can also be formed by an electrochemical polymerization of azulene (15). However, polyazulene, electrochemically formed is amorphous.

A particularly interesting diacetylene is

$$CH_3(CH_2)_2-C\equiv C-C\equiv C-Hg-C\equiv C-C\equiv C-(CH_2)_2-CH_3.$$
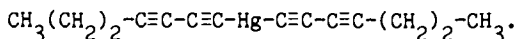
This material can be polymerized by u.v. radiation at a high temperature. We have found that in the solid state, it reacts explosively with AsF_5. However, the reaction can be controlled by mixing AsF_5 with argon and using this gas mixture to react slowly with the diacetylene. The IR spectra of the monomer, the photopolymerized product and the product formed by reaction with AsF_5 are compared in Figure 2. The IR spectra of the AsF_5 reaction product correlate with that of the polymer. In addition, it shows features due to the dopant confirming that the polymer is formed in a doped state.
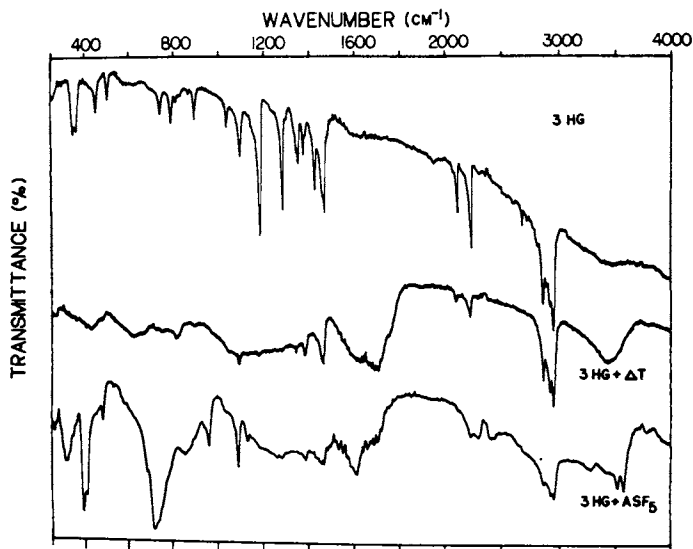
Figure 2. IR spectra of the diacetylene:
$CH_3(CH_2)_2-C\equiv C-C\equiv C-Hg-C\equiv C-C\equiv C-(CH_2)_2 CH_3$ (abbreviated as 3HG), thermally polymerized product ($3HG^2 + \Delta T$), and the product obtained by the gas-solid interface reaction with AsF_5.

Conclusions

Phonon spectroscopy has been found to be a powerful method to
investigate the reaction dynamics in solid state. Also, non-linear
laser spectroscopic study has been used to probe the dynamics of
photochemical reactions. Future directions are clearly a more
quantitative and theoretical formulation of the importance of energy
state dynamics in determining reactivity in the condensed phase.
Non-linear spectroscopy as well as time-resolved X-ray
crystallography using synchrotron radiation can be expected to
provide valuable approaches for future development of a dynamic
model of solid state polymerization.

Acknowledgment

Literature Cited

1.   Prasad, P. N.; Swiatkiewicz, J.; Eisenhardt, G. Applied
     Spectroscopy 1982, 18, 59.
2.   Prasad, P. N.; Swiatkiewicz, J.; Mol. Cryst. Liq. Cryst. 1983,
     93, 25.
3.   Swiatkiewicz, J.; Prasad, P. N. J. Polym. Sci. Polym. Phys.
     1984, 22, 1417.
4.   Hasegawa, M. In "Advances in Polymer Sciences; Springer-Verlag,
     1982, Vol. 42, p. 1.
5.   Dwarakanath, K.; Prasad, P. N. J. Am. Chem. Soc. 1980, 102,
     4254.
6.   Sukenik, C. N.; Bonapace, J.; Mandel, N. S.; Lau, P.-Y.; Wood,
     G.; Bergman, R. G. J. Am. Chem. Soc. 1977, 99, 851.
7.   Cruickshank, D. W. Acta Cryst. 1956, 9, 1005.
8.   Misra, T. N.; Prasad, P. N. Chem. Phys. Lett. 1982, 85, 381.
9.   McCaffrey, R. R.; Prasad, P. N.; Fornalik, M.; Baier, R. J.
     Polym. Sci. Polym. Phys. 1985, 23, 1523.
10. Burzynski, R.; Prasad, P. N.; Biegajski, J.; Cadenhead, D. A.
     Macromolecules (in Press).
11. Day, D.; Ringsdorf, H. Makromol. Chem. 1979, 180, 1059.
12. Olmsted, J.; III, J.; Strand, M. J. Phys. Chem. 1983, 87, 4790.
13. Biegajski, J.; Burzynski, R.; Cadenhead, D. A.; Prasad, P. N.
     (to be published).
14   Burzynski, R.; Prasad, P. N. J. Polym. Sci. Polym. Phys. 1985,
     23, 2193.
15. Burzynski, R.; Prasad, P. N.; Bruckenstein, S.; Sharkey, J.
     Synthetic Metals 1985, 11, 293.

<center>Chapter 9</center>

Interaction of Halogens with Single Crystals of Poly(1,6-di-*N*-carbazolyl-2,4-hexadiyne)

Daniel J. Sandman, B. S. Elman, G. P. Hamill, J. Hefter, and Christopher S. Velazquez

GTE Laboratories, Inc., Waltham, MA 02254

The reactions of macroscopic single crystals of poly-DCH with bromine and chlorine provide the first examples of reactivity of a polydiacetylene where the product is homogeneous by electron microscopy. Reaction conditions and product compositions are presented. Infrared and solid-state electronic spectroscopy, x-ray powder diffraction, scanning electron microscopy, and thermogravimetric analysis are techniques used to characterize the reaction products. The structures of the reaction products were deduced by ^{13}C CP-MAS NMR studies presented elsewhere. Bromination leads to a crystal-to-crystal transformation, and material which has gained 6 Br atoms per repeat unit was concluded to have a mixed polyacetylene structure. Poly-DCH and the bromination reaction products were characterized by static magnetic susceptibility, and possible structural origins for the paramagnetic species are presented. Mechanistic aspects of the interaction of bromine with the backbone are discussed and the possible involvement of conjugation defects (soliton-like species) is considered. Chlorination of poly-DCH results in amorphous solids where reaction has occurred primarily in the side chain. Experimental conditions under which poly-DCH crystals are inert to iodine are summarized, and comments are made on a recent reported reaction of iodine with poly-DCH.

The systematic chemical modification of a polymer, such as a polydiacetylene (PDA, *1*), which is crystallographically fully ordered, is of interest because such a process could lead to materials which might not be accessible by solid-state polymerization of relevant monomers. Because of their low solid-state ionization energies (*2*), PDA might be expected to undergo redox chemistry with reagents ("dopants") which render the partially crystalline polyacetylene $(CH)_x$, conductive. However, due to van der Waals tight-packed structures, the interaction of reactive gases and liquids with PDA crystals typically results in reaction only at crystal surfaces (*1a*).

Recently, we observed that the PDA from 1,6–di–N–carbazolyl–2,4–hexadiyne (*2a*), i.e., poly-DCH (*2*), reacts with assorted gaseous and liquid species to give modified materials which appear homogeneous on microscopic examination (*1*). Our studies to date of the interaction of chlorine, bromine, and iodine with single crystals of poly-DCH are presented herein.

Bromination of Poly-DCH

The bromination of poly-DCH is of interest because the degree of bromine uptake can be controlled, by choice of experimental conditions, between 3 and 8 Br atoms per polymer repeat unit and because a crystal-to-crystal transformation is observed. Scheme 1 summarizes the reactions of liquid bromine with poly-DCH. Interaction of poly-DCH crystals with dense vapors of bromine or cyanogen bromide for months did not lead to detectable weight gain. By contrast, DCH monomer (2a), which has a crystal structure similar to the polymer (6), readily reacts with bromine vapor to give an amorphous material which has gained ca 12 Br atoms per molecule.

Poly-DCH crystals which have gained 3–6 Br per repeat have a bronze appearance rather than the brassy appearance of the pristine polymer. A straw color is noted for the material which has gained 7–8 Br per repeat, and the solid-state spectrum of this material exhibits a broad shoulder at ca 450 nm, a shift to higher energy compared to poly-DCHBr$_6$ (1a), indicative of disruption of conjugation. When samples of poly-DCH which have 3–6 Br per repeat are treated with refluxing bromine, they are not converted to poly-DCHBr$_8$. Rather, they add sufficient bromine to approach the poly-DCHBr$_6$ composition.

The introduction of bromine into poly-DCH decreases the temperature at which weight loss begins in thermogravimetric analysis (TGA). While poly-DCH loses no weight below 450 °C, samples of poly-DCH which have gained 3.2 and 8 Br atoms per repeat have lost 20% of their weight at 400 and 410 °C, respectively. Parenthetically, during isothermal heating at 370 °C, samples of poly-DCH lose 55% of their initial weight within 6 hours.

X-ray powder diffraction of poly-DCHBr$_6$ reveals at least twenty reflections. From rotation photographs of these crystals (7), a repeat distance along the polymer chain of 4.75 Å may be deduced. Corresponding Weissenberg photographs reveal that the crystallites are well aligned in the chain direction, but are poorly correlated perpendicular to that axis. From such photographs and powder diffraction from oriented samples, the following lattice is deduced for poly-DCHBr$_6$: $\underline{a}$ = 14.21 Å; $\underline{b}$ = 4.75 Å; $\underline{c}$ = 20.67 Å; β = 106.8°; and V = 1328 Å^3. Compared to pristine poly-DCH (6), the $\underline{a}$ and $\underline{c}$ lattice constants reveal significant expansion. The disorder introduced by the bromination precludes a structure determination by crystallographic methods.

We therefore turned to spectral methods to determine the location of the Br atoms. Comparison of the out-of-plane aromatic CH deformation vibrations of pristine and modified poly-DCH in their FTIR spectra reveals that ring substitution has occurred. In the case of nitration (1a), comparison with a model molecular compound strongly indicated the expected (1a) 3,6 substitution. FTIR spectra of brominated poly-DCH which has gained 3–8 Br per repeat reveal strong absorption at ca 645, 795, 835, and 867 cm^{-1}. The 3,3',6,6' brominated DCH monomer 2b (8) exhibits IR absorption at 650, 720, 735, 785, 805, 835, 865, 885, and 830 cm^{-1}, while the octabromomonomer 2c (8) exhibits IR absorption at 645, 725, 795, 850, 860, 945, and 985 cm^{-1}. Hence, for brominated poly-DCH, the IR data are consistent with 3,6 carbazole substitution, but other more complex substitution pattterns cannot be ruled out. The IR data give no information on possible reactions involving the conjugated backbone.

The positions of Br addition to poly-DCH were deduced by a solid-state ^{13}C NMR study using cross-polarization and magic angle spinning (CP-MAS) techniques on the brominated polymers and model molecular compounds, including 2b and 2c (7–9). The studies indicate that for poly-DCHBr$_{3-8}$, the first process is bromination of the carbazole ring at the 3,6 positions. For poly-DCHBr$_6$, it was deduced (7–9) that the triple bond is converted to a brominated double bond, i.e., the PDA backbone is converted to a mixed polyacetylene structure; this conclusion is illustrated in Scheme 2.

The conversion of a PDA backbone to a mixed polyacetylene is without precedent and is of further interest. With one exception (10), in a monomer which also contains a diacetylene, it has not been possible to obtain fully ordered polyacetylenes by solid-state polymerization (3, 11, 12).

RCH₂

$$\left[\begin{matrix} RCH_2 \\ | \\ C - C \equiv C - C \\ | \\ CH_2R \end{matrix} \right]$$

1

a , R = N — Carbazolyl (**2a**)

R = CH₃—⟨benzene⟩—SO₂O —

2d

RCH₂C ≡ C — C ≡ CCH₂R

2

R =

a , X = Y = H

b , X = Br; Y = H

c , X = Y = Br

POLY-DCHBr₃₋₆ —→ $\frac{Br_2}{REFLUX}$ ✕ —→ POLY-DCHBr₇₋₈

Br₂

-5° TO 25°C

Br₂ OR
75% Br₂/CCl₄
REFLUX

POLY-DCH

Scheme 1.

6Br —→
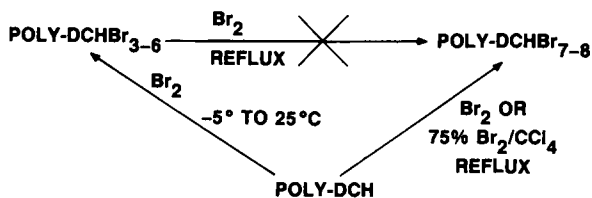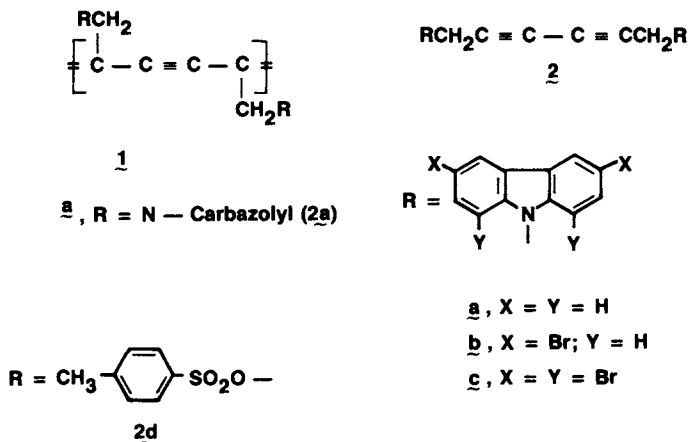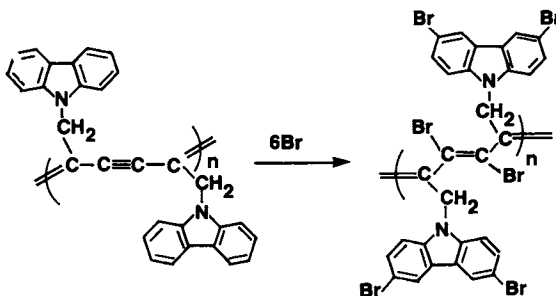
Scheme 2.

The Chlorination of Poly-DCH

We have found that poly-DCH may be chlorinated by liquid or gaseous chlorine, solutions of chlorine in dichloromethane, and by *aqua regia*. Poly-DCH is inert to refluxing thionyl chloride, and reaction with chlorine gas sufficient to introduce 6 Cl atoms per repeat unit leads to an inhomogeneous material.

The reaction products of chlorination are less well characterized to date than the brominated materials. The features that these reactions have in common are the largely amorphous nature of the product, the introduction of at least 10 Cl atoms per repeat unit, and the partial solubilization (complete in the case of *aqua regia*) of the reaction product. FTIR spectra clearly reveal substitution of the carbazole ring.

The product of the interaction of chlorine gas with poly-DCH was studied by scanning electron microscopy (SEM); our SEM studies of pristine and brominated poly-DCH were previously reported (1b). A sample at magnification 1500 is shown in Figure 1. Compared to pristine poly-DCH, Figure 1 reveals that a fibrous morphology is retained, but the fibers of the chlorinated polymer appear thicker and rougher than those of the reactant.

From a combination of ^{13}C CP-MAS studies (9) and mass spectrometry of soluble extracts, it appears that gaseous chlorine interacts primarily with the carbazole group. The NMR studies reveal the presence of the triple bond at 102 ppm, indicating preservation of the conjugated system, and broad resonances near 50 ppm, assigned to — CHCl — groups. Mass spectrometry of evaporated dichloromethane extracts reveals a 6 Cl isotopic cluster with a composition $C_{12}H_5NCl_6$, which requires chlorine addition to the ring and loss of aromaticity. The FTIR spectra of the products of chlorination by the gas and the chlorine solution in dichloromethane are indistinguishable.

Aqua regia is primarily a chlorinating agent, in that the product has gained 12 Cl atoms per repeat unit. The FTIR spectrum and elemental analysis indicate that some degree of ring nitration occurs. The reaction product is soluble in dimethylformamide.

Poly-DCH was inert to nitrosyl chloride in both liquid and vapor phases.

Iodine and Poly-DCH Single Crystals

Given the reactions described above for poly-DCH with chlorine and bromine, it is natural to seek reactivity with iodine. In the course of the above work, we had noted that poly-DCH single crystals were inert to iodine vapor at 20 °C and to heating with a ten-fold molar excess of iodine at 125–130 °C for 16 hr.

It was recently (13) observed that single crystals of the PDA from the bis –p-toluenesolfonate of 2,4–hexadiyne–1,6–diol (PTS, 2d), held at 100 °C for 14 days in an apparatus similar to that used for graphite intercalation, react with iodine vapor to give a material with a room-temperature dc conductivity in the range 10^{-4} to 10^{-2} Ω-cm^{-1}. We found that poly-DCH is inert to iodine vapor under those conditions, and that poly-DCH kept at 200 °C for 7 days did not react with iodine heated to 80 °C, as judged by lack of weight gain and no observed change in the FTIR spectrum.

In view of the above observations, we were surprized to learn that "single crystals" of poly-DCH, prepared by thermal polymerization, reacted with molten iodine at 140 °C to give a material with a room-temperature dc conductivity of ca 10^{-3} Ω-cm^{-1} (14). The obvious remark to make is that it is firmly established that thermal polymerization of DCH results in a fibrous polymer which is not a single crystal, due to separate nucleation of polymer domains (5a). Earlier, we had noted a difference in reactivity toward antimony pentahalides between thermal and gamma-radiation polymerized DCH (3). We have observed that single crystals of poly-DCH are inert to iodine under the conditions reported (14), as judged by a lack of weight gain and an FTIR spectrum indistinguishable from that of poly-DCH.

Static Magnetic Susceptibility of Brominated Poly-DCH

These studies were undertaken to gain initial information concerning the concentration and nature of the magnetic species involved in the reactions of the conjugated backbone. Data were taken over the temperature range 6–300 K, and, since the materials were found to be largely diamagnetic, data processing followed a Curie law treatment for the molar susceptibility (χ_m = A + C/T). Table I lists values of A and C for poly-DCH and samples which have gained ca 6 or 8 Br atoms per repeat, as well as a sample of thermally polymerized PTS *(2d)*.

Table I. Static Susceptibility of PDA Materials

PDA	A × 10^6 (emu)	C × 10^6 (emu/K)
PTS	– 190.3	92.4
DCH	– 239.9	162.4 – 494.5
DCHBr$_6$	– 411	1535 – 3258
DCHBr$_8$	– 443	815 – 1404

Satisfactory agreement was noted between the observed values for core dia-magnetism (A) in Table I and those estimated from Pascal's constants for the PDA repeat unit. The data for poly-DCHBr$_6$ indicate a concentration of spin 1/2 species of ca 10^{21} per mole.

Compared to poly-PTS, we infer that the bulk of the paramagnetic term for poly-DCH arises from paramagnetic defects associated with radiation damage caused by the gamma radiation used to produce single crystals. Derivative to our deduction that poly-DCHBr$_6$ has a mixed polyacetylene structure, it is possible that the bulk of the paramagnetism in this material is associated with conjugation defects (15), as illustrated in Figure 2, where A is the alkylcarbazole chain and B is Br. The g-value (g = 2.023) of electron-spin resonance spectra (1b, 16) of these materials indicates the involvement of bromine with the unpaired electron.

From a consideration of the defects in Figure 2 as they relate to the product struc-ture in Scheme 2, it is possible to describe the mixed polyacetylene case as an alter-nating copolymer of AC=CA and BC=CB, or a homopolymer of AC=CB. The latter situation invites a synthetic experiment, that is, the attempted solid-state polymeriza-tion of N–(3–bromo–2–propynyl)carbazole (17). We have isolated this compound in two polymorphic forms. Both forms are melt-stable, but undergo reaction upon exposure to ^{60}Co gamma radiation. Characterization of the reaction products has been initiated.

Mechanistic Aspects of Reaction on the Conjugated Chain

The experiments summarized above for reactions of bromine with poly-DCH indicate that bromine has reacted with the PDA chain in the formation of the materials which have gained ca 6 or 8 Br atoms per repeat. It is thus appropriate to inquire into the types of mechanistic processes which might be involved, and three possibilities come to mind. They are (1) reaction via electron transfer, (2) the "classical" addition mechanisms, and (3) reaction via conjugation defects.

Possible electron transfer processes merit discussion, a priori, because of the relatively low solid-state ionization energy of the PDA backbone (2) and the strong acceptor character of bromine. Since the resultant products of bromination are largely diamagnetic, a long-lived electron transfer product is not involved. Moreover, when the bromination reaction is monitored by electron-spin resonance (1b), no buildup of a paramagnetic species was noted. In view of these observations, reaction via electron transfer as a major process is ruled out.
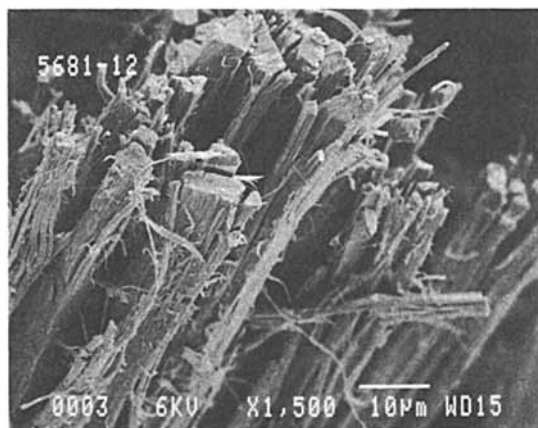
Figure 1. SEM of chlorinated poly -DCH (gain of *ca* 12 Cl per repeat unit), 1500X.

"AB" DEFECT

"BB" DEFECT

SIMILARLY, "AA" DEFECT
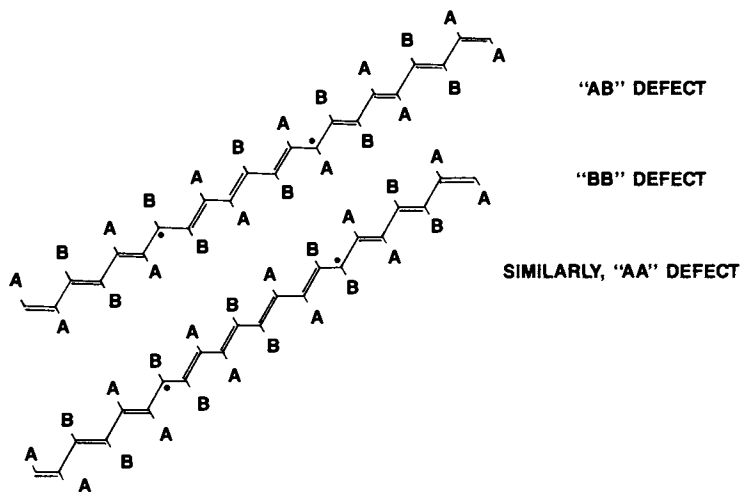
Figure 2. Representation of conjugation defects in a mixed polyacetylene.

By "classical" addition mechanisms, we include the large number of mechanisms advanced to date to rationalize various aspects of the bromination of double and triple bonds. The major reaction deduced thus far, conversion of the triple bond to a dibromo double bond, could be a very localized process. Yet the triple and double bonds of the backbone are in an extended conjugated system and do not have the energetics of the isolated systems. It is not possible to rule out such mechanisms at present.

A discussion of possible involvement of conjugation defects in PDA reactions is motivated by the voluminous literature involving such species ("solitons") in the redox chemistry of polyacetylene (15). Conjugation defects in PDA have been discussed (4, 18, 19) and may involve both neutral and charged species (4). The most widely discussed PDA defect contains $4n + 2$ carbons, n an integer, of the backbone involving two double bonds and a triple bond for the $n = 1$ case. Redistribution of electron density in the six-carbon defect can lead to a four-carbon defect. Other types of defects are conceivable (20). A plausible reaction pathway leading from the six-carbon defect in its neutral form to poly-DCHBr$_6$ is given in Figure 3. It is readily apparent that reaction of the 1 and 6 carbons of this defect with a Br moiety would disrupt the conjugated system. This situation could be relevant to poly-DCHBr$_8$ formation.

Summary

We have described herein the first chemical reactions involving macroscopic PDA crystals leading to homogeneous products when examined by the electron microscopy. In their initial stages, the reactions of chlorine and bromine with poly-DCH are anisotropic and involve the carbazole side chain. For the case of bromination, a crystal-to-crystal transformation is observed, and reactivity of the conjugated backbone, deduced from solid-state ^{13}C NMR studies presented elsewhere, involves conversion of the PDA structure to that of a mixed polyacetylene. Possible structural origins for the paramagnetic species in poly-DCHBr$_6$ include soliton-like species. A consideration of mechanistic aspects of the reaction of the conjugated backbone leads to the suggestion that conjugation defects may play a role in these reactions.

Experimental Section

General. Elemental analyses were performed by Schwarzkopf Microanalytical Laboratory, Woodside, NY. Thermogravimetric analysis (TGA) was performed on a DuPont 950 instrument in a nitrogen atmosphere at a heating rate of 20 °C per minute. Diffuse reflectance was recorded using 1 %-by-weight dispersions in sodium chloride on a Varian Cary 17 instrument. Electron microscopy was performed on a JEOL JSM-840 II analytical SEM using an electron-beam accelerating voltage of 6 kV. A Nicolet Fourier transform instrument was used to record spectra between 4000 and 400 cm^{-1}. The static susceptibility measurements were performed at the Francis Bitter National Magnet Laboratory at Massachusetts Institute of Technology using a SQUID device.

Interaction of Poly-DCH With Bromine at 25 °C. Poly-DCH (3) (0.139 g) was allowed to stand in liquid bromine (2 ml) at 25 °C for 24 hours. After isolation and vacuum drying, the material had gained 0.173 g in weight, corresponding to 6.3 Br atoms per repeat unit, and was copper in color. The FTIR spectrum revealed, *inter alia,* absorption at 867, 831, and 794 cm^{-1}. The x-ray powder diffraction of this material exhibited over 20 reflections, including strong ones at d = 6.96, 4.86, 4.14, 3.62, 3.53, 3.19, and 3.00 Å. The material had an electrical resistivity greater than 10^{10} Ω-cm.

Analysis. Calcd for $C_{30}H_{16}N_2Br_{6.3}$: C, 39.68; H, 1.82; N, 3.17; Br, 55.46. Found: C, 37.30; H, 1.45; N, 3.08; and Br, 58.80. The observed analysis corresponds to $C_{30}H_{14}N_{2.1}Br_{7.1}$.

Figure 3. Possible reaction pathway for backbone reactivity involving conjugation defects in poly-DCHBr₆ formation.

Interaction of Poly-DCH With Bromine at Reflux. Poly-DCH (121 mg) was heated at reflux with bromine (10 ml) for 23 hours. The resulting tan-straw-yellow material weighed 319 mg (163% weight gain, 8.3 Br per repeat). The FTIR spectrum exhibited absorption at, *inter alia*, 867, 833, and 796 cm⁻1. Reflections were observed at 7.06, 4.92, 3.66, 3.59, 3.21, 3.14, and 2.94 Å in x-ray powder diffraction. Diffuse reflectance revealed a shoulder at 450 nm and features in the ultraviolet similar to poly-DCHBr$_6$ (**1a**). TGA of this material reveals a 20% weight loss upon heating to 410 °C, while poly-DCH loses no weight below 450 °C.

Analysis. Calcd for $C_{30}H_{16}N_2Br_8$: C, 34.51; H, 1.55; N, 2.68; Br, 61.26. Found: C, 33.76; H, 1.49; N, 2.73; Br, 62.56. The observed analysis corresponds to $C_{28.8}H_{15.2}N_{2.0}Br_{8.03}$.

Interaction of Poly-DCH With Liquid Chlorine. To liquid chlorine (5 ml) was added poly-DCH (57.4 mg) and the mixture was kept in a dry-ice/acetone bath for 22 hours, after which the remaining liquid chlorine was swept into a trap containing aqueous NaOH. The resultant orange solid, found to be amorphous by x-ray diffraction, was washed with dichloromethane to give 107 mg of product. This FTIR spectrum of this material exhibited absorption, *inter alia*, at 1440, 1085, 852, 799, and 744 cm⁻¹, and its diffuse reflectance exhibited a broad maximum at ca 410 nm which tailed to beyond 600 nm. The material was partially soluble in hot dimethylformamide.

Analysis. Calcd for $C_{30}H_{14}N_2Cl_{13}$: C, 41.72; H, 1.63; N, 3.25; Cl, 53.40. Found: C, 40.42; H, 1.63, N,3.01; Cl, 52.54. The observed analysis corresponds to $C_{31}H_{15}N_{2.0}Cl_{13.8}$.

Interaction of Poly-DCH With Chlorine Gas. Poly-DCH (65.5 mg) was placed in a one-liter, three-neck flask filled with dense chlorine vapor. After 20 hours at 20 °C, the polymer became orange in color and gained 74.7 mg in weight after vacuum drying, corresponding to 13.5 Cl atoms per repeat unit. X-ray powder diffraction of this material revealed it to be largely amorphous, with a weak reflection at d = 7.62 Å. The FTIR spectrum of this material revealed, *inter alia*, strong absorptions at 1480, 1435, 1360, 1330, 1300, 1180, 1100, 1040, 1000, 851, 798, and 745 cm⁻¹.

Analysis. Calcd for $C_{30}H_{14}N_2Cl_{13}$: C, 41.72; H, 1.63; N, 3.25; Cl, 53.40. Found: C, 41.74; H, 1.81; N, 3.50; Cl, 51.29. The observed analysis corresponds to $C_{30.0}H_{15.5}N_{2.1}Cl_{12.5}$.

Interaction of Poly-DCH With Aqua Regia. Poly-DCH (81.7 mg) was exposed to 40 ml of a 3:1 mixture of concentrated hydrochloric and nitric acids at 0 °C for 29 hours. The material gained 149% in weight, became orange in color, was amorphous by x-ray powder diffraction, and dissolved in dimethylformamide. The FTIR spectrum revealed absorption at, *inter alia*, 1535, 1355, 854, 881, 755, 746, 719, 707, 697, and 693 cm⁻¹.

Analysis. Found: C, 35.87, H, 2.04, N, 3.35, Cl, 52.49. The observed analysis corresponds to a composition of $(C_{30}H_{20}N_{2.4}Cl_{14.9})$.

Acknowledgments

Literature Cited

1. Earlier accounts of portions of this work have been presented at the *7th Int. Conf. on the Chem. of the Org. Solid State,* Iraklion, Greece, July 7–12, 1985.
   (a) Sandman, D.J.; Elman, B.S.; Hamill, G.P; Velazquez, C.S.; Samuelson, L.A. *Mol. Cryst. Liq. Cryst.* 1986, *134,* 89.
   (b) Sandman, D.J.; Elman, B.S.; Hamill, G.P.; Hefter, J.; Velazquez, C.S.; Jones, M.T. Mol. Cryst. Liq. Cryst. 1986, *134,* 109; and at the Workshop on Conduct. Polym., Brookhaven National Laboratory, Upton, NY, October 7–9, 1985.
   (c) Sandman, D.J.; Tripathy, S.K.; Elman, B.S.; Samuelson, L.A. *Synth. Met.,* 1986, *15,* 229.
2. (a) Arnold, S. *J. Chem. Phys.* 1982, *76,* 3842.
   (b) Murashov, A.A.; Silinsh, E.A.; Bässler, H. *Chem. Phys. Lett.* 1982, *93,* 148.
3. Sandman, D.J.; Hamill, G.P.; Samuelson, L.A.; Foxman, B.M. *Mol. Cryst. Liq. Cryst.* 1984, *106,* 199.
4. Sandman, D.J.; Carter, G.M.; Chen, Y.J.; Elman, B.S.; Thakur, M.K.; Tripathy, S.K. in "Polydiacetylenes"; Bloor, D.; Chance, R.R., Eds.; Martinus Nijhoff: Dordrecht, Boston, 1985; pp. 299-316.
5. (a) Enkelmann, V.; Leyrer, R.J.; Schleier, G.; Wegner, G. *J. Mater. Sci.* 1980, *15,* 168.
   (b) Galiotis, C.; Read, R.T.; Yeung, P.H.J.; Young, R.J.; Chalmers, I.F.; Bloor, D. *J. Polym. Sci., Polym. Phys. Ed.* 1984, *22* 1589.
6. Enkelmann, V. *Adv. Polym. Sci. 1984,* 63, 91.
7. Sandman, D.J.; Elman, B.S.; Hamill, G.P.; Velazquez, C.S.; Yesinowski, J.P; Eckert, H. *Nature,* submitted.
8. Yesinowski, J.P.; Eckert, H.; Sandman, D.J.; Velazquez, C.S. *J. Am. Chem. Soc.,* accepted.
9. Yesinowski, J.P.; Eckert, H.; Sandman, D.J.; Velazquez, C.S. In "Solid State Polymerization and the Structure and Properties of Polymers Produced by Lattice-Controlled Processes"; Sandman, D.J., Ed.; ACS SYMPOSIUM SERIES, to be published.
10. Grasso, R.P.; Thakur, M.K.; Lando, J.B. *Mol. Cryst. Liq. Cryst.* 1985, *118,* 377.
11. Foxman, B.M.; Jaufmann, J.D. *Mol. Cryst. Liq. Cryst.* 1984, *106,* 189.
12. Sandman, D.J.; Samuelson, L.A.; Velazquez, C.S. *Polym. Commun.* 1986, *27,* 242.
13. Sakamoto, M.; Wasserman, B.; Dresselhaus, M.S.; Wnek, G.E.; Elman, B.S.; Sandman, D.J. *J. Appl. Phys.,* 1986, *60,* 2788.
14. Zhu, D.; Shi, S.; Qian, R. *Makromol. Chem., Rapid Commun.* 1986, *7,* 313.
15. Brédas, J.L.; Street, G.B. *Acc. Chem. Res.* 1985, *18,* 309.
16. Jones, M.T.; Roble, J.; Sandman, D.J. In this volume.
17. Schleier, G. Ph.D. Thesis, University of Freiburg, 1980 (unpublished).
18. Baughman, R.H.; Chance, R.R. *J. Appl. Phys.* 1976, *47,* 4295.
19. Wegner, G. In "Molecular Metals"; Hatfield, W.E., Ed.; Plenum Press: New York, 1979; pp. 209-242.
20. Sandman, D.J., unpublished, 1986.

Chapter 10

Structural and Spectroscopic Studies of Polydiacetylenes

D. Bloor

Department of Physics, Queen Mary College, London E1 4NS, United Kingdom

Many aspects of the preparation and properties of poly-
diacetylenes are the subject of lively debate. This
review presents recent results that bear on some of
these controversies. First the relationship of diacety-
lene monomer crystal structure and solid-state reactiv-
ity is discussed. Secondly the temporal evolution of
solvato-chromic transitions of soluble polydiacetylenes
is displayed. Optical and Raman spectra reveal the oc-
currence of an intermediate form of the polymer. A
model compatible with these results is described.

The polydiacetylenes, $+CR-C\equiv C-CR'+_n$, hereafter abbreviated PDAs, have
been extensively studied since the late 1960s ($\underline{1}$). This research
has been the subject of several reviews and a recent book ($\underline{2}$).
Current studies continue to bring to light interesting and unexpected
phenomena and much of this is the subject of a series of lively deb-
ates. The importance of PDAs stems from the availability of macros-
copic single crystals with larger inter-chain separations, obtained
by solid-state polymerisation of diacetylene monomers. Such samples
enable the fundamental properties of the quasi-one-dimensional, fully
extended, conjugated polymer chains to be probed free from the comp-
lications imposed by the complex morphologies usually encountered in
polymeric materials. Such direct studies are not possible with other
conjugated polymers which can, at best, be obtained as aligned but
disordered samples. The PDAs may be obtained in less perfect form so
that the influence of disorder on their physical properties can be
properly assessed. Thus, PDAs provide us with a class of model mat-
erials for the study of conjugated polymers.
A basic requirement of the subject is to obtain an understanding of
the solid-state reactivity of diacetylene monomers. This can, in
principle, be used to develop a predictive capability and enable re-
active monomer molecules to be 'engineered'. Progress towards this
goal has been achieved by the correlation of lattice packing and re-
activity. Some recent studies, providing further information on this
topic, are reviewed in the following section.
PDAs can be disordered by a variety of processes but to date there

has been little detailed characterisation reported in the literature.
An exception to this is the class of PDAs which dissolve, without de-
gradation, in a range of common solvents. These PDAs display thermo-
chromism and solvent composition dependent colour changes. These ef-
fects derive from order-disorder transitions but there is not yet a
concensus about the details of the structure of the ordered and dis-
ordered phases. Obtaining a proper understanding of these effects is
complicated by the marked differences that exist in the sidegroups of
PDAs. Thus, though there is a generality of chromic effects, there
are many differences in detail. Examples illustrating the effect of
changes of sidegroups structure on the solvato-chromism will be pre-
sented in the final section. In particular, the temporal evolution
of the spectra after a stepwise change in solvent composition are
described. The relevance of these results to the current models for
PDA chains in solution is discussed.

Solid State Reactivity

The colouration of certain diacetylene compounds on prolonged storage
or exposure to light has been known for over 100 years. Though the
true nature of this reaction was not shown experimentally by Wegner
($\underline{1}$) until 1969, a number of earlier workers identified some of the
salient points ($\underline{3}$). Most notable was the work of Strauss et al ($\underline{4}$)
in 1930. They observed colour changes leading to metallic, lustrous
crystals of dihalogen-diacetylenes. This was attributed to the cry-
stal packing giving rise to interactions of the molecules rendering
the structure unstable. Molecular rotation within the crystal could
then allow bonds to form between the individual molecules producing a
polymer. The metallic appearance was presumed to derive from loosely
bound electrons in the product. The authors surmised that x-ray str-
uctural studies would provide a deeper insight into the process.
This essentially correct description went unnoticed; apparently
these insights were ahead of their time. Part of the lack of inter-
est may have been due to the fact that the dihalogen-diacetylene cry-
stals exploded under impact. In any event, it was a further 39 years
before the important x-ray studies were undertaken.
The lattice packing of reactive diacetylenes is most conveniently dis-
played using the monomer separation and tilt angles (d and γ) first
introduced by Baughman ($\underline{5}$), see Figure 1(a). Crystal structure data
for both reactive and unreactive compounds was used in a comparison
of the lattice packing of diacetylene monomers and their solid-state
reactivity. This showed that a reasonable criterion for reactivity
is that the reacting (1 and 4') carbon atoms must be separated by
less than 0.4 nm ($\underline{3}$).   This criterion was originally proposed by
Schmidt ($\underline{6}$). More recent compilations have come to the same general
conclusion ($\underline{7}$). It is also found to hold, even when there are com-
plex molecular re-arrangements during polymerisation ($\underline{8}$). The rate
of polymerisation is strongly influenced in these cases but not the
occurrence of solid-state reactivity. Since the close packing of
monomers is determined by the van der Waals radii of the diacetylene
carbons, the values of d and γ for reactive packing must lie within
the shaded area of Figure 1(b). Here the lower curve is the limit of
closer packing and the upper curve is set by Schmidt's criterion.
Thus, for any given monomer separation d_{mon} there is a range of
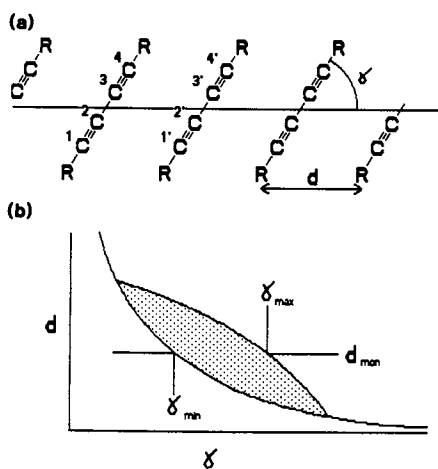
Figure 1. Solid-state polymerization of diacetylenes
(a) Monomer array in crystal lattice
(b) Reactive packing (shaded area) shown in terms of d and γ.

values from γ_{min} to γ_{max} which allows solid-state polymerisation to occur.

The arrangement shown in Figure 1(a) presupposes an extended conformation of the diacetylene molecule. For monomers with bulky end groups, the flexibility of the monomer molecule can result in a compact molecular structure in the crystal. The sidegroups then impede the reaction, in contrast to the situation in reactive monomers where the sidegroup interactions bring the diacetylene moieties into the desired reactive contact.

Both these general rules are illustrated in the structures of a series of monomers related to 2,4-hexadiynylene bis(p-toluene sulphonate), (TS) (9). The parent compound of this series is 2,4-hexadiynylene bis(benzene sulphonate),(BS), R = $-CH_2-O-SO_2-C_6H_5$ (10). The nature of the substitution of the terminal benzene ring has marked effects on molecular conformation and packing. Five compounds have the conformation shown in Figure 2(a): these have terminal H (BS), F (FBS), CH_3 (TS), OCH_3 (MBS), Cl (CBS) and the triply CH_3 substituted ring (mesitylene sulphonate, MS). This is known from the structures of BS (10), TS (9), FBS (11) and MS (12). CBS and MBS are polymorphic and the reactive phases are available only as small crystals grown from highly supersaturated solutions (13,14). From the similarities in polymer structure of TS and MBS (15) and the powder data which indicates a monomer separation of 0.518 nm in MBS, a similar conformation can be inferred for MBS. It seems probable that reactive CBS adopts the same form. The d_{mon}, γ_{min}, γ_{max} and γ values are listed in Table I. The observed packing and reactivity correlates as expected.

Table I. Lattice packing of BS related monomers

Monomer	d_{mon}(nm)	γ_{min}	γ_{max}	γ	Reaction
BS	0.528	40°	49°	45.2^{o}	Yes
FBS	0.515	41°	50.5^{o}	44.8^{o}	Yes
TS	0.515	41°	50.5^{o}	43.4^{o}	Yes
MS	0.547	37°	46°	66.3^{o}	No
CBS	0.503	42°	51°	66.7^{o}	No
MBS	0.580	36°	43°	60.9^{o}	No
PM	0.645	32°	35°	68°	No

The unreactive form of CBS has a unique conformation not seen in other monomers, except for the bromine substituted analogue. The molecular form is extended but the molecular tilt is too great for reactivity (Table I). The unreactive form of MBS adopts a folded conformation, see Figure 2(b), drastically increasing d, γ is also large and reaction is precluded (14). The same form occurs for the penta-methyl substituted monomer (PM), see Figure 2(c) (17). The bulky substituents force the monomer units further apart and increase
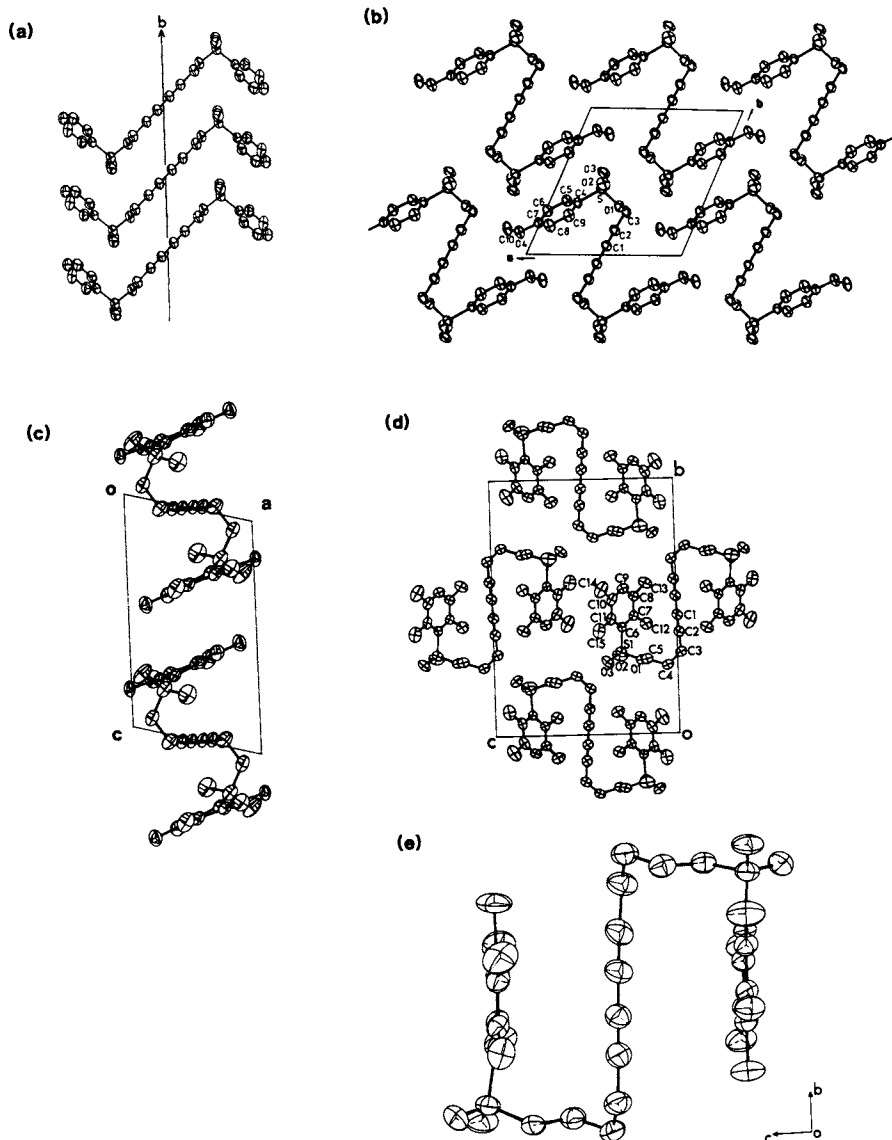
Figure 2. Crystal structures of (a) BS, (b) MBS, (c) PM, (d)
DSD, (e) PMD, see text for abbreviations. Reproduced with
permission from refs. (10, 14, 17, 18, 18). Copyright 1979,
1985, 1986, International Union of Crystallography.

the tilt angle so that a solid state reaction is impossible. Similar folded conformations occur for the durene sulphonate and penta-methyl sulphonate derivatives of 4,6-decadiynylene, Figure 2(d) (DSD) and 2(e) (PMD) (18). The shortest 1-4' carbon distances are 0.626 and 0.821 nm in these compounds, close to the molecular separations since δ is nearly 90°.
The addition of bulky substituent groups produces large changes in conformation but the overall effect is to increase both d and δ , which is clearly unfavourable. Thus, multiply substituted conjugated rings should not be incorporated in the substituent groups of diacetylene monomers.

Chromism in solutions

The chromism displayed by soluble PDAs as a function of solvent temperature and composition, has generated both interest and controversy (19,20). On cooling, or the addition of a non-solvent, a bathochromic shift is observed in the absorption peak produced by excitation of the conjugated backbone of the polymer. The absorption in good solvents peaks at about 470 nm (yellow form). In such solutions it is generally agreed that the polymer chains are disordered though there is disagreement as to whether the conformation is a random coil with pronounced kinking of the polymer, or a worm-like chain with only small local deformations. The down shifted absorptions occur at about either 540nm (red form) or 620nm (blue form). The change is due to an order-disorder transition with the red and blue forms being the more ordered. An active debate centres on whether the ordering is of individual chains, a coil to rod transition (19) or the result of aggregation and crystallisation (20). The phenomenon is a general one occuring both in polymers with strongly and weakly interacting sidegroups (21,22). This has led to the proposal that the ordering is a backbone driven phenomenon.
Most investigations have concentrated on two of the nBCMU series of polymers (R=-(CH$_2$)$_n$OCONHCH$_2$CO$_2$C$_4$H$_9$) with n = 3 and 4. 3BCMU has a yellow to blue transition and 4BCMU a yellow to red transition in chloroform/hexane solvent mixtures and when hot toluene solutions are cooled.
It has been assumed that the transition between disordered and ordered forms is direct since an isobestic point is observed in the spectra, either as a function of temperature (23), or as a function of solvent composition over the range where both ordered and disordered forms co-exist (24).
Indications that intermediate forms can occur are found firstly, in increased absorption at intermediate wavelengths for 3BCMU immediately after addition of the non-solvent (25), and in studies of water soluble PDAs (26). For the latter polymers, three absorption peaks are observed at high, intermediate and low energies with no isobestic points during interconversion of the three species.
Recently the higher homologue, 9BCMU, has been synthesised and characterised (27). This polymer shows yellow to blue, yellow to red, yellow to red and blue and red to blue transitions. These transitions are observed using the same solvent/non-solvent mixture, chloroform/hexane, as for 3 and 4BCMU (28). Examples of these transitions are shown in Figure 3.
For 9BCMU the nature of the transitions from the disordered form and
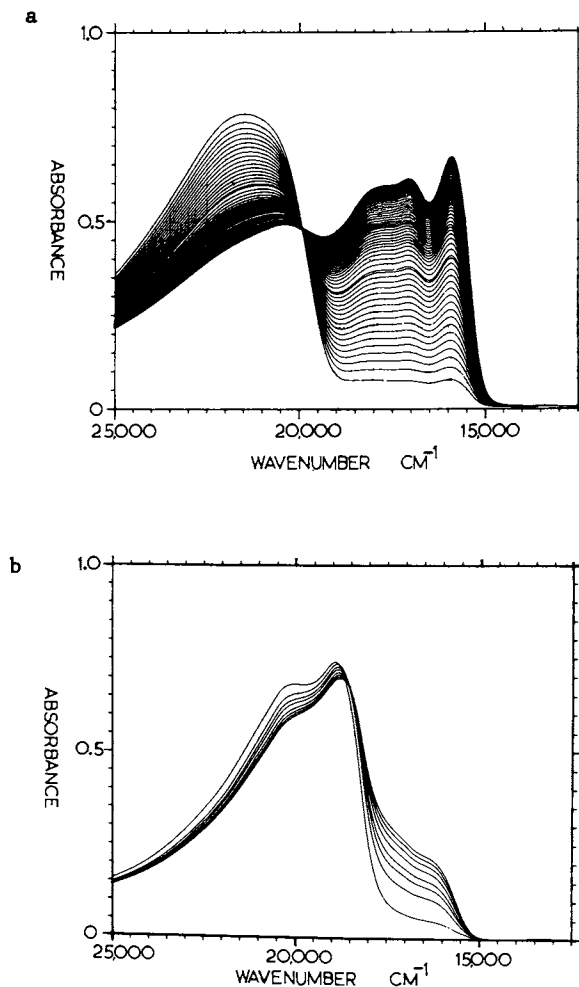
Figure 3. Sequential spectra of 9BCMU in chloroform-hexane
solutions
(a) composition 0.49:0.51 total duration of the experiment 140
hours,
(b) composition 0.33:0.67 duration of experiment 45 min.
In both cases the concentration in repeat units is of the order
4×10^{-5} mol/litre.
Reproduced with permission from ref. (28) Copyright 1986, Hüthig
and Wepf Verlag.

its kinetics are controlled by the fraction of non-solvent added to
the chloroform solution. The yellow solution is stable up to approx-
imately 50% hexane. Small further additions of hexane lead to a yel-
low to blue colour change, the rate of which is determined by the
quantity of hexane added. When the quantity of hexane added is very
small the transformation takes in excess of 10^5 secs. At higher
hexane concentrations the transformation produces both red and blue
forms, in a ratio determined by the composition of the mixed solvent.
When the hexane content is about 70%, the solution converts rapidly,
i.e. in much less than 1 sec, to almost 100% of the red form. The
red solution then undergoes a slower transformation, time scale of
the order 10^3 secs, to the blue form. These changes are independent
of the concentration of the solution in the range 4×10^{-5} to 3×10^{-6} mol/lit, in terms of repeat units, see Figures 3 and 4. The
yellow to blue and red to blue transformations show isobestic points
while the yellow to red and blue does not. The kinetics of these
transitions are of a log(t) form, the data for 3BCMU is similar (25).
Such behaviour is typical of systems with a random distribution of
potential barriers (29).

These results strongly suggest that the red form of 9BCMU is a meta-
stable partially disordered intermediate. Other evidence for this is
provided by Raman spectra (30). The yellow solution has C=C and C≡C
stretching bands at 1520 and 2120 cm^{-1}, and weak, broad bands between
700 and 1500 cm^{-1}. The crystal and the blue solution polymer have
identical spectra with C=C and C≡C frequencies of 1450 and 2070 cm^{-1}
and a few sharp bands between 700 and 1500 cm^{-1}. The red solution
has C=C and C≡C bands at 1455 and 2075 cm^{-1} and a sequence of weak
bands between 700 and 1500 cm^{-1}, see Figure 5. The 700-1500 cm^{-1} re-
gion is characterised by Fermi resonances with sidegroup vibrational
modes. Thus, the yellow solution has disordered sidegroups, the blue
solution perfectly ordered sidegroups and the red form partially ord-
ered sidegroups.

Similar effects are observed in other nBCMU polymers. Both 2 and 6
BCMU go through an intermediate red form to a final more ordered form
e.g. see Figure 6. The spectral shifts are small so that there is no
visible change in the colour of the solution. The large differences
in the final absorption energies is a well established result of side
group interactions producing deformation of the PDA backbone (31-33).
Thus, the occurrence of an intermediate form in solutions is a general
phenomenon. The Raman results and the insensitivity of the spectra
of the yellow solutions to changes in sidegroups show that the side-
groups are disordered in this form. For sidegroups containing paraf-
finic sequences this will involve the presence of gauche conformers,
as observed in paraffinic solids and micelles (34). This will lead
to repulsion of polymer chains since the sidegroups act in a manner
analogous to that of paraffinic surfactants used to stabilise coll-
oids. On the addition of a nonsolvent the polymer attempts to strai-
ghten but it is constrained by residual disorder in the sidegroups.
The dependence of the spectra on sidegroups is slightly greater in
this phase. The residual disorder then relaxes to give an ordered
form on a time scale determined by the particular sidegroups. As the
chains order, the repulsive interaction is replaced by an attractive
one and the polymers crystallise, even at low dilutions. The spectra
are then strongly dependent on the sidegroups. Strong evidence for
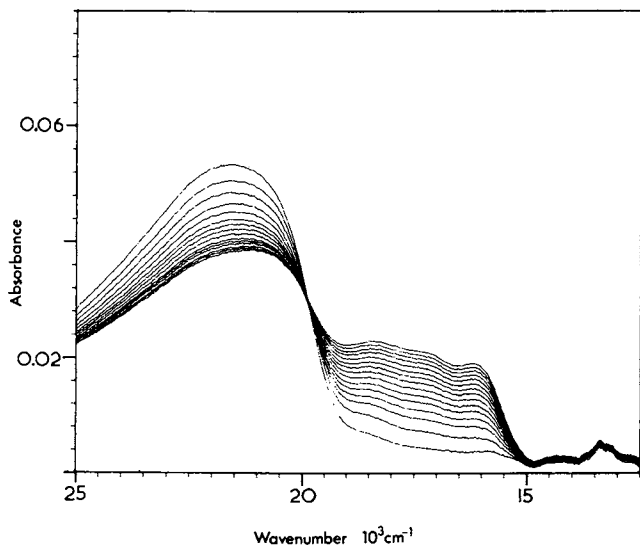
Figure 4. Sequential spectra of 9BCMU in chloroform-hexane with
a slight excess of hexane, concentration 3 x 10^{-6} mol/litre, 16
min between scans.
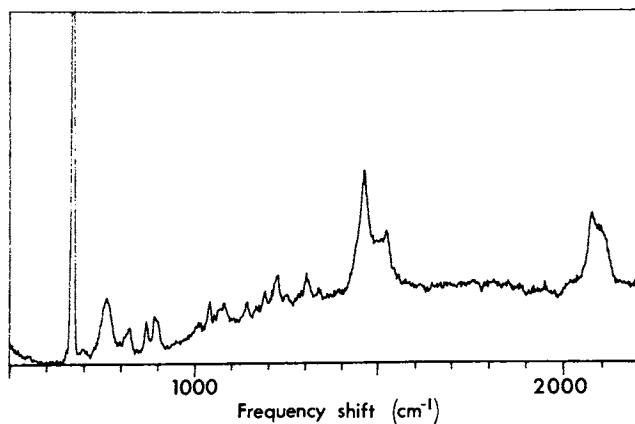
Figure 5. Resonance Raman spectrum of the red and, less intense,
yellow forms of 9 BCMU in chloroform-hexane solution excited with
515 nm Ar laser.
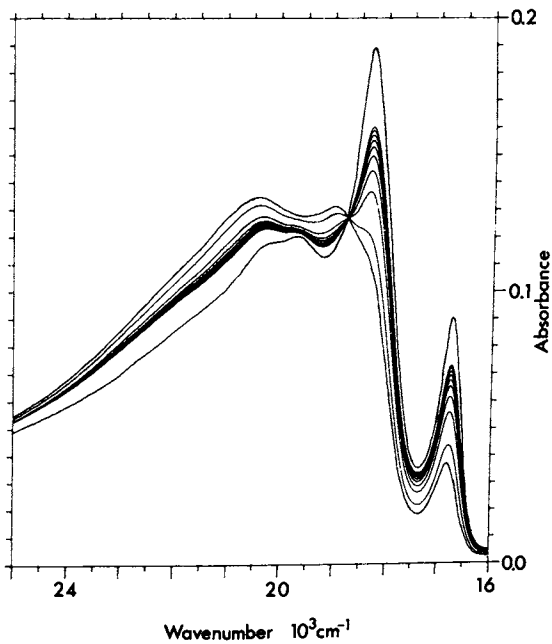
Figure 6.   Sequential spectra of 2 BCMU in chloroform-hexane solution, showing transformation from the partially to fully ordered forms, duration of experiment 4 hours.

crystallisation is provided by 2BCMU, Figure 6, since the transition
to the final double peaked spectrum has a clear isobestic point.
Thus, these peaks must be attributed to two distinct polymer conform-
ations produced in the crystals since the transformation to equal
amounts of two independent polymer chains in solution seems improb-
able.

Conclusions

Brief reviews of the structure-reactivity relationship of diacetylene
monomers and the evolution of solution spectra after changes in sol-
vent composition have been presented. Much remains to be done to
formulate a precise set of guidelines for the production of reactive
diacetylenes. The presence of multiple substitution of conjugated
rings in the end groups of monomers has been shown to be unfavourable.
The presence of intermediate partially ordered PDA chains in solution
has been shown to occur for several nBCMU substituted polymers. A
simple model consistent with the spectroscopic data is introduced.
This does not address the question of the form of the polymer in
yellow solutions. The presence of disordered sidegroups attached to
a rigid backbone is, however, compatible with the model of a wormlike
chain (35).

Acknowledgments

Literature Cited
  1. Wegner, G. Z. Naturforsch. 1969, 24b, 824.
  2. "Polydiacetylenes"; Bloor, D; Chance, R. R., Eds.; Martinus
      Nijhoff Publ., Dordrecht, 1985.
  3. Bloor, D. In "Developments in Crystalline Polymers - I";
      Bassett, D. C., Ed.; Applied Science Publ., London, 1982,
      p. 151.
  4. Strauss, F.; Kolleck, L; Heyn, W. Ber. Deutsch. Chem. Ges.
      1930, 63, 1868.
  5. Baughman, R.H. J. Polym. Sci. Polym. Phys. Ed. 1974, 12, 1511.
  6. Schmidt, G. M. J. "Reactivity of the Photo-excited Organic
      Molecule'; Wiley, N. Y., 1967, p. 227.
  7. Enkelmann, V. Adv. in Polym. Sci. 1984, 63, 91.
  8. Enkelmann, V.; Wenz, G.; Muller, M. A.; Schmidt, M.: Wegner, G.
      Mol. Cryst. Liq. Cryst. 1984, 105, 11.
  9. Enkelmann, V.; Leyrer. R. J.; Wegner, G. Makromol. Chem. 1979,
      180, 1787.
 10. Ando, D. J.; Bloor, D.; Hursthouse, M. B.; Motevalli, M. Acta
      Cryst. 1985, C41, 2245.
 11. Enkelmann, V. Makromol. Chem. 1983, 184, 1945.
 12. Werninck, A. R.; Blair, E.; Milburn, H. W.; Ando, D. J.; Bloor,
      D.; Motevalli, M; Hursthouse, M. B. Acta Cryst. 1985, C41, 227.

13. Enkelmann, V. J. Mater. Sci. 1980, 15, 951.
14. Fisher, D. A.; Ando, D. J.; Bloor, D.; Hursthouse, M. B. Acta
     Cryst. 1979, B35, 2075.
15. Williams, R. L.; Ando, D. J.; Bloor, D.; Hursthouse, M. B.
     Polymer 1980, 21, 1269.
16. Williams, R. L. Ph.D. Thesis, University of London, 1982.
17. Motevalli, M.; Norman, P. A.; Hursthouse, M. B.; Werninck, A. R.;
     Milburn, H. W.; Blair, E.; Bloor, D.; Ando, D. J. Acta Cryst.
     in press.
18. Day, R. J.; Ando, D. J.; Bloor, D.; Norman, P. A.; Blair, E.;
     Werninck, A. R.; Milburn, H. W.; Motevalli, M.; Hursthouse,
     M. B. Acta Cryst. 1985, C41, 1456.
19. Lim, K. C.; Sinclair, M.; Casalnuovo, S. S.; Fincher, C. R.;
     Wudl, F.; Heeger, A. J. Mol. Cryst. Liq. Cryst. 1984, 105, 329.
20. Wenz, G.; Muller, M. A.; Schmidt, M.; Wegner, G. Macromols.
     1984, 17, 837.
21. Rughooputh, S. D. D. V.; Phillips, D.; Bloor, D.; Ando, D. J.
     Polymer Commun. 1984, 25, 242.
22. Plachetta, C.; Rau, N. O.; Hauck, A.; Schultz, R. C. Makromol.
     Chem. Rapid. Commun. 1982, 3, 249.
23. Lim, K. C.; Fincher, Jr. C. R.; Heeger, A. J. Phys. Rev. Lett.
     1983, 50, 1934.
24. Patel, G. N.; Chance, R. R.; Witt, J. D. J. Chem. Phys. 1979,
     70, 4387.
25. Chance, R. R.; Washabaugh, H. W.; Hupe, D. J. Chemtronics,
     1986, 1, 36.
26. Bhattachargee, H. R.; Preziosi, A. F.; Patel, G. N. J. Chem.
     Phys. 1980.
27. Bloor, D.; Ando, D. J.; Obhi, J. S.; Mann, S.; Worboys, M. R.
     to be published.
28. Bloor, D.; Ando, D. J.; Obhi, J. S.; Mann, S.; Worboys, M. R.
     Makromol. Chem. Rapid. Commun. submitted.
29. Gibbs, M. R. J.; Evetts, J. E.; Leake, J. A. J. Mater. Sci.
     1983, 18, 278.
30. Bloor, D.; Ando, D. J.; Obhi, J. S.; Batchelder, D. N.; Kwok, H.
     to be published.
31. Batchelder, D. N.; Bloor, D. J. Phys. C. Sol. St. Phys. 1978,
     11,   L629.
32. Chance, R. R. Macromols. 1980, 13,   396.
33. Bloor, D. ACS Symp. Ser. No. 162, p. 81.
34. Maroncelli, M.; Strauss, H. L.; Snyder, R. G. J. Chem. Phys.
     1985, 82, 2811.
35. Allegra, G.; Bruckner, S.; Schmidt, M.; Wegner, G. Macromols.
     1986, 19, 399.

Chapter 11

Urethane-Substituted Polydiacetylenes

Solid-State Polymerization, Crystal Optics, and Conformational Transitions

R. R. Chance[1,3], H. Eckhardt[1], M. Swerdloff[1], R. R. Federici[1], J. S. Szobota[1], E. A. Turi[1], D. S. Boudreaux[1], and M. Schott[2]

[1]Allied–Signal Corporation, Morristown, NJ 07960
[2]Groupe de Physique des Solides, University of Paris VII, Paris, France

Urethane-substituted polydiacetylenes display a wide variety of interesting chemical and physical phenomena. The diacetylene crystals which serve as the precursors to these polymers are among the most photochemically reactive of studied diacetylenes. Yet they show almost no thermal reactivity. Thermochromic phase transitions are observed in PDA crystals with urethane substituent groups of the form $-(CH_2)_4OCONH-X$, where X can be any one of a number of organic moieties. Spectroscopic (Raman and visible) and thermodynamic (DSC and TMA) characterizations of the thermochromic phase changes are discussed and compared with theoretical calculations of distorted PDA backbones. Hydrogen-bonding of the urethane substituent is suggested as playing an important role in the reactivity of the monomer crystals and in distortions of the polymer chain which affect the optical properties.

Urethane-substituted polydiacetylenes have been investigated for over ten years and now constitute the most widely studied class of polydiacetylenes (PDAs). There are several reasons for the large interest in these materials. First, the PDA crystals are highly ordered and can be produced with macroscopic dimensions suitable for detailed optical studies. Urethane-substituted PDAs with substituents of the form, $-(CH_2)_4OCONH-X$ where X can be a variety of organic moieties, display thermochromic phase transitions during which crystalline order is maintained. A possible origin of this thermochromism is discussed herein. Second, this class of materials provided the first soluble, high molecular weight PDAs. Studies of

[3]Current address: Exxon Research & Engineering Company, Clinton Township, Annandale, NJ 08801

PDA solutions have provided the first determination of the molecular weight of a PDA and the discovery of interesting thermally- and solvent-induced chromic transitions of the individual PDA chains in solution. Finally, the polymerization of the monomers in the solid state is interesting for two reasons: 1) they display the highest photochemical reactivity of studied diacetylenes and 2) they show almost no thermal reactivity. A possible explanation of the difference in thermal and photochemical reactivity is discussed in the next section.

Solid-State Reactivity

The solid-state reaction of diacetylene crystals proceeds by a 1,4-addition reaction of adjacent monomer units to produce a fully conjugated, polymer single crystal with nearly one-dimensional electronic properties. Initiation of the reaction can be accomplished by either heat or radiation in many cases. Once initiated, the chains propagate in a highly exothermic reaction ($\underline{1}$) to produce a final polymer containing over 1000 monomeric units in some instances ($\underline{2}$). Little is known about chain termination. Though urethane-substituted diacetylenes show almost no thermal reactivity, they are highly reactive to UV, X-ray, and gamma-ray radiation. The most studied example is 4BCMU, $RC \equiv C-C \equiv CR$ where R is $-(CH_2)_4OCONHCH_2COOC_4H_9$ ($\underline{3-5}$). The initial quantum yield for UV polymerization is about 100 monomer repeat units per absorbed photon at low polymer conversions; the X-ray and gamma-ray yields are also high ($\underline{5}$). As is typical of this class of materials, there is a small degree of thermal reactivity to produce about 0.5% polymer. Since this thermal reaction cannot be taken to higher yield even with extensive heating at high temperatures, the polymer produced in the thermal process is thought to initiate from defect sites in the monomer crystal.

The heat of photopolymerization has been measured for 4BCMU, $\Delta H_p = 1.0$ eV ($\underline{4}$). Thus, each propagation event releases 1.0 eV on the average. This value is significantly less than that obtained for thermal polymerization of other diacetylenes, $\Delta H_t = 1.6$ eV ($\underline{1}$). The explanation put forth for this large difference involves the hydrogen bond networks in 4BCMU monomer and polymer. By analogy to TCDU ($R = -(CH_2)_4OCONHC_6H_5$) ($\underline{6}$), we expect that reacting monomers in 4BCMU are hydrogen bonded to one another. This hydrogen bonding is maintained in the polymer, though molecular models suggest that some strain is required in the $(CH_2)_4$ linkage connecting the conjugated backbone and the chains of hydrogen bonds ($\underline{7}$). This strain energy would decrease ΔH_p from its nominal value. Since similar geometric rearrangements are required in the initiation step, we can expect that the activation energy for thermal polymerization would be increased due to hydrogen bonding. This effect could explain the low thermal reactivity of urethane-substituted diacetylenes ($\underline{4}$).

Though the quantum yield for photopolymerization with UV light is high at low polymer conversions, it rapidly decreases as the polymer concentration increases ($\underline{3}$). The limiting yield for UV polymerization in 4BCMU is about 35%. It is believed that this effect has its origin in quenching of the monomer excited states by the polymer chains, i.e., the monomer excited states created on irradi-

ation are quenched via nonradiative energy transfer to the polymer
chains in the lattice before they have time to initiate a new chain
(3). Only gamma-ray irradiation has been established to yield
nearly quantitative conversion to polymer (5).

We were also interested in determining if we could suppress UV
and enhance gamma or x-ray induced polymerization of diacetylenes
relative to 4BCMU by changing the nature of the X groups in
diacetylene urethanes. We first attempted to enhance radiation
induced photopolymerization by introducing a bromine into the side
chain. Accordingly, using standard synthetic procedures, BrPU (X =
$(CH_5)_5Br$) and HU (X = $(CH_2)_5CH_3$) were prepared and their
reactivities determined relative to 4BCMU. Both of these compounds,
however, as thin films coated on filter paper, were found to be as
reactive as 4BCMU and produced similar dark blue colors upon expos-
ure to either UV or x-ray irradiation (from a copper target). The
aromatic derivatives BrPhU (X = $p-BrC_6(H_4)$) and TolU (X = $p-CH_3C_6H_4$)
were also prepared and studied. Two crystal modifications of BrPhU
were obtained. The crystals formed from acetone/hexane were moder-
ately reactive and turned red-purple in the presence of UV light and
orange-purple in the presence of x-rays. Crystals obtained by pre-
cipitating BrPhU from acetone/hexane with pentane turned blue in the
presence of UV light and blue-purple in the presence of x-rays.
These reactions, however, occurred at a slower rate than with
4-BCMU. TolU, on the other hand, was much less reactive and only
slowly turned light pink or yellow in the presence of x-rays or UV
light. In this case, it appeared that the presence of a bromine did
promote irradiation induced polymerization. Finally, NU (X =
1-naphthyl) was prepared. This compound was found to be externally
stable in the presence of UV light but gradually turned blue in the
presence of x-rays. Presumably, the naphthyl group acted as an
internal photoquencher and suppressed photopolymerization, in a
manner similar to that occurring in DCHD which has a carbazole in
the substituent group (8). One would predict from these results
that a bromonaphthalene derivative would thus be ideal for suppres-
sing photopolymerization and enhancing radiation polymerization.

Optical Properties

The optical properties of urethane-substituted PDAs are typical in
that they show a lowest energy absorption peak at about 16,000 cm^{-1}
(630 nm). This peak is followed by a vibrational sideband whose
dominant components are vibrational modes associated with the double
and triple bonds of the backbone. Polymers with substitutent groups
of the general formula $-(CH_2)_4OCONH-X$ are unique in displaying a
thermochromic phase change. The color change during the phase
transition is blue to red for thin films or green-gold metallic to
red for large crystals. Crystalline order is maintained during the
phase change, which is reversible at least for several cycles. The
spectroscopic changes that take place on temperature cycling are
shown in Figures 1 and 2 for the example of poly-IUPDO
[X = $-CH(CH_3)_2$]. The normal incidence reflection spectra (Figure 1)
show a dramatic shift to higher energies when the crystal is heated
above about 120°C (9). The spectral shift is about 2800 cm^{-1}
(0.35 eV). There is a significant hysteresis in the transition, the
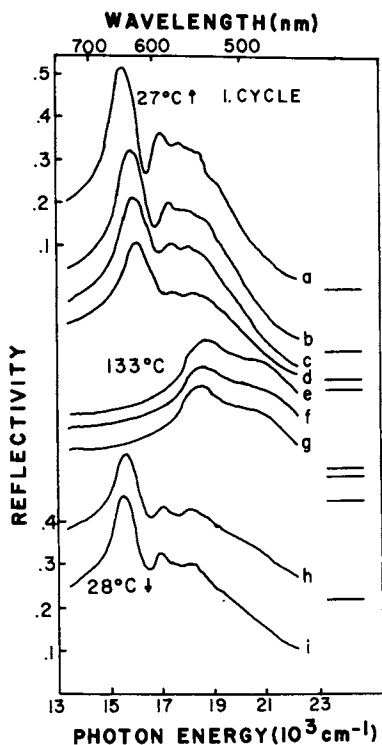
Figure 1. Normal incidence specular reflectance spectra as a function of temperature for PolyIUPDO (9). Temperatures are: a, 27 C; b, 66 C; c, 100 C; d, 114 C; e, 133 C; f, 117 C; g, 78 C; h, 64 C; i, 28 C. The spectra were recorded in the order a to i on the first thermochromic cycle.

red-to-blue color change occurring at about 70 C on cooling. Figure 2 shows Raman spectra in the double and triple bond regions at temperatures above, below, and "during" the phase change. The low temperature spectra have vibrational frequencies, $\nu_{C=C}$ = 1460 cm^{-1} and $\nu_{C=C}$ = 2080 cm^{-1}, which are typical of single crystal PDAs. The high temperature phase has vibrational frequencies which are shifted to higher energies by about 30 cm^{-1}. Similar shifts in reflection and Raman spectra are seen in polyETCD, X = -C$_2$H$_5$ (10,11).

The thermochromic phase change can also be following calorimetrically with differential scanning calorimetry (DSC). Both polyIUPDO and polyETCD have been studied with DSC. The blue-to-red phase change is exothermic by about 1 kcal/mol. The DSC signals closely parallel the changes in optical spectra, including the rather large hysteresis in the transition. On cycling the energy released during the transition decreases gradually, as does the temperature for the blue-to-red change and the size of the hysteresis loop. Thermal mechanical analysis (TMA) has also been performed on polyETCD (which is available as small fibers). Results are shown in Figure 3. The polymer elongates abruptly at the phase change, and on cooling returns to its original length in a manner which parallels the optical and DSC measurements described above.

PolyTCDU (X = C$_6$H$_5$) can be synthesized so that the red, high-temperature phase is stable at room temperature (12). Conversion to the blue phase can be achieved at low temperatures (at least partially) (13) or under a strain field (14). The optical properties of the red and blue phases of polyTCDU are nearly identical to those of polyETCD and polyIUPDO (9,10). The X-ray structure of polyTCDU (15) suggested that this polymer existed in the butatriene conformation, -(R)C=C=C=C(R)-, rather than the commonly observed (and theoretically more stable) acetylenic conformation, =(R)C-C≡C-C(R)=. This led to the suggestion that thermochromism involved an acetylenic-to-butatrienic conformational change (10).

Recent theoretical and experimental results, however, cast doubt on the correctness of this interpretation. All calculations predict that the butatrienic form would display a lower bandgap than the acetylenic form (16,19), contrary to what is observed experimentally. On the experimental side, a new crystal structure determination of polyTCDU shows no evidence for the existence of a butatrienic backbone (20) and instead yields results consistent with a distorted acetylenic-like structure. As in the earlier polyTCDU structure, the distortion is extended into the sidechain with considerable bond alternation in the (CH$_2$)$_4$ linkage. In addition the end phenyl ring appears highly distorted. All this points to the fact that distortion is a major factor in the polyTCDU structure and that X-ray diffraction may not give reliable answers concerning the bond sequence of the backbone. It has been pointed out that inter- and intra-molecular sidegroup interactions, particularly in systems with strong hydrogen bonding like polyTCDU, may strain the polymer backbone and have a strong effect on the optical properties of the polymer (21).

We have employed the recently developed Valence Effective Hamiltonian technique (16) and MNDO calculations (22) to study the influence of strain in the sidegroups on the geometry of the backbone and the resulting polymer band structure, bandgap, and ionization potential. The molecule used in our simulation of strain
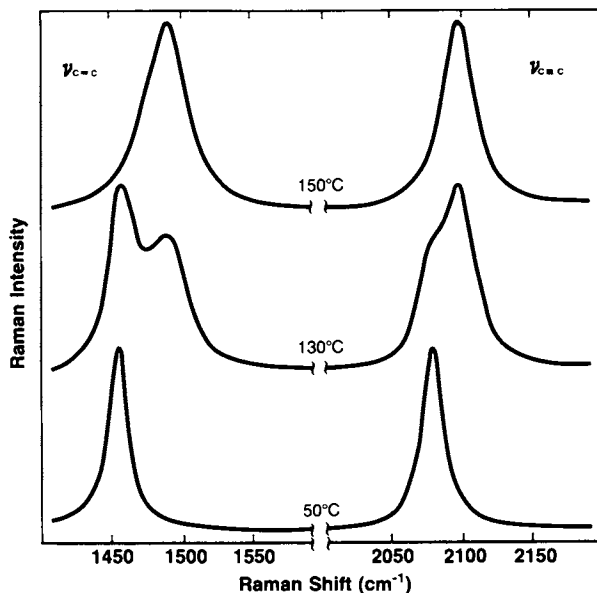
Figure 2. Raman spectra for polyIUPDO at various temperatures in the regions of the double and triple bond stretches. The exciting wavelength was 6471 A.
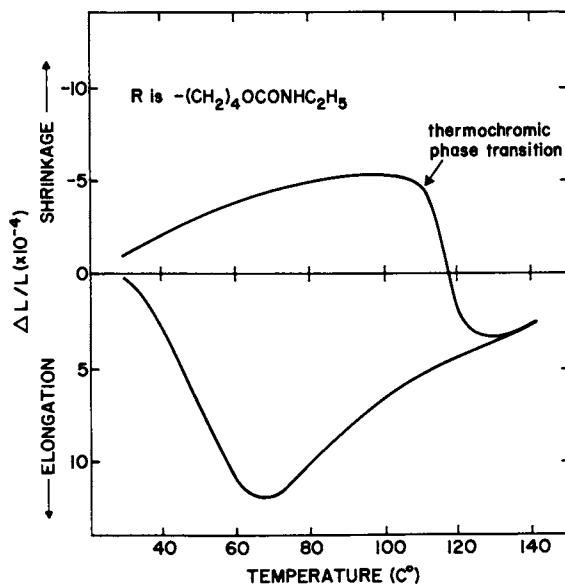
Figure 3. Thermal mechanical analysis (TMA) of polyETCD.

effects is shown in Figure 4. In order to minimize endgroup effects on the central diacetylene unit the backbone was terminated with a triple bond on both sides. This was found to be sufficient to shield the central unit from endgroup effects. The addition of one or two additional PDA repeat units had only a marginal effect on the C1-C2, C2-C3, and C4-C5 bond lengths of the central unit. The sidechains consisted of one methyl group. For most calculations the geometry was kept planar including the side group carbons. Only the H-atoms were allowed to deviate from the plane. The center of symmetry of the molecule was retained in all calculations. Two parameters, the bond distance between the methyl carbon and the diacetylene linkage and the angle between this carbon and the polymer chain, were used to model the influence of sidegroup distortion on the backbone geometry. Strain effects were simulated by keeping these parameters fixed and allowing the backbone geometry to relax in the MNDO calculations. For different sets of bond distances and bond angles of the side chain, different geometries for the repeat unit were obtained. These geometries were then used as input for the VEH calculation for both the short oligomer in Figure 4 and the polymer using the polymer repeat unit derived from the oligomer. The VEH method and the parameters used for linear conjugated polymers are described in detail in references 16 and 23. The calculated band-structures, bandgaps, and ionization potentials for the different strain configurations are then compared to the calculated results using experimentally determined geometries from references 15, 20, and 24.

The geometries obtained from the MNDO calculations are shown in Table I together with the X-ray results for polyPTS ($R=CH_2SO_3C_6H_4CH_3$) and polyTCDU.

Cases a to c are results from the X-ray experiments, while configuration d is the fully optimized structure. The central bond C2-C3 comes close to a triple bond for all three experimental structures although it appears that the values for the two polyTCDU cases are too short for a true triple bond. Notice the reversal of the bond order for C1-C2 and C4-C5 for the two polyTCDU cases. The reported 1.38 A bond distance in b for C1-C2 has been considered as the main argument for the existence of the butatrienic backbone. This result is not confirmed in the new structure determination (case c). As can be seen from Table I, the Enkelmann-Lando structure (case b) deviates the most from an idealized diacetylene configuration. In cases e, f, and g the distance of the methyl group to the backbone and the side group angle has been varied to simulate strain conditions.

The results of the VEH calculations for monomers and polymers for geometries a-g from Table I are listed in Table II. Consider first the experimental geometries (a-c). The VEH results for the polyPTS geometry (case a) are in good agreement with experiment for both E_g and IP. For the poly-TCDU geometries (cases b and c) agreement with experiment is not good; in particular the experimentally observed blue-shift in optical absorption is not predicted by VEH in either case. Note the large difference in E_g predicted by VEH for cases b and c; this results from the reversal in bond lengths for the single and double bonds (C1-C2 and C4-C5).

Table I. Geometries

	Sidechain		Backbone				Comment
	C4-C7	C7-C4-C5	C1-C2	C2-C3	C4-C5	C5-C4-C3	
a)	1.51	120.3°	1.428	1.191	1.356	121.9°	polyPTS (Ref. 24) fixed geometry
b)	1.56	114.4°	1.38	1.17	1.45	127.7°	polyTCDU (Ref. 15) fixed geometry
c)	1.50	122.1°	1.435	1.177	1.40	120.0°	polyTCDU (Ref. 20) fixed geometry
d)	1.513	123.7°	1.423	1.203	1.373	121.9°	All angles and distances optimized by MNDO
e)	1.56	122.0°	1.420	1.202	1.369	124.4°	Sidegroup fixed
f)	1.35	122.0°	1.431	1.203	1.399	120.9°	Sidegroup fixed
g)	1.56	135.0°	1.435	1.202	1.365	114.9°	Sidegroup fixed

Table II. Results of the VEH calculations for bandgap (E_g) and
           ionization potential (IP). For the experimentally derived
           geometries (a, b, and c), experimental results, where
           known, are shown in parentheses.

	Monomer		Polymer	
	E_g	IP	E_g	IP
	(eV)	(eV)	(eV)	(eV)
a)	3.63	5.7	2.16 (2.0)(12)	4.9 (5.2)(25)
b)	2.67	5.2	0.86 (2.3)(12)	4.4
c)	3.35	5.6	1.92 (2.3)(12)	4.8
d)	3.41	5.6	1.89	4.8
e)	3.46	5.7	1.92	4.9
f)	2.93	5.3	1.70	4.3
g)	3.65	5.7	2.18	4.9

     For case d, the geometry predicted by MNDO for a PDA
backbone with unstrained methyl sidegroups, the VEH E_g value is very
close to that commonly observed in PDA crystals. (Most PDA crystals
yield E_g values which are somewhat less than that of polyPTS.)
Cases e, f, and g represent our simulations of sidegroup strain.
For case e, the bond to the sidegroup is lengthened and the angle is
kept close to the MNDO and experimental values. Little change in E_g
or IP compared to case d is observed. In case f, the bond angle is
kept the same and the bond length is decreased to 1.35 A. This
change results in a decrease in E_g to 1.67 eV. In case g, both the
bond and the angle to the sidegroup are increased. This variation
results in a significant increase in E_g (about 0.3 eV shift to the
blue). This increase in E_g is very similar to that observed experi-
mentally for polyTCDU versus polyPTS, and to the overall shift
observed during the thermochromic phase change (Figure 1). Thus
VEH calculations predict that a substantial variation in sidegroup
geometry can induce signficant shifts in optical spectra. The side-
group distortion needed to produce this shift is well beyond any
distortion indicated by the X-ray structures, but this could reflect
either inaccuracies in the X-ray studies or difficulties in simulat-
ing the sidegroup distortion with one methyl group.
     We have also carried out Hückel calculations on the
various backbone geometries considered in this paper. Hückel theory
only considers nearest neighbor overlap integrals, ρ, for the
backbone carbon atoms and has no sensitivity to bond angles. The
Hückel result for E_g as a function of overlap integrals for the
three different bonds in the PDA backbone is:[18]

$$E_g = 2 \left\{ 2\beta_{12}^2 + \beta_{25}^2 + \beta_{45}^2 - [(\beta_{23}^2 + \beta_{45}^2)^2 + 4\beta_{12}^2(\beta_{23} + \beta_{45})^2]^{1/2} \right\}^{1/2}$$

where β_{ij} is the overlap intergral between carbons i and j. An exponential relationship between β and bond length is usually assumed;

$$\beta_{ij} = B \exp(-Ad_{ij}) \qquad (2)$$

Various values for the parameters A and B have been suggested in the literature. We have chosen three for comparison of VEH and Hückel predictions: A=2.59 A^{-1} and B=102.9 eV from Chance et al. (19); A=2.36 A^{-1} and B=67.3 eV from Boudreaux and Chance (18), and A=2.68 A^{-1} and B=67.8 from Salem (26). Backbone geometries from Table I are inserted into equation (2) and three resulting β values are inserted in equation (1) to calculate E_g. Results are summarized in Figure 5. There is a near linear correlation between Hückel and VEH results for all three parameter sets; the A and B values from Boudreaux and Chance and Chance et al. most closely represent the VEH results. Not surprisingly, the highly strained geometry (case g in Table I) yields the largest deviation from the linear correlation indicated in Figure 5. In other words, Hückel theory predicts a blue-shift of about 0.2 eV for cases g versus d whereas VEH theory predicted a shift of 0.3 eV. Nevertheless, we conclude that Hückel calculations can, for the most part, simulate the effects of strain as well as VEH theory. If these same three parameter sets are used to predict the bandgap of polyacetylene (using the MNDO prediction for the geometry of polyacetylene) (27), the results are respectively 1.47, 1.21, and 0.88 eV compared to an experimental value of 1.4 eV. VEH theory predicts a bandgap of 1.4 eV for polyacetylene (16). A detailed account of this work will be presented elsewhere (28).

Summary

An underlying theme in the study of urethane-substituted PDAs is hydrogen bonding, which affects the energetics of the polymerization process and probably plays a dominant role in thermochromism. One reason for this important role is the fact that the ideal repeat distance for a chain of urethane hydrogen bonds is 4.9 Å, which is essentially an exact match to the ideal repeat distance for a PDA chain (29). Hydrogen bonding has also been invoked in the explanation of the solvent-and temperature-induced color transitions in polyBCMU solutions (7). We suggest that hydrogen bonding can induce strain on the backbone causing significant variations in optical properties. Simulations of the effect of strain on the PDA backbone induced by the sidegroups yield variations in the optical properties which are similar to those observed experimentally in thermochromic urethane-substituted PDA crystals. Recent spectroscopic studies of thermochromic PDAs in the infrared region are also consistent with our theoretical approach (30). We conclude that variations in optical properties of these materials are related to strain and not to fundamental changes in backbone geometry such as acetylenic-to-butatrienic transformation.
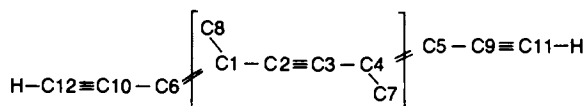
Figure 4. Model oligomer for MNDO calculations.
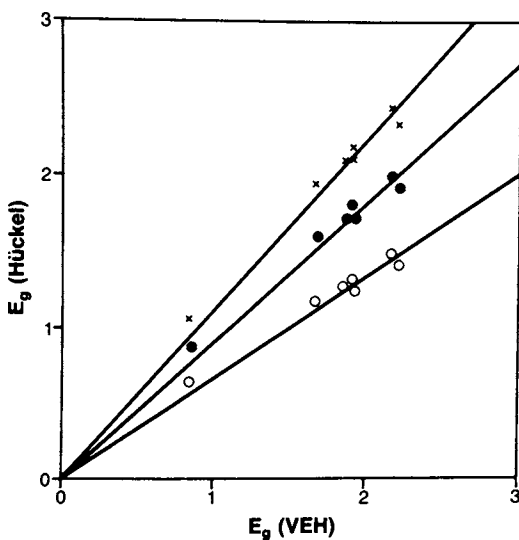
Figure 5. Huckel results for polymer bandgap, E_g, versus corresponding results from VEH theory for various backbone geometries (See Table I). All energies are given in eV. The three dates sets represent three different choices for the β-bond length relationship in Huckel theory: reference 19 (x), reference 18 ($\bullet$), and reference 26 (o).

Literature Cited

1. Chance, R. R.; Patel, G.; Turi, E.; Khanna, Y. J. Amer. Chem. Soc. 1978, 100, 1307; 1978, 100, 6444.
2. Patel, G. N.; Walsh, E. J. Polym. Sci. 1979, 17, 203.
3. Prock, A.; Shand, M.; Chance, R. R. Macromol. 1982, 15, 238; J. Chem. Phys. 1982, 76, 5834.
4. Eckhardt, H.; Prusik, T.; Chance, R. Macromol. 1983, 16, 732.
5. Patel, G. N.; Khanna, Y.; Ivory, D.; Sowa, J.; Chance, R. J. Polym. Sci. 1979, 17, 899.
6. Lando, J. B., unpublished X-ray data on TCDU monomer and polymer.
7. Patel, G. N.; Chance, R.; Witt, J. J. Chem. Phys. 1979, 70, 4387.
8. Chance, R. R.; Baughman, R. H. In "Eighth Molecular Crystals Symposium Abstracts"; M. El Sayed, Ed., UCLA, 1977 p. 81. See also R. R. Chance in Ency. Polym. Sci. Eng., Vol. 4, J. Kroswitz, Ed., Wiley: New York, 1986; p. 767.
9. Eckhardt, H.; Eckhardt, C.; Yee, K. J. Chem. Phys. 1979, 70, 5498.
10. Chance, R. R.; Baughman, R.; Mueller, H.; Eckhardt, C. J. Chem. Phys. 1977, 67, 3616.
11. Exharos, G.; Risen, W.; Baughman, R. J. Am. Chem. Soc. 1976, 98, 481.
12. Mueller, H.; Eckhardt, C.; Chance, R. R.; Baughman, R. Chem. Phys. Lett. 1977, 50, 22.
13. Iqbal, Z.; Chance, R.; Baughman, R. J. Chem. Phys. 1977, 66, 5520.
14. Mueller, H.; Eckhardt, C. Mol. Cryst. Liq. Cryst. 1978, 45, 313.
15. Enkelmann, V.; J. Lando Acta Crystallogr. 1978, B 34, 2352.
16. Bredas, J. L.; Chance, R. R.; Baughman, R. H.; Silbey, R. J. Chem. Phys. 1982, 76, 3673.
17. Suhai, S. Phys. Rev. B 1984, 29, 4570.
18. Boudreaux, D. S.; Chance, R. R. Chem. Phys. Lett. 1977, 51, 273.
19. Chance, R. R.; Shand, M.; Hogg, C.; Silbey, R. Phys. Rev. B 1980 22, 3540.
20. Baughman, R. H.; Eckhardt, H., unpublished results.
21. Chance, R. R. Macromolecules 1980, 13, 396.
22. Dewar, M. J. S.; Thiel, W. J. Am. Chem. Soc. 1977, 99, 4899; 1977, 99, 4907.
23. Bredas, J. L.; Silbey, R.; Boudreaux, D.; Chance, R. J. Am. Chem. Soc. 1983, 105, 6555.
24. Kobelt, D.; Paulis, E. Acta Crystalogr. 1973, B 30, 232.
25. Arnold, S. J. Chem. Phys. 1982, 76, 3842.
26. Salem, L. "The Molecular Theory of Conjugated Systems"; Benjamin: New York, 1966.
27. Boudreaux, D. S.; Chance, R.; Bredas, J.; Silbey, R. Phys. Rev. B 1983, 28, 6927.
28. Eckhardt, H.; Boudreaux, D. S.; Chance, R. R. J. Chem. Phys., in press.
29. Karpfen, A.; Chance, R., unpublished results.
30. Rubner, M., unpublished results.

Chapter 12

Electronic Spectra of a Series
of Polydiacetylene Crystals

C. J. Eckhardt, J. Sartwell, M. Morrow, and H. Müller

Department of Chemistry, University of Nebraska, Lincoln, NE 68588-0304

The spectra of the lowest energy electronic
transitions of a series of polydiacetylene crystals
are presented. Crystals comprised of polymer
chains containing urethane side groups with
differing numbers of methylene linkages (n = 1 to
4) provide the possibility of observing coupling
between chains. Thermochromism is observed for the
series. Piezomodulation spectroscopy is used to
further investigate the role of stress in the
optical response of polydiacetylenes. The role of
strain induced defects on the electronic spectra is
discussed.

The nature of the lowest energy electronic transition observed in
the polydiacetylenes (PDA) has been of interest since the first
spectroscopic observations of these systems. The crystals
display two different but characteristic spectra which are
largely independent of the nature of the substituents on the
polymer chain. This leads to association of the observed
transitions with the pi orbitals of the polymer backbone. For
some systems, the two characteristic spectra may be observed for
the same material but at different temperatures or pressures
(1-4). Thermochromic behavior is not uncommon for PDAs and it is
possible to observe a change, often reversible, from one of the
characteristic bandshapes to the other. The low temperature (LT)
spectrum, sometimes referred to as acetylenic, is exemplified by
a highly structured band which originates around 16,500 cm^{-1}
which is consistent with the gold sheen of the crystals. The
second spectrum, previously called butatrienic, which may appear
at higher temperatures (HT), is devoid of any significant

structure and is found to be blue-shifted to a region around 18,000 cm^{-1} and is typified by the crystal's green luster. Photoconductivity experiments indicate that both of the band systems are excitonic ([5]).

The origins of the characteristic HT and LT spectra are unresolved. An initial hypothesis was that the two arose from different valence tautomers of the PDA backbone ([4]). Quantum chemical calculations have cast doubt on this since the trends for transition energies appear to be in the wrong direction ([6-8]). Interpretation of the color change observed for PDA oligomers in solutions of varying hydrogen bonding capabilities led to the idea that strain placed on the spine by the side groups interacting with solvent molecules was the cause of the color change ([9]). Calculations on "strained" geometries for the spine have supported this view ([10]). As with all such necessarily approximate calculations on large systems, caution must temper judgment, and a definitive experimental conclusion is still awaited.

The nature of the interchain coupling of excitation has not been studied in detail. While exciton splitting has been reported where expected ([11]), additional investigation regarding the nature of the interchain coupling has not been pursued. This may be attributed to the phase and thermochromic changes in the PDAs as well as to difficulty in understanding the intramolecular transitions of the polymer.

One way in which the intermolecular coupling may be studied is to alter the nature of the side chain substituents. If their length is altered, the side chains may be expected to perturb the solid state interactions by affecting the packing in the crystal. By using electronically "neutral" spacers such as methylene groups to vary sidechain lengths, a closely related series of PDA crystals may be generated with differing interchain distances. Because the coupling is a function of the distance between the polymer spines, such a series of crystals may be expected to provide some information on the coupling, especially since the oscillator strengths of the transitions would be expected to be nearly the same.

Another approach to understanding the electronic spectra of PDAs and, in particular, the problem of coupling is to use stress to perturb the energy of the lattice. This can be most profitably approached through piezomodulation spectroscopy. In this experiment, a periodic stress is applied to the crystal and the change in the optical signal is detected synchronously with the stress. This approach can give the strain sensitivity of the transition, the transverse and longitudinal frequencies of the band and, if elastic constants are available, the amount of mechanical energy associated with the modulation of the states involved in the transition ([12]). This is different from the approach using Seraphin coefficients which is commonly employed in the modulation spectroscopy of metals and semiconductors ([13]). Because the coefficients are rapidly varying functions of frequency for the PDAs, they cannot be usefully employed for analysis of the PDA modulation spectra ([14]).

The research presented here pursues the question of the electronic spectra of PDA crystals by employing both of these approaches. In the first, the spectra of a series of PDAs with differing urethane sidechains (Table I) are investigated. Variance of the number of sidechain methylenes is expected to affect the distance between the polymer spines in the lattice thereby altering the spectral response.

Table I. Polydiacetylene Series

$$-(CH_2)_n-O\overset{O}{\overset{\|}{C}}-\underset{H}{N}-R$$

Polymer	n	R
HDU	1	phenyl
POD	2	phenyl
DDU	3	phenyl
TCDU	4	phenyl
DDMU	3	methyl
ETCD	4	ethyl

The second approach is to use low temperature piezomodulation spectroscopy to obtain a more detailed picture of the electronic spectra. In this case, the low temperature spectrum of PTS, which is known to show excitonic interaction, is studied.

Pertinent experimental details are given in the following section after which are presented the spectra of a phenylurethane series of PDA crystals. The nature of the coupling between the transitions is pursued using these results. The subsequent section presents the low temperature piezomodulation spectrum for PTS. The nature of the vibronic structure in this spectrum and its relation to the electronic structure is discussed.

Experimental

Samples were provided by R. R. Chance then of Allied Corporation. The samples were used without further processing. Both the normal incidence specular reflection (15) and piezomodulated reflection experiments are described elsewhere (16). The size and physical character of the first three members of the phenylurethane series of PDA crystals prevented their investigation with our low temperature apparatus.

Crystals for the low temperature piezomodulation experiments were placed in a uniaxial stress mount which was itself located in a CTI helium refrigerator. Spectra were measured in 10 or 25 cm^{-1} intervals using a Jobin-Yvon THR-1500 double pass monochromator.

Table 2 lists the known crystallographic data for the systems studied. Of the phenylurethane series, only TCDU has complete structural information in the literature (17). Apparently, more recent structural data for TCDU exists but it has yet to be published (10). While a drawing relevant to the crystal structure of HDU is published (18), no quantitative crystallographic parameters have been located in the literature. No structural information is available for POD. The specular reflection spectra for ETCD and TCDU have been published elsewhere (3,19).

Spectra of the Phenylurethane Series of Polydiacetylenes

The varying sizes of the pendant groups of the PDAs should alter the distance between the separate polymer spines of the crystal thereby affecting the excitation interactions. The usual criterion for the strength of the vibronic coupling of polariton states in molecular crystals is based on the analysis of Simpson and Peterson (20).

$$\Theta = \frac{4 \pi d^2}{V_o} >> \Delta$$

Here, Θ, is the bandwidth of the calculated stopping band for a crystal of unit cell volume, V_o, and dipole strength, d, and, Δ, is essentially the bandwidth of the free molecule. Of course, in the case of the PDAs, the solution spectrum of the oligomers of some systems is all that is available to approximate the free molecule. It is clear from the expression that the greater the stopping band width, the greater the coupling should be. The criterion cannot be exactly applied because of the lack of the free polymer spectrum, but it can be reasonably approximated from the solution spectra of the oligomers at concentrations where aggregation is unlikely. Thus, the nature of the coupling can be reasonably identified for a series of closely related crystals such as those studied here.

Coupling in PDA Crystals. The polarized specular reflection spectra for the most highly reflective principal directions are shown in Figure 1. For the first three members of the series, the characteristic LT spectrum is observed. Backreflection was a severe problem because of the thinness of the crystals and, in the case of the less reflective principal direction, structure was altered sufficiently to render the spectra unuseable. Thus, direct measurement of exciton splitting, if present, was not possible. In the spectra reported, the backreflection in the intensely reflecting principal directions was corrected using a curve fitting procedure described elsewhere (21).

In Table III are listed the calculated stopping bandwidths and the bandwidths (FWHM) of the actual reflection spectra for the PDA urethane sidechain series of crystals studied here. Because the value of the background dielectric constant is

Table 2. Lattice Constants for Selected PDA Crystals

	Lengths (Å)	Angle (deg)		Interchain Distances (Å)
HDU[b]	a = 4.89 b = 12.53 c = 16.78	α = 69.3 β = 96.8 γ = 96.2	P1̄ Z = 2	6.3
POD	?	?	?	?
DDU[a]	a = 19.46 b = 4.90 c = 10.78	β = 94.55	P2$_1$/c Z = 4	5.4
TCDU[c]	a = 6.23 b = 39.03 c = 4.90	β = 106.85	P2$_1$/c Z = 4	6.23
ETCD[a]	a = 17.90 b = 5.26 c = 4.84	β = 95.2	P2$_1$/c Z = 2	5.26
DDMU[a]	a = 16.35 b = 4.85 c = 9.47	β = 91.9	P2$_1$/c Z = 2	<4.8

a) Provided by R.R. Chance
b) Ref. 18
c) Ref. 17
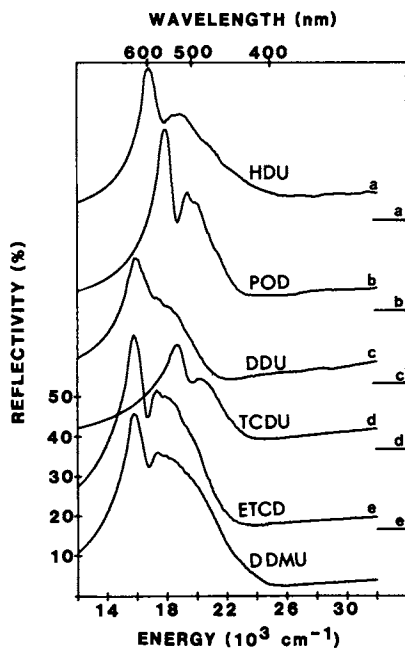
Figure 1. Reflection spectra of a series of PDA crystals with light polarized along the maximally reflecting direction. Spectra were taken at 300K. Lines on the right locate the zero of the designated spectrum.

normally greater than one, it is clear that the coupling in these
systems is at most intermediate in the cases of ETCD and possibly
DDMU, but is weak for all of the phenylurethanes. This
correlates well with the bandwidths of the experimental
reflection bands. In the case of POD, where crystallographic
data is not available, it appears that the coupling is very weak
since the observed reflection band is significantly narrower than
for the other PDAs in the series. Thus, polariton coupling is
not particularly important for PDAs and displays no clear
dependence on the length of the sidechains.

Table III. PDA Bandwidths in Crystal and Solution

Solution	FWHM(cm^{-1})	
	Yellow	Blue
PTS	4,400	
3BCMU	4,840	4,840

Crystal	Reflection (300K)	Coupling
HDU	5,500	Weak-Intermediate
POD	2,550	Weak
DDU	5,000	Weak
DDMU	6,950	Intermediate

The general bandshapes are similar and are strongly
reminiscent of those of PTS or DCHD. Significant structure to
the blue of the most intense peak is observed for all of the
crystals. Most striking, however, are the variances of the
bandwidths of the entire reflection bands and frequencies of
the first peaks. The frequencies range from 15,800 cm^{-1} for
DDMU and DDU to 18,300 cm^{-1} for POD, but the bandshape of the
characteristic LT spectrum is seen in all cases.
    For POD, the peak frequency is close to the 18,800 cm^{-1}
peak observed for the HT TCDU spectrum. The frequency shift
within the phenylurethane series is, therefore, nearly
equivalent to that observed when PDAs such as ETCD or TCDU
undergo thermochromic or pressure induced changes. A major
difference here, however, is the retention of the fairly well
defined vibronic structure characteristic of the LT bandshape.
Application of the strain hypothesis of the thermochromic shift
in PDA spectra would imply that the strain on the polymer
spines would increase in the order: DDMU = DDU < ETCD < HDU <
POD < TCDU. This extreme shift of the LT electronic spectra of
the phenylurethane substituted PDAs presents a problem, since,
if it is strain induced, it has not caused the disappearance of
the "fine structure" in the vibronic envelope which occurs when
the HT phase is induced by temperature or pressure. However,
it has caused essentially the same shift of energy of the pi
transition of the spine as observed in the thermochromics.

A similar, although not as extreme, variation in spectra has been observed with PDAs having fluorobenzene side chains. In these systems there is also significant change in the lengths of the side chains (22).

The spectra could be taken to indicate that crystals of HDU, DDU and DDMU may contain significant numbers of defects or that the polymers are strained significantly. It is also possible that the distribution of chain lengths may be quite broad. All of these could cause the ill-defined structure observed in these spectra. The physical appearance of the materials supports these conjectures. HDU is essentially fibrous while DDU and DDMU are ill-formed solids.

The behavior of POD is of particular interest since it shows only a slight energy shift of its lowest peak on transition to the HT form. It appears to wither rather than decompose or melt upon heating.

While it may be expected that the interchain separation will be a function of the length of the pendant sidechain, the relation is unlikely to be linear. For example, folding becomes more likely with an increasing number of constituents in the methylene chains connecting the urethane functional group to the polymer spine. Upper bounds on the interchain distances for the PDAs investigated are given in Table II. That for POD is unavailable because of lack of crystallographic data but it may be expected to be between those of HDU and DDU.

Although not of the phenylurethane series, DDMU and ETCD are useful for comparison. ETCD is used to complete the series because it is linked to the polymer spine by four methylenes and shows the typical LT spectrum. TCDU is the proper $n = 4$ member of the phenylurethane series but it shows the HT spectral bandshape and thus does not allow spectral comparison. Given the possible effect of strain on the spectra, it is possible that linewidth arguments are not applicable and that most of the broadening arises from the distribution of conjugation lengths of the polymers in the crystals.

Thermochromic Behavior of Phenylurethane Polydiacetylenes.
Since other PDAs with urethane sidechains display thermochromism, the phenylurethane series was investigated for this effect. All were found to be thermochromic. Because of the remote location of the hot stage thermometer from the sample, an accurate transition temperature was not determined but a range could be defined. The color change was determined visually.

HDU had an apparent change from 91-92 C. The fibrous nature of the sample made observation somewhat difficult. Measurement using a differential scanning calorimeter showed a slight change of curvature indicating the possibility of a second order phase change at 117 C. The "transition" does not appear to be reversible. No return to the LT color was observed after two weeks of observation.

POD showed a transition in about the same temperature region as HDU. This sample, however, withered almost immediately after the change. The thermal inertia of the apparatus prevented more refined control of the temperature. DDU displayed a reversible thermochromic shift from 148 to 150 C. It reverted from the HT to the LT form upon cooling. The small amounts of the samples prevented any meaningful DSC measurements. The samples were not checked for hysteresis.

Both ETCD and TCDU have been previously reported to undergo thermochromic changes (1,3). With the former, the change is reversible which is not the case with the latter. All samples gave the greenish metallic color typical of the HT phase observed with the thermochromic PDAs.

Stress Modulation Spectra of Polydiacetylenes

Another approach to the investigation of the intermolecular polariton coupling, as well as to the effects of strain, is piezomodulation spectroscopy. In this experiment a periodic uniaxial stress, within the elastic regime, is applied to the sample and the optical signal is detected synchronously with the stress. The measurement can yield information on the coupling, the strain dependence of the spectra, and more extensively resolved structure (12). Because of sample size and stability, PTS was studied by piezomodulation spectroscopy at low temperature.

A previous report has demonstrated how the temperature dependence of the piezomodulation spectra has been able to produce a more detailed picture of the interaction of the side chains with the polymer spine (23). It was shown that different vibronic modes became active at different temperatures for a uniaxial stress along the b-axis of the crystal.

The piezomodulation spectra for the two factor group directions of the PTS (001) face are shown in Figure 2. The spectra were taken at 14K with a uniaxial stress along the b-axis of the crystal.

There are two quite striking differences in the b-axis and a-axis piezomodulation spectra. First, the sense of the strain response is reversed, i.e. the transverse frequencies appear as minima in the a-axis spectrum rather than as maxima as seen for the b-axis spectrum. Second, the a-axis structure virtually vanishes at frequencies greater than 16,000 cm^{-1}.

The reversal of the response of the piezomodulation is not surprising since it arises from the extreme anisotropy of the system. It would be expected that an extensive stress for the polymer spine would appear as a compression for a direction perpendicular to the spine.

The two minima for the a-axis piezomodulation spectrum occur at 15,610 and 15,860 cm^{-1} thereby exhibiting the characteristic 250 cm^{-1} energy difference typical of the doubled bands seen in the low temperature phase of PTS.
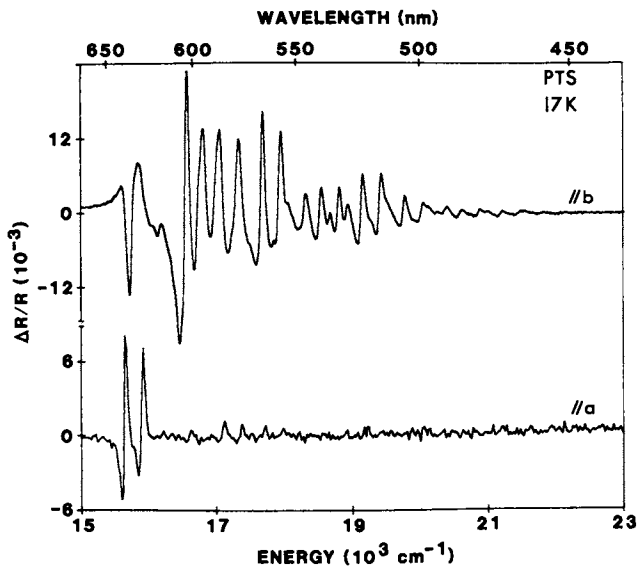
Figure 2.   Piezomodulated specular reflection spectra of PTS at 17K with light polarized along the b and a (b) axes.   The uniaxial stress was along the b-axis.

Within the resolution of the experiment, these are the same
values of the peaks in the piezomodulation spectrum for the
b-axis. Thus, the Davydov splitting is less than 10 cm^{-1}.
Characteristic shoulders are seen approximately 50 cm^{-1} to the
blue of the a-axis minima. Their origin is unknown but
suggestive of a lattice mode.

The lack of any significant Davydov splitting is further
evidence for weak coupling between the spines and argues for
most of the observed broadening as arising from defects. In
addition, the absence of any structure at energies higher than
16,000 cm^{-1} suggests that a quite different interaction is
present at these frequencies. However, there is weak structure
observed at approximately 17,150 and 17,400 cm^{-1} with
additional structure at 17,750 and 18,000 cm^{-1}. Both pairs are
separated by 250 cm^{-1} thereby suggesting that they are related
to the polymer transition. In fact, they appear at essentially
the same frequencies where structure is observed in the b-axis
spectrum. This is in a region where there exists much
unassigned structure. Since this a-axis structure is so
isolated and does not follow the rest of the structure in this
frequency region, it is possible that the unassigned structure
in the b-axis spectrum may be associated with another
electronic state (see Soos, Kuwajima and Mazumdar in these
proceedings).

Discussion of Results

The small upper limit of the Davydov splitting established by
the low temperature piezomodulation spectra of PTS indicates
that the interchain coupling of electronic transitions is
negligible for that system. While the sidechains of the
phenylurethane series may change this somewhat, it is unlikely
that the interaction will exceed the weak coupling case. This
is confirmed by the bandwidth studies of the reflection spectra
where the coupling may approach the intermediate case.
However, a more likely explanation is broadening arising from
defects.

The spectral behavior of the PDA phenylurethanes indicates
that understanding of the electronic properties of these
systems, and PDAs in general, still requires development.
Calculations simulating strain on the backbone have not been
able to address the observed distribution of intensity amongst
the vibronic levels nor the changes in the vibrational
frequencies or their distribution (6-9). While a substantial
blue shift has been calculated, it is unclear what the strain
should do to the shape of the electronic band envelope. The
higher energy spectrum has previously been taken to be that of
the HT form.

It is clear that the low temperature bandshape of the
phenylurethane series is observable over the frequency region
spanned by the low and high temperature bandshapes of the
thermochromics. Strain on the polymer spine may be used to
explain this shift from DDU to POD with retention

of essential bandshape. However, it then becomes necessary to
explain the thermochromism of the phenylurethane PDAs. Of
course, more strain may be invoked. The question concerning
the distinctive and essentially reversible change of bandshape
then remains. It is necessary that the role of strain in the
electronic spectra of the PDAs be more refined if it is to be
used to rationalize the changes in PDA spectra.

If strain is invoked to describe the changes observed in
the spectra, it must explain: (1) the large blue shift seen in
the phenylurethane LT spectra, (2) the additional blue shift
with attendant lack of structure observed in the HT spectra of
the same series, and (3) the usual reversibility of the LT-HT
transition. Since the electronic spectrum arises only from the
polymer spine, it is necessary to better define the role of the
strain effects on the pi conjugation of the spine. It may
prove that not all of these changes, particularly the
thermochromic ones, can be attributed to strain.

The scenario would envisage that the crystal strain
increases in the phenylurethane series such that a blue shift,
which is essentially that of the LT to HT transition, would
result. The loss of detailed structure occurring on the
thermochromic transition to the HT spectrum would result from
an extreme increase in disorder which could be mainly
attributed to dynamic processes, such as sidechain motions,
which are intensified at higher temperatures. A theoretical
approach not unlike this has been recently advanced by
Schweizer (24). Both weak and strong disorder regimes are
considered in that treatment.

The important contribution of Schweizer's approach is the
explicit consideration of the distribution of conjugation
lengths and the subsequent effect on the electronic spectrum.
This is augmented by a consideration of the nature of the
defects causing the varied conjugation lengths and possible
correlations between the defects. The calculated model
absorption spectra show an increasing broadening and blue shift
with decreasing value of the mean conjugation length. All the
spectra for non-infinite mean conjugation lengths show a
persistent high energy tail. The latter is seen in the spectra
for the phenylurethane PDAs.

There is also experimental discrepancy with this approach.
The phenylurethane PDA which has the most blue-shifted LT
spectrum, POD, is also the one which displays the most resolved
structure and narrowest band. Increasing disorder of the side
chains is associated with decreasing conjugation length and,
presumably, a diminution in spectral structure. Perhaps POD is
exceptional and manages to have a narrow distribution of short
conjugation lengths with little disruption of the pendant
groups. Its relatively low temperature thermochromic
transition and resulting instability argues for a highly
strained crystal. It would be expected that the DDU would show
the most resolved structure since it shows the spectrum
farthest to the red. In contrast, it has the most congested
spectrum in the series although not the broadest.

The results suggest the existence of both long and short conjugation lengths in something like a bimodal distribution. This may imply that some conjugation lengths are favored over others. Upon heating, this distribution may become essentially that of the shorter lengths with an accompanying increase of disorder. The present weak disorder picture may be modified by further findings on the absolute intensities of the transitions. More detailed study of the weak defect limit and the effect of correlation of defects may also explain the present inconsistencies.

Conclusions

A series of phenylurethane substituted PDAs have spectra with structure characteristic of the low temperature phases of other PDAs such as PTS. However, the frequency region spanned by these is equivalent to that for PDAs undergoing thermochromic transitions. The series also displays thermochromic transitions. Varying conjugation lengths caused by defects in the polymer spine due to rotations of side groups may be used to rationalize the spectra. The high temperature spectra observed after the thermochromic transition may be broadened and shifted due to dynamic effects not accounted for in the present theory. Present explanations of the spectral changes positing strain require significant elaboration. Disagreement with a current theory of defect created distributions of conjugation lengths is also found, however, since the most blue-shifted member of the series also shows the least broadening and sharpest structure.

Acknowledgment

Literature Cited

1. Müller, H.; Eckhardt, C. J. Cryst. Liq. Cryst. 1978, 45, 313.
2. Eckhardt, H.; Eckhardt, C. J. J. Chem. Phys. 1979, 70, 5498.
3. Chance, R. R.; Baughman, R. H.; Müller, H.; Eckhardt, C. J. J. Chem. Phys. 1979, 67, 3616
4. Iqbal, Z.; Chance, R. R.; Baughman, R.H. J. Chem. Phys. 1977, 66, 5520.
5. Chance, R. R.; Baughman, R. H. J. Chem. Phys. 1976, 64, 3889.
6. Bredas, J. L.; Chance, R. R.; Silbey, R.; Nicolas, G.; Durand, Ph. J. Chem. Phys. 1981, 75, 255
7. Bredas, J. L.; Chance, R. R.; Baughman, R. H.; Silbey, R. ibid. 1982, 76, 3673.

8.   Suhai, S. Phys. Rev. B **1984**, 29, 4570
9.   Patel, G. N.; Chance, R. R.; Witt, J. D. J. Chem. Phys.
     1979, 70, 4387; Patel, G., N.; Witt, J. D.; Khanna, Y. P.
     J. Polymer Sci., Polym. Phys. Ed. **1980** 18, 1383.
10. Eckhardt, H.; Boudreaux, D. S.; Chance, R. R. J. Chem. Phys.
     1986, 85, 4116.
11. Müller, H.; Eckhardt, C. J. J. Chem. Phys. **1977**, 67, 5386.
12. Luty, T.; Eckhardt, C. J. J. Chem. Phys. **1984**, 81, 520.
13. Cardona, M. Modulation Spectroscopy, in Solid State Physics,
     Supplement 11, edited by Ehrenreich, H.; Seitz, F.;
     Turnbull, D. (Academic Press, New York, 1969).
14. Seraphin, B. O., in Optical Properties of Solids, edited by
     Abeles, F. (North-Holland, Amsterdam, 1972), p. 167.
15. Pennelly, R. R.; Ph.D. thesis, University of Nebraska, 1972.
16. Eckhardt, C. J. Mater. Sci. **1984**, 10, 355.
17. Enkelmann, V.; Lando, J. Acta Crystallogr. Sec. B **1978**, 34,
     2352.
18. Hädicke, E.; Mez, E. C.; Krauch, C. H.; Wegner, G; Kaiser,
     J. Angew. Chem. Internat. Edit. **1971**, 10, 266.
19. Müller, H.; Eckhardt, C. J.; Chance, R. R.; Baughman, R.
     H. Chem.   Phys. Letters **1977**, 50, 22.
20. Simpson, W. T.; Peterson, D. L. J. Chem. Phys. **1957**, 26,
     588.
21. Pennelly, R. R.; Eckhardt, C. J. Chem. Phys. **1976**, 12, 89.
22. Tokura, Y.; Koda, T.; Itsubo, A.; Miyabayashi, M.; Okuhara,
     K.; Ueda, A. J. Chem. Phys. **1986**, 85, 99.
23. Morrow, M.; Eckhardt, C. J. Chem. Phys. Letters, in press.
24. Schweizer, K. S. J. Chem. Phys. **1986**, 85, 4181.

Chapter 13

Nonlinear Optical and Excited-State Processes in Polydiacetylenes

Measurements Using Picosecond and Femtosecond Time Scales

Gary M. Carter, Mrinal K. Thakur, John V. Hryniewicz, Yung Jui Chen, and Stephen E. Meyler

GTE Laboratories, Inc., Waltham, MA 02254

Time resolved degenerate four-wave mixing experiments in good optical quality PTS-polydiacetylene have been performed on the picosecond and femtosecond time scale. From the picosecond data the magnitude and temporal response of material's third order nonlinear optical susceptibility were determined. The large measured value of this nonlinearity, 5 x 10^{-10} esu, obtained below the absorption edge (transparent region) and its fast time response make this material an attractive candidate for ultrafast signal processing concepts. The femtosecond measurements were performed in the material's absorption region and the data imply $\approx$ 2 picosecond lifetime for the excited state. Preliminary results indicate the nonresonant nonlinear response time is shorter than can be resolved with 300 fsec duration optical pulses.

Members of the organic polymeric materials system, the polydiacetylenes, have attracted attention as possible candidates for ultrafast nonlinear optical signal processing schemes. These are based on the modification of the material's dielectric constant with applied optical intensity via its third order nonlinear optical susceptibility $\chi^{(3)}$ (1,2). This interest stems from the observation that polydiacetylenes in the solid state have the largest measured value for a nonresonant $\chi^{(3)}$ for wavelengths compatible with optical communication systems ($\approx$ .8 - 2 μm). In the following we will describe recent progress in interdisciplinary research performed at our laboratory which is aimed at developing these materials for the anticipated technological application.

Thin Film Single Crystal Growth

Since the nonlinear optical signal processing schemes require materials in thin film form (either etalons or waveguides) with good optical quality surfaces, we initiated research in the area of growth of thin films of the polydiacetylenes. Recently, this effort has lead to the development of a novel solution-shear technique which has provided the first good optical quality large area ($\geq$ 50 mm^2) single crystal thin ($\approx$ 1 μm) films of PTS-polydiacetylene(3). These good optical quality single crystal platelets should support planar waveguide modes with relatively long propagation lengths, and we are currently employing several techniques to couple to waveguide modes in these films to verify this conjecture. This is a step towards demonstrating

nonlinear waveguiding as a "proof of concept" for the signal processing applications. In the meantime we have been able measure both the magnitude and temporal response of $\chi^{(3)}$ in these platelets, and thus gain information to help judge the suitability of these polymers for the anticipated technology. These results and their significance are discussed in the following.

Picosecond Degenerate Four-Wave Mixing Experiments

Figure 1 shows the measured transmission through a typical 1 μm thick PTS platelet. The oscillations are due to the interference of multiple reflections from the film-air interfaces. As the wavelength is decreased the period of the oscillations increase while their amplitude decreases. The increase in period is due to the increase in index of refraction as one approaches resonance, and the amplitude decreases due to absorption. For wavelength's ≥ 690 nm the sum of the transmission and reflection from the sample was ≈ 100% (estimated error, 1%) indicating that the sample was essentially transparent at these wavelengths. At 650 nm the losses are evenly split between first surface reflection and absorption. The observed absorption in Figure 1 is due to the tail of the excitonic state in PTS (4) which has its resonance at 620 nm (observed in reflection). As we will demonstrate in the following these platelets are ideal for measuring $\chi^{(3)}$ for the wavelengths shown in Fig. 1 via degenerate four-wave mixing experiments. Figure 2 shows a schematic of the four-wave mixing experiment. A 1 kW peak power laser beam (≈ 6 psec pulse duration) is separated into three beams which are focused onto the same 20 μm diameter spot on the sample. Each beam path contains a retro-reflecting prism which is mounted on a translation stage. By varying the position of the retro-prism, one can vary the arrival time at the sample for that pulse. A fourth beam is generated via $\chi^{(3)}$ by the interaction of the three incident beams in the sample. The temporal evolution of the fourth beam was investigated by delaying one of the incident beams in time relative to the other two. At all wavelengths measured the fourth beam was observed only when all three pulses were overlapped in time indicating that the reponse time of the material was much shorter than our optical pulse duration of 6 psec (5). Since the temporal and spatial profile of the input beams are known, by measuring the power in the fourth beam one can derive a value for $\chi^{(3)}$. In the transparent region (≈ 700 nm) we determined $\chi^{(3)} \approx 5 \times 10^{-10}$ esu (5). When this data is corrected for the elliptical projection of the beams on the sample $\chi^{(3)} \approx 10^{-9}$ esu which is in good agreement with values obtained by a different technique at 1.9 μm using nsec duration laser pulses(6). These values represent the largest measured nonresonant $\chi^{(3)}$. This large value coupled with the fast temporal response and the material's excellent optical quality suggest that PTS-polydiacetylene is an attractive candidate for the applications mentioned in References 1 and 2.

At this point in the discussion it is important to discuss what further measurements (if any) of $\chi^{(3)}$ are necessary for assessing its ultility for optical signal processing. There are two basic reasons for using a nonresonant nonlinearity: 1) Ideally the optically induced change in the index of refraction responds "instantaneously" (i.e. it is not limited by an excited state lifetime in the nonresonant regime allowing a high data rate of information to be processed in the material (1); 2) Slow responding thermal changes in the index (as well as thermal damage) due to absorption are minimized. Therefore one needs to determine if the measurement at 700 nm is truly in the nonresonant region. Even at 650 nm which is in the absorptive region the nonlinear response was faster than could be resolved with the 6 psec duration pulses. One might argue that at 700 nm one could be observing a nonlinearity due to a (small) tail of the absorption. However, the fact that the magnitude of the nonlinearity is close to that obtained far off resonance would seem to indicate that this is not the case. Non-degenerate four-wave mixing data taken on several polydiacetylenes in solution indicate that there is a two-photon state which is
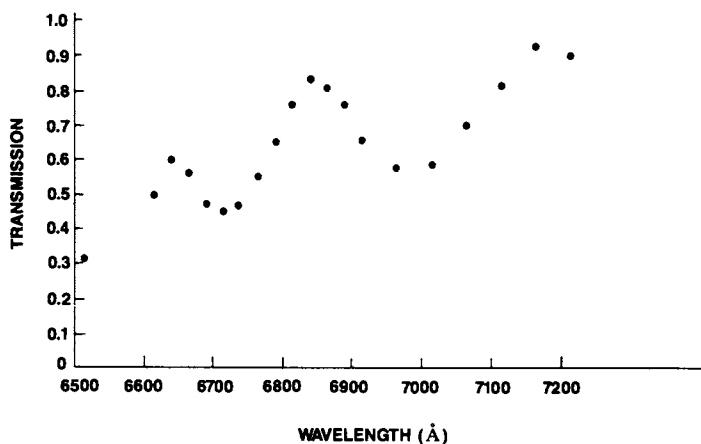
Figure 1. The measured transmission through a 1 μm thick single crystal platelet of PTS-polydiacetylene.
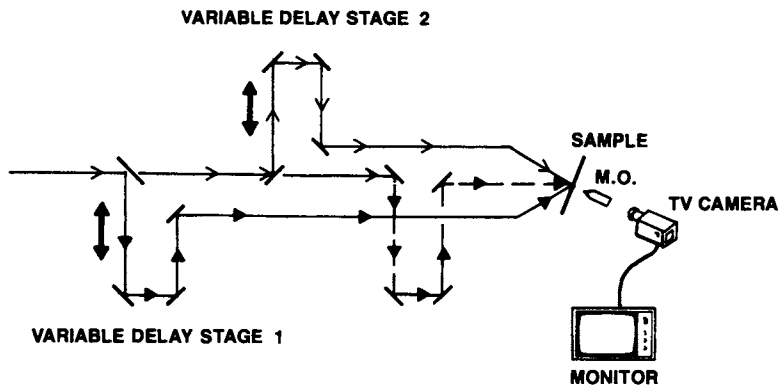
Figure 2. A schematic of the four-wave mixing experiment. The microscope objective (M.O.) and TV camera combination is used to observe spatial overlap of the three incident beams on the same spot on the sample during intial beam alignment.

at shorter wavelengths than the peak of the one-photon absorption curve (7). From the model presented in Reference 7 when the incident photon energy is one-half that of the energy of the two-photon state (relative to the ground state) two-photon absorption would become the dominant term in $\chi^{(3)}$. Such a process could then slow down the response of the nonlinearity to that of the lifetime for the two-photon state or even longer times due to thermal index changes induced by the absorption. The location of the two-photon state and its relative contribution to $\chi^{(3)}$ have not been determined for polydiacetylenes in the solid state. Even if one uses the model presented in Reference 7 which predicts the two-photon level is at 480 nm, then twice the photon energy used in our experiments is far away from the two-photon state. In fact the 700 nm result is 80 nm from the one-photon resonant state, and thus we feel that it is unlikely that there are any significant contributions at this wavelength from two-photon absorptive effects. Another point to consider is that for the application, one can use a wavelength for signal processing which is far below one-half of the two-photon energy to eliminate any two-photon absorptive effects and still be within the optical communication band (e.g. 1.6 μm). Since the nonlinear optical response time even in the absorptive region (650 nm) which one expects to be limited to the excited state lifetime is shorter than 6 psec, it is important to: 1) determine the excited state lifetime and then ; 2) perform time resolved off-resonant measurements of $\chi^{(3)}$ with optical pulse durations shorter than this lifetime to insure that the nonlinear response is not limited by the lifetime effects.

In the following we describe the first step in this process, the determination of the excited state lifetime. The measurement of dynamical processes in the excited state is also part of another component of research in this area. Another goal of the research effort at our laboratory is to develop a microscopic model of $\chi^{(3)}$. To do this one needs to know the nature (i.e. the wavefunctions) of the excited states, and measurements of excited state dynamics provide key insight into the nature of the excited states.

Excited State Lifetime Determination with Femtosecond Laser Pulses

As pointed out in the preceding discussion the degenerate four-wave mixing experiments performed in the absorption region of PTS at 650 nm show the material response time is shorter than 6 psec. One would expect the response time to be determined by the excited state lifetime for the state accessed by this wavelength. Since this state is below the energy gap of the photo-conductive states in this material it has been suggested the state is excitonic in nature and has a large charge transfer component (8). This state has been investigated experimentally by reflection spectroscopy (4), electro-reflectance techniques, and piezomodulation techniques(9). Even though this state possesses a large oscillator strength no luminesence is detected from highly ordered samples(10). This behavior is consistent with a fast non-radiative decay of the excited state. Thus we initiated degenerate four-wave mixing experiments with pulse durations of 300 fsec duration. The wavelength range picked for these experiments, 650-660 nm, is a balance between absorption which is required to observe lifetime effects, and detectability which requires minimal attenuation in the sample.

To produce sub-picosecond high peak power optical pulses the output of the laser used in Reference 5 was coupled into a single mode optical fiber. The resulting self-phase modulation broadens the laser bandwidth from 0.1 to 2 nm. The increased frequency varies almost linearly with time and hence can be compressed in time by passing it through a medium, in this case a grating, with the right sign of dispersion (11). This pulse compression technique produces pulses of ≈ 300 fsec duration and 1 kW peak power. The compressed laser pulse is then directed to the rest of the apparatus shown in Figure 2.

Figure 3 shows the optical power in the fourth beam (λ = 660 nm) as a function

of relative time delay between one of the input beams and the other two which are aligned in time. Negative time delay means that the third beam arrives at the sample after the other two beams. This data shows a clear asymmetry with respect to zero relative time delay unlike the data taken with longer pulse durations (5). The long tail for large negative time delays is due to the excited state lifetime as we will justify in the following.

The four-wave mixing signal in Figure 3 can be described as a transient grating experiment which can be easily understood if the process is dominated by excited state population effects. We assume the input laser intensity causes population to be transferred from the ground to the excited state. The population transfer rate then is proportional to the intensity and the total population is the integrated intensity convolved with the exponential decay of the excited state. Thus the four-wave mixing data in this model (i.e. for the absorbing wavelengths) is a result of two input beams interfering in the sample to produce a population grating in the sample. The third beam diffracts from this grating producing the fourth beam. For pulse durations shorter than the population lifetime the grating decay due to the excited state population decay can be observed by delaying the third beam several optical pulse widths. One can easily show that for negative (in the convention in Figure 3) relative delay times longer than the integrated optical pulse duration the signal decays with at time constant of $T_1/2$ where T_1 is the excited state lifetime.

To further test this simple model we performed saturated transmission experiments as shown schematically in Figure 4. In this case we use only two of the input beams and monitor the transmission of one of them (attenuated) which we designate as the probe beam and the other as the pump beam. From our model the population tranfer to the excited state due to the pump beam will cause a change in the absorption coefficient of the sample. The sample will become more transmitting until the population decays. Figure 5 shows the change in transmitted power of the probe beam as a function of relative time delay between the pump and probe pulses ($\lambda = 650$ nm). In this case positive relative time delay indicates the pump pulse arrives at the sample before the probe. The simple model would then predict that the exponential decay of this change in transmission (i.e. for positive relative times in Figure 5 that are greater than the integrated pulse intensity) should have a time constant of T_1. Preliminary analysis of the data like that shown in Figures 3 and 5 indicates that the decay of the signal is exponential and yields a value of $T_1 \approx 2$ psec. The fact that the lifetime is the same for both experiments indicates that the grating decay is not due to diffusion of excited state species over the distance of a grating spacing (1-2 μm) because the probe beam is measuring the change in transmission over the entire 20 μm spot on the sample illuminated by the pump beam. In fact the proposed model links the transient grating and saturated absoprtion measurements. The index of refraction of the material is proportional to the difference between the excited and ground state population. Therefore the change in the excited state population produces a change in the index of refraction. The change in the real part of the index changes the phase of the optical wave in the material and the change in the imaginary part of the index produces a change in absorption coefficient. Both the change in the real and imaginary components of the index lead to the transient grating signal and only the imaginary component leads to the saturated absorption signal. In this model the change in transmission $\Delta T/T$ (T= total transmission through the sample) squared is equal to the part of the four-wave mixing signal in Figure 3 that comes from the change in the imaginary part of the index. Experimentally the peak value of $\Delta T/T \approx 10^{-2}$ and the peak diffraction efficiency for the four-wave mixing experiments is $\approx 10^{-4}$ which implies that most of diffraction (in Figure 3) is coming from an absorption grating as one would expect near resonance.

If we assume that there are only two states involved in this decay process, the model implies that the nonradiative decay is back to the ground state. In fact, the saturated absorption measurements show that for delay times (positive in the
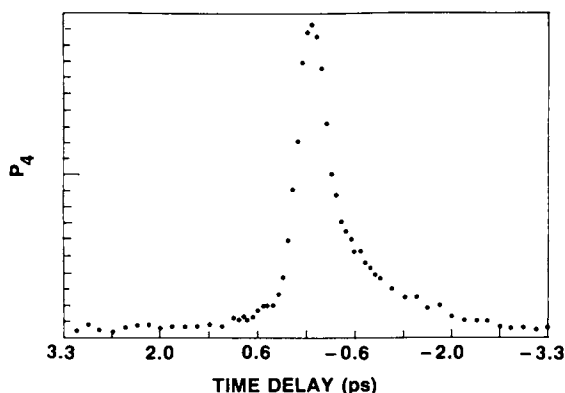
Figure 3. P_4, the power in the generated fourth beam as a function of relative time delay between one of the incident beams and the other two incident beams. Negative time delay means that the third incident beam arrives at the sample after the other two. The laser wavelength is = 660 nm.
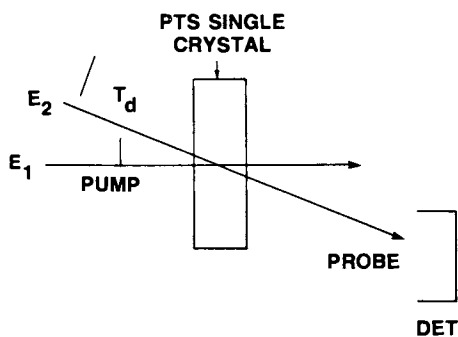
Figure 4. Schematic of pump-probe (saturated absorption) experiment performed in single crystal PTS-polydiaceytlene platelet. E_1 is the intense pump beam and E_2 is the attenuated probe beam, T_d is the relative time delay between the two beams, and DET is the photo-detector used to measure the transmitted probe power.
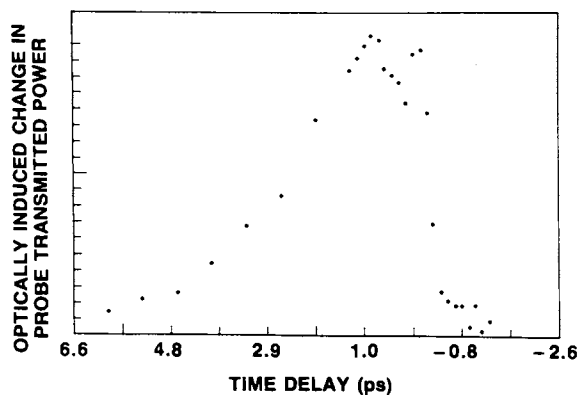
Figure 5. The change in transmitted power of the probe beam due to the pump beam as a function of relative time delay between the two pulses. Positive relative time delay means the pump beam arrives at the sample before the probe beam. Laser wavelength = 650 nm.

convention of Figure 5) $\cong$ 10psec the transmission always returns to its original value indicating that within the context of this model the population does return to the ground state, and the branching ratio to any long-lived intermediate states must be small. This type of behavior is observed in molecules where strong ground and excited state coupling causes rapid non-radiative decay(12). Although a lower lying intermediate state has been observed in PTS, it has been suggested that its existence is due to the generation of a free electron -hole pair(13). Since the excitonic state is 0.4 eV below the gap for free electron-hole pair generation in PTS, it is unlikely that this state decays into the observed intermediate state.

Off-Resonant Data

Recently the solution-shear crystal growth technique was extended to yield thicker samples of PTS-polydiacetylene. Since the degenerate four-wave mixing signal increases as the square of the interaction length in the material (until one approaches the depth of focus of the beams in the sample), these thicker samples are ideal for off-resonant measurements of the temporal response of $\chi^{(3)}$. Figure 6 shows time resolved four-wave mixing data taken at 720 nm with 300 fsec duration optical pulses using a 11 μm thick PTS-polydiacetylene single crystal. Note that the asymmetry with respect to zero time delay which is evident in Fig. 3 (resonant data) has disappeared. Although data taking and analysis are continuing, this data indicates the response time of the nonlinearity is shorter than can be resolved with the 300 fsec duration optical pulses.

Conclusions

From time and wavelength resolved four-wave mixing data, for PTS-polydiacetylene the magnitude of the nonresonant third order nonlinear susceptibility, $\chi^{(3)}$ was determined to be $\approx 10^{-9}$ esu and its response time to be less than 6psec. This result coupled with the availability of good optical quality single crystal thin films of the material indicate that the polydiacetylenes are indeed attractive candidates for nonlinear optical signal processing schemes. Further the lifetime of the excitonic state in PTS located at 2.0 eV above the ground state was determined to be $\approx$ 2 psec by transient grating and saturated absorption measurements. Recent data indicates the off-resonant response time for the optical nonlinearity is shorter than can be resolved with 300 fsec duration optical pulses.
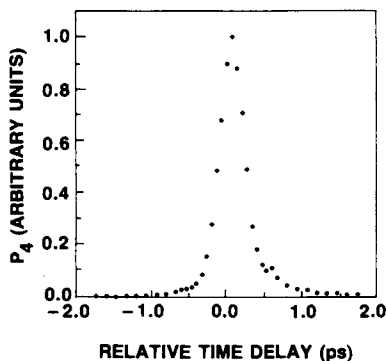
Figure 6. P_4, the power in the generated beam as a function of relative time delay between one of the incident beams and the other two incident beams. Data were taken at 720 nm with 300 fsec duration optical pulses.

<u>Literature Cited</u>

1. Smith, P.W. <u>Bell Sys. Tech. J.</u> 1982, <u>61</u>, 1975.
2. Lattes, A.; Haus, H.A.; Leonberger, F.J.; Ippen, E.P. <u>IEEE Journ. of Quantum Electron.</u> 1983, <u>QE-19</u>, 1718.
3. Thakur, M.; Meyler, S. <u>Macromolecules</u> 1985, <u>18</u>, 2341.
4. Bloor, D.; Ando, D.J.; Preston, F.H.; Stevens, G.C. <u>Chem. Phys. Lett.</u> 1974, <u>24</u>, 407.
5. Carter, G.M.; Thakur, M.K.; Chen, Y.J.; Hryniewicz, J.V. <u>Appl. Phys. Lett.</u> 1985, <u>47</u>, 457.
6. Hermann, J.P.; Smith, P.W. <u>Proc. 11th Interntl Quantum Electron. Conf.</u>, 1980, pp.656-657.
7. Shand, M.L.; Chance, R.R. In "Nonlinear Optical Properties of Organic and Polymeric Materials"; Williams, David, Ed.; ACS Symposium Series No. 233, American Chemical Society: Washington, D.C., 1983; Chap. 9.
8. Philpott, M.R. <u>Chem. Phys. Lett.</u> 1977, <u>50</u>, 18.
9. Eckhardt, C.J.; Muller, H.; Tylicki, J.; Chance, R.R. <u>J. Chem. Phys.</u> 1976, <u>65</u>, 4311.
10. Pope, M.; Swenberg, C.E. "Electronic Processes in Organic Crystals "; Oxford University: New York, 1982; pp. 677-696.
11. Nikolaus, B.; Grischkowsky, D. <u>Appl. Phys. Lett.</u> 1983, <u>43</u>, 228.
12. Shank, C.V.; Ippen, E.P.; Teschke, O.; Fork, R.L. <u>Chem. Phys. Lett.</u> 1978, <u>57</u>, 433.
13. Orenstein, J.; Etemad, S.; Baker, G.L. <u>J. Phys. C</u> 1984, <u>17</u>, L297.

Chapter 14

Nonlinear Optics: Organic and Polymeric Systems

A. F. Garito, Y. M. Cai, H. T. Man, and O. Zamani-Khamiri

Department of Physics and Laboratory for Research on the Structure of Matter,
University of Pennsylvania, Philadelphia, PA 19104-6396

Organic and polymer structures exhibit
unusually large, ultrafast second and third
order nonlinear optical properties that are
important to the fields of nonlinear optics
and optical device technologies. These
important properties have been demonstrated
in a large number of structures, phases and
states. Experimental and theoretical
studies of such systems have achieved sig-
nificant advances in the understanding of
these macroscopic nonlinear optical
responses based on theoretically calculated
microscopic electronic mechanisms. One
recent example of the electronic origin of
second order nonlinear optical processes in
conjugated linear chain structures is
reviewed.

Organic and polymer structures exhibit unusually large,
ultrafast second and third order nonlinear optical proper-
ties that are important to the fields of nonlinear optics
and optical device technologies. These important
properties have been demonstrated in a large number of
structures, phases, and states that, as previously
reviewed (1-9), include organic crystals and films, conju-
gated polymers, monomolecular films, liquid crystals,
liquid crystal polymers, and more recently, high perform-
ance ordered polymers (10,11), and polymer glasses (12).
For these classes of conjugated molecular and polymer
structures, the principal property is that their nonreson-
ant, nonlinear optical responses are dominated by ultra-
fast, virtual excitations of the π-electron states. This
was directly demonstrated by MNA (2-methyl-4-nitroaniline)
single crystal measurements of macroscopic second order
susceptibilities at dc (13) and optical frequencies (13-
15) and combined second harmonic measurements and theo-

retical calculations of the frequency dependent molecular second order susceptibility ($\underline{3,16,17}$). Similar results are being obtained for third order properties of liquid crystal monomers and polymers ($\underline{18\text{-}22}$), and single crystal polymers ($\underline{23\text{-}24}$). Importantly, π-electron excitations are intrinsically ultrafast of order 10^{-15} seconds (1fs) ($\underline{25}$) whereas other potential excitation modes such as phonons, or ion motions, involve slower nuclear displacements and vibrations of order 10^{-12} seconds (1ps).

Currently, the π-electron excitations are viewed as occurring on individual molecular, or polymer chain, sites and providing macroscopic sources of nonlinear optical response through the corresponding on-site microscopic nonlinear optical susceptibility. Thus, in a rigid lattice approximation, the macroscopic second order $\chi^{(2)}(-\omega_3;\omega_1,\omega_2)$ and third order $\chi^{(3)}(-\omega_4;\omega_1,\omega_2,\omega_3)$ responses are expressed by the equations

$$\chi^{(2)}{}_{ijk}(-\omega_3;\omega_1,\omega_2) = N\langle R_{im'}R_{jn'}R_{ko'}f_{j'n'}^{\omega_1}f_{k'o'}^{\omega_2}f_{m'i'}^{\omega_3}$$

$$\beta_{i'j'k'}(-\omega_3;\omega_1,\omega_2)\rangle \tag{1}$$

and

$$\chi^{(3)}{}_{ijkl}(-\omega_4;\omega_1,\omega_2,\omega_3) = N\langle R_{im'}R_{jn'}R_{ko'}R_{lp'}$$

$$f_{j'n'}^{\omega_1}f_{k'o'}^{\omega_2}f_{l'p'}^{\omega_3}f_{m'i'}^{\omega_4}\gamma_{i'j'k'l'}(-\omega_4;\omega_1,\omega_2,\omega_3)\rangle$$

$$\tag{2}$$

where N is the number of molecular, or polymer, sites per unit volume, $\beta_{i'j'k'}$ and $\gamma_{i'j'k'l'}$ are the respective microscopic second and third order nonlinear optical susceptibilities, f^{ω_i} local field tensors, R the rotation matrix transforming the molecular frame to the laboratory frame, the bracket $\langle...\rangle$ an average over the orientational distribution, and the unprimed (primed) coordinates designate the laboratory (molecular) fixed axes. Thus, unlike inorganic semiconductors and dielectric insulators, the fundamental problem of understanding the origin of the large macroscopic responses $\chi^{(2)}{}_{ijk}$ and $\chi^{(3)}{}_{ijkl}$ of conjugated π-electron organic and polymer structures reduces to experimental and theoretical studies of the corresponding microscopic susceptibilities β_{ijk} and γ_{ijkl} of single molecular, or polymer chain, units, and the orientational distribution functions of assemblies of such units comprising the nonlinear optical medium.

The π-electron states are true many-body states because electron correlations due to natural repulsive Coulomb interactions tend to localize the otherwise delocalized electrons. Electron correlations play an important role in the nonlinear optical responses of conjugated organic structures ($\underline{1\text{-}3,16,17,26}$), and their description of β_{ijk} and γ_{ijkl} differs markedly from independent particle models. In calculating the sign, magni-

tude, and dispersion of β_{ijk} or γ_{ijkl}, suitable descriptions of the correlated π-electron motion occurring in the higher order virtual excitations can be obtained by self consistent field molecular orbtial procedures (SCF-MO) that include single and double configuration interactions (SDCI) to account for electron correlations (1-3,16,17,26).

For the microscopic second order response β_{ijk} of resonant ring structures such as MNA and its parent PNA, detailed theoretical and experimental analyses show that, of the many π-electron excited states, only those states possessing highly asymmetric charge correlations principally contribute in the virtual excitation processes responsible for the measured magnitude, sign, and dispersion of β_{ijk} (3,16,17). These states characteristically possess relatively large values for both their transition moments and dipole moment differences. Important to third order procesess in centrosymmetric structures such as conjugated linear chains, the correlated motion of π-electrons leads to formation of two photon excited states (27). For example, in centrosymmetric <u>trans</u> linear polyenes (28,29) (alternating single and double bonds) such as diphenyloctatetraene (DPO), both spectroscopic measurements and SCF-MO-SDCI calculations have demonstrated that a dipole forbidden two photon ^1A_g state appears immediately below the well-known one photon allowed ^1B_u state. More recently, SCF-MO-SDCI calculations (3,7,30,31) and third harmonic generation measurements (7,22,29) show that introduction of triple bonds in <u>trans</u> linear polyenynes such as diphenyldivinyldiacetylenes (DVDA) results in the 2 photon ^1A_g state lying above ^1B_u.

SOLVENT INDUCED SHIFTS OF THE EXCITATION ENERGIES OF LINEAR POLYENYNES AND π-ELECTRON STATE ORDERING

Solvent induced shifts of absorption and emission spectra of dissolved symmetric conjugated linear chains as a function of solvent refractive index can provide experimental evidence of the relative state ordering (28,29). The frequency shift $\Delta\omega$ is approximated by the mutual polarizability expression

$$\Delta\omega = \frac{-1}{\hbar a^3}\frac{(n^2-1)}{(n^2+2)}\frac{\omega}{(\omega'+\omega)}\left[\mu_{ng}^2 - \hbar\omega(\alpha_g-\alpha_n)\right] \quad (3)$$

where n is the refractive index of the solvent, a solute cavity radius, μ_{ng} electric dipole transition moment of the solute, ω and ω' mean excitation frequencies of the solvent and solute, respectively, and α's polarizabilities of the solute in the ground (g) and excited (n) states.

Representative experimental absorption and emission spectra of DVDA1 (<u>trans-trans</u>-1,8-bis(methylphenyl)-1,7-

diene-3,5-octadiyne) dissolved in a solvent, in this case
hexadecane, are shown in Figure 1. As illustrated in the
comparative Figure 2, with increased solvent polarizabil-
ity $(n^2-1)/(n^2+2)$, the DVDA1 absorption and emission spec-
tra shift linearly to lower energy and extrapolate to
their respective gas phase values of 27,700 and 27,100 cm^{-1}
which essentially correspond to the same electronic state
within experimental error. According to eq. 3, strongly
allowed transitions with large transition dipole moments
μ_{ng} should exhibit a relatively large dependence of their
excitation energy on solvent polarizability. The slope of
the absorption data for DVDA1 in Figure 2b corresponds to
about -7,400 cm^{-1} per unit change of $(n^2-1)/(n^2+2)$, and
the emission slope to the even larger value of -10,300
cm^{-1}. In contrast, for DPO in Figure 2a, absorption to
the ^1B_u and emission from the dipole forbidden 2^1A_g yield
widely differing slopes of -10,800 and -1,100 cm^{-1} respec-
tively (28). For another linear polyene, decatetraene, the
emission slope is actually of opposite sign (29). Thus,
analysis of solvent effects for DVDA1 and related struc-
tures leads to the conclusion that, in contrast to linear
polyenes, absorption and emission in linear polyenynes
occurs from the same ^1B_u excited state and that the 2^1A_g
state consequently lies above the ^1B_u state.

ELECTRONIC ORIGIN OF SECOND ORDER NONLINEAR OPTICAL
RESPONSES IN CONJUGATED LINEAR CHAIN STRUCTURES AND HIGHLY
CHARGE CORRELATED π-ELECTRON STATES

Linear polyenes and polyenynes represent the finite chain
limit to the corresponding quasi-one dimensional
conjugated polymer chain, and phase matched second
harmonic generation, for example, has been demonstrated
for noncentrosymmetric conjugated polymer structures (see
Figure 3) (1,2,3,7,32). In this regard, for the funda-
mentally important case of a noncentrosymmetric conjugated
linear chain, NMDVDA [trans-trans 1-(4 methylphenyl)-8-
(4'-nitrophenyl)-1, 7-diene-3,5-octadiyne] (3), the first
results have been obtained
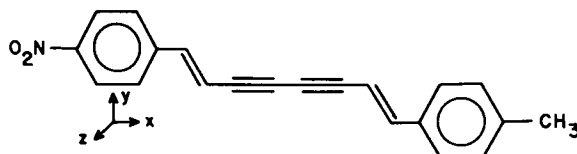
for the frequency dependent $\beta_{ijk}(-2\omega;\omega,\omega)$ as determined
by DC induced second harmonic generation (DCSHG) measure-
ments and corresponding all valence electron, self
consistent field molecular orbital calculations (SCF-MO)
with single and double configuration interactions (SDCI)
(26).
     The vector part $\beta_x(-2\omega,\omega,\omega)$ of $\beta_{ijk}(-2\omega;\omega,\omega)$ was
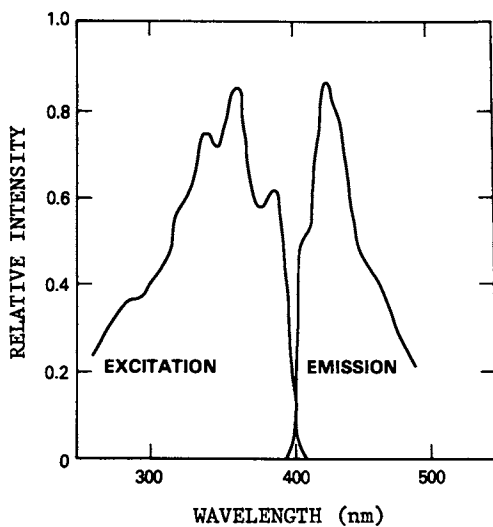
Figure 1.   Typical solution absorption and emission spectra of DVDA1 in hexadecane.
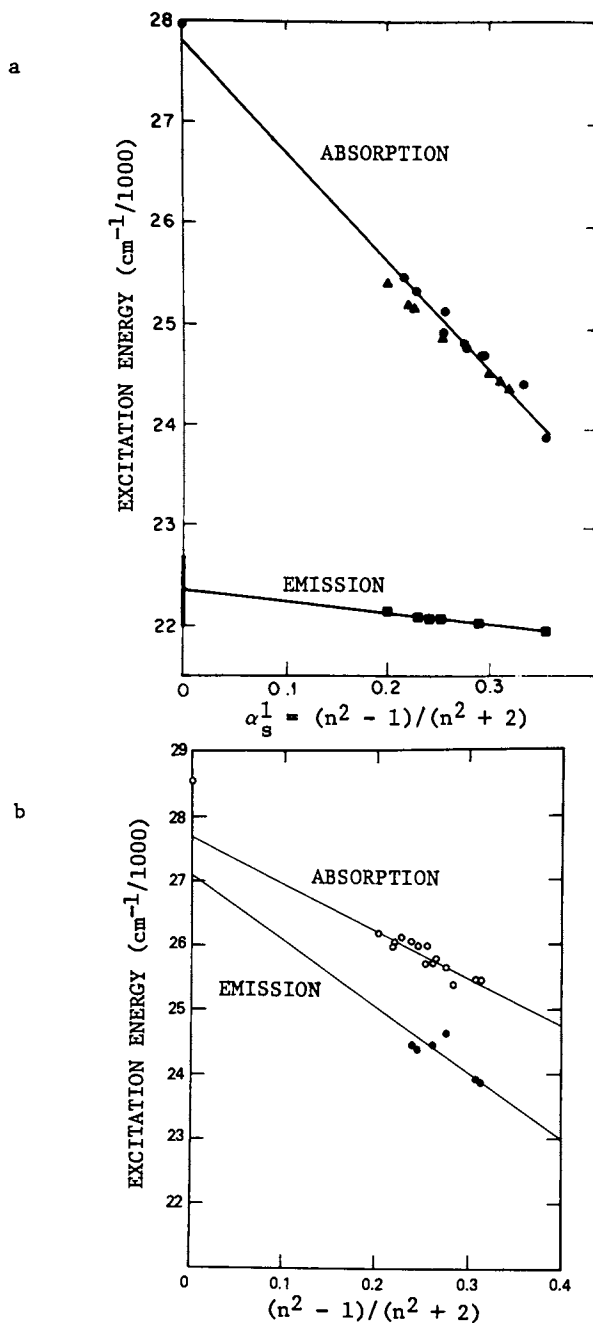
Figure 2. Comparison of solvent effects on absorption and emission processes where n is the solvent linear refractive index: (a) diphenyloctatetraene (DPO) and (b) bis(methylphenyl)divinyl-diacetylene (DVDA1). (Reproduced with permission from reference 28. Copyright 1973.)

CONJUGATED POLYMER
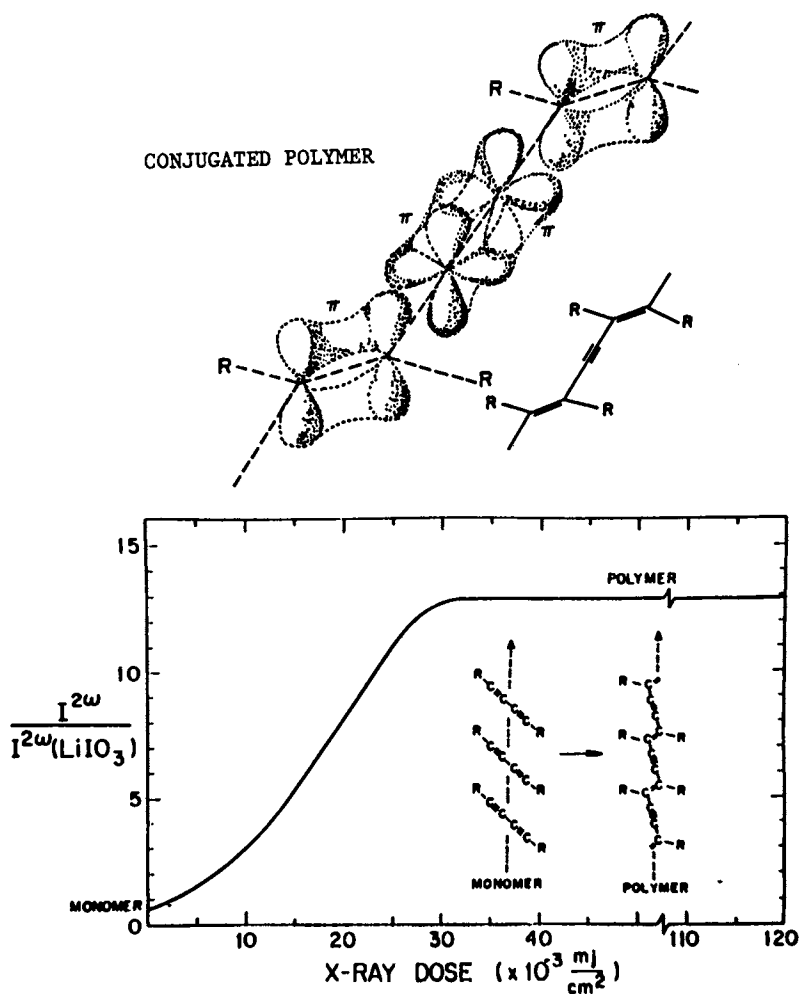
Figure 3.   Second harmonic intensity of MNA substituted diacetylene monomer (NTDA) microcrystals referenced to lithium iodate powder with increasing X-ray induced polymer formation.   (Reproduced with permission from reference 3.   Copyright 1984.)

experimentally determined by DCSHG (2,3,14,16,33,34) liquid solution measurements of NMDVDA dissolved in dioxane using wedge cell and infinite dilution methods described earlier (2,3,16,34). The measured macroscopic susceptibility Γ_L for a two component solution of solvent (o) and solute (1) is given by the infinite dilution equation (34)

$$\frac{(2\epsilon_0+n_1^2)(2n_0^2+n_1^2)^3 M_1}{(n_1^2+2)^4 n_0^6 \epsilon_0} \{v_0 \frac{\partial \Gamma_L}{\partial w}\big|_0 + \Gamma_0 \frac{\partial v}{\partial w}\big|_0 + v_0 \Gamma_0 - v_0 \Gamma_0 \ (\frac{1}{n_0^2} \frac{\partial n^2}{\partial w}\big|_0 +$$

$$(\frac{1}{\epsilon_0} - \frac{2}{2\epsilon_0+n_0^2})\frac{\partial \epsilon}{\partial w}\big|_0)\} = N_A \gamma_i' \qquad\qquad (4)$$

where γ_i is $\beta_i \mu_i / 5 k_B T$ with μ_i the dipole moment; w solute weight fraction; v is the specific volume; ϵ static dielectric constant; n index of refraction; and N_A Avogadro's number. Solvent induced shifts in solute excitation energies for β_x were analyzed as described previously (16). The dipole moment (5.1 $\pm$ 0.3D) of NMDVDA in dioxane was standardly determined by infinite dilution procedures (34).

The experimental values of β_x for NMDVDA as a function of frequency are plotted in Figure 4. With increased frequency, the positive β_x values starting at approximately 40×10^{-30} esu increase smoothly to greater than 300×10^{-30} esu in approaching the 2ω singularity which corresponds to the observed excitation energy 3.31 eV (0.375 μm) of the major absorption peak of NMDVDA in dioxane (Figure 4 insert).

The frequency dependent β_{ijk} components and singlet-singlet excitation spectrum of NMDVDA were theoretically calculated by the original SCF-MO-CI method (3,17) in the rigid lattice CNDO/s approximation. Included were all (16) possible singly excited (SCI) and 100 lowest energy doubly excited configurations (DCI) involving the four highest occupied π-orbitals and the four lowest virtual π-orbitals along with the SCF ground state. The results were unchanged by increased CI.

For $\beta_x = \beta_{xxx} + 1/3(\beta_{xyy} + \beta_{xzz} + 2\beta_{zzx} + 2\beta_{yxx}))$, the theoretical gas phase components are, for example, at 0.650 eV (λ =1.907 μm) β_{xxx}:34.2; β_{xyy}:1.9; β_{xzz}:0; β_{zzx}:0; and β_{yxx}:1.4 ($\times 10^{-30}$ esu). The calculated dispersion curve for β_x is plotted as the solid line in Figure 4 after accounting for dipole mediated solvent induced shifts (16). The comparison between experiment and theory for the magnitude, sign, and dispersion of β_x is quite satisfactory.

The largest β_x component is β_{xxx}, having diagonal β_{xxx}^{nn} and off-diagonal β_{xxx}^{nn} contributions of 54% and 46%, respectively. The diagonal component β_{xxx}^{nn} is given by the expression

Figure 4. Frequency-dependent $\beta_x(-2\omega;\omega,\omega)$ for NMDVDA: (■) experiment; (—) theory. Comparison of singlet-singlet excitations spectra with large oscillator strength transitions to states I, III, and IV. Dielectric shift due to dipole-mediated solvent interactions (26).

$$\beta_{xxx}^{nn} = \frac{-3}{2\hbar^2} \left\{ \sum_n \mu_{ng}^x \mu_{ng}^x \, \Delta\mu_n^x \; \omega_{ng}^2 (\omega_{ng}^2 - \omega^2)^{-1} \, (\omega_{ng}^2 - 4\omega^2)^{-1} \right\} \tag{5}$$

where $\mu_{ng}^x = -er_{ng}^x$ is the x-component of the transition moment between the ground (g) and excited (n) states; $\Delta\mu_n^x = -e \Delta r_{ng}^x$ is the x-component of the dipole moment difference between the ground and excited states, and the sum is over all states. The dominant NMDVDA singlet excited states are I, III and IV with calculated gas phase values, respectively, for ω_{ng} of 3.83, 4.49 and 4.96 eV; μ_{ng}^x of 9.6, 4.9, and 2.3 D; and $\Delta\mu_{ng}^x$ of 18.7, 4.2 and 33.5 D. The state I contribution to β_{xxx}^{nn} is largest (90%) because both values of μ_{I}^x and $\Delta\mu_{I}^x$ are relatively large and the excitation energy ω_{Ig} is lowest.

The off-diagonal component $\beta_{xxx}^{nn'}$ is given by the expression

$$\beta_{xxx}^{nn'} = \frac{-1}{2\hbar^2} \sum_{\substack{n \neq n' \\ n \neq g \\ n' \neq g}} (\mu_{gn'}^x \mu_{nn'}^x \mu_{ng}^x) \; [(\omega_{ng} - \omega)^{-1}(\omega_{n'g} - 2\omega)^{-1}$$
$$+ (\omega_{ng} - \omega)^{-1}(\omega_{n'g} + \omega)^{-1} + (\omega_{ng} + \omega)^{-1}(\omega_{n'g} + 2\omega)^{-1}] \tag{6}$$

where $\mu_{nn'}^x = -er_{nn'}^x$ is the x-component of the transition moment between excited states n and n'. As in the diagonal term, the important NMDVDA singlet excited states are I, III and IV with calculated gas phase values of $\mu_{I,III}$: 8.3D; $\mu_{I,IV}$: 12.8D; and $\mu_{III,IV}$: 4.0D. The largest contribution to $\beta_{xxx}^{nn'}$ results from excitations between states I and III (59%) and states I and IV (36%).

Density matrices of the state functions provide a compact graphical representation of important microscopic features for second order nonlinear optical processes. The transition moment $\mu_{nn'}^i$ is expressed in terms of the transition density matrix $\rho_{nn'}(r,r')$ by $\langle \mu \rangle_{nn'} = -e \int_{r=r'} r \, \rho_{nn'}(r,r')dr$ and the dipole moment difference $\Delta\mu_n^i$ by the difference density function $\rho_n - \rho_g$ between the excited and ground state functions $\langle \Delta\mu_n \rangle = -e \int r(\rho_n - \rho_g)dr$ where ρ_n is the first order reduced density matrix. Contour diagrams of $\rho_n - \rho_g$ and $\rho_{nn'}$ for states I, III and IV are plotted as examples in Figure 5 where the solid and dashed lines correspond to negative and positive values, respectively. In each case, upon virtual excitation in the second order process, large asymmetric redistribution of electron density occurs along the conjugated chain, especially in the x direction, resulting in large dipole moment differences $\Delta\mu_n^x$ (Figures 5a and 5b) and transition moments $\mu_{nn'}^x$ (Figure 5c) that determine β_x. Thus, for example, $\rho_{IV} - \rho_g$ of Figure 5b corresponding to $\Delta\mu_{IV}^x$ of 33.5D exhibits a large correlation distance
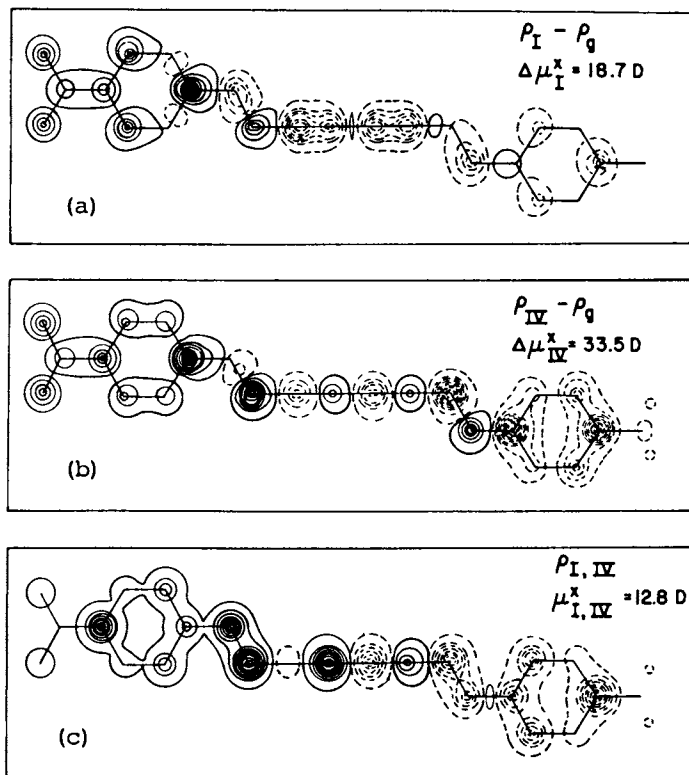
Figure 5. Contour diagram of difference density functions for $\rho_g - \rho_I$ (5a) and $\rho_g - \rho_{IV}$ (5b) and of transition density matrix $\rho_{I,IV}$ (5c) (26).

between positive and negative regions along the x-direction in comparison to $\rho_I - \rho_g$ with its associated value of $\Delta\mu_I^x$ of 18.7D. The same charge correlated features are exhibited by $\rho_{I,IV}$ of Figure 5c where the $\mu_{I,IV}^x$ of 12.8D is relatively large. Similar features were found in resonant benzene ring structures such as MNA (2,3,5,13,17).

Thus, experimental and theoretical results for the frequency dependent second order nonlinear optical response $\beta_{ijk}(-2\omega;\omega,\omega)$ for the noncentrosymmetric all trans-polyenyne NMDVDA show that the microscopic origin resides in highly charge correlated states of the π-electron singlet excited state manifold whose virtual excitations contribute to both the diagonal and off-diagonal components of $\beta_x(-2\omega;\omega,\omega)$. In addition to studies of nonlinear optical conjugated polymers, these recent results serve as a basis for a variety of futher studies such as the effects of photoisomerism and electron-lattice coupling; second harmonic generation in mono-molecular layers; and the design of conjugated structures with intrinsic second order optical responses orders of magnitude larger than the prototype NMDVDA system. The results of these studies are being reported separately.

ACKNOWLEDGMENTS

LITERATURE CITED

+ Presented in part: Molecular Crystal Symposium XI, Lugano, 1985, and International Quantum Electronics Conference, San Francisco, 1986.

1.   Garito, A.F.; Singer, K.D. Laser Focus 1982, 18, 59.
2.   "Nonlinear Optical Properties of Organic and Polymeric Materials"; Williams, D., Ed.; Plenum Press: New York, 1983.
3.   Garito, A.F.; Teng, C.C.; Wong, K.Y.; Zammani-Khamiri, O. Mol. Cryst. Liq. Cryst. 1984, 106, 219.
4.   Shen, Y.R. Rev. Mod. Phys. 1976, 48, 1.
5.   Girling, I.R.; Cade, N.A.; Kolinsky, P.V.; Montgomery, C.M. Electron. Lett. 1985, 21, 169.
6.   Lalama, S.J.; Sohn, J.E.;Singer, K.D. SPIE Integrated Optical Circuit Engineering II. 1985, 578, 168.
7.   Garito, A.F. SPIE Adv. in Mats. For Active Optics 1985, 567, 51.
8.   Williams, D.J. Angew. Chem. Intl. Ed. Eng. 1984, 23, 690.
9.   Zyss, J. J. Molec. Electron. 1985, 1, 25.

10.   Garito, A.F. SPIE Nonlinear Optics and Applications 1986, 613.
11.   Rao, D.N.; Swiatkiewicz, J.; Chopra, P.; Ghoshal, S.K.; Prasad, P.N. Appl. Phys. Lett. 1986, 48, 1187.
12.   Singer, K.D.; Sohn, J.E.; Lalama, S.J. Appl. Phys. Lett. (in press).
13.   Lipscomb, G.F.; Narang, R.S.; Garito, A.F. Appl. Phys. Lett. 1981, 38, 663; J. Chem. Phys. 1981, 75, 1509.
14.   Levine, B.F.; Bethea, C.G.; Thurmond, C.D.; Lynch, R.T.; Bernstein, J.L. J. Appl. Phys. 1979, 50, 2523.
15.   C. Grossman and A.F. Garito, Opt. News 1985, 11, 88.
16.   Teng, C.C.;Garito, A.F. Phys. Rev. Lett. 1983, 50, 350; Phys. Rev. B 1983, 28, 6766.
17.   Lalama, S.J.; Garito, A.F. Phys. Rev. A 1979, 20, 1179.
18.   Durbin, S.D.; Shen, Y.R. Phys. Rev. A 1984, 30, 1419.
19.   Meredith, G.R.; Van Dusen, J.G.; Williams, D.J. in ref. 2.
20.   Khoo, I.C.; Normandin, R.; So, V.C.Y. J. Appl. Phys. 1982, 53, 7599.
21.   Wong, K.Y.; Garito, A.F. Phys. Rev. B, in press.
22.   Wong,K.Y.; Teng, C.C.; Garito, A.F. J. Opt. Soc. Am. B 1984, 1, 434.
23.   Sauteret, C.; Hermann, J.P.; Frey, R.; Pradiere, F.; Ducuing, J.; Baughman, R.H.; Chance, R.R. Phys. Rev. Lett. 1976, 36, 959; Optics Commun. 1976, 18, 55.
24.   Carter, G.M.; Thakur, M.K.; Chen, Y.J.; Hryniewicz, J. Appl. Phys. Lett. 1985, 47, 457.
25.   For a recent example, see Weiner, A.M.; DeSilvestri, S.; Ippen, E.P. J. Opt. Soc. Am. B 1985, 2, 654.
26.   Cai, Y.M.; Man, H.T.; Teng, C.C.; Zamani-Khamiri, 0.; Garito, A.F. XIV Intl. Quant. Elec. Conf. Tech. Digest 1986, p. 84.
27.   Schulten, D.K.; Ohmine, I.; Karplus, M. J. Chem. Phys. 1976, 64,4222.
28.   Hudson, B.S.; Kohler, B.E. Chem. Phys. Lett. 1972, 14, 299; J. Chem. Phys. 1973, 59, 4984.
29.   Hudson, B.S.; Kohler, B.E.; Schulten, K. "Excited States", Lim, E.C. Ed.; Academic Press: New York, 1982; Vol. 6, p. 1-97.
30.   Garito, A.F. Conf. Proc. Unconventional Photoactive Solids, Schur, H. Ed.; Cleveland, 1985.
31.   Garito, A.F. Mol. Cryst. Symp. XI 1985, 97.
32.   Garito, A.F.; Singer, K.D.; Hayes, K.; Lipscomb, G.F.; Lalama, S.J. J. Opt. Soc. Am. 1981, 32, 1306.
33.   Ouder, J.L. J. Chem. Phys. 1977, 67, 446.
34.   Singer, K.D.; Garito, A.F. J. Chem. Phys. 1981, 75, 3572.

Chapter 15

Extended Pariser–Parr–Pople Model
for Polydiacetylene Excitations

Z. G. Soos[1], S. Mazumdar[2], and S. Kuwajima[1]

[1]Department of Chemistry, Princeton University, Princeton, NJ 08544
[2]GTE Laboratories, Inc., Waltham, MA 02254

The Pariser–Parr–Pople (PPP) model for π-electrons is
extended to polydiacetylene (PDA) excitations. Dynamic
Coulomb correlations between the two π systems of the
PDA triple bonds lower and split the excitonic $1\,^1B$
absorption in short segments. Such coupling occurs in
correlated states of ene–yne molecules, qualitatively
changes their low-lying excited states, and admixes
pseudocovalent valence-bond (VB) structures describing
simultaneous transfers in both π systems.

Recent theoretical and experimental advances[1-5] in the area of planar
π-conjugated molecules and polymers have convincingly demonstrated
the need for going beyond single-particle concepts by explicitly
including strong Coulomb interactions between π-electrons. To be
sure, the ground state geometries are usually found within single-
particle theories. Even in the ground state, however, correlations
lead to antiferromagnetic coupling[6] and to negative spin densities in
polyacetylene[7] (PA) and in alternant radicals[8]. More pervasive correla-
tion effects occur in excited electronic states. Even[9,10] at the
Hartree–Fock (HF) level, for example, the positions[9,10] of the two-
photon $2\,^1A_g$ and dipole-allowed $1\,^1B_u$ level of octatetraene and longer
polyenes are in the wrong order[11]. The same ordering of $2\,^1A_g$ below
$1\,^1B_u$ has recently been reported[12] for PA. The absence of a mid-gap
neutral soliton absorption[12] in trans-PA and its occurrence at the
optical band edge of the pristine material show the importance of

correlations for the band gap E_g. It may be useful to consider π-conjugated polymers to be Mott-Hubbard semiconductors[13] with a Peierls-typebroken symmetry in the ground state.

The relative roles of electron-electron and electron-phonon coupling have long been debated[14] even in ideal cases. But the amorphous morphology of PA and other conducting polymers is far from ideal. Polydiacetylenes (PDAs), on the other hand, are crystalline polymers[1,4,5] with large interstrand separations that should permit sharper comparisons between theory and experiment. Although the PA absorption at E_g has been interpreted as a band-to-band transition,[15] the lowest optical state in PDA is generally agreed to be an exciton,[16] mainly because the threshold for photoconduction is still higher. But there is no microscopic picture for the exciton and band (Hückel) theory is invoked for other aspects of PDA.

We initiate here the microscopic description of PDA within the π-electron framework of Pariser-Parr-Pople (PPP) theory. Quite aside from the crystallinity and interesting nonlinear optical properties of PDAs, we are convinced that related π-electron descriptions should apply to PA, PDA, and other conjugated polymers. Furthermore, the nature of the low-lying excited states of polymers is a prerequisite for understanding their relaxation and dynamics. In sharp contrast to π-electron models, a more realistic treatment of triple bonds leads to important and previously overlooked Coulomb correlations. We focus below on the novel aspects of excitations in ene-yne systems.

Typical π-bonding in HC≡CH is shown in Fig. 1(a) for the two sets of π-electrons denoted as π and π'. Their simultaneous transfer in the opposite direction leads to the pseudocovalent diagram in Fig. 1(b). Such a dicarbene contains π and π' ion pairs that
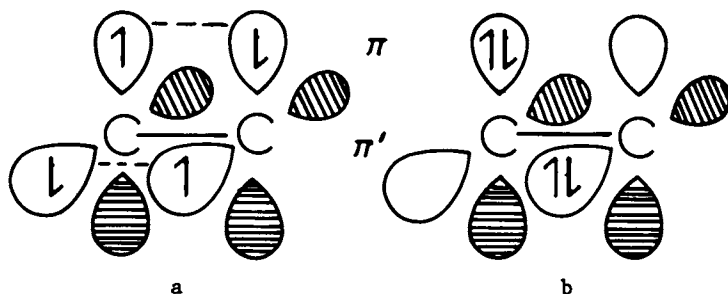
Figure 1.   (a) Covalent diagram with π and π' bonds; (b) pseudocovalent diagram with π, π' lone pairs on adjacent sites.

form neutral sites. Explicit inclusion of Coulomb correlations leads
to strong admixture of pseudocovalent states. Parallel transfers in
Fig. 1(a), by contrast, produce $C^{+2}C^{-2}$ pairs with very high energy
and thus negligible weight. Pseudocovalent diagrams reflect coupling
between systems with low-lying excited states. The 2.0 ev exciton in
PDA is associated below with the π system, while the localized π'
dimers have a ~ 7 ev excitation. The far higher (>10 ev) σ^* excita-
tions are consequently more weakly coupled. Thus $\pi-\pi'$ Coulomb corre-
lations must at the very least alter PPP parameters derived for
purely ene systems.

Extended PPP Model

     In free-electron or in Hückel theory the orthogonal π-systems of
diacetylene (HC$\equiv$C-C$\equiv$CH) or other linear ynes are decoupled and merely
lead to different bond lengths or resonance integrals t_{ij} than occur
in butadiene (H$_2$C=CHCH=CH$_2$) or other enes. Such decoupling persists
at the HF level. The polyene backbone of PA in Fig. 2 contains
alternating double and single bonds, while the PDA backbone consists
of double-single-triple-single sequences. The difference between PDA
and PA is then entirely associated with the bond lengths and thus t_{ij}
= t_1, t_2, t_3 for single, double and triple bonds, respectively,
involving sp and sp^2 centers in Table I.

     We retain these t_{ij} for the PPP description of the extended
π-system of PDA. Now the in-plane or π'-electrons of the triple bond
formally[18] belong to the σ network, but their identity is well pre-
served[18] in vinylacetylene (HC$\equiv$C-CH=CH$_2$) and other yne-enes. We also
assign t_3 to π' dimers in Fig. 1 and exclude $\pi-\pi'$ transfers. A PDA
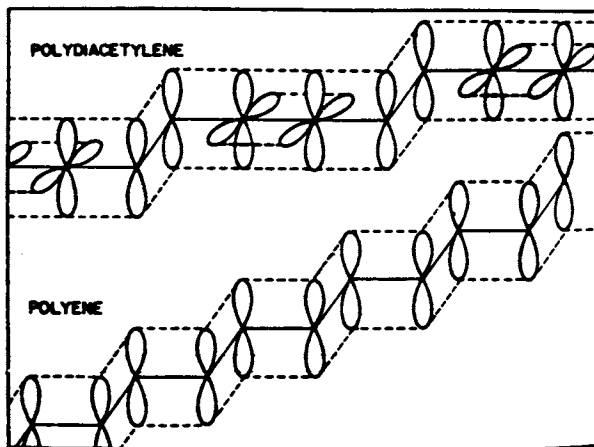
Figure 2. Schematic representation of π electron backbones in
PDA and PA. (Reproduced with permission from reference 17.
Copyright 1976 John Wiley & Sons.)

Table I. Bond lengths and transfer integrals for PDA and PA$_2$
          calculations; the C-C bond angles are $2\pi/3$ at sp^2
          centers and π at sp centers

C-C Bond	R(Å)	-t(ev)
single	1.45	2.24
double	1.35	2.56
triple	1.20	3.04

segment of 4n carbon atoms then contains precisely 4n π-electrons delocalized over the entire segment and 2n π'-electrons localized to n dimers. Coulomb interactions $V_{pp'}$ among C^+ and C^- sites are given by the Ohno interpolation[19] between $U = V_{pp} = 11.26$ ev and unshielded interactions $\pm e^2/r_{pp'}$ at large separation. Equal site energies (α integrals) were chosen for simplicity at sp and sp^2 sites. These parameters[10] completely specify the PPP model for PDA and automatically incorporate Coulomb correlations $U' = U$ between π and π' ions at the same site. Different α, U', and t_3 for the π' electrons need careful examination before making definitive assignments.

The extended PPP model is solved exactly via diagrammatic valence-bond (DVB) methods.[20] Each π' dimer increases the dimensions of the configuration-interaction matrices by about a factor of 3. We have found the ^{1}A ground state and lowest two ^{1}B excited states of two N = 6 molecules, I = $H_2C=CH-C\equiv C-CH=CH_2$ and II = $HC\equiv C-CH=CH-C\equiv CH$. We have also found the corresponding states of a cyclic molecule III with N = 8 and two PDA unit cells. N = 10 chains and N = 12 rings should also be accessible. In addition to $\pi+\pi'$ results, we solve the simpler PPP model with only π-electrons, standard parameters and the PDA geometry in Table I. Such calculations demonstrate the extent of π-π' coupling, while comparisons with polyenes probe changes in the backbone geometry.

The probability that orbital ϕ_i is empty or doubly-occupied, and therefore not covalent, in state $|r\rangle$ is simply

$$P_i^{(r)} = \langle r | n_i^2 | r \rangle - 1 \tag{1}$$

where n_i is the number operator and $\langle n_i \rangle = 1$ follows exactly from the electron-hole symmetry of the half-filled PPP model. The π or π' bond orders in $|r\rangle$ are given by

$$2p_j^{(r)} = (\partial E_r/\partial t_j) \tag{2}$$

for transfer integral t_j connecting sites j and $j+1$. The uncorre-
lated Hückel result for ethylene gives $p = 1.0$ for equal admixture
of a covalent Heitler-London bond and ionic VB diagrams. The contri-
bution of pseudocovalent diagrams is approximated by

$$P_{\pi\pi'}^{(r)} = -\langle r \mid n_\pi n_{\pi'} \mid r \rangle + 1 \qquad\qquad (3)$$

for the π and π' orbitals at the same site; the operator gives 1 for
pseudocovalent diagrams, vanishes when either orbital is singly
occupied, and gives -3 for the small admixture of C^{-2} diagrams. To
the extent that adjacent like charges have negligible weight, we may
also use (3) for the weights of ion pairs C^+C^- at adjacent sites i
and j. Such expectation values and transition moments provide
direct insight into correlated states containing linear combinations
of many ($< 10^5$) VB diagrams. Indeed, there is no "dominant" diagrams
even though trends and ideas are often best understood by considering
Kekulé, Dewar, ionic or other special cases.

Table II lists results for molecule II, which has inequivalent
sp centers. Values in parentheses are π-only results. Similar
calculations have been carried out on I and III. We consistently
find weak $\pi-\pi'$ effects in the ^1A ground-state bond orders (2), ion-
pair correlations (3), or ionicities P_i in (1). The ~ 12% admixture
of pseudocovalent structures increase P_i slightly at sp centers. The
situation is quite different for the 1^1B and 2^1B excited states in
Table II. The different admixtures of pseudocovalent states, dif-
ferent bond orders and different P_i or P_{ij} all point to dynamic $\pi-\pi'$
coupling. Comparable effects are found in I and III, although the
cyclic system seems to have 1^1B and 2^1B interchanged.

The excitation energies $\Delta E(ev)$ and transition dipole $M(D)$ in
Table II are also changed qualitatively on including $\pi-\pi'$ coupling.
$E(2^1B)$ is strongly lowered, while $E(1^1B)$ is slightly red shifted.
Their transition dipoles become comparable, with 2^1B having the
larger M in both I and II. Preliminary results on longer fragments,
where the intensity is increasingly concentrated in 1^1B for purely π
systems, suggest that $\pi-\pi'$ coupling still results in similar M for
1^1B and 2^1B. In contrast to a single strong absorption in polyenes,[10]
$\pi-\pi'$ coupling in ene-ynes results in two dipole-allowed transitions
with comparable intensities and energies.

The largest changes between 1^1A and either ^1B states in Table II
involve C^+C^- ion pairs across single bonds. Their amplitude is
comparably small in the ground states of I, II, and III, presumably
because the dominant ionic contributions involve ion pairs across
multiple bonds with larger t. The electron-hole symmetry of the ^1B
states, on the other hand, rigorously excludes purely covalent
diagrams and leads to admixture of states with one or more ion pairs.
The expectation value of $(-)^{\pm}$ in 1^1B increases sharply to ~25% in all
three molecules; its small negative value in 2^1B indicates greater
admixtures of like charges. Detailed information in Table II about
correlated states has not been previously accessible and its
interpretation is far from complete.

Table II Extended PPP results for $HC_1 \equiv C_2C_3H = CHC \equiv CH$, with t_{ij} parameters from Table I; in parentheses, same geometry but without the π' electrons

States	$1\,^1A$	$1\,^1B$	$2\,^1B$
Excitation energy, ΔE(ev)	–	4.669(5.238)	6.125(8.149)
expt, ref. (22)		4.74	
Transition Moment, M (D)	–	3.66(6.79)	5.29(3.36)
Ionicity, $\langle n_i^2 \rangle - 1$			
$\quad sp^2 \qquad C_3$	.363(.362)	.466(.658)	.650(.574)
$\quad sp(\pi) \qquad C_1$	.426(.374)	.626(.507)	.437(.529)
$\qquad\qquad C_2$	.441(.399)	.576(.500)	.479(.528)
$\quad sp(\pi') \quad C_1, C_2$	.430	.530	.530
Pseudocovalent (eq. 3)			
$\qquad\qquad C_1$	.132	.310	.167
$\qquad\qquad C_2$	.123	.249	.187
Bond Order (eq. 2)			
$\quad \pi'$	.959	.844	.808
$\quad \equiv$ (sp–sp)	.917(.923)	.668(.740)	.865(.649)
$\quad = (sp^2 - sp^2)$	.868(.865)	.712(.411)	.385(.389)
$\quad - (sp - sp^2)$	.286(.295)	.410(.483)	.308(.265)
Ion pair[a] $(1 - \langle n_i n_j \rangle)$			
$\quad (-)^{\pm}$	.056(.065)	.209(.262)	–.030(–.130)
$\quad (=)^{\pm}$	.293(.290)	.323(.454)	.431(.495)
$\quad (\equiv)^{\pm}$	.397(.342)	.512(.370)	.386(.477)

a, charges in π orbitals only.

We have also compared PDA results with earlier PPP calculations[10] on trans polyenes with $t_1 = -2.26$ and $t_2 = -2.56$ ev for single and double bonds of 1.45 and 1.35Å, respectively. The larger PDA alternation due to the triple bond ($t_3 = -3.04$ ev, r = 1.20Å) increases as expected the excitation energy to 1^1B for the π system, but this is more than compensated by $\pi-\pi'$ coupling. The optical gap of II in Table II and of 4.543 ev for I are both lower than all-trans hexatriene gap of 5.04 ev. The larger PDA alternation is clearly seen in the larger bond-order alternation.[6] On-site and nearest-neighbor correlations fortunately converge very rapidly with the segment size N, as does the oscillator strength per site, while optical gaps vary significantly with N. Thus results for molecules I, II, and III already suggest several features of infinite PDA strands.

Evidence for π' Participation

Coulomb correlations in the PPP model automatically couple the π and π' subsystems even in the strict absence of $\pi-\pi'$ transfers. The same situation prevails in extended Hubbard models and the coupling becomes more important when both subsystems have low-energy excitations. Such correlations have been neglected previously because, in the absence of $\pi-\pi'$ transfers, two subsystems merely change each other's self-consistent field. We expect previously studied ene-yne molecules to corroborate $\pi-\pi'$ coupling now that specific predictions can be tested.

Extrapolations for PDA are more delicate, since smaller N is accessible with $\pi-\pi'$ coupling and there is no rigorous basis for such extrapolations. We nevertheless propose that the PDA spectra in Fig. 3 should be analyzed in terms of two excitonic transitions, a 1^1B state around 2.0 ev with weak exciton-phonon coupling and a 2^1B state around 2.1-2.2 ev with vibronic sidebands.
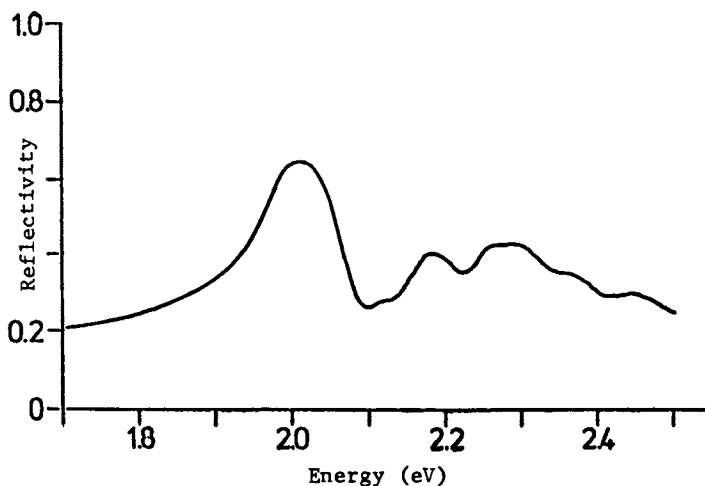
Figure 3. Reflectivity of a PDA crystal at 300 K. (Reproduced with permission from reference 16. Copyright 1976 North-Holland Physics Publishing.)

Standard PPP parameters have successfully accounted for the positions of the 2^1A_g and 1^1B_u states of finite polyenes,[10] for the low-lying states and fine structure constants of naphthalene,[21] for negative spin densities in radicals,[8] and for $\pi-\pi^*$ absorptions of anions.[10] Their extension to ene-ynes is also satisfactory. The longest wavelength absorption[22] of I is 4.66 ev in methanol vs. 4.543 ev for $\pi-\pi'$ coupling and 5.27 ev for the π system alone. The experimental value[22] for II is 4.74 ev in methanol vs. 4.669 ev with $\pi-\pi'$ coupling and 5.238 ev for π only. Replacing the terminal H in II with t-butyl groups leads[23] to an absorption at 4.51 ev in hexane. Solvents usually give red shifts due to the higher polarizability of the excited state. The strength of the $\pi-\pi'$ coupling is also open, since its relative change from higher-energy σ excitations in sp^2 centers must be estimated in obtaining new PPP parameters for sp centers. The present $\pi-\pi'$ coupling is consequently maximal and defines the full range of energy shifts relative to the π-only result.

The C-C bond lengh of HC≡CH increases[24] by 0.18 Å in the lowest excited state to 1.38Å. The 120.2 C-C-H bond angles point to sp^2 hybrids. This bent excited molecule is quite suggestive of the pseudocovalent diagram in Fig. 1(b), except for placing the lone pairs in sp^2 orbitals. The bond length also indicates contributions from double-bonded VB diagrams. While such major distortions are neither possible in polymeric crystals nor expected for delocalized excitations, the HC≡CH excitation illustrates nicely how bending vibrations could be excited by pseudocovalent contributions.

The π' excitation of an isolated dimer with r = 1.20Å and t = 3.04 ev is

$$\Delta E' = [(x^2+16t^2)^{1/2} + x]/2 = 7.79 \text{ ev.} \qquad (4)$$

with $x = V_{11} - V_{12} = 3.05$ ev. The polarization is along the PDA backbone, but $\Delta E'$ is not lowered through delocalization. Tokura et al.[25] observe a high-energy polymeric transition around 6.7-7.6 ev for different R groups in PDA. They reject the interpretation of π' excitation due to the broadened line and too high energy within SCF theory. We note, on the contrary, that standard PPP parameters are quite appropriate and that $\pi-\pi'$ coupling offers promising possibilities for R-group and broadening effects. Additional work and refinements of sp parameters should provide a more quantitative treatment of the high-energy PDA peak polarized along the chain.

Recent optical data on both PDAs and their finite-chain analogs provide quite independent and equally preliminary support for two low-lying excitons. In higher resolution low temperature work on single crystals, Eckhart[26] has been led to consider two nearby O-O frequencies in an effort to obtain a satisfactory fit. In finite PDA analogs with R = H side group add t-butyl caps, Wudl[23] reports two $\pi-\pi^*$ absorptions whose separation depends weakly on chain length. Standard PPP parameters account for the lowest $\pi-\pi^*$ excitation of the smallest molecule in this series, the t-butyl-capped version of II in

Table II. The calculated 2^1B excitation is far higher than the
second observed $\pi-\pi^*$ transition, however, and either improved para-
metrization of the π' interactions or another explanation must be
sought.

    More persuasive qualitative evidence for π' participation emerges
on comparing molecular ene-yne and polyene excitations. The lowest
absorptions[23] of N = 6 and 10 ene-ynes are below that of the
corresponding polyenes.[9] Thus bond alternation does not dominate
the optical gap, since either one-electron or full PPP treatments
for π electrons predict a larger gap at any N for the larger bond-
length alternation of ene-ynes. As discussed above, $\pi-\pi'$ coupling
red shifts the lowest 1^1B transition. The red shift decrease with N
since the π and π' excitation energies become more separated; the π
system has $E_g \sim 2$ ev as N → ∞ while the nonconjugated π' dimers
remain around 7 ev in (4). The stronger alternation in PDAs then
leads to a larger E_g than in PA.

    Such preliminary comparisons clearly support the $\pi-\pi'$ coupling
found on extending the PPP model to ene-ynes. More extensive and
quantitative applications are in progress. Possible changes of the
microscopic parameters, the nature of electron-phonon coupling in
these correlated states, and an assessment of extrapolations all need
further work in both PA and PDA.

Discussion

    Not even improved finite-chain calculations, however, can
demonstrate directly the occurrence of two excitonic states separated
by ~ 0.2 ev in Fig. 3. Any finite-chain analysis leads to discrete
eigenstates and therefore to multiple absorptions. Thus N → ∞ extra-
polations require caution. We discuss below why we believe that the
1^1B and 2^1B transitions will persist as separate entities in PDA
polymers.

    The oscillator strengths in discrete systems generally decrease
with increasing transition energy, as shown by the familar absorption
edge of a one-dimensional band. As seen in Table II, on the other
hand, $\pi-\pi'$ Coulomb interactions reverse this trend: 2^1B has a higher
transition dipole than 1^1B. The latter is considerably smaller than
the polyene transition moment for N = 6 or 8. Thus something fun-
damentally new and different is occurring even in the finite system.

    The novel features of $\pi-\pi'$ coupling may be illustrated with the
aid of some characteristic VB diagrams. The covalent and pseudocova-
lent diagrams in Fig. 1 are nearly degenerate electrostatically.
Admixtures of covalent and pseudocovalent segments may consequently
be envisioned in eigenstates of PDA chains. There is now a new kind
of low-energy charge-transfer (CT) involving the triple bonds of the
extended π system. CT involving π double bonds is independent of
whether the neighboring yne is covalent or pseudocovalent. But two
different CT processes involving π electrons are shown in Fig. 4 for
the triple bond. In the atomic limit ($t_3 = 0$) both CT processes

require $U-V_1$. The new π-CT process in Fig. 4(b) persists in polymers even on admixing CT transitions outside the triple bonds and, in our opinion, is the origin for two nearly degenerate adsorptions.

We note that the lower E_g of short ene-ynes relative to polyenes is readily understood by associating the 1^1B ene-yne excitation with Fig. 4(a). There the final configuration is directly connected to a pseudovovalent diagram, albeit through a π' CT process that costs more energy. Thus π-π' Coulomb coupling lowers 1^1B <u>indirectly</u> through configuration interactions. The correlation functions in Table II provide further support for the CT processes in Fig. 4. From the energetics alone, we expect the 1^1B and 2^1B excitations to be more influenced, respectively, by CT process (a) and (b). It then follows that the π-electron ionicity in the triple bond should increase in 1^1B due to non zero $U_{\pi\pi'}$, but the same π-electron ionicity should decrease in 2^1B, where a C^+C^- is replaced by C-C. This aspect of the sp(π) ionicities in Table II is clearly seen on comparing 1^1B and 2^1B with the π-only result. The slight ionicity increase in 2^1B relative to 1^1A reflects the rigorous exclusion in the former of all purely covalent VB diagram. We have verified the same results in molecule I and in an N = 8 PDA segment.

Such considerations are no more definitive than the preceding experimental evidence for π-π' coupling. While the 7-8 ev absorption discussed above is clear evidence for excitation of π' dimers, it does not require π-π' Coulomb coupling. Our preliminary discussion of the extended PPP model has been restricted to standard ene parame-
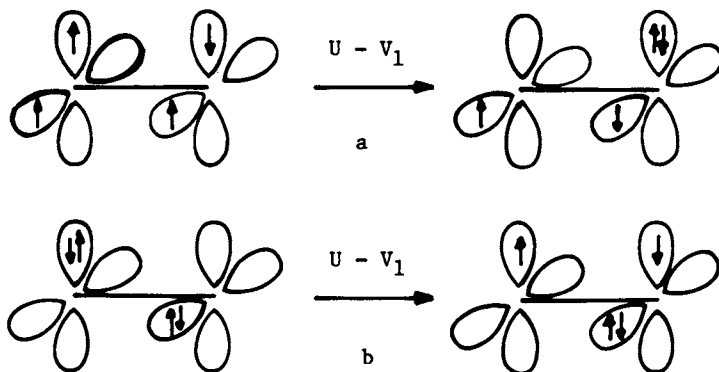
Figure 4. Schematic representation of CT processes in the π subsystem: (a) CT in covalent diagram; (b) CT in pseudocovalent diagram.

ters and to small molecules. We have focused on the dipole-allowed
^{1}B excitations. The less accessible 2^1A or triplet excitations are
equally amenable^{27} to exact analysis within the extended PPP model and
should provide both additional comparisons with experiment and new
$\pi-\pi'$ contributions. There are good reasons both experimentally and
theoretically to explore more carefully the implications of Coulomb
correlations afforded by low-lying excited states of both π and π'
subsystems of ene-yne molecules and polymers.

References

1. Polydiacetylenes, NATO ASI Series E102 (eds. D. Bloor and R. R.
    Chance, Martinus Najhoff, Dordrecht, The Netherlands, 1985).

2. Proceedings of the International Conferences on the Physics
    and Chemistry of Low-Dimensional Synthetic Metals, Abano Terme,
    Italy, Mol. Cryst Liqu. Cryst. 117-121 (1985).

3. G. Wegner, Angew. Chem. Int. E. Engl. 20, 361 (1981);
    "Proc. of VI Int. Conf. Org. Solid State," Freiburg,
    1982, Mol. Cryst. Liqu. Cryst. 93, 96 (1983).

4. V. Enkelmann, Adv. Polymer Science 63 (ed. H. Cantow,
    Springer-Verlag, 1984) p. 91. See also the articles by
    H. Bässler and by H. Sixl in the same volume.

5. D. Bloor, in Photon, Electron, and Ion Probes of Polymer
    Structure and Properties, (eds. D. W. Dwight, T. J. Fabish,
    H. R. Thomas, ACS Symposium Series 162) p. 81 (1981).

6. S. Ramasesha and Z. G. Soos, Phys. Rev. B32, 5368 (1985).

7. H. Thomann, L. R. Dalton, Y. Tomkiewicz, N. S. Shiren, and
    T. C. Clarke, Phys. Rev. Lett. 50, 553 (1983).

8. Z. G. Soos and S. Ramasesha, Phys. Rev. Lett. 51, 2374 (1983);
    H. M. McConnell and D. B. Chesnut, J. Chem. Phys. 27, 984 (1957).

9. B. S. Hudson, B. E. Kohler, and S.Schulten, Excited States 6,
    1 (1982) and references therein.

10. Z. G. Soos and S. Ramasesha, Phys. Rev. B29, 5410 (1984).

11. S. Etemad, APS meeting, Las Vegas (1986).

12. Z. G. Soos and L. R. Ducasse, J. Chem. Phys. 78, 4092 (1983);
    B. R. Weinberger, C. B. Roxlo, G. L. Baker, and J. Orenstein,
    Phys. Rev. Lett. 53, 86 (1984).

13. S. Mazumdar and D. K. Campbell, Synth. Metals $\underline{13}$, 163 (1986) and referenes therein.

14. S. Dixit and S. Mazumdar, Phys. Rev. $\underline{B29}$, 1824 (1984) and references therein.

15. S. Etemad, A. J. Heeger, and A. G. McDiarmid, Ann. Rev. Phys. Chem. $\underline{33}$, 443 (1983).

16. D. Bloor, F. H. Preston, and D. J. Ando, Chem. Phys. Lett. $\underline{38}$ 33 (1976); see also the D. N. Batchelder in ref. 1 and D. Bloor in ref. 5; M. R. Philpott, Chem. Phys. Lett. $\underline{50}$, 18 (1977).

17. R. H. Baughman and R. R. Chance, J. Pol. Sci. $\underline{14}$, 2037 (1976).

18. U. Dinur and M. Karplus, Chem. Phys. Letters $\underline{88}$, 171 (1982).

19. K. Ohno, Theor. Chim. Acta. $\underline{2}$, 219 (1964).

20. S. Ramasesha and Z. G. Soos, Int. J. Quantum Chem. $\underline{25}$, 1003 (1984); J. Chem. Phys. $\underline{80}$, 3278 (1984).

21. S. Ramasesha and Z. G. Soos, Chem. Phys. $\underline{91}$, 35 (1984).

22. G. J. Exarhos, W. M. Risen, Jr., and R. H. Baughman, J. Am. Chem. Soc. $\underline{98}$, 481 (1976).

23. F. Wudl and S. P. Bitler, these precedings and private communication.

24. C. K. Ingold and G. W. King, J. Chem. Soc. $\underline{1953}$, 2702; K. K. Innes, J. Chem. Phys. $\underline{22}$, 263 (1954).

25. Y. Tokura, T. Mitani, and T. Koda, Chem. Phys. Lett. $\underline{75}$, 324 (1980); Y. Tokura, Y. Oowaki, Y. Kaneko, T. Koda, and Y. Mitani, J. Phys. Soc. Japan $\underline{53}$, 4054 (1984).

26. C. J. Eckhart, these procedings and private communication.

27. Z. G. Soos, S. Mazumdar, and S. Kuwajima, Physica B (in press).

Chapter 16

Solitary Wave Acoustic Polaron Motion on Polydiacetylene Chains

K. J. Donovan and E. G. Wilson

Department of Physics, Queen Mary College, London E1 4NS, United Kingdom

An extra electron put on a polymer chain
deforms the chain and forms a SWAP
(Solitary Wave Acoustic Polaron). The SWAP
dynamics and energy dissipation are such
that the smallest field causes it to move
at approximately the sound velocity; its
mobility is ultra high, higher than that of
any conventional semiconductor. Increasing
field changes the shape of the SWAP, but
does not increase the speed.
    Pulse photoconductivity experiments on
polydiacetylenes have established that
charge carriers move along the chains, with
the intrinsic chain motion, for up to 1 mm
distance before trapping at some extrinsic
defect. The intrinsic motion is that of the
SWAP.
    The SWAP is expected to be the
universal form of intrinsic motion on all
polymer chains.

Polydiacetylene (PDA) crystals have virtually perfect
straight polymer chains. They are thus ideal for the
study of electron motion in one dimension. This paper
describes pulse photo conduction experiments which have
established that charge carriers move along the chains,
with the intrinsic chain motion, for up to 1 mm distance
before trapping at some extrinsic defect. Two defects
have been identified, namely traps (or barriers) and
recombination centres; Fig. 1 illustrates what is
established (1,2) on two particular PDA's.The intrinsic
velocity between the defects is saturated; the smallest
field causes the carriers to move at approximately the
sound velocity S; the mobility is ultra high, higher than
that of any conventional semiconductor. The phenomenology
leading to these results is described in Section 3.
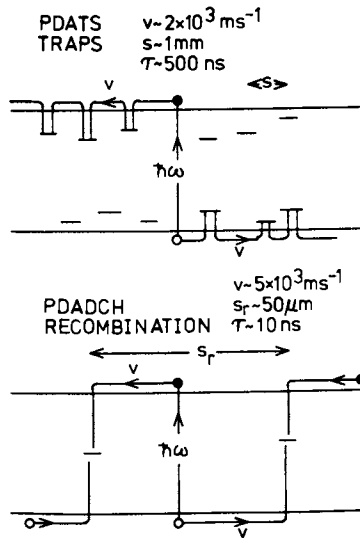
Figure 1. Time evolution of photocarriers in PDATS and PDADCH. (Reproduced with permission from reference 1. Copyright 1985 Springer Verlag.)

Such motion is extraordinary and was a great
surprise when discovered by us (3). The greatest
resistance to acceptance of the result was that there was
no model known to account for such extraordinary motion
at the time of its discovery. Attempts were made (4) to
use the theories that work in conventional three
dimensional (3D) semiconductors such as Silicon, but
without success (5).

The motion was later asserted (6) to be that of the
Solitary Wave Acoustic Polaron (SWAP). Fig. 2 shows the
structure of the SWAP. The electron localises in a region
of the chain; it thus causes a force F_n on the chain in
that region which in turn causes a local contraction of
the chain; the contraction of the chain causes the
localisation of the electron in the first place. In this
way a self consistent object is created. The motion along
the chain is that of the electron plus its accompanying
distortion; the whole SWAP moves. The dispersion relation
of the SWAP is shown in Fig. 3. The important point is
that the velocity of the SWAP, being the slope of the
dispersion relation, approaches an assymptotic limit,
which is the sound velocity S, as the energy is
increased. Thus, in the absence of dissipation or break
up, the SWAP velocity is essentially constant in the
presence of an applied field. The SWAP is essential in
one dimensional (1D) electron motion because an electron
will always localise in a deformation in 1D: in 3D the
deformation has to be of a sufficient size and range.
Thus difference of dimensionality leads to difference of
kind.

Figs. 2 and 3 also show an ambient phonon of wave
vector q_1 scattering off the SWAP as a Doppler shifted
phonon q_2 . These illustrations are for PDA; the SWAP has
thermal energy, and the phonon wave vectors illustrated
give half the maximum scattering probability which is
given by long wavelength phonons. This scattering gives
dissipation, for energy can transfer from the SWAP to the
lattice. The point to stress however (6) is that the
dissipation is weak compared to that operative in 3D. The
dissipation in 3D is due to Cerenkov emission or
absorption of a phonon in a first order process. Such a
Cerenkov process cannot occur with the SWAP: it violates
energy momentum conservation. An object, like the SWAP,
always moving at less than the sound velocity cannot emit
or absorp sound, it can only scatter sound. The weak SWAP
dissipation is the reason for the ultra high low field
mobility. Again the difference of dimensionality leads to
a different kind of behaviour.

Section 2 describes further the properties of the
SWAP. But first we relate it to other polarons discussed
in polymers, so as to bring out similarities and
differences.
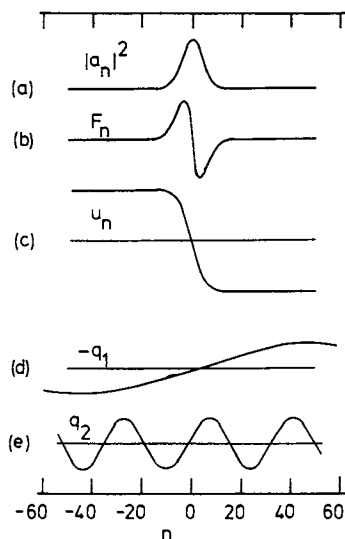
Figure 2. The SWAP: the abcissa is number of unit cells; a, electron density; b, force on lattice by electron; c, lattice displacement; d, incident phonon; e, scattered phonon. (Reproduced with permission from reference 5. Copyright 1985 Nijhoff.)
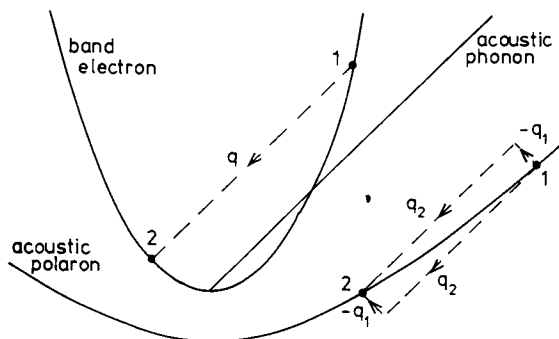
Figure 3. Schematic illustration of dispersion curves of an acoustic phonon, a band electron, and the SWAP. The incident phonon $-q_1$ is scattered as q_2. (Reproduced with permission from reference 5. Copyright 1985 Nijhoff.)

1 The SWAP and other Polarons

We do not intend to give a history of the evolution of
ideas about polarons. We restrict ourselves to picking
out threads which are relevant to motion, and are
relevant to one dimension, with the aim of sharpening
contrasts. Table 1 shows the make up of a quartet of
polarons. The SWAP, being an electron in an acoustic
deformation, was described by Whitfield and Shaw (7):
these workers obtained an analytical solution for the
moving SWAP. Wilson (6) went on to show the scattering
was weak, and the mobility ultra high, and to identify
Donovan and Wilson's (3) experimental discovery as being
the SWAP. Much of this theoretical work had in fact
already been done independently by Davydov.

TABLE 1 Four Polarons made from two Particles and two
Distortions

| | LATTICE DISTORTION | |
PARTICLE	Acoustic	Optic
Electron	SWAP Whitfield and Shaw (7) Donovan and Wilson (3) Wilson (6)	OPTIC POLARON Holstein (10) Su Shrieffer and Heeger (11)
Vibrational Exciton	DAVYDOV SOLITON Davydov (8) Scott (9)	CARRERI's POLARON Carreri (13) Alexander (14)

       In the early seventies Davydov (8) proposed his
Soliton as a means of energy transfer in biological
systems. In particular he proposed that the imide CO
vibration of the polypeptide causes an acoustic
deformation of the polymer chain and forms the Davydov
Soliton. He showed how the vibrational exciton coupling
to the acoustic phonon is strong in this system on
account of the strong hydrogen bonding between CO and NH
groups. The mathematical description given by Davydov is
virtually identical to that given for the SWAP, for both
the static and moving solution. Scott (9) and coworkers
conducted complementary studies of the Davydov Soliton,
particularly using computer simulations.
       The essential difference between the SWAP and the
Davydov Soliton (apart from numerical matters) lies in
the effect of the acoustic deformation: in the former it
changes the electron inter site transfer energy, whereas
in the latter it changes the on site exciton vibrational
energy. The difference between on site and inter site
will not show up for polarons larger than the lattice
spacing.

Earlier than all of this Holstein (10) described his optic polaron, in which the deformation of the 1D chain is an optic deformation. His was the first polaron solution which was a Solitary Wave or Soliton. In such a deformation there is no change in lattice density in the polaron; there is only a rearrangement of atoms without a change of density. In the case of the optic polaron there is no analytical solution for the moving polaron. However it is clear that on increase of the optic polaron energy due to motion there is no perturbation as the velocity goes through the sound velocity. In the pure optic polaron the sound velocity is not in the model at the outset. It is in the motion of the polaron at velocities up to the sound velocity that the profound difference between the acoustic and optic polarons occurs; the difference in properties of the polarons at rest is less important.

The work of Su Shrieffer and Heeger (11) focussed on conjugated polymers having two valence bond structures, say A and B. In the case of trans polyacetylene, where A and B are degenerate, they showed intrinsic defects can occur, in which A phase goes continuously over to B phase, forming a soliton kink. They further considered the charged kink, which is then a polaron. Elaborations have been developed for polymers with non degenerate A and B phases; they include polarons and bi polarons in which one or two electrons are localised in an A to B and B to A kink anti kink pair. It is common to all this work that it is an optic deformation that carries a structure from A to B phase, and optic deformations only are included in the make up of the polarons. In this sense they are an elegant extension of Holsteins polaron: in the wide band gap limit they go over to Holsteins solution (12). There is no analytic solution for the moving polarons of Su Shrieffer and Heeger. But again, being made of optic deformations, there is no perturbation to their motion as accelerated through the sound velocity.

It is worth stressing that the SWAP and the Holstein Polaron can exist in any polymer, for example in polyethylene or nylon, as well as in conjugated polymers.

Carreri et al (13) found infra red absorptions in polypeptides and their model crystal acetanilide which they suggested might be the Davydov Soliton. However it is more likely that they are due to the remaining member of the quartet of Table 1, namely the imide vibration bound in a range of optic deformation (14).

The stress we lay on the difference between optic and acoustic deformation is a reaction to the enormous literature on exclusively optic polarons in conjugated polymers. Yet as the Davydov Soliton and SWAP show, it is the acoustic deformation which dominates the motion of the polaron. In so far as it is motion which is the essential quality of a Soliton, it is the Acoustic deformation which it is essential to consider. In reality

a polaron will have both optic and acoustic deformation
in its make up; as it moves the ratio of acoustic to
optic component will increase, and dominate as the sound
velocity is approached. We are unaware of analytical
studies of this behaviour; it manifests in some computer
simulations.

2 Theory of the SWAP

The Su Schrieffer Heeger (11) Hamiltonian for one extra
electron added to an insulator is

$$H = \sum (1/2M) p_n^2 + \sum (1/2) C(u_{n+1} - u_n)^2$$
$$- \sum t_{n+1,n} (c_{n+1}^\dagger c_n + c_n^\dagger c_{n+1}),$$
$$t_{n+1,n} = t_o - \alpha(u_{n+1} - u_n) \tag{1}$$

Here M, C, u_n and p_n are the mass, force constant,
displacement and momentum of the n th unit cell. The
electron in an undeformed lattice exists in a conduction
band of effective mass m. From this band are constructed
Wannier states $c_n^\dagger |0\rangle$, ie. molecular-like states localised
at the unit cells. Then $t_o = \hbar/2ma^2$, where a is the lattice
spacing. α measures the variation of the transfer energy
t with lattice spacing. It is related to the deformation
potential D by $D = 2\alpha a$. Thus D and m can be freely used to
replace the α and t_o of the Hamiltonian.
     The electron in the SWAP exists in a localised state

$$\phi = \sum a_n c_n^\dagger |0\rangle \tag{2}$$

Consider the adiabatic Hamiltonian defined by

$$H_A = \langle \phi | H | \phi \rangle = H_L + H_e \tag{3}$$

where H_L is the Hamiltonian of the free lattice, and H_e
contains all electron coordinates. Then classical
equations of motion for the lattice in the adiabatic
approximation are

$$\dot{u}_n = \partial H_A / \partial p_n = p_n / M \tag{4}$$

$$M\ddot{u}_n = \dot{p}_n = -\partial H_A / \partial u_n = C(u_{n+1} - u_n) - C(u_n - u_{n-1}) + F_n, \tag{5}$$

where the continuum limit of F_n is

$$F_n = (D/a) \, \partial |a_n|^2 / \partial n. \tag{6}$$

Thus F_n is the force on lattice site n due to the
localised electron; its magnitude depends on the gradient
of the electron density. The force gives rise to the
lattice deformation u_n. Suppose the SWAP to move at
velocity V, such that the force also moves ie.

$$F_n = F(na - Vt) \tag{7}$$

Then the classical displacements due to such a moving force are found from Equ.s 4,5 and 6 to be

$$u(na - Vt, t) = [-1/MS^2 (1 - \beta^2)] \iint F(x) d^2 x \tag{8}$$

Here a parameter β, which is the ratio of polaron velocity to sound velocity has been introduced:-

$$S^2 = a^2 C/M \quad , \quad \beta = V/S \tag{9}$$

Thus the lattice deformation, which also moves at velocity V, has a shape which is the double spatial integral of the force. Fig. 2 illustrates the spatial variation of the electron density, force, and lattice displacement. The deformation diverges as V increases towards S. This is the physical reason for the polaron energy diverging as the velocity approaches the velocity of sound. There is no equivalent effect in the optic polaron. For such a divergence it is necessary that the different lattice waves making up the localised displacement have the same phase velocity; ie. the effect only exists for the continuum acoustic polaron and for the lattice acoustic polaron provided it is larger than the lattice spacing.

For this system of equations, and going to the continuum limit in which the lattice becomes a string, there is a complete analytic solution (6,7,8). The eigenfunction a_n describing the polaron electronic wavefunction via Equ. 2 is

$$a_n = (\gamma/2)^{1/2} \operatorname{sech}[\gamma(n - n_0)] \tag{10}$$

where

$$\gamma = \gamma_0/(1 - \beta^2), \qquad \gamma_0 = (D^2 m a^2)/(2MS^2 \hbar^2) \tag{11}$$

and the centre X of the SWAP is at $X = Vt = an_0$. The binding energy of the electron within the SWAP is

$$\epsilon_e = \quad - U/(1 - \beta^2)^2 \tag{12}$$

where

$$U = (1/8)(m/\hbar^2)(D^4 a^2/M^2 S^4) \tag{13}$$

The binding energy increases as V increases, and diverges as V approaches S. This is illustrated in Fig. 4. The polaron in this sense becomes more stable when it moves, and the adiabatic approximation becomes more accurate.

The lattice deformation is

$$u_n = -[Da/MS^2 (1 - \beta^2)] \tanh[\gamma(n - n_0)] \tag{14}$$
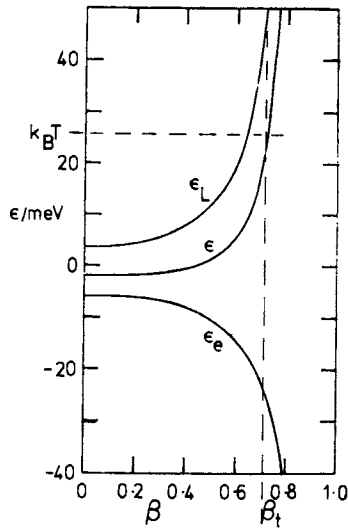
Figure 4. The dependence on $\beta = V/S$ (β_t is the value for a thermal polaron) in PDATS of the lattice energy ϵ_L, the electron energy ϵ_e, and the total energy of the SWAP. (Reproduced with permission from reference 6. Copyright 1983 Institute of Physics.)

The increase in lattice energy due to the deformation is

$$\mathcal{E}_L = (2U/3)(1+\beta^2)/(1-\beta^2)^3 \tag{15}$$

This energy is also displayed in Fig. 4. The total energy is then

$$\mathcal{E} = \mathcal{E}_e + \mathcal{E}_L$$
$$= (U/3)(-1+5\beta^2)/(1-\beta^2)^3 \tag{16}$$

This energy is also displayed in Fig. 4
It can be shown that (6,7,8) the momentum conjugate to X is then

$$P = (4U/3S)\beta/(1-\beta^2)^3 \tag{17}$$

and the velocity is the slope of the curve of $\mathcal{E}$ against P,

$$V = \partial\mathcal{E}/\partial P . \tag{18}$$

There is no simple expression for $\mathcal{E}$ as a function of P. Fig. 3 shows an example. The slope of the dispersion curve $\mathcal{E}(P)$, which is the velocity, asymptotically approaches S as the energy tends to infinity.
In an electric field $\mathcal{E}$ the equation of motion for P is

$$\dot{P} = -|e|\mathcal{E} \tag{19}$$

Hence a SWAP, in the absence of dissipation, would increase its conjugate momentum P at a uniform rate in response to an external force. The energy would correspondingly increase without limit; the velocity would however saturate at S.
Wilson (6) considered the strength of the Doppler shifted phonon bouncing illustrated in Fig. 3. He went on to solve the Boltzmann transport equation for the SWAP response to the field. He found that the energy loss by phonon bouncing is insufficient, above a threshold polaron energy, to overcome the energy gain from the applied field. Moreover the threshold energy increases as the field is reduced, but it always exists. That is, saturation of the polaron drift velocity at the velocity of sound occurs at all fields no matter how small. Thus the low field mobility of the SWAP in the continuum limit approximation is predicted to be infinite.

3 Experimental Evidence for SWAP Motion

The different evolution of photo carriers in TS and DCH, following a 10 ns laser pulse, as established by experiment (1,2) is illustrated in Fig 1. There are four remarks we now make.

First remark The long distance apart of traps in TS
allows of a determination of the trap time τ. This is
defined by the theoretically expected decay of the photo
current following illumination

$$I(t)/I(0) = E_2(t/\tau), \quad \tau = s/v, \tag{20}$$

which is expected for carriers created at random
positions drifting at velocity v to randomly positioned
traps in 1D (16). Here E_2 is the exponential integral
function and s is the mean distance between traps. The
characteristic time τ is found experimentally (15) to be
independent of field. This reflects the independence of v
on field characteristic of the motion of a SWAP. If v
were linear in field then τ is expected to fall inversly
with field in 1D, s remaining a constant. On the good
sample of Fig. 1 τ is 500 ns. The subsequent dispersive
trap controlled motion, which in 1D follows

$$I(t) \sim t^{-\alpha}, \tag{21}$$

has been established (17). Thus it is clearly possible to
distinguish the initial motion at the intrinsic velocity
v from the subsequent trap limited motion at velocity
$\langle v(t) \rangle$.

Second remark It has been possible to establish the
absence of recombination centres in TS (1,2) and to
measure their distance apart s_r in DCH (18), by a novel
experiment possible only in a one dimensional material.
It is possible experimentally to integrate over time the
decaying currents by measuring the charge accumulating at
the electrodes with an electrometer. The excess charge Q_m
over and above that due to the dark current is due to
motion of the photo created charge. Figure 5 illustrates
two experiments. The first experiment is to cut the
chains, by physical removal of material (3); the second
experiment is the creation of invisible cuts, or
electronic walls, in which there is no removal of
material. They are made by scanning a high energy
electron beam, as used in electron beam lithography,
across the sample surface (18). This produces sufficient
change of material properties, probably by cross linking,
that the charge carriers stop at the walls and recombine.
Wall spacings as small as 12.5 μm have been made in this
way.In both these ways a sample of length D can be
divided, for the depth of the cuts only, into lengths d.
The cuts are deeper than the optical skin depth but much
less than the sample thickness. The dark current and
applied field are unaffected by the cuts. It is found
that carriers are stopped at the cuts and eventually
recombine at the cuts. The cuts only affect the
accumulated charge Q_m when d is less than the distance

apart of recombination centres s_r . Thus s_r is measured
directly.

<u>Third remark</u> It is possible to determine the magnitude
of the drift velocity. The peak current at the end of the
laser pulse is

$$I_p = Q \ v/D \tag{22}$$

provided the carriers are still free, which it is
possible to establish, as described in the first remark.
Here Q is the charge created by the laser pulse, which is
related to the accumulated charge Q_m measured by

$$Q = Q_m \qquad \text{in TS} \quad \text{where } s_r > D,$$
$$= Q_m (D/s \ ) \ \text{in DCH where } s_r < D \tag{23}$$

where these equations follow from the second remark. In
this way the magnitude of the drift velocity is found. In
TS, Fig. 6 shows I_p and Q_m over four decades of applied
field (2); the ratio of these observables is according to
Equs 22 and 23 the value of v/D; thus v is independent of
field over four decades; its magnitude is within a factor
two of the sound velocity; the low field mobility is
greater than 20 $m^2 \ s^{-1} \ V^{-1}$. In DCH the method yields
similar results (18).

<u>Fourth remark</u> There is an independent method of
determining the drift velocity. The cuts can be
sufficiently close that carriers made during the 10 ns
laser pulse transit between the cuts in the duration of
the pulse. The current detector is not fast enough to
resolve these time effects; however they also reduce the
current magnitude and can be so detected. The reduction
of current is by a factor d/vT, where T is the laser
pulse duration: for this is the fraction of otherwise
free carriers that have not hit the walls. Thus

$$I(d)/I(\infty) = d/vT \quad \text{for } d < vT = d_c$$

$$= 1 \qquad \text{for } d > vT \tag{24}$$

This behavior has been established in DCH (18). v is
found to be close to S, and independent of field over at
least one decade.

4 Conclusion

In conclusion, a complete experimental phenomenology now
exists for the photo creation, free motion, trapping,
trap release, and recombination of charge carriers in
PDA. The most striking result is the velocity of free
motion, which is independent of field. This finds a
natural explanation as the motion of a SWAP, which is an
essential consequence of one dimensionality.
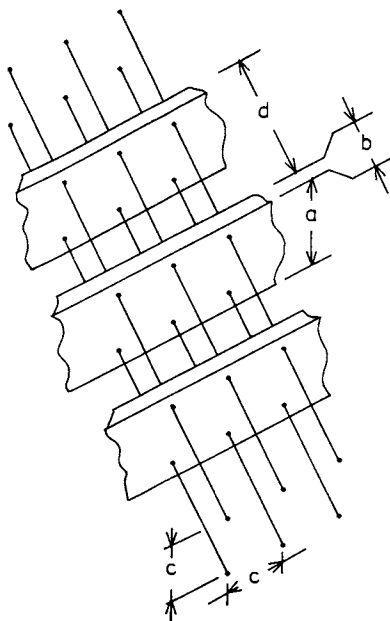
Figure 5.   Polymer wires of spacing c=0.7 nm with cuts or walls
of spacing d.   (Reproduced with permission from reference 18.
Copyright 1985 Institute of Physics.)
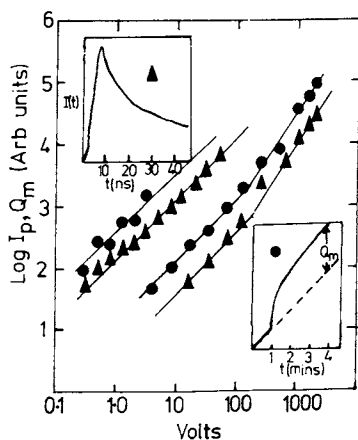
Figure 6. I_p and Q_m in PDATS over 4 decades of applied field;
their ratio according to equations 22 and 23 measures the drift
velocity of free carriers.   (Reproduced with permission from
reference 2.   Copyright 1985 Nijhoff.)

Literature Cited

1   K J Donovan, P D Freeman and E G Wilson "Electronic
    Properties of Polymers and Related Compounds",
    Springer Series in Solid State Sciences 63, 256 (1985)
2   K J Donovan, P D Freeman and E G Wilson
    "Polydiacetylenes", ed D Blooor and R R Chance, NATO
    ASI No 102 Nijhoff 165 (1985)
3   K J Donovan and E G Wilson Phil Mag B 44 9 (1981)
4   E G Wilson J Phys C 15 3733 (1982)
5   E G Wilson "Polydiacetylenes", ed D Bloor and R R
    Chance, NATO ASI No 102 Nijhoff 155 (1985)
6   E G Wilson J. Phys. C. 16 6739 (1983)
7   G Whitfield and P B Shaw Phys Rev B 14 3346 (1976)
8   A S Davydov "Biology and Quantum Mechanics" Pergamon
    Press (1982)
9   A C Scott Phys Rev A 26 578 (1982)
10 T Holstein Ann Phys 8 325 (1959)
11 W P Su,J R Schrieffer and A J Heeger Phys Rev B 22
    2099 (1980)
12 D K Campbell, A R Bishop and K Fesser Phys Rev B 26
    6862 (1982)
13 G Carreri et al Phys Rev B 30 4689 (1984)
14 D M Alexander Phys Rev Lett 54 138 (1985)
15 K J Donovan and E G Wilson J Phys C 18 L51 (1985)
16 E G Wilson J Phys C 13 2885 (1980)
17 B Movaghar, D W Murray, K J Donovan and E G Wilson J
    Phys C 17 1247 (1984)
18 K J Donovan, P D Freeman and E G Wilson J Phys C 18
    L275 (1985)

Chapter 17

Time-Resolved Photoconduction in the Polymer of the Bis(*p*-toluenesulfonate) of 2,4-Hexadiyne-1,6-diol

T. Blum and H. Bässler

Fachbereich Physikalische Chemie, Philipps-Universität, Hans-Meerwein-Straße,
D-3550 Marburg, Federal Republic of Germany

Peak photocurrents excited in a polymer of bis(p-toluene-
sulfonate) of 2,4-hexadiyne-1,6-diol (PTS) by N_2-laser
pulses vary superquadratically with electric field. The
ratio $i_p(E)/\phi(E)$, where ϕ denotes the carrier generation
efficiency, increases linearly with field. This indicates
that on a 10 ns scale the carrier drift velocity is a
linear function of E. Information on carrier transport
kinetics in the time domain of barrier controlled motion
is inferred from the rise time of photocurrents excited
by rectangular pulses of 488 nm light. The intensity de-
pendence of the rate constant for carrier relaxation
indicates efficient interaction between barrier-localized
carriers and chain excitons promoting barrier crossing.

This paper addresses the problem of charge transport in single crystal-
line polydiacetylene (PDA), special emphasis being placed in the distinc-
tion between defect controlled and free chain motion. It has been gene-
rally accepted by now that transport of a charge carrier across a PTS
crystal of macroscopic dimension is a dispersive process, manifested in
a temporal decay of the transport velocity following a $t^{-\alpha}$ law with
$\alpha \approx 0.85$ ([1]). The underlying idea, derived from principles of motion in a
disordered one-dimensional system ([2]), is that a moving carrier is
occasionally stopped by barriers whose crossing rate W is subject to an
exponential distribution

$$\rho(W) = \frac{\alpha-1}{W_0} \left(\frac{W}{W_0}\right)^{-\alpha} \qquad (0<\alpha<1, \ 0<W<W_0) \qquad (1)$$

It seems straightforward to associate the barriers with gaps between
polymer chain ends and/or crystallographic imperfections. If W^{-1} exceeds
the time a carrier needs to reach the barrier, the crossing event becomes
the rate limiting step for transport and the average drift velocity must
become virtually field independent provided that W is no function of the
applied electric field. There is good evidence that this description
applies to PTS for times $\gtrsim 1$ µs. A time of flight experiment conducted on

a macroscopic sample is therefore principally unable to probe motion of a
carrier while travelling along an intact conjugated chain.
     The provocative idea Donovan and Wilson (DW) (3,4) introduced into
the discussion is that even for times t<W^{-1} where free chain motion pre-
vails the transport velocity is still field-saturated because of forma-
tion of an acustic polaron which becomes bigger as it moves in an elec-
tric field (5). A transition between defect controlled to free chain mo-
tion will therefore not be revealed by a change in the current voltage
relation measured in course of a transient photoconductivity experiment.
We briefly recall the experiment (3,4) that led to the above conclusion:
A short pulse of strongly absorbed above band gap light (N photons per
sample area) creates Nηφ carriers, η being the primary efficiency for
generating geminate e...h pairs and φ(E) their dissociation probability
as a function of applied field E. At short times where loss processes are
still negligible, the resulting peak photocurrent is

$$i_p(E) = eN\eta\phi(E)v(E)d^{-1} \tag{2}$$

d being the electrode separation and v the carrier drift velocity. Since
PTS has been shown not to contain defects that catalyze carrier recombi-
nation (4) every generated carrier eventually reaches the contact and an
integrating current measurement yields the total amount of charges pro-
duced, Q = eNηφ(E). Hence i_p/Q = v/d. DW showed this quantity to be field
independent.
     In order to check the conclusions of DW we repeated their transient
photoconductivity experiment under conditions allowing for higher elec-
tric fields. We find that the peak photocurrent excited by a N$_2$-laser
pulse follows an i_p~Eφ(E) relationship which results in a linear field-
dependence of the drift velocity as expected for conventional transport.
A field effect is also seen in the photocurrent decay time at high light
intensity, interpreted in terms of bimolecular carrier recombination.
Finally we discuss the rise time of a photocurrent following a rectangu-
lar light pulse. The latter results pertain to the time domain where
transport is barrier controlled and bear out the importance of photo-
induced barrier crossing processes.

Experimental

All experiments were performed with PTS crystals carrying on their (001)
face evaporated, non-transparent Ag-electrodes, 0.3 mm apart, the elec-
tric field directed along the polymer chain axis. A N$_2$-laser (fwhm 5 ns,
energy per pulse ≈1μJ m^2) was used for ns-resolved transient photocurrent
experiments carried out at 293 K and <10^{-5} torr. The RC time constant of
the circuit was 3.5 ns. photocurrent rise time studies were done at both
148 K and 293 K using rectangular light pulses of duration up to 1 s cut
from the 488 nm beam of a cw-Ar laser by means of a Pockels cell (rise
time 10 μs). Photocurrent signals were recorded by a Tektronix 7D20 sto-
rage oscilloscope and, after sampling, fed to a computer for further
analysis. In this case the RC time of the circuit was ≈1 μs.

Results

Transient Studies with ns Time Resolution

The photocurrent transients observed upon flashing a PTS crystal with a
periodic train of N_2-laser pulses are very similar to the those published
by Donovan, Freeman and Wilson (6). There appears to be an order of magni-
tude difference in scale between the original Donovan et al. data shown
in the inset of their Figure 2 of ref. (6) and the log-log representation
(Figure 4 in ref. (6)). Replotting the oscilloscope traces on a semilo-
garithmic scale (Figure 1) reveals some deviation from exponentiality.
Although the decay functions can be fitted reasonably well by an exponen-
tial integral function proposed by Wilson (7) to treat trapping in an 1D
system, we are nevertheless reluctant in making this assignment because it
ignores onset of carrier release events at longer times and also because
of the ambiguity in locating the time origin. Because of difficulties in
deconvoluting the laser pulse and signal response, we assume that the time
origin coincides with the photocurrent maximum (i_p) attained by the end
of the laser pulse. Figure 1 indicates that the photocurrent decay be-
comes faster as the light intensity increases. As a measure of the decay
constant k we take the reciprocal time after which the current has dropped
to i_p/e. Data shown in Figure 2 follow $k(I) = k_0 + const.I$. This suggests
attributing the increase of k with I to the onset of bimolecular recombi-
nation (8), i.e.

$$k = k_0 + \gamma n \qquad\qquad (3)$$

where γ is the relevant rate constant and n the carrier density.
   Photocurrent relaxation is also enhanced by the applied electric
field (Figure 1). This effect, not noted before, might be attributed to
the quasi 1D nature of a PTS crystal. By analogy with carrier trapping
(9-11) one expects that in an ideal 1D system only those carriers recom-
bine that travel on the same chain. At realistic field strengths the re-
combination time should be drift rather than diffusion limited and, hence,
should scale with E^{-1} provided the drift velocity is not saturated. How-
ever, Monte Carlo simulation of bimolecular recombination in anisotropic
lattices (12) indicated that because of transient localization of charge
carriers entering their mutual coulombic potential genuine 1D electron-
hole recombination requires anisotropies not exhibited by any material
known to date. Therefore we reject the dimensionally argument to explain
k(E) and attribute the effect to field-assisted generation of free charge
carriers. Recall that the field dependence of the probability $\phi(E)$ for
thermally dissociating an optically produced geminate e...h pair is a
slightly superlinear function of E in the field range under considera-
tion, in accord with the 1D version of Onsager's theory (13). Taking the
$\phi(E)$ data of Seiferheld et al. (14) allows translating the k(E) data into
a k(n) relation. Comparing the functional dependences of k(I) and k(n)
indicates good agreement (Figure 2) confirming that the field effect on
the photocurrent relaxation can be traced back to a carrier density
effect, dimensionality effects remaining unresolved. In the context of
the present experiments it is important to note that recombination limi-
ted photocurrent transients carry direct information on the field depen-
dence on the carrier density generated by a laser flash.
   The crucial experimental information we wish to present is contained
in Figure 3. It shows the variation of the peak photocurrent with applied
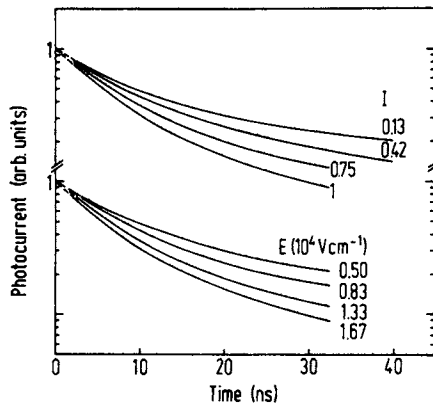
Figure 1. Photocurrent decay as a function of the applied
electric field at maximum light intensity (lower portion) and
of the relative light intensity at a field of $1.67 \cdot 10^4$ V cm^{-1}
(upper portion). I = 1 is equivalent to a pulse energy of
≈ 1 μJ mm^{-2}.
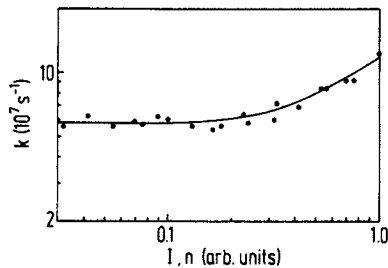
Figure 2. Decay constant of the photocurrent as a function of
the normalized charge carrier concentration n at t = 0 which is
proportional to the relative light intensity I. Closed circles
indicate data obtained from field-dependent decay profiles of
Figure 1.

electric field at various light intensities. While the $i_p(I)$ relation is
linear, confirming that (i) the photogeneration is a first order process
and (ii) spacecharge effects are negligible, $i_p(E)$ is a slightly super-
quadratic function of E. No hysteresis effect is observed upon increasing
or decreasing E. Dividing $i_p(E)$ by $\phi(E)$ measured under steady state con-
ditions (14) and confirmed by the above analysis of the photocurrent de-
cay yields a linear relation. By virtue of Equation 2 we have to conclude
that the carrier drift velocity increases linearly with field, contrary
to the DW claim.

At present we can only speculate why DW did not see this effect. Ex-
cept for higher fields applied in the present study, the only difference
in the experimental set-up is the way the contacts are made. DW used sil-
ver paste contacts applied to the side faces of the crystals. The advan-
tage of their configuration compared with the coplanar arrangement used
in   this   work is the improved field homogeneity and that it alleviates
the problem of interchain jumps required by a carrier for reaching sur-
face contacts. However, as long as the penetration depth of the exciting
light (~ 1µm) and, hence, the thickness of the current path is much
smaller than the electrode gap (0.03 cm), the field inhomogeneity within
the current path is negligible. Further, interchain jumps are not trans-
port limiting in the early (10 ns) time domain. On the other hand, silver
paste electrodes have been reported to inject holes (15,16) and it is
conceivable that at low fields photo-detrapped charge carriers contribute
significantly to the total photocurrent pulse.

In claiming (i) that v~E and (ii) that photocurrent relaxation sets
in on a ~10 ns time scale we also have to cope with the experiment of
Baumann et al. (17) who report on photocurrent pulses excited by 25 ps
laser flashes falling off with an instrument limited decay time (~100 ps)
and increasing linearly with field. A numerical estimate which will be
presented elsewhere indicates that, contrary to earlier reasoning (18),
these photocurrent pulses can be associated with the primary generation
of geminate e...h pairs whose dipole moments will preferentially align
parallel to the applied field as E increases (19,20).

Photocurrent Rise Time Studies

In this section we summarize the result of photocurrent rise time studies
conducted at a time resolution of $\cong 10$ µs (21). Their goal was to gain
further insight into the transport process within the time domain where
barrier crossing controlls the average transport velocity. In particular,
we wanted to understand why the decay of the photocurrent after termina-
ting optical carrier generation depends on the previous irradiation con-
ditions, notably the light intensity. This phenomenon suggests (i) that
carrier photon interaction is of importance and (ii) that the sample re-
tains a memory of interaction events.

The rise time of a photocurrent excited by a rectangular light pulse
reflects the establishment of equilibrium between generation and loss
processes, expressed in terms of a generalized rate equation for the
carrier density

$$\dot{n} = G - K(t)n \tag{4}$$

In the absence of bimolecular recombination, experimentally verified via
the intensity dependence of the steady state photocurrent, and of defect-
catalyzed recombination ("Shockley-Read recombination") (4), K must con-

tain terms accounting for carrier localization by barriers and subsequent revitalisation as well as for discharge at the contacts. Due to the distribution of barrier crossing rates (Equation 1) K is time-dpendent and solution of Equation 1 will in general require numerical methods. If one measure the build-up of a stationary photocurrent i_∞, K(t) is accessible via numerical differentation,

$$K(t) = \frac{\partial \ln \frac{i_\infty - i(t)}{i_\infty}}{\partial t} \qquad (5)$$

Here i(t) is the photocurrent at a time t after onset of the irradiation.

Figure 4 presents experimentally determined photocurrent time profiles as a function of the irradiation intensity and normalized to the saturation value attained in the long time limit. There is a fast, intensity-independent initial rise followed by a gradual approach of saturation which becomes faster with increasing I. Data analysis in terms of Equation 5 yields the k(t) curves collected in Figure 5. K(t) falls off rapidly according to a power law, approaches as saturation value, called K_{opt}, in the intermediate time domain and continues decaying according to a t^- law at longer times. If $K(t) \sim t^{-\alpha}$, Equation 4 can be solved analytically to yield $n(t) = n_\infty (1-\exp|-K(t)t|)$, K(t) can then be extracted with greater accuracy from a semilog plot of $(i_\infty -i(t))/i_\infty$ giving $K(t) \sim t^{-0.85}$ for 30 µs t≤300≤µs. The interesting observation is that K_{opt} increases with light intensity in an almost linear fashion $(K_{opt} \sim I^{0.85})$ testifying the existence of bimolecualr carrier photon interaction.

A straightforward interpretation of the effect is based on the concept of photostimulated barrier crossing, analoguous to optical release of carriers trapped at defects in a molecular crystal (22). Consider a charge carrier moving in a crystal containing barriers characterized by an exponential distribution of crossing rates W, equivalent to the exponential distribution of tail states in an amorphous semiconductor. Immediately after generation a carrier moves along an unperturbed polymer chain, typically a few hundred to a thousand repeat units long (23), until it reaches the chain end. Transfer between adjacent chain ends can yet need not necessarily determine the velocity of motion. The condition that it will is that W be smaller than the reciprocal passage time of a carrier along the chain. The conclusion that not all chain ends act as rate-controlling barriers comes from the observation that the initial decay time of the photocurrent is $k_0^{-1} \sim 15$ ng (Figure 2) implying a schubweg of order of a few µm assuming $v = 2 \cdot 10^5$ cm s^{-1} (4), i.e. $\mu = 20$ cm^2/(Vs) at $E = 10^4$ V cm^{-1}. Therefore a carrier will sample several chains until stopped by a large barrier having $W< k_0$ and the 1D character of the motion is likely to be eroded. A field-independent initial photocurrent decay time cannot, therefore, be taken as evidence for field-saturated motion since it need not be drift-controlled. For $t>k_0^{-1}$ transport becomes barrier limited and dispersive. In presence of a photon field a carrier will eventually have relaxed to a state that empties slowly enough to render photostimulated barrier crossing occurring at a rate $W = r(I)$ competitive with non-stimulated barrier crossing by tunnelling. The optically liberated carrier will be resubjected to the relaxation process and again relaxe to the level characterized by $W = r$ which can be considered as the analogue to the demarcation energy in amorphous semiconductors (24,25). Carrier-photon interaction therefore establishes dynamic equili-
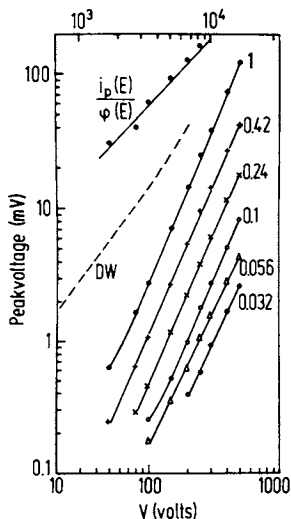
Figure 3. Peak photovoltage measured across a 50Ω resistor as a function of applied voltage and electric field, respectively. Parameter is the relative light intensity. The dashed curve is the Donovan et al. (6) result in arbitrary ordinate units. The quantum efficiency φ(E) for geminate dissociation used to calculate $i_p(E)/\phi(E)$ is taken from reference 14.
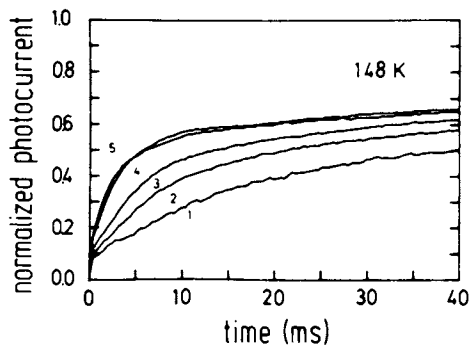
Figure 4. Photocurrent transients recorded at 148 K at variable intensity of a rectangular light pulse. 600 ms in duration and polarized perpendicular to the PTS chain (1 to 5: $7 \cdot 10^{16}$; $1.3 \cdot 10^{17}$; $2.8 \cdot 10^{17}$; $5 \cdot 10^{17}$; and $9.3 \cdot 10^{17}$ quanta cm^{-2} s^{-1}, respectively). Curves are normalized relative to the steady state photocurrent attained after several minutes of irradiation. The electric field was $2 \cdot 10^4$ V cm^{-1}. (Reproduced from reference 21. Copyright 1986 American Chemical Society.)
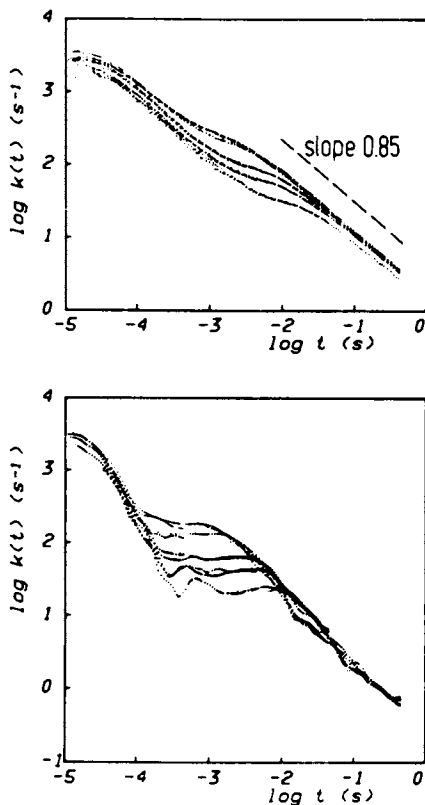
Figure 5. Rate constant K(t) derived from the rise time functions of Figure 4. Bottom section: Data obtained by numerical differentiation (Equation 5). Top section: Data obtained assuming that $K(t) \sim t^{-n}$, n>0. Since the photocurrent signal is the superposition of three data sets recorded under different time resolutions, K(t) plots display some mismatch in the regions of data overlap. (Reproduced from reference 21. Copyright 1986 American Chemical Society.)

brium between the carriers and the density of states distribution while irradiation continues. Within the pertinent time domain carrier transport is non-dispersive and the average transport velocity increases with light intensity. Carrier discharge at the contact occurs at a rate $K_{opt}=r/n$, where $n=L/2$ 1 is the number of photoexcitation events a carrier experiences, L is the electrode gap and 1 the schubweg between subsequent photoexcitation events. From the time interval where photostimulated transport prevails, $n=r/K_{opt} \sim 20$ and, since $L=0.3$ cm, $1 \approx 10$ µm is estimated. At times $t>K_{opt}^{-1}$ those carriers will discharge that experienced no or only few excitation events. A surprising feature, born out by quantitative data analysis, is that photostimulated barrier crossing is a very efficient process. It is interpreted in terms of interaction between the localized carrier and a chain exciton which promotes barrier crossing. This is another manifestation of the delocalization of electronic excitation along a PTS chain, known to be responsible for the large non-linear optical response of PDAs (26). The above concept also provides a straightforward explanation for the memory effect observed in course of photocurrent relaxation studies after switching off the light source. Since the dynamic equilibrium during irradiation is governed by the rate r(I), the fastest relaxation rate observed afterwards is also r(I).

Concluding Remarks

The challenging information of this contribution is that in the short time limit a PTS crystal behaves like a conventional semiconductor as far as carrier transport is concerned. Clearly, more work is required, notably, quantitative assessments. However, for reasons of concistency, the drift velocities measured at highest fields employed in this study cannot exceed those measured earlier (4). This yields a mobility of order 10 cm^2 $(Vs)^{-1}$. A similar estimates results from the schubweg travelled by a carrier before immobilized by a large barrier. It has to be shorter than the distance travelled between localization events (~10 µm). The conclusion is that carrier motion is polaronic as described by Cade and Movaghar (27).

Acknowledgment

Literature Cited

1. Movaghar, B.; Murray, D.W.; Donovan, K. J.; Wilson, E.G. J. Phys. C. 1984, 17, 1247.
2. Alexander, S.; Bernasconi, J.; Schneider, W. R. Rev. Mod. Phys. 1981, 53, 175.
3. Donovan, K. J.; Wilson, E. G. J. Phys. C. 1979 12, 4857.
4. Donovan, K. J.; Wilson, E. G. Phil. Mag. B 1981, 44, 31.
5. Wilson, E. G. In "Polydiacetylenes"; Bloor, D.; Chance, R.R., Eds.; NATO ASI, Series E, No 102, Niejhoff, M. Publishers, 1985; p. 155, and J. Phys. C. 1983, 16, 6739.
6. Donovan, K. J.; Freeman, P. D.; Wilson, E. G. In "Polydiacetylenes", (see ref. 5), p. 165.
7. Wilson, E. G., J. Phys. C. 1980, 13, 2885.

8. Reimer, B.; Bässler, H. Chem. Phys. Lett. 1976, 43, 81.
9. Haarer, D.; Möhwald, H. Phys. Rev. Lett. 1975, 34 1447.
10. Movaghar, B.; Murray, D. W.; Pohlmann, B.; Würtz, D. J. Phys. C.
    1984, 17, 1677.
11. Seiferheld, U.; Bässler, H.; Movaghar, B. Phys. Rev. Lett. 1983,
    51, 813.
12. Ries, B.; Bässler, H. Chem. Phys. Lett. 1984, 108, 71.
13. Ries, B.; Schönherr, G.; Bässler, H.; Silver, M. Phil.Mag. B 1983,
    48, 87.
14 Seiferheld, U.; Ries, B.; Bässler, H. J. Phys. C. 1983, 16, 5189
15. Siddiqui, A. S.; Wilson, E. G. J. Phys. C. 1979, 12, 4237.
16. Siddiqui, A. S. J. Phys. C. 1980, 13, L1079.
17. Baumann, T.; Donovan, K. J.; Goebel, E.; Roth, S. Materials Science
    (Wroclaw), 1984, Vol.X, 23.
18. Bässler, H. In "Polydiacetylenes" (see ref. 5), p. 135.
19. Lukin, L. V.; Tolmachev, A.V.; Yakovlev, B.S. Chem. Phys. Lett.
    1983, 99, 16.
20. Sauer, M. C.; Trifunec, A. D., Cooper, R.; Meisel, D. Chem. Phys.
    Lett. 1982, 92 178.
21. Blum, T.; Ries, B.; Bässler, H. J. Phys. C. 1986, 19, 3659.
22. Rohrbacher, H.; Karl, N. phys. stat. sol. (a) 1982, 29, 517.
23. Braunschweig, F.; Bässler, H. Chem. Phys. 1985, 93, 307.
24. Tiedje, T.; Rose, A. Solid State Comm. 1981, 37, 49.
25. Monroe, D.; Phys. Rev. Lett. 1985, 54, 146.
26. Sandman, D. J.; Carter, G. M.; Chen, Y. J.; Elman, B. S.; Thakur,
    M. K.; Tripathy, S. K. In "Polydiacetylenes", (see ref. 5), p. 299.
27. Gade, N. A.; Movaghar, B. J. Phys. C. 1983, 16, 539.

Chapter 18

Solid-State Reaction
of Poly(1,6-di-N-carbazolyl-2,4-hexadiyne) with Electrophiles
A 13C Cross-Polarization/Magic Angle Spinning NMR Study

James P. Yesinowski[1], Hellmut Eckert[1], Daniel J. Sandman[2], and Christopher S. Velazquez[2]

[1]Division of Chemistry and Chemical Engineering, California Institute of Technology, Pasadena, CA 91125
[2]GTE Laboratories, Inc., Waltham, MA 02254

^{13}C cross-polarization/magic angle spinning (CP-MAS) NMR at 50.36 MHz reveals that the reaction of the crystalline polymer poly-N-dicarbazolyl-2,4-hexadiyne (poly-DCH) with the electrophilic reagents liquid bromine, gaseous chlorine, and nitric acid fumes results in the formation of covalent bonds in the polymer. Spectra have been obtained both of the products formed as well as of model compounds, and factors influencing the quantitative interpretation of peak intensities have been taken into consideration. The observed disappearance of peaks from carbon atoms either bonded to or adjacent to bromine atoms is due to a dipolar interaction not averaged to zero by magic-angle spinning. The NMR results show that the initial anisotropic reaction is a selective attack of the bromine at the 3,6 positions of the aromatic rings of the carbazole moiety, resulting in a polymer with four Br/repeat unit. At higher bromination levels electrophilic addition to the multiple bonds in the backbone occurs. Other evidence suggests that the triple bond may react preferentially, resulting in formation of a mixed polyacetylene for products of composition poly-DCH($Br_{6.0}$). The reaction of poly-DCH with nitric acid fumes appears to result in substitution at the 3,6 positions of the carbazole ring. In contrast, exposure of poly-DCH to chlorine gas most likely effects both electrophilic substitution and addition in the carbazole sidechains.

Macroscopic polymer single crystals with a high degree of perfection can be produced by the homogeneous topochemical polymerization of conjugated diacetylene monomers (1). The polydiacetylenes thus formed have a fully conjugated planar backbone and possess unusual optical and electronic properties

that suggest applications in electronic devices. Unlike polyacetylenes, however, which can be doped readily with electron-donor or -acceptor molecules to produce highly conductive polymers, the polydiacetylenes do not react in this fashion because of their high crystallinity. Thus the opportunities for modifying the physicochemical properties of this class of compounds have been severely limited by lack of reactivity.

Recently two of us have found (2) that exposure of single crystals of poly-N-dicarbazolyl-2,4-hexadiyne (poly-DCH, Fig. 1, see ref.(3) for the crystal structure) to liquid bromine produces highly crystalline materials with reproducible bromine contents ranging from 3 to 6 Br per repeat unit, with a concomitant color change from the brassy appearance of the starting polymer to a coppery-bronze color. Reaction with refluxing solutions of bromine produces straw-colored products with 7 to 8 Br per repeat unit; the reaction in this case appears to proceed in a different fashion, which is not yet well-understood. Furthermore, homogeneous, albeit amorphous, products can be obtained from analogous reactions with chlorine gas and nitric acid fumes.

While the reaction of halogens with the chemically-related polyacetylene, $(CH)_x$, can be explained in terms of an ionic intercalation model (4), the significantly higher halogen uptake encountered with poly-DCH, as well as the non-metallic character of both starting material and products, suggest a different mode of reaction involving formation of covalent C-Br bonds. Potential bromination sites are the double and triple bonds, the allylic methylene group, and the aromatic carbazole moiety. However, the products cannot be predicted simply on the basis of the relative reactivities of these groups toward bromination, since anisotropic solid-state diffusion of bromine must be a major factor in governing the course of reaction.

Detailed experimental identification of the products has proven elusive so far. Single crystal x-ray diffraction methods have been hindered by the presence of crystallographic disorder. FTIR spectroscopy indicates carbazole substitution (2), but is neither unequivocal nor quantitative. In addition the insolubility of all of the brominated products precludes the use of traditional solution-state characterization methods. However, the pioneering work of Schaefer and Stejskal (5), starting in 1975, has demonstrated that the cross-polarization (CP) method (6), developed by Pines, Gibby, and Waugh (7) for enhancing the sensitivity of detection of ^{13}C NMR in natural abundance in solids, could be combined with the magic angle spinning (MAS) technique discovered independently by Andrew (8) and Lowe (9), to provide a means of obtaining high resolution natural abundance ^{13}C NMR spectra of polymers. In the years following, many additional useful modifications of the basic experiment have appeared and ^{13}C CP-MAS NMR has proven to be an extremely valuable method for characterizing organic polymers in the solid state (10), including various polydiacetylenes (11,12).

In the present study we have used this method to clarify the course of bromination of poly-DCH. Preliminary results have also been obtained on the chlorination and nitration of this polymer. Information about the chemical structure
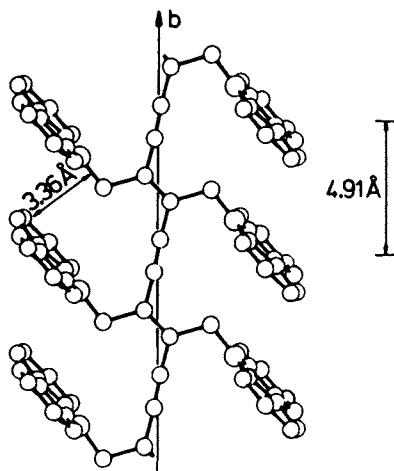
Fig. 1. Structure of poly-DCH. Reproduced with permission from reference (1). Copyright 1984, Springer Verlag Berlin, Heidelberg, New York.

of the reaction products has been obtained by utilizing CP-MAS NMR data on model compounds as well as solution NMR data to aid in the assignments. Through the combined use of different CP-MAS NMR experiments, assignments have been obtained and the conditions for semi-quantitation have been established. Complications arising from the presence of quadrupolar bromine nuclei in the samples have been observed and can be taken into account in the interpretation of the results.

Basic Principles of the ^{13}C CP-MAS NMR Technique.

Unlike the high resolution easily achieved in solution state NMR, the resolution of a ^{13}C NMR spectrum in the solid state is severely degraded by broadening due to the anisotropic direct ^{1}H-^{13}C dipolar interaction (which varies as the inverse cube of the distance between the carbon and proton) and the anisotropy of the ^{13}C chemical shift. High-resolution spectra can be obtained, in principle, if these interactions are removed by high-power proton decoupling and magic angle spinning, respectively. Even under these conditions, the observation of a ^{13}C NMR signal is frequently difficult, because the low natural abundance (1.1%) and the long spin-lattice relaxation times of the ^{13}C nucleus, which can be on the order of several minutes, severely limit the detection sensitivity. Cross-polarization can be used in order to overcome these problems. The method takes advantage of the large nuclear polarization of the proton spin system, which can be partially transferred to the ^{13}C spin system. The ^{1}H magnetization is spin-locked along the x-axis in the rotating frame, while a ^{13}C pulse with a radiofrequency field strength H_{1C} satisfying the Hartmann-Hahn "matching" condition

$$\gamma_C H_{1C} = \gamma_H H_{1H}$$

is applied during the contact time t_m (γ_H and γ_C are the gyromagnetic ratios of ^{1}H and ^{13}C, respectively). Under these conditions the ^{1}H-^{13}C dipolar coupling effects polarization transfer between both spin systems, which takes place with a characteristic cross-relaxation time T_{C-H}. At the end of the contact period, the proton radiofrequency field H_{1H} is left on in order to provide high power decoupling during the period during which the ^{13}C "free induction decay" is acquired. The sensitivity enhancement not only results from the polarization process described above (which would be four-fold in theory), but also from the fact that the ^{1}H spin-lattice relaxation time T_1, which is usually much shorter than the ^{13}C T_1, is now the crucial parameter limiting the rate at which the experiment can be repeated to obtain successive acquisitions.

Furthermore, the sequence can be modified in order to discriminate between protonated and non-protonated carbon atoms by utilizing the large differences in their ^{1}H-^{13}C dipolar interactions. Adding a delay time of 60 μs after cross-polarization prior to acquisition and decoupling leads to a dephasing of all signals arising from protonated carbon atoms, and thus enables the selective observation of non-protonated carbon atoms (13). On the other hand, protonated carbon atoms can be selectively identified by measurements with short

contact times (100 μs or less), since the proton-carbon cross-relaxation times T_{C-H} are greatly reduced due to the stronger dipolar coupling for these carbon atoms.

The relative areas of peaks obtained by the cross-polarization method are not necessarily proportional to the number of carbon atoms giving rise to these peaks. In order to obtain quantitative results, the contact time must be long enough to ensure that all carbon atoms, including those ones remote from protons and therefore having long cross-relaxation times T_{C-H}, have been maximally polarized by the protons. Experiments employing variable contact times can establish the necessary conditions. On the other hand, decay of the spin-locked proton magnetization with a characteristic relaxation time $T_{1\rho}$ during a long contact time may be significant. Distortions in the relative intensities will result if the proton $T_{1\rho}$ values differ for the various protons in the sample. In order to address this possibility, the proton $T_{1\rho}$ values are obtained indirectly by measuring the ^{13}C signal intensity with constant contact time as a function of a variable delay time before cross-polarization (14). Finally, additional complications arise from the presence of isotopes with nuclear electric quadrupole moments, such as ^{14}N, $^{79,81}Br$, and $^{35,37}Cl$, experiencing nonzero electrostatic field gradients, since these nuclei cannot be efficiently decoupled by irradiation. If these quadrupolar interactions are sufficiently large, the dipolar coupling is not averaged to zero by magic angle spinning, since the quadrupolar spins now tend to be quantized along the principal axis of the electric field gradient rather than along the external magnetic field. As has been previously discussed (15, 16), a complicated powder pattern results, the actual appearance of which is determined by the dipolar and scalar coupling constants, as well as by the magnitude of the quadrupolar coupling constant relative to the Zeeman interaction. Although such powder patterns have actually been detected in favorable cases (15), the resonance of the carbon atom directly-bonded to a quadrupolar nucleus can be broadened beyond detection, as has been observed for ^{13}C in a polymer containing quadrupolar chlorine nuclei (17). We note that this effect may disappear if molecular motion causes the quadrupolar nucleus to relax rapidly. Such is not the case in the compounds we have studied, and thus the evaluation of their ^{13}C spectra must take these effects into consideration.

Experimental.

DCH was synthesized and polymerized under the conditions reported previously (2). Brominated compounds were obtained by exposing the large, rod-like crystals to liquid Br_2 at -5°C for several hours, resulting in uptakes of 3 to 6 Br per polymer repeat unit, and have been represented in formulae of the type poly-DCH(Br_x). The initial brassy color of the pristine polymer becomes coppery bronze upon this reaction. Straw-colored polymers with higher Br contents (7.4 and 8.2 per repeat unit) were synthesized by refluxing poly-DCH in either liquid Br_2 or a 75:25 w/w solution of Br_2 and CCl_4. Compositions of the brominated polymer inferred by weight gain were in good agreement with those

found by complete elemental analysis. The synthesis of the monomeric model compounds has been described elsewhere (2). Poly-DCH(NO$_2$)$_{7.6}$ was prepared by exposing poly-DCH to nitric acid fumes at room temperature in a desiccator. Chlorinated poly-DCH was obtained by exposing the polymer to aqua regia at 0 °C for 26 hours, resulting in the uptake of 14.9 Cl per repeat unit. All products appear homogeneous by both scanning and transmission electron microscopy. X-ray studies of crystals which have gained ca. 6 Br atoms per repeat reveal a slight decrease of the chain repeat distance from 491 ± 1pm (in the pristine material) to 475 ±5 pm, as well as new reflections which are more diffuse than those of poly-DCH.

The solid state NMR data were obtained on a home built spectrometer controlled by a Nicolet 1280 computer and 293B pulse programmer, operating at a ^{13}C frequency of 50.36 MHz. Experiments were done using a CP-MAS probe from Doty Scientific with 7mm o.d. sapphire rotors. The achievable spinning speeds were 2.5-5 kHz, depending on the sample packing characteristics. ^{1}H 90° pulse lengths of 5 μs were used, corresponding to 1.2 mT decoupling power. Cross-polarization contact times were typically 3 to 5 ms, and the Hartmann-Hahn matching condition was set using an adamantane standard, whose methylene peak also provided a secondary chemical shift reference at 38.56 ppm from TMS (18). High power decoupling was applied during the acquisition period of 20 ms. The cross-polarization pulse program incorporated spin temperature inversion (19) to suppress artifacts, and "flipback" of the ^{1}H magnetization into the z-direction by an additional 90$^\circ_{-x}$ pulse at the end of the acquisition period. Further experiments were done with delayed decoupling and variable contact times, as described above. ^{1}H T$_{1\rho}$ relaxation times were determined by spin-locking the protons for a variable delay time before cross-polarization with a constant contact time of 3 ms (14) and measuring the integrated areas of the peaks (no changes in the relative intensities of peaks were observed).

The free'induction decays were multiplied by an exponential filter function, equivalent to a Lorentzian line-broadening of 10-20 Hz, and were zero-filled from 1K to 4K data points prior to Fourier transformation. A "rolling baseline" in some spectra was eliminated by left-shifting the free induction decay by 0-100 μs or by using a baseline fit routine in the Nicolet NMC software. Integrations of peak intensities were carried out using the same software. Because the needle-like crystals may have been partially oriented during packing into the rotor, we did not attempt to calculate chemical shift anisotropies from the relative intensities of the spinning sidebands.

High resolution solution state ^{13}C NMR spectra were obtained using a 10 mm broadband probe on a Bruker WM 500 spectrometer with a 45° flip angle, power-gated broadband decoupling and a relaxation delay of 6 seconds.

Results and Discussion.

This section will begin by establishing the conditions required for quantitative results. We will then discuss the spectral changes observed upon the polymer-

ization of DCH to yield the pristine polymer (Fig. 2). Finally, we will discuss
the nature of the chemical modification of poly-DCH by bromine (using results
obtained on model compounds (Figs. 3 and 4)), as well as nitric acid (Figs. 5
and 6), and chlorine (Fig. 7).

To follow the chemistry of these reactions it is important to establish that
the relative area of a peak is proportional to the number of carbon atoms giving
rise to that peak. The cross-polarization technique is required for obtaining
spectra since the ^{13}C spin-lattice relaxation times are very long. (An attempt
to obtain a ^{13}C MAS spectrum of poly-DCH using 5μs carbon 90° pulses, high-
power proton decoupling, a recycle delay of 120 s, and 12 hrs accumulation time
was unsuccessful). We therefore considered several potential sources of quantita-
tion error in the CP-MAS experiment arising from non-uniform relaxation times
(20) for both poly-DCH as well as poly-DCH(Br$_{3.0}$). No change in the relative
intensities of peaks was observed upon increasing the recycle delay to 240 s, in-
dicating a uniform ^{1}H spin-lattice relaxation time. Likewise, the ^{1}H $T_{1\rho}$ values
were found to be equal for all protons ($T_{1\rho}$ = 30 ms). Furthermore, constant
ratios among all of the peak areas could be obtained with cross-polarization
contact times of 3 ms or longer. The peak areas thus observed in poly-DCH
agree reasonably well (within 10 percent) with those predicted from the molecu-
lar structure. Although we did not measure ^{13}C $T_{1\rho}$ values directly, they must
be substantially longer than the 3 ms or 5 ms contact times used, since the
absolute signal intensities increase up to a contact time of approximately 5 ms
before beginning to decrease. We have thus established that our ^{13}C CP-MAS
experiments should be reasonably quantitative; the complication caused by the
presence of bromine nuclei will be addressed later.

Pristine poly-DCH. Fig. 2 shows the ^{13}C CP-MAS spectra of unreacted N-
dicarbazolyl-2,4-hexadiyne and of the polymerized material. The appearance of
a new peak at 129 ppm in the spectrum of poly-DCH, resulting from the forma-
tion of a double bond, is evident from the spectra. Furthermore, polymerization
causes a marked downfield shift of the triple bond resonance(s) from 68.3 and
75.0 ppm in the diacetylenic monomer to 104.3 ppm in poly-DCH. This effect
is well-documented for many polyconjugated systems containing triple bonds
(12,21), and presumably reflects an increasing cumulene contribution to the
original enyne electronic structure of such systems.

The above changes in the spectrum are very distinct, demonstrating that
^{13}C CP-MAS NMR could be used as a highly sensitive means of monitoring the
solid state polymerization of DCH. The peak positions in the aromatic region,
however, are very similar for both monomer and polymer as well as for solid
carbazole itself. Detailed assignments were obtained by comparison with liquid
state spectra (22,23), and by delayed decoupling experiments. In addition,
measurements as a function of contact time serve to enhance the resolution in
the crowded region around 119-124 ppm and provide additional confirmation
for the assignments which are listed in Table I. For carbazole, close agreement
between the solution and solid state chemical shifts is observed.
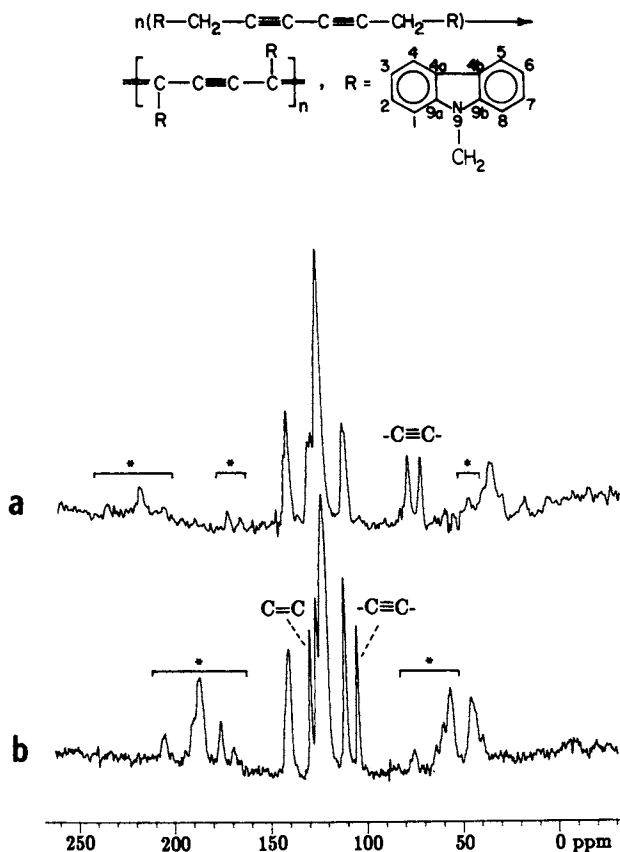
Fig. 2a. ^{13}C CP-MAS spectrum at 50.363 MHz of DCH monomer. Spinning sidebands are indicated by asterisks. The spectrum was obtained under the following conditions: spinning speed 5 kHz, 3 ms contact time, recycle delay 6 s (with magnetization flipback), 1108 scans.

Fig. 2b. ^{13}C CP-MAS spectrum at 50.363 MHz of poly-DCH. Spinning sidebands are indicated by asterisks. The spectrum was obtained under the following conditions: spinning speed 3.2 kHz, 10 ms contact time, recycle delay 60 s (no magnetization flipback), 292 scans.

Table I.

Solid state ^{13}C chemical shift assignments (in ppm) of pure and chemically modified poly-DCH and model compounds. See text for details of assignments. C-9a,b denotes the ring C-atoms directly bonded to nitrogen while C-4a,b denotes the aromatic quaternary carbons. Error limits (unless indicated otherwise by the number of significant digits) are ± 0.2 ppm for unbrominated compounds, ± 0.5 ppm for poly-DCH(Br$_{3.0}$), poly-DCH(Br$_{3.8}$), and bis(3',6' dibromo-N-carbazolyl)-2,4-hexadiyne, and ± 1 ppm for the remaining compounds.

Sample	C-9a,b	C-1	C-2	C-3	C-4	C-4a,b	C=C	C≡C	CH$_2$
poly-DCH	141.3	110.7	125.4	119.9	121.0	122.9	129.0	104.3	44
poly-DCH(Br$_{3.0}$)	139.6	111.1	125.2	peak around 121		123.7	123.7	102.4	44
poly-DCH(Br$_{3.8}$)	139.4	111.7	broad envelope around 122-123			123.9	128.5	102.2	44
poly-DCH(Br$_{6.0}$)	139	113	broad envelope around 122-123			123	not observed		44
poly-DCH(Br$_{7.4}$)	139	113	broad envelope around 122-123			123	not observed		44
poly-DCH(NO$_2$)$_{7.6}$	143	111	117* 123*‡	143	117* 123*‡	122	not observed		45
poly-DCH(Cl$_{14.9}$)	138	112	broad envelope around 116-128					102	†
carbazole	139.8	111.5	126.4	absorption around 120		121.5	—	—	—
3,6-dibromo-carbazole	138	116	broad envelope around 122-123			122.9	—	—	—
1,3,6,8-tetra-bromocarbazole	very broad spectrum, no assignments possible					—	—	—	—
di-N-carbazolyl-2,4-hexadiyne	139.0	108.8 107.6	127.6 125.7	peak around 120.6		122.5	—	75.0 68.3	32
bis(3',6'-dibromo-N-carbazolyl)-2,4-hexadiyne	137.4	109.9 106.8	broad features at 122 and 128			122.4	—	73.2 71.9	32
bis(1',3',6',8'-tetra-bromo-N-carbazolyl)-2,4-hexadiyne	135	broad pattern around 130				124	—	74	39
N-ethyl-3,6-dinitrocarbazole	140.8	110.0	115.9* 124.6*	144.7	115.9* 124.6*	121.9	—	—	39.0

* these two possible assignments cannot be decided.
† overlaps with broad CHCl resonance (40-70 ppm)
‡ based on relative peak intensities; resolved peak is only seen in solution NMR spectrum

Chemically modified poly-DCH. Previous ^{13}C NMR studies of poly-acetylenes doped with bromine, iodine and AsF$_5$ show the appearance of new resonance lines attributed to the formation of carbocationic species (24 − 26). In accord with this, Mössbauer studies of systems containing iodine (4, 27) or antimony pentahalide (28) indicate a partial reduction of the dopant species. These results correspond to a redox intercalation mechanism for the doping reaction, resulting in the formation of a compound stabilized primarily by an ionic interaction between the positively charged host lattice and the negatively charged guest species. In sharp contrast, the ^{13}C CP-MAS NMR spectra obtained with all derivatized polydiacetylenes investigated in the present study show no resonances typical of carbocationic species. Thus, an intercalation mechanism can be discounted as a reaction model for the present materials. Instead, the results presented and discussed below prove that covalent bonds are formed, first in the polymer sidechains and then in the backbone. In the following, our descriptions of the bromination products should be understood as average structures, since it is unlikely that a solid state diffusion process would affect every repeat unit in an identical manner.

Bromination of poly-DCH. The effects of bromination upon the ^{13}C CP-MAS NMR spectrum of poly-DCH are shown in Fig. 3. With increasing bromine content, a progressive marked broadening of resonances occurs and intensity losses for certain peaks of the polymer are observed. This phenomenon is not due to a distribution of chemical shifts since the same behavior is seen for the specifically brominated derivatives of both carbazole and the DCH monomer (Fig. 4). Rather, these effects arise from the dipolar coupling of the ^{13}C nuclei to nearby quadrupolar bromine nuclei as discussed above ([79]Br and [81]Br, the only naturally-occurring isotopes of bromine, both have spin 3/2). The experimental results obtained with the brominated model compounds (Fig. 4) indicate that the resonances from carbon atoms directly bonded to bromine as well as of adjacent carbon atoms are broadened to such an extent that they do not yield identifiable peaks in the spectrum. The broadening effects are more severe in the brominated carbazoles than in the brominated DCH monomers, presumably because of stronger *inter*molecular dipolar interactions in the former compounds. For this reason we believe that the brominated DCH monomers represent better model compounds for identifying the chemical changes taking place upon bromination of poly-DCH.

It should be noted that the CH$_2$ group and the nitrogen-bound carbon atom of the carbazole moiety are subject to the same effect, arising from the dipolar coupling to the quadrupolar ^{14}N nucleus. In this case, however, since the quadrupole coupling constant is much smaller than for the bromine isotopes (2.16 MHz for N-methyl pyrrole (29)) the interaction is much weaker and manifests itself only as a moderate broadening of the peaks with some ill-resolved structure. For these asymmetric resonances, the chemical shifts were measured at the center of gravity.
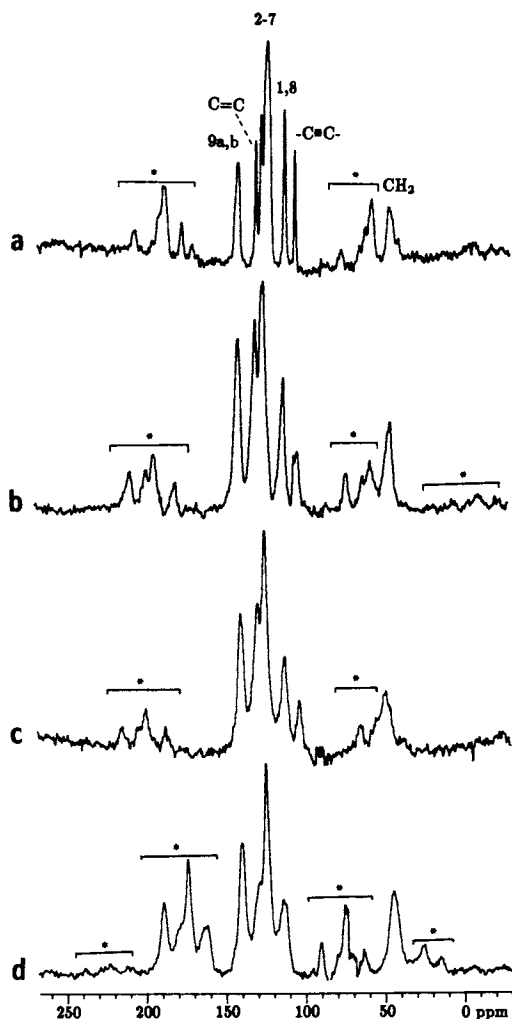
Fig. 3. ^{13}C CP-MAS spectra at 50.363 MHz of poly-DCH and its bromi-
nated reaction products. Spinning sidebands are indicated by an asterisk.
a) poly-DCH: spinning speed 3.2 kHz, 10 ms contact time, recycle delay 60
s (no magnetization flipback), 292 scans.
b) poly-DCH(Br$_{3.0}$): spinning speed 3.4 kHz, 5 ms contact time, recycle
delay 5 s (with magnetization flipback), 1444 scans.
c) poly-DCH(Br$_{3.8}$): spinning speed 3.9 kHz, 5 ms contact time, recycle
delay 20 s (no magnetization flipback), 230 scans.
d) poly-DCH(Br$_{6.0}$): spinning speed 2.5 kHz, 3 ms contact time, recycle
delay 5 s (with magnetization flipback), 500 scans.
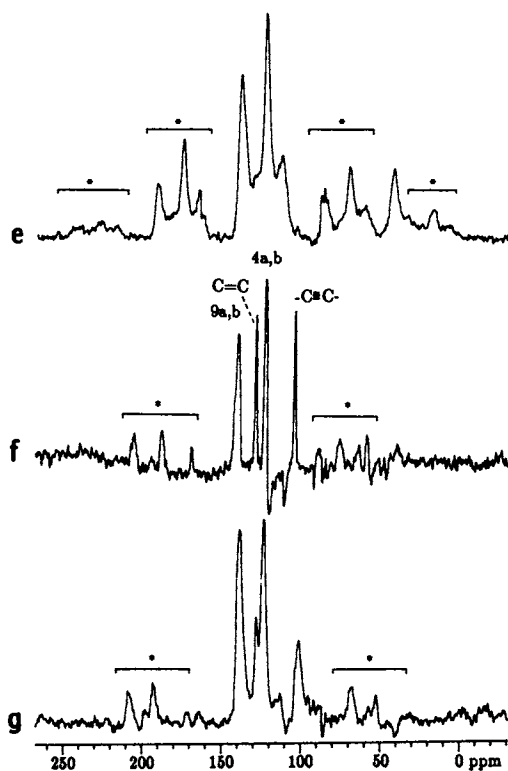
Fig. 3. (Continued)

e) poly-DCH(Br$_{7.4}$): spinning speed 2.6 kHz, 3 ms contact time, recycle delay 5 s (with magnetization flipback), 700 scans.

f) pristine poly-DCH: spinning speed 3.3 kHz, 10 ms contact time, decoupling delay 60 μs, recycle delay 60 s (no magnetization flipback), 252 scans.

g) poly-DCH(Br$_{3.0}$): spinning speed 3.5 kHz, 3 ms contact time, decoupling delay 60 μs, recycle delay 5 s (with magnetization flipback), 1000 scans.
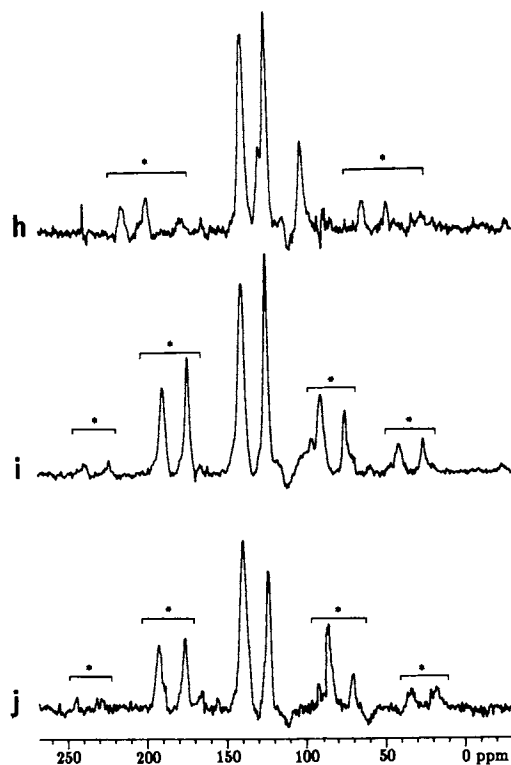
Fig. 3.   (Continued)
h) poly-DCH(Br$_{3.8}$): spinning speed 3.9 kHz, 5 ms contact time, decoupling delay 60 μs, recycle delay 60 s (no magnetization flipback), 228 scans.
i) poly-DCH(Br$_{6.0}$): spinning speed 2.5 kHz, 3 ms contact time, decoupling delay 60 μs, recycle delay 5 s (with magnetization flipback), 3000 scans.
j) poly-DCH(Br$_{7.4}$): spinning speed 2.6 kHz, 3 ms contact time, decoupling delay 60 μs, recycle delay 5 s (with magnetization flipback), 1104 scans.
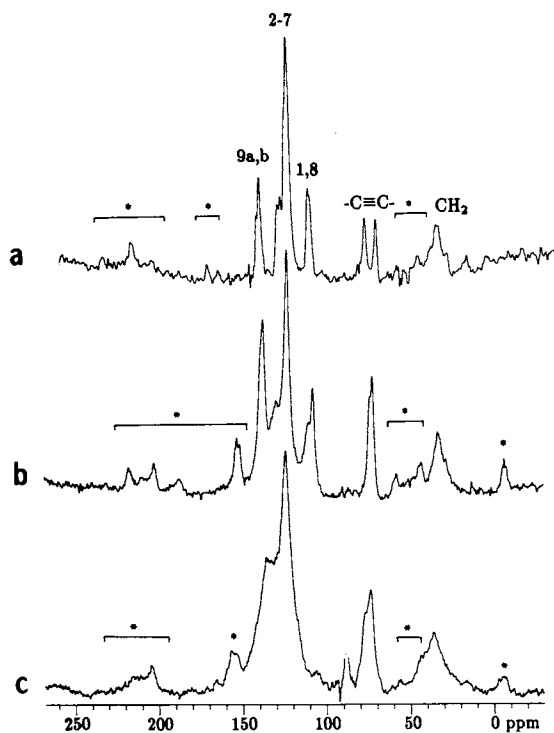
Fig. 4. ^{13}C CP-MAS spectra at 50.363 MHz of monomeric model compounds. Spinning sidebands are indicated by an asterisk.

a) N- carbazolyl-2,4-hexadiyne: spinning speed 5 kHz, 3 ms contact time, recycle delay 6 s (with magnetization flipback), 1108 scans.

b) bis(3',6'- dibromo-N-carbazolyl)-2,4-hexadiyne: spinning speed 4.0 kHz, 10 ms contact time, recycle delay 60 s (without magnetization flipback), 172 scans.

c) bis(1',3',6',8'- tetrabromo-N-carbazolyl)-2,4-hexadiyne: spinning speed 4.2 kHz, 3 ms contact time, recycle delay 5 s (with magnetization flipback), 1120 scans.
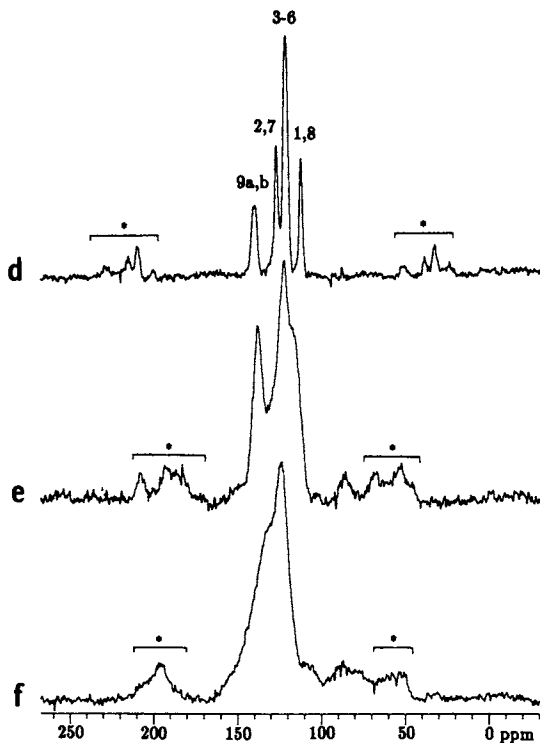
Fig. 4. (Continued)
d) carbazole: spinning speed 4.4 kHz, 5 ms contact time, recycle delay 4 s
(with magnetization flipback), 227 scans.
e) 3,6- dibromocarbazole: spinning speed 3.5 kHz, 10 ms contact time, re-
cycle delay 20 s (without magnetization flipback), 60 scans.
f) 1,3,6,8- tetrabromocarbazole: spinning speed 3.6 kHz, 10 ms contact time,
recycle delay 20 s (without magnetization flipback), 440 scans.

We can now attempt to explain the changes observed upon bromination in the spectra of Fig. 3 in terms of the chemical reactions taking place. Conceivable possibilities include electrophilic addition to the double or triple bonds, electrophilic substitution at the aromatic carbazole rings or bromination of the allylic methylene group. The latter possibility can be ruled out immediately, since the methylene peak remains unaffected by the reaction at all levels. Comparison of Fig. 3 with the spectra of the model compounds (Fig. 4) reveals that the spectral pattern in the aromatic region observed at all levels of bromination (Figures 3c,d,e) closely resembles that of the 3,3',6,6'-tetrabrominated monomer (Fig. 4b). This close resemblance is also observed in additional experiments involving delayed decoupling and variable contact times. Furthermore, these experiments establish that the peak pattern of Fig.'s 3c-e and 4b comprises the resonances of the 9a,9b, 4a,4b, and 1,8 carbon atoms, whereas the atoms C-2, C-3, C-4, C-5, C-6, and C-7 do not yield resolvable peaks. This result is consistent only with 3,6 bromination, in view of the experimentally established fact that C-atoms directly bonded or adjacent to bromine do not yield resolvable peaks. Thus we conclude that selective bromination of the aromatic rings takes place exclusively at the 3,6 positions.

Bromination of the carbazole group in the poly-DCH(Br$_{3.8}$) sample results in a small (2 ppm) upfield shift of the acetylenic carbon resonance. Wenz et al. (12) have shown that the chemical shift of the triple bond resonance may be a very sensitive measure of the number of conjugated carbon bonds. Thus the slight decrease observed in the brominated polymer could reflect a decrease in the average conjugation length, indicating the possibility of some minor degree of attack on the backbone even at low bromination levels. Alternative explanations cannot be ruled out, however. The acetylenic region of the poly-DCH(Br$_{3.0}$) spectrum contains peaks in both the original position and the upfield-shifted position in a ratio of roughly 1:3. This result suggests that the reaction does not produce a polymer with a statistical distribution of carbazole rings containing zero, one, and two bromine substituents, but rather results in a heterogeneous mixture of unbrominated polymer and polymer containing completely dibrominated carbazole rings.

Up to a level of 4 Br/repeat unit, bromination appears to be confined to the carbazole moiety, occurring selectively at the 3,6 sites. Four Br per repeat unit are required to completely brominate these sites. Above this level, the absorption pattern assigned to the carbazole moiety remains unchanged, indicating that no further ring bromination takes place. Instead, the peaks associated with the double and triple bonds become unobservable (30). Although the olefinic and especially the acetylenic carbon atoms are remote from protons and hence cross-polarize rather slowly, the experiments discussed in the previous section establish that the spectra obtained should be reasonably quantitative. It is worth noting that these unsaturated carbons are most likely cross-polarized by the methylene protons which are respectively two and three bonds distant. Since the NMR results show that these protons are retained during bromination, cross-polarization should occur even at the highest bromination levels. The fact

that these resonances actually disappear at a bromination level of 6 Br/repeat unit is likely due to the electrophilic addition of Br_2 to the multiple bonds. Since bromination is expected to render the ^{13}C resonances of both the carbon atoms directly bonded to bromine as well as the adjacent carbon atoms unobservable, these results are consistent with attack at either double or triple bonds, or a combination of both. In this context it should be pointed out that the chemical shift of multiple bonds is very sensitive to conjugation effects. Thus even if addition of bromine to the double or triple bonds to form single bonds occurred to only a minor extent, the disruption of backbone poly-conjugation would result in a broad distribution of chemical shifts which could render the corresponding resonances unobservable. However, since four Br per repeat unit appears to be the maximum extent of substitution on the carbazole rings, and since the methylene group does not react, we conclude that all bromine atoms above four Br per repeat unit must add to the multiple bonds. Furthermore, since in poly-$DCH(Br_{6.0})$ the backbone conjugation appears to be maintained (as suggested by the strong resonance Raman absorption at 632.8 nm excitation wavelength), we infer that bromine adds mainly to the triple bond in this material, resulting in the formation of a polyacetylene structure containing only poly-conjugated double bonds.

Levels of bromination above six Br per repeat unit can only be achieved under more vigorous reaction conditions. The straw-colored appearance of the products indicates a loss of backbone conjugation. This result is consistent with the observation that the carbazole region in the spectrum closely resembles that of bis(3',6'-dibromo-N-carbazolyl)-2,4-hexadiyne rather than that of bis(1',3',6',8' tetrabromo-N-carbazolyl)-2,4-hexadiyne. The comparison indicates that even at this high bromination level the attack upon the carbazole moiety in this polymer has been limited to the 3,6 positions (four Br per repeat unit). Since only two additional Br atoms can be added to (the triple bond of) the backbone while preserving polyconjugation, the stoichiometry of 7-8 Br per repeat implies that extensive disruption of polyconjugation in the backbone must have occurred. Further NMR evidence concerning the bromine addition to the multiple bonds in the polyconjugated polymer backbone could be obtained by monitoring the carbon-carbon bond lengths using ^{13}C nutation NMR, an experiment recently carried out on ^{13}C-dilabeled polyacetylene (31).

Nitration of poly-DCH. In contrast to the bromination reaction, the nitration reaction cannot be as easily controlled, and the resultant products are all highly nitrated. The results of some preliminary studies are shown in Fig. 5, where the spectra of a sample of composition poly-$DCH(NO_2)_{7.6}$ and the model compound N-ethyl-3,6-dinitrocarbazole are compared. The sites of nitration, unlike those of bromination, can be directly observed in the CP-MAS NMR spectra, although they are somewhat broadened by the dipolar interaction with the quadrupolar nitrogen nucleus as discussed above. No triple bond resonance is detected in the nitrated polymer, while some poorly resolved absorption in the region near 130 ppm in the spectra obtained with delayed decoupling indi-
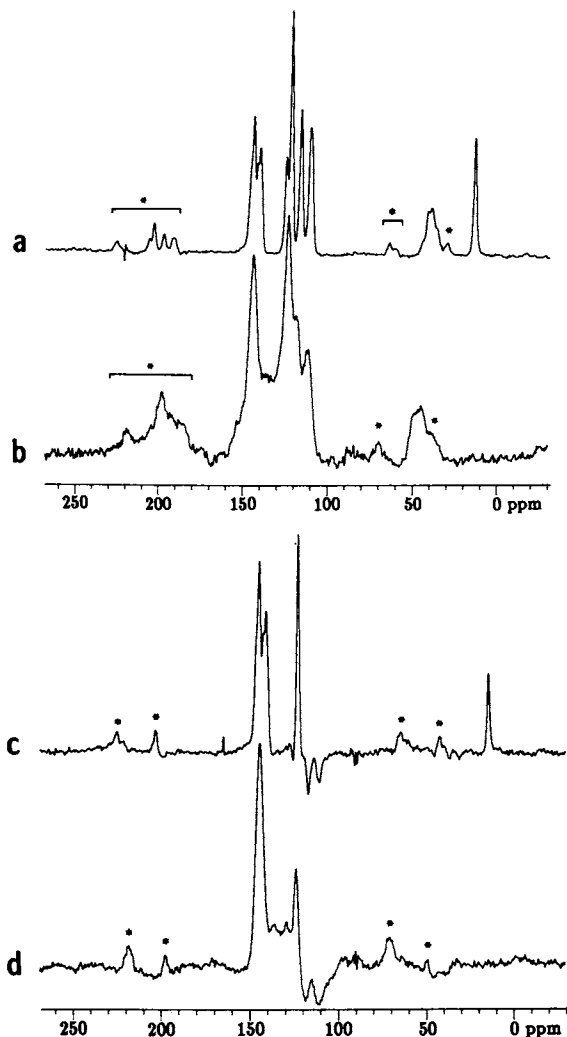
Fig. 5: ^{13}C CP-MAS studies at 50.363 MHz of the nitration of poly-DCH. Spinning sidebands are indicated by an asterisk.

a) N-ethyl-3,6-dinitrocarbazole (model compound): spinning speed 4.1 kHz, 10 ms contact time, recycle delay 5 s (with magnetization flipback), 311 scans.

b) poly-DCH(NO$_2$)$_{7.6}$: spinning speed 3.7 kHz, 10 ms contact time, recycle delay 5 s (with magnetization flipback), 304 scans.

c) N-ethyl-3,6-dinitrocarbazole: spinning speed 4.1 kHz, 10 ms contact time, decoupling delay 60 μs, recycle delay 4 s (no magnetization flipback), 2388 scans.

d) poly-DCH(NO$_2$)$_{7.6}$: spinning speed 3.7 kHz, 10 ms contact time, decoupling delay 60 μs, recycle delay 20 s (no magnetization flipback), 176 scans.

cates that some double bonds are still present. As in the case of bromination, the close similarity of the chemical shifts in Fig. 5 for the nitrated polymer and the model compound suggests that the chemical derivatization occurs at the 3,6 positions of the carbazole moiety. Additional evidence for the 3,6- ring nitration is shown in Figure 6, where the corresponding high resolution NMR spectra in DMSO solution are compared (in contrast to the other derivatized polydiacetylenes, the nitration product is soluble). The close agreement observed would not be expected if nitration occurred at other positions and we thus conclude that only low levels of other nitrated isomers are present. The broad bases of the peaks in Fig. 6b are attributed to the higher molecular mass fractions. Weaker peaks observed between 108 and 143 ppm have not been assigned. Further studies are needed in order to identify nitration sites other than the 3,6- positions.

Chlorination of poly-DCH. Like the reaction with nitric acid fumes, the derivatization of poly-DCH with gaseous chlorine cannot be controlled to yield compounds with low or moderate chlorine uptakes. The only compound which can be synthesized with a reproducible stoichiometry is poly-DCH(Cl_{15}), which is largely amorphous. The ^{13}C CP-MAS NMR spectrum of this product is displayed in Fig. 7a. Broadened aromatic carbazole peaks around 120-140 ppm can be observed, but in the absence of model compound data no specific substitution patterns can be ascertained. In addition, a strong broad resonance is observed in the chloroalkane region around ca. 50 ppm. Since this resonance appears in experiments using short (50 μs) contact times (Fig. 7b) and is completely absent in delayed decoupling experiments, it can be assigned to CHCl groups. The ability to observe this resonance shows that the broadening effects due to dipolar coupling to the directly-bonded quadrupolar chlorine nuclei are less severe than in the case of bromine, a not unexpected result. The intensity of this CHCl resonance is much greater than would be expected if it arose from chlorination of the allylic methylene group, which is, in any event, still observable. The results suggest that some addition of chlorine to the carbazole unit has occured, with concomitant loss of aromaticity. Another striking feature of Fig. 7a is the observation of a triple bond resonance at 102 ppm, as verified also by delayed decoupling experiments. This chemical shift, which is similar to that in poly-DCH, reveals that polyconjugation of the backbone has remained intact (the double bond resonance is presumably obscured by the broadened carbazole resonances).

Overall, these results demonstrate that the chlorination reaction differs markedly from bromination and seems to be restricted to the carbazole groups. Although the sample appears to be homogeneous by electron microscopy, the simultaneous appearance of aromatic and non-aromatic sidegroup resonances in the reacted polymer is difficult to explain without invoking sample heterogeneity.
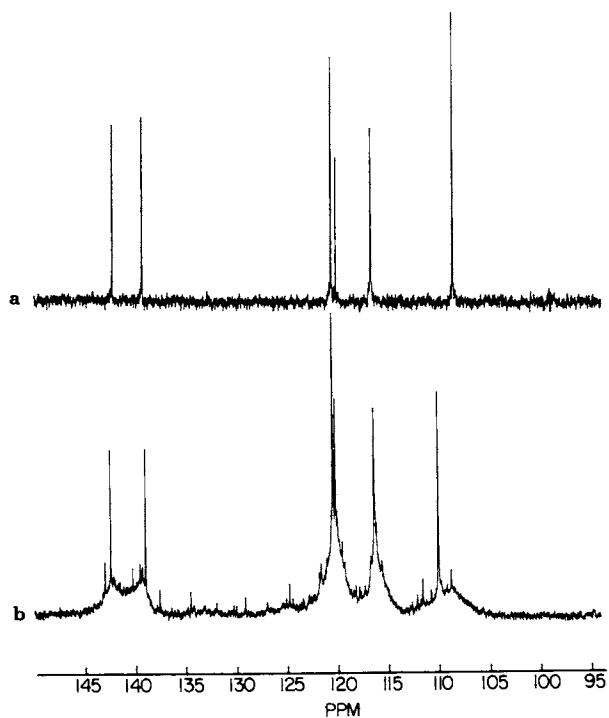
Fig. 6: High resolution ^{13}C NMR spectra in DMSO, at 125.76 MHz, power-gated proton decoupling, of:
a) N-ethyl-3,6- dinitrocarbazole
b) poly-DCH(NO$_2$)$_{7.6}$
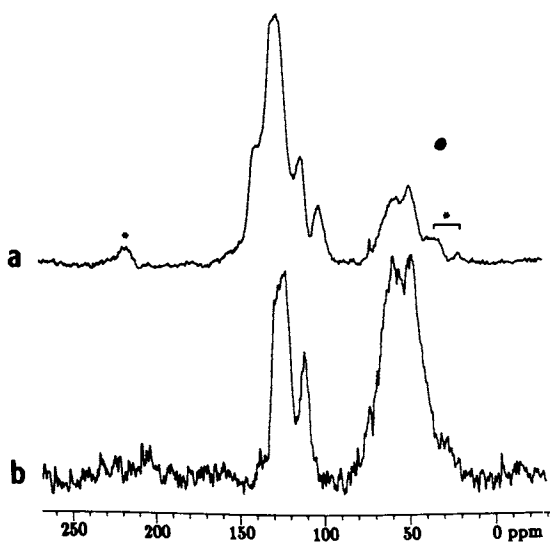
Fig. 7: ^{13}C CP-MAS spectra at 50.363 MHz of:
a) poly-DCH(Cl$_{14.9}$), spinning speed 5.0 kHz, 3 ms contact time, recycle
delay 10 s (with magnetization flipback), 1537 scans.
b) same conditions as a), except with a short contact time (50 μs), 400 scans.

Conclusions.

The reactions of poly-DCH crystals with liquid bromine, gaseous chlorine, or nitric acid fumes represent rare cases of solid state transformations of a polydiacetylene. Cross-polarization magic-angle spinning ^{13}C NMR techniques allow one to monitor the course of this reaction in a semi-quantitative fashion. The results indicate that the redox intercalation model which describes the chemical derivatization of polyacetylenes is not appropriate here. Instead, the reaction leads to the formation of new covalent bonds in the polymer. Studies of model compounds and solution state spectra lead to the conclusion that the bromine reagent selectively substitutes at the 3,6 positions of the aromatic rings of the carbazole moiety, forming a polymer with four Br/repeat unit. Further bromination of the ring does not take place even at the highest bromination levels (8.2 Br/repeat unit). Instead, bromine appears to add to acetylenic and ultimately to olefinic carbon atoms. While the nitration of poly-DCH appears to be governed by similar principles, the reaction with chlorine proceeds quite differently and leads to both addition and substitution on the carbazole moieties.

Acknowledgments.

Literature Cited.

1. Enkelmann, V. in "Polydiacetylenes", Cantow, H.-J., Ed., Springer Verlag Berlin, Heidelberg, New York, Tokyo 1984, p. 91.
2. Sandman, D. J.; Elman, B. S.; Hamill, G. P.; Hefter, J.; Haaksma, R.; Velazquez, C. S. Proc. ACS Div. PMSE 1986, 54, 297.
3. Apgar, P. A.; Yee, K. C. Acta Crystallogr. 1978, B34, 957.
4. Kaindl, G.; Wortmann, G.; Roth, S.; Menke, K. Solid State Commun. 1982, 41, 75.
5. Schaefer, J.; Stejskal, E. O.; Buchdahl, R. Macromolecules 1975, 8, 291.
6. Hartmann, S. R.; Hahn, E. L. Phys. Rev. 1962, 128, 2042.
7. Pines, A.; Gibby, M. G.; Waugh, J. S. J. Chem. Phys. 1972, 56, 1776.
8. Andrew, E. R.; Bradbury, A.; Eades, R. G. Nature 1959, 183, 1802.
9. Lowe, I. J. Phys. Rev. Lett. 1959, 2, 285.
10. Yannoni, C. S. Acc. Chem. Res. 1982, 15, 201 and references therein.
11. Havens, J. R.; Thakur, M.; Lando, J. B.; Koenig, J. L. Macromolecules 1984, 17, 1071.
12. Wenz, G.; Müller, M. A.; Schmidt, M.; Wegner, G. Macromolecules 1984, 17, 837.
13. Alla, M.; Lippmaa, E. Chem. Phys. Lett. 1976, 37, 260.

14. Stejskal, E. O.; Schaefer, J.; Sefcik, M. D.; McKay, R. A. Macromolecules 1981, 14, 275.
15. Menger, E. M.; Veeman, W. S. J. Magn. Reson. 1982, 46, 257.
16. Zumbulyadis, N.; Henrichs, P. M.; Young, R. H. J. Chem. Phys. 1981, 75, 1603.
17. Fleming, W. W.; Fyfe, C. A.; Lyerla, J. R.; Vanni, H.; Yannoni, C. S. Macromolecules 1980, 13, 460.
18. Earl, W. L.; VanderHart, D. L. J. Magn. Reson. 1982, 48, 35.
19. Stejskal, E. O.; Schaefer, J. J. Magn. Reson. 1975, 18, 560.
20. Alemany, L. B.; Grant, D. M.; Pugmire, R. J.; Alger, T. D.; Zilm, K. W. J. Am. Chem. Soc. 1983, 105, 2133 and 2142; Alemany, L. B.; Grant, D. M.; Alger, T. D.; Pugmire R. J. J. Am. Chem. Soc. 1983, 105, 6697.
21. Levy, G. C.; Lichter, R. L.; Nelson, G. L. In "Carbon-13 Nuclear Magnetic Resonance Spectroscopy", John Wiley & Sons, New York 1980.
22. Begtrup, M.; Claramunt, R. M.; Elguero, J. J. C. S. Perkin Trans. (II) 1978, 99.
23. Katritzky, A. R.; Saczewski, F.; Marson, C. M. J. Org. Chem. 1985, 50, 1351.
24. Heinmaa, I.; Alla, M.; Vainrub, A.; Lippmaa, E.; Khidekel, M. L.; Kotov, A. I.; Kozub, G. I. J. Phys. Colloq. 1983, 44, C3, 357.
25. Terao, T.; Maeda, S.; Yamabe, T.; Akagi, K.; Shirakawa, H. Solid State Commun. 1984, 49, 829.
26. Clarke, T. C.; Scott, J. C.; Street, G. B. IBM Res. Develop. 1983, 27, 313.
27. Matsuyama, T; Sakai, H.; Yamaoka, H.; Maeda, Y.; Shirakawa, H. Solid State Commun. 1981, 40, 269; J. Phys. Soc. Jpn. 1983, 52, 2238.
28. Friedt, J. M.; Poinsot, K.; Soderholm, L. Solid State Commun. 1984, 49, 223.
29. Lucken, E. A. C. In "Nuclear Quadrupole Coupling Constants", Academic Press, London 1969.
30. Recent results obtained at higher spinning speeds reveal the presence of some residual absorption in the triple bond region (95 to 102 ppm) for the material with 6 Br per repeat unit.
31. Clarke, T. C.; Kendrick, R. D.; Yannoni, C. S. J. Phys. Colloq. 1983, 44, C3, 369.

Chapter 19

Electron Paramagnetism
in Poly(1,6-di-*N*-carbazolyl-2,4-hexadiyne)
and Its Bromine Derivatives

M. T. Jones[1], J. Roble[1], and Daniel J. Sandman[2]

[1]Department of Chemistry, University of Missouri—St. Louis, St. Louis, MO 63121
[2]GTE Laboratories, Inc., Waltham, MA 02254

ESR studies of pristine poly-[1,6-bis(N-carbazolyl)-2,4-
hexadiyne](poly-DCH), a member of the general class of
materials known as polydiacetylene, of the reaction of
poly-DCH with bromine, and of poly-DCHBr$_6$ are reported
and compared to previously reported ESR studies on
similar systems. The ESR studies include measurements
of the spectral linewidths, the g-tensors and the
relative ESR signal intensity as a function of
temperature for poly-DCH and poly-DCHBr$_6$. Briefly, for
pristine poly-DCH, two superimposed ESR spectra are
observed. The spectral linewidths and g-tensors are
independent of temperature. In contrast, the ESR
signal intensity is thermally activated and displays two
activation energies. The kinetics of the disappearance
of the original ESR spectrum observed in pristine poly-
DCH and its replacement with a different ESR spectral
envelope is presented as are the kinetic parameters
which describe the reaction of poly-DCH with bromine.

Poly-[1,6-bis(N-carbazolyl)-2,4-hexadiyne](poly-DCH)   is   of
considerable interest because it is a member of a class of materials
known   as   polydiacetylenes(PDA's)   which   can   be   prepared   as
polyconjugated, single crystal polymers(1, 2). Additionally, these
materials are possible one dimensional semiconductors with a wide
band gap(3).   It has been found recently that single crystals of
poly-DCH react with chlorine, bromine, and nitric acid to give
products which appear homogeneous on examination by scanning and
transmission electron microscopy(4, 5).   We report ESR studies here
on poly-DCH, its bromination, and its bromination products since the
bromination reaction yields products with partial crystallographic
order, whereas, the other reactions produce amorphous solids. Thus,
the purpose of this study is several-fold: 1.   to learn more about
the electronic and molecular structure of pristine poly-DCH,   2. to
learn more about the source of the electron paramagnetism associated

with poly-DCH,   3.   to learn more about the details of the reaction
of bromine with poly-DCH and, finally, 4.   to learn more about the
electronic and molecular structure of the reaction products of poly-
DCHBr with bromine.

Experimental Techniques

The details of the preparation of the poly-DCH samples used in this
investigation are given in Ref. 3.   The crystal structure of poly-
DCH is given in ref. 6.   More detail regarding the chemistry of the
reaction of poly-DCH with bromine is given ref 7.

      The   ESR   measurements were performed on   a   Varian   E-12
spectrometer equipped with a dual cavity and interfaced with an IBM
PC/XT   for   data   collection.   The dual cavity   spectra   were
simultaneously recorded with a dual channel L & N Speedomax XL
recorder.   The g-values were measured at various temperatures using
the dual cavity technique which has been previously described in
detail(8-10) as has the ESR spectrometer and associated equipment
used in these studies.   The spin counts were made in comparison with
reference samples of a known amount of solid DPPH or   the Varian
Strong   Pitch   Sample.   Where   necessary,   the   ESR   spectral
intensities(i.e.,   the double integral of the derivative curve) were
calculated using a computer program based on a Riemann sum algorithm.
The digitized input data for the computer program were obtained
directly from the analog output of the ESR spectrometer.

ESR of Partially Oriented Pristine Polycrystalline Poly-DCH

The polycrystalline samples of poly-DCH used in this portion of the
study were partially oriented in the magnetic field. The long
crystalline(i.e., needle) axes were perpendicular to the magnetic
field but the other two crystalline axes were fanned out in all
directions   perpendicular to the crystalline long   axis.   The
conjugation chain direction is parallel to the long crystal axis.
Samples prepared in two different ways were studied: 1. the monomer
was crystallized from dimethyl formamide(DMF) and polymerized by
gamma irradiation, and 2. the monomer was crystallized from ethyl
acetate(EtOAc) and polymerized by gamma irradiation.

Sample Type #1. Room temperature ESR spectra taken at low microwave
powers(1 mw) show a single asymmetric line whose linewidth   varies
from approximately 16.5 to 20 G depending upon the sample orientation
in the magnetic field(i.e., rotation of the sample about the sample
holder axis). At low microwave powers and a temperature of ca 110 K,
additional absorption is observed in the wings of the single line.
However, the ESR spectral linewidth is independent of temperature.
At much larger microwave powers(ca 100 mw) two additional peaks
appear, one each, on either side of the single line observed at lower
microwave powers. Again there is no change in the observed linewidth
as the temperature is reduced. These two sets of superimposed spectra
do not have the same spin-lattice relaxation rates as demonstrated by
the difference in their saturation behaviour.

Figure 1 shows a series of ESR spectra recorded at room temperature as a function of increasing microwave power for sample type #1. The central line saturates(i.e., a plot of ESR signal amplitude as a function of microwave power reaches its maximum value) at ca 10 mw whereas the high power spectrum saturates at ca 100 mw. At a given power level and sample orientation in the magnetic field, the width of the center line is independent of temperature. The positions of the outer peaks which are observed at the higher microwave powers also depend on sample orientation. Based on these observations plus additional studies made as a function of temperature and microwave power, we have concluded that the spectrum of poly-DCH consists of two overlapping spectra. One consists of a single spectral line of ca 17 G which is rather easily saturated. The other consists of three spectral lines of relative intensity 1:2:1, such as might arise from the interaction of an unpaired electron with a methylene group, and which is rather difficult to saturate. The hyperfine splitting observed in the 1:2:1 pattern ranges from 25-30 G depending upon sample orientation. The single line of the first spectrum is superimposed upon the center line of the triplet of the second spectrum. Low microwave power, room temperature spin count measurements yield a value of 3×10^{17} spins per gram for the single line spectrum and ca one to two times that amount($3-6 \times 10^{17}$) for the 1:2:1 triplet spectrum.

At low microwave powers(i.e., 1 mw) and in the temperature range of 126 to 373 K, the ESR spectral lineshape of the center "line" is asymmetrical with an asymmetry parameter(A/B) of value greater than unity and which is not a strong function of temperature. However, as the microwave power is increased, the asymmetry parameter of the center line decreases to values below unity and shows a stronger dependence on temperature.

Measurement of the paramagnetic susceptibility at low microwave power(1 mw) as a function of temperature from 126 to 290 K shows(see Figure 2) that it is activated and that it can not be described with a single activation energy. In the temperature range 225 to 290 K, the activation energy has the value of 0.032 ev., whereas, it has the value of 0.016 ev from 126 to 225 K. This behaviour can be rationalized in terms of the presence of two different radicals each with a different energy of activation and/or different spin-lattice relaxation rates. The exact activation energies and the temperature of the knee depends upon the level of the microwave power used in the study. The magnetic susceptibilities for several different poly-DCH samples were studied as a function of temperature. All displayed behaviour as described above. A number of other polydiacetylene systems(11-13) have been reported to display multiple activation energies for magnetic susceptibilities. However, this is the first instance in which two distinct radical species have been observed to be the cause of such behaviour.

The g-value at the crossover point of the ESR spectrum is independent of temperature for a given sample orientation. However, the g-value is dependent upon sample orientation.

Poly-DCH is thermally stable up to 373 K as measured by the
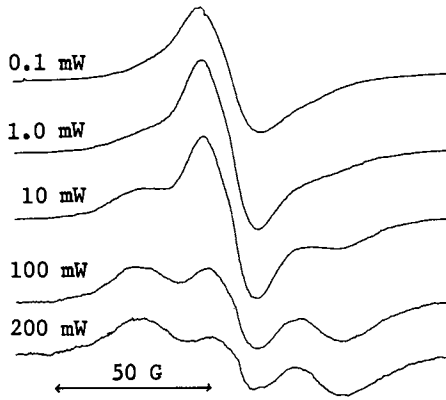
Figure 1.   Room temperature ESR spectra of poly-DCH(sample type #
1) shown as a function of microwave power.
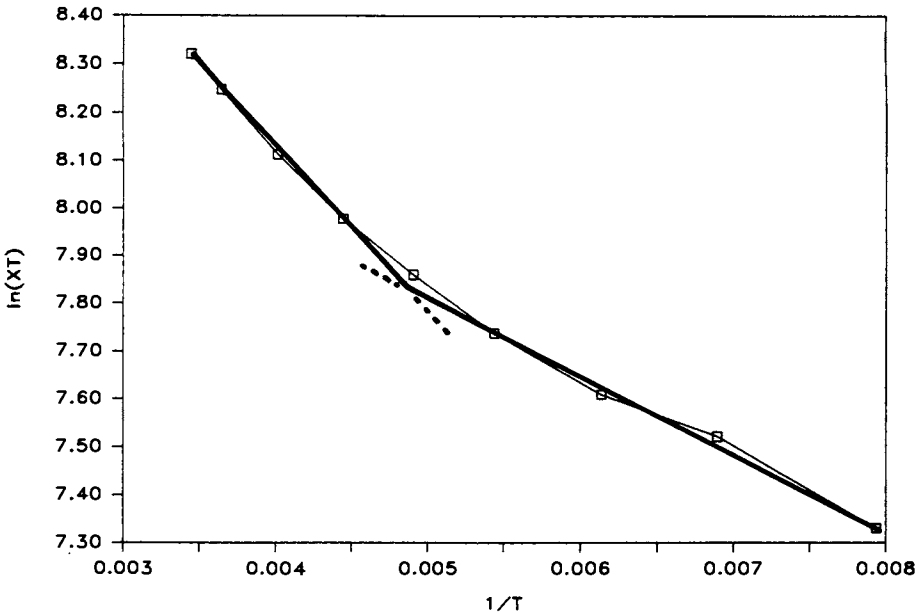
Figure 2. Plot of ln(XT) against 1/T for polycrystalline poly-DCH.
The   dashed lines trace the loci for activation energies equal to
0.016   and 0.032 ev for the low and high   temperature regions,
respectively.

process outlined below. A polycrystalline sample of poly-DCH was subjected to the following heat cycle: A. from room temperature to 333 K for 15 min and back to room temperature, B. from temperature to 373 K for 15 min and back to room temperature for 15 min, C. from room temperature to 373 K for 15 min and back to room temperature. While, at the higher temperatures, there was an increase in the ESR signal intensity due to the presence of thermally activated paramagnetic species and, perhaps, a slight increase in ESR linewidth, the process is completely reversible and there were no observable changes in the room temperature spectra after each cycle nor upon completion of the entire experiment.

ESR spectra were recorded from 0 to 10,000 G at ca 110 K and 298 K and at several different power levels. The only ESR absorption observed was near $g \sim 2$. No fine structure splitting was observed. These experiments will be repeated a liquid helium temperatures in the near future in our laboratory.

Sample Type #2. ESR studies of sample #2 yield results similar to those observed with sample #1 with one exception(see Figure 3). An additional third resonance line of width ca 0.5 G and integrated area equal to less than 1% of the other two radicals. The two samples have the same crystal structure but different morphology. It has been reported(13) that certain solvents either become trapped in the crystalline matrix or are incorporated in the crystalline lattice in a regular manner. Since the latter did not occur, we can only conclude that perhaps the former occurred and that we are looking at some type of radiation damaged solvent molecule.

ESR of Single Crystals of Pristine Poly-DCH

The single crystal samples of poly-DCH were 5 mm long(i.e., along the conjugation axis) and 3 mm and 1 mm along the other two axes. While complete anisotropic studies are planned, only data taken for rotation about the conjugation axis are reported here. The narrowest ESR spectral linewidths(20 G) are observed when the magnetic field is parallel to the broad face of the single crystal. The g-value at this orientation is 2.0029. The linewidth is equal to ~25 G when the magnetic field is perpendicular to the broad face of the crystal. There is only a slight dependence of the linewidth on temperature. It decreases by about 1 G at 108 K from room temperature. The paramagnetic susceptibility is activated and just as in the case of the polycrystalline sample shows two regions, each with its own activation energy. The values of the activation energies and the temperature ranges for the two different regions differ somewhat for each type of sample, however, this is not believed to be significant as noted above. At low microwave power, spin count measurements show the number of unpaired spins in the single crystals of poly-DCH is 3.7×10^{17} spins per gram at room temperature.
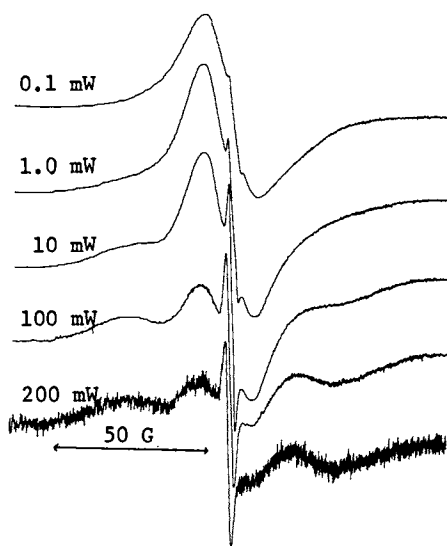
Figure 3. Room temperature ESR spectrum of poly-DCH(sample type #2) shown as a function of microwave power.

ESR Studies of the Reaction of Partially Oriented Pristine

Polycrystalline Poly-DCH with Bromine

As described in the Introduction and in references 3-5, poly-DCH has been found to react with bromine at 268 K. The purpose of these experiments was to see if there were any free radical intermediates found during the reaction. However, none were found. Instead, the radicals observed in pristine poly-DCH disappear and two new radical species at lower concentrations reappear.

ESR was used to monitor the ESR intensity as a function of time as pristine polycrystalline poly-DCH was allowed to react with bromine at 268 K. The reaction can be divided into three phases.

A. Initial phase(t < 80 min): First order reaction during which the initially observed ESR signal disappears at a rate of 1.19×10^{-2}/min. The parameters which describe the initial ESR spectrum are linewidth = 20 G and g at crossover = 2.00292. The initial ESR spectrum is replaced by a second spectrum whose parameters are given below.

B. Second phase(t > 120 min): First order reaction during which the second spectrum disappears at a rate of 2.1×10^{-3}/min. The parameters which describe the second spectrum are linewidth = 17 G and g at crossover = 2.0069.

C. Third phase(t > 16 - 20 hours): Final ESR intensity reduced to 10-15% of its original intensity. The final spectrum is described by the parameters given for the second phase.

Figure 4 shows a plot of the ESR signal intensity for poly-DCH as a function of time during reaction with bromine at 268 K.

A second experiment gave essentially the same results except that the rate constants were found to have different values than those reported above. We believe this to be a characteristic of a two phase reaction where the ratio of sample surface area to sample volume is an important variable over which we had no control.

ESR Studies of Poly-DCHBr$_3$

In the symbolism used here, poly-DCHBr$_x$, represents X bromine atoms per repeat unit in the polymer. Thus, poly-DCHBr$_3$ represents poly-DCH which on the average contains three bromine atoms per repeat distance. As discussed in references 3-5 and 7, the first four bromine atoms substitute in the two carbozlyl rings. The next two bromine atoms add across the triple bond. Further bromination destroys the crystalline nature of the poly-DCH.

Figure 5 compares the ESR spectra of poly-DCH, poly-DCHBr$_3$, and poly-DCHBr$_6$. The ESR spectrum of poly-DCHBr$_3$ shown in Figure 5 is quite consistent with that observed during the second phase of the bromination reaction. Of the two radical species observed in the
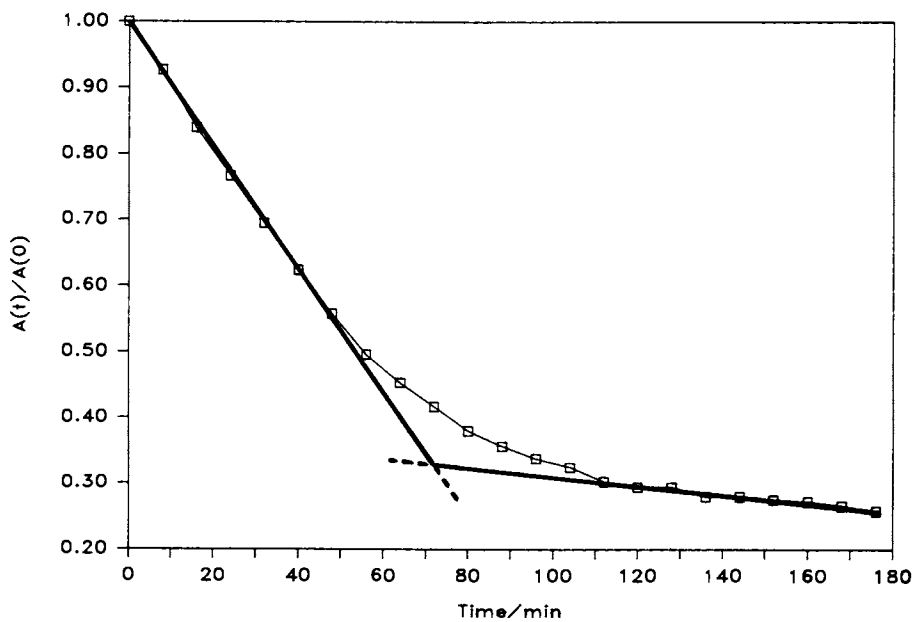
Figure 4.   Plot of ESR signal intensity for poly-DCH(sample type
#1) as a function of time during reaction with bromine at 268 K.
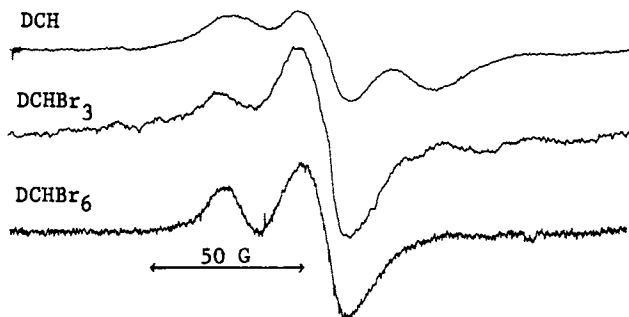
Figure 5.   Room temperature ESR spectra of poly-DCH(sample #1),
poly-DCHBr$_3$, and poly-DCHBr$_6$.

pristine poly-DCH, the first to disappear is that which gives rise to the three line spectrum. As the reaction proceeds, the central spectral line narrows and the g-value shifts to a slightly larger value. A new low field line begins to appear at g = 2.01977.

ESR Studies of Poly-DCHBr$_6$

The ESR spectrum observed for polycrystalline samples of poly-DCHBr$_6$ is shown in Figure 5. The most important question to be answered about this spectrum is whether it arises from a single species with a pseudo axial g-tensor or from two different radical species. Based on variable temperature and variable microwave power studies of this material we have concluded that the spectrum arises from two different radical species. However, the evidence in that regard leaves some uncertainty. Additional experiments are planned.

ESR Studies of Poly-DCHBr$_8$

The ESR spectrum of poly-DCHBr$_8$ is a single line of ca 1200 G with g = 2.256. Its signal amplitude is activated. All chemical evidence indicates that the original crystallinity of pristine poly-DCH and that of the poly-DCHBr$_6$ are completely destroyed upon the addition of 8 bromine atoms per repeat distance. The ESR results are in agreement with other chemical evidence which suggests a drastic change takes place upon the addition of two more bromine atoms to poly-DCHBr$_6$.

Spin Concentration Measurements, g-Values and Spectral Linewidths

Spin concentrations, g-values and spectral linewidths have been measured for each of the samples studied. The results are summarized in Tables I and II.

Table I Summary of Room Temperature ESR Results

Sample	<g>	LW/G	A/B	Mag. Sus	Spin Density
DCH-EtOAc	2.00414	17.5	1.05	Act.	3.9×10^{17},[a]
DCH-DMF	2.00413	17.5	1.07	Act.	3.0×10^{17},[a]
DCH/Br$_3$	2.00384	16.5	--	--	7.7×10^{16}
DCH/Br$_6$(1)	2.01977	10.2	--	C.L.	2.0×10^{15}
(2)	2.00467	12.1	--	C.L.	1.0×10^{16}
DCH/Br$_8$	2.2559	1215	0.833	Act.	----------

[a]Low power measurement of center line.

Table II Summary of Room Temperature g-values

Sample	g_1	g_2	g_3	$<g>$	LW/G
DCH-EtOAc	2.00941	2.00380	1.99937	2.00414	17.5
DCH-DMF	2.00951	2.00390	1.99897	2.00413	17.5
DCH/Br$_3$	2.00892	2.00365	1.99896	2.00384	16.5
DCH/Br$_6$(1)	2.02271	2.02007	2.01655	2.01977	10.2
(2)	2.00834	2.00467	2.00101	2.00467	12.1
DCH/Br$_8$	2.6199	2.2629	1.8848	2.2559	1215

Discussion of Results and Conclusions

Spectral Lineshapes and Linewidths. The spectral lineshapes and
linewidths are independent of temperature for all of the systems
studied and reported upon here. In the case of poly-DCH, where the
magnetic susceptibility is thermally activated, this implies that
even though individual paramagnetic sites are being randomly created
and annihilated as a function of time, the rate at which this occurs
is too slow to affect the ESR spectral envelope. Based on a spectral
linewidth of 17 G and an estimated unresolved hyperfine splitting of
3-5 G an upper limit for any motional process is estimated to be in
the range of 10^8 Hz. Only at temperatures of 373 K is there a hint
of possible line narrowing.

Spin Concentrations. It is of interest to answer the question, what
is the mean molecular weight per unpaired electron(i.e., per radical
sites)? Based on the assumption of two unpaired electrons per
"molecule" and a total spin concentration of 6 x 10^{17} spins per gram,
the mean molecular weight per pair of unpaired electrons is 2 x 10^6.
This is a number that falls into the range of expected molecular
weights for this particular polymer system.

Identification of the Source of the Electron Paramagnetism in Poly-
DCH. We have investigated a series of possible radical site
structures and models to explain the observed electron paramagnetism
in poly-DCH and poly-DCHBr$_6$. The model which holds the most promise
for poly-DCH is that proposed by Sixl and co-workers([14]).

Assume the ground state of poly-DCH is described by the ene-iyne
structure. The ends of the polymer consist of dicarbene structures
which can be either of the ground state singlet or triplet type. The
experimental evidence appears to favor the singlet. However, this
point needs further study. Upon thermal excitation the carbene,
breaks up into two radicals. One, a sigma(i.e. sp^2) radical centered

on end of the polymer at the original site of the carbene and two, a pi radical which moves into the polymer chain sufficiently far away from the sigma radical site to reduce the magnetic interaction between the two sites is observed. The two radicals observed in poly-DCH appear to be consistent with this model. The 1:2:1 three line spectrum is identified as the sigma radical and the single line spectrum is identified as the pi type radical. These identifications are consistent with the different ESR spectral parameters which describe the two different spectra. For example, the sigma radical is expected to have somewhat larger methylene proton hyperfine splittings than those of a similar pi radical. The sigma radical is expected to exhibit a somewhat enhanced spin-lattice relaxation rate in comparison with the pi radical.

Literature Cited

1. "Polydiacetylenes", Advances in Polymer Science, Vol. 63, Cantow, H.-J., ed., Springer-Verlag, 1984.

2. "Polydiacetylene: Synthesis, Structure, and Electronic Properties", NATO-ASI Series, Bloor, D.; Chance, R. R., Martinus Nijhoff, Dordrecht, Boston, 1985.

3. Sandman, D. J.; Hamill, G. P.; Samuelson, L. A.; Foxman, B. M.; Mol. Cryst. Liq. Cryst. 1984, 106, 199.

4. Yesinsowoski, J. P.; Eckert, H.; Sandman, D. J.; ACS, Div. Polymeric Materials, Preprint,(1986).

5. Sandman, D. J.; Elman, B. S.; Hamill, G. P.; Velazquez, C. S.; Yesinowski, J. P.; Eckert, H.; J. Am. Chem. Soc., Submitted

6. Apgar, P. A.; Yee, K.C.; Acta Cryst. 1978, B34, 957-9.

7   Sandman, D. J.; Elman, B. S.; Hamill, G. P.; Velazquez, C. S.; Samuelson, L. A.; Mol. Cryst. Liq. Cryst. 1986, 134, In Press.

8. Jones, M. T.; Kuechler, T. C.; J. Phys. Chem. 1977, 81, 360.

9. Jones, M. T.; Ahmed, R.; Kastrup. R.; Rapini, V.; J. Phys. Chem. 1979,83, 1327

10. Rataiczak, R. D.; Jones, M. T.; Reeder, J. R.; Sandman, D. J.; Mol Phys, 1985, 56 ,65.

11. Freitas, Jr., J. A.; Greenbaum, S. G.; J. Polym. Sci. Polym. Phys. Ed 1983, 21, 2045.

12. Eichele, H; Schwoerer, M.; Huber, R.; Bloor, D.; Chem. Phys. Lett. 1976, 42, 342.

13.   Baughman, R. H.; Exarhos, G. J.; Risen, Jr., W. M.; J.
      Polym. Sci Polym. Phys. Ed. 1974, 12, 2189.
14.   Sixl, H.; Neumann, W.; Huber, R.; Denner, V.; Sigmund, E.; Phys.
      Rev., 1985, B31, 142.

Chapter 20

Relationship between Structure and Mechanical Properties of Polydiacetylenes

R. J. Young

Department of Polymer Science and Technology, Manchester Institute of Science and Technology, University of Manchester, Manchester M60 1QD, United Kingdom

Polydiacetylenes offer a unique opportunity of studying
structure/property relationships in polymers. This
paper is concerned with structural factors which control
mechanical properties. The effect of the size of side-
groups upon the Young's moduli of different polydiacety-
lenes is discussed briefly. The effect of internal
and surface defects upon the strengths of individual
fibres is also described. Examples are given of how
Raman spectroscopy can be used to follow the deformation
of fibres and it is shown how this can be extended to
fibres in composites. The general mechanical properties
of the composites are also described.

Polydiacetylene single crystals produced by the solid-state polymer-
ization of substituted diacetylene single crystal monomers (1,2) offer
a unique opportunity of studying structure/property relationships in
polymers. The solid-state polymerization technique enables highly-
perfect polydiacetylene single crystals to be produced as either
lozenges (3) or fibres (4) with macroscopic dimensions. This can be
contrasted with the case of conventional polymers such as polyethy-
lene which is obtained as polycrystalline spherulitic samples when
crystallized from the melt (5) or as microscopic chain-folded
lamellar single crystals from dilute solution (6). Neither of these
two morphologies are particularly useful for the study of structure/
property relationships. Spherulitic polymers have complex structures
(5) and the lamellar single crystals can generally only be studied in
the electron microscope (6). Many of the fundamental investigations
of structure/property relationships in metal crystals have involved
the use of large single crystal specimens (7).
    In the past there have been several attempts to investigate the
relationship between structure and mechanical properties in
polyethylene. It has proved possible to produce samples of the
polymer with a single-crystal texture (8) but they are still
polycrystalline and certain ambiguities remain concerning the
detailed deformation mechanisms in such samples (9). There have also
been reports of studies of the deformation of single crystals of
polyethylene on extensible substrates (10,11). Because the polymer

molecules are oriented perpendicular to the surface of the lamellar crystals (5) deformation is limited to directions perpendicular to the chain direction. Also forces or stresses cannot be measured for the microscopic crystals. Polymer scientists were therefore frustrated for many years by the lack of polymer crystals with suitable morphologies.

It was realised that the fundamental problem was the difficulty of arranging the long tangled and coiled molecules of a molten polymer or polymer solution in a single crystal. Hence, there was considerable excitement when polymer chemists started to examine the possibility of producing polymer crystals by the solid-state polymerization of single crystal monomers (1). Some of the first attempts, however, were rather disappointing. For example, single crystals of trioxane were found to undergo polymerization to polyoxy-methylene in the solid state but the polymer produced was found to be polycrystalline with a complex morphology (12). Such problems are not normally encountered with the topochemical polymerization (1) of a large number of differently substituted diacetylene derivatives. This has led to the development of highly-perfect polydiacetylene single crystals with macroscopic dimensions which have enabled significant advances to be made in our understanding of the relation-ship between the optical, electronic and mechanical properties and the structure of polymer crystals (2).

This paper reviews recent work upon structure/mechanical-property relationships in polydiacetylenes. It is shown how this has led to the development of high strength polydiacetylene single crystal fibres and their performance as reinforcing fibres in composites is described.

Structure

Morphology. In general, polydiacetylene single crystals are found in one of two crystal morphologies, either as lozenges or as fibres. The morphology is controlled by the conditions under which the monomer is crystallized although the exact reasons why a particular morphology is obtained are not fully understood. The toluene sulphonate derivative (TSHD) (3) is normally obtained in the form of lozenges from most solvents whereas the carbazolyl derivative (DCHD) (4) is usually obtained as fibres, the aspect ratio of which depends upon the solvent, solution concentration and crystallization conditions. In contrast the ethyl urethane derivative (EUHD) (13,14) can be obtained in three crystal forms, only one of which can undergo solid-state polymerization to give fully-polymerized single crystal fibres (13). An example of fibrous crystals of this derivative is given in Figure 1a.

Electron Microscopy. X-ray diffraction methods have been used to determine the crystal structures of many polydiacetylene derivatives to a high degree of accuracy and precision (15-17). This depth of knowledge of the crystal structures is invaluable for the purpose of relating mechanical behaviour to structure. Although X-ray diffraction is the most accurate method of determining crystal structures considerable extra information can be obtained using transmission electron microscopy (18-20). Studies upon polydiacety-lene single crystals have enabled the detailed structure of defects
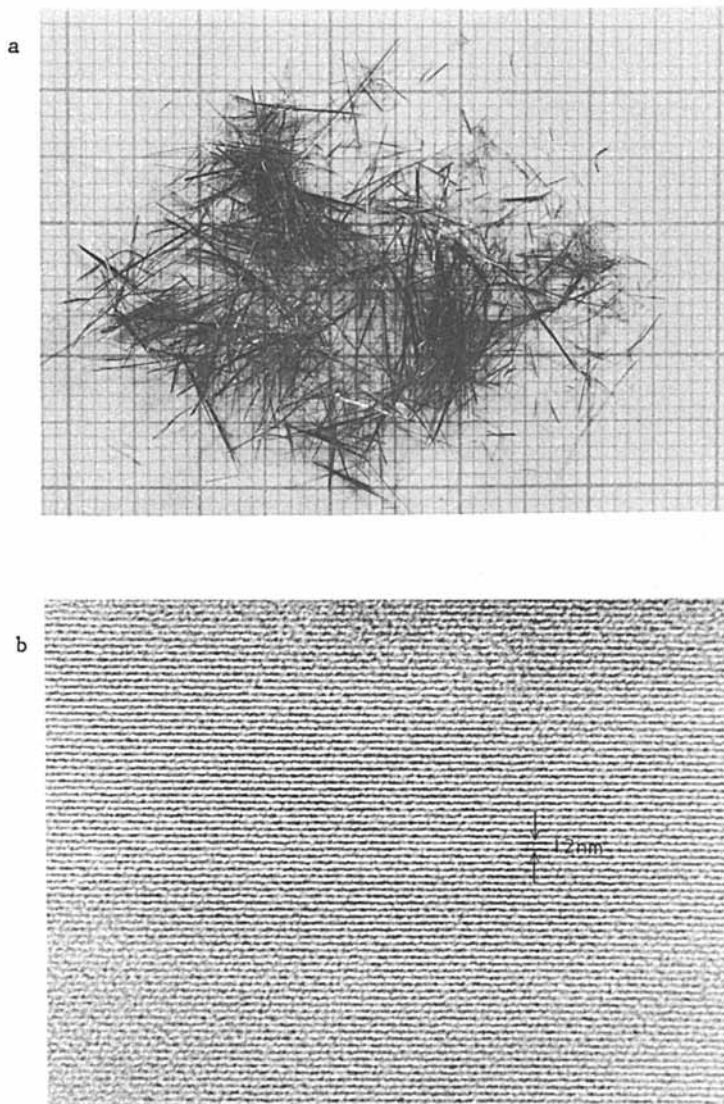
Figure 1 (a) Photograph of polydiacetylene single crystal fibres
on mm graph paper. (b) Lattice planes in poly DCHD, spacing
1.2 nm.

such as twins (21), dislocations (19,22) and stacking faults (23) to
be elucidated. It has also enabled the geometry of surface defects
such as steps (24), which control the strength of single crystal
fibres, to be analysed in detail.
     One problem normally encountered with organic materials such as
polymers in the electron microscope is radiation damage whereby the
crystal structure is destroyed by exposure to the electron beam (19).
It has been found that most polydiacetylenes are relatively stable
and that polyDCHD is particularly outstanding in its ability to
resist damage in the electron beam (19) being over 20 times more
resistant than polyethylene. This high stability has allowed
detailed studies to be made of the structure of polyDCHD at high
magnification. It has been found that the crystal lattice can be
imaged directly in the electron microscope (19,24) and an example of
this is shown in Figure 1b where planes parallel to the chain
direction can be seen. As well as being an interesting exercise in
electron microscopy this imaging of the crystal lattice shows the
perfect alignment of the polymer molecules in polyDCHD crystals and
the relatively defect-free nature of these materials.

Mechanical Properties

Stress/strain behaviour. In 1974, Baughman, Gleiter and Sendfeld (25)
demonstrated that fibre-like crystals of the phenyl urethane
substituted polydiacetylene, polyPUHD could be deformed elastically
to strains of over 3%. The crystals were found to have high values
of Young's modulus in the chain direction of the order of 45GPa.
The work has since been extended to other polydiacetylenes with
modulus values of 45GPa being reported for polyDCHD (24) and 62GPa
for polyEUHD (14).
     A typical stress/strain curve for a polyDCHD single crystal
fibre is given in Figure 2. The curve is linear up to a strain of
about 1.8% and there is a slight decrease in slope above this strain
until fracture occurs at a strain of about 2.8%. It has been
suggested (25) that this non-linear behaviour, which is not a yield
process, might be due to the anharmonic part of the interaction
potential between neighbouring atoms on the polymer backbone. This
has been confirmed using Resonance Raman Spectroscopy (26) where it
has been shown that the frequencies of all the main-chain carbon-
carbon stretching modes decrease with applied strain. The consequent
reduction in the force constants is one of the factors leading to a
reduction in the slope of the stress/strain curve at high strains
(14,24,25)

Young's modulus. Polydiacetylene single crystal fibres have very high
values of Young's modulus when account is taken of the relatively
high cross-sectional area of the molecules caused by the presence of
relatively large side-groups. For example, each molecule in polyDCHD
(24) supports an area of about 1 nm^2 compared with the cross-sectional
area of a polyethylene molecule (0.18 nm^2). Hence polyDCHD has about
the same per-chain modulus as polyethylene and both have about the
same value of diamond (27). This indicates the tremendous potential
that polymer crystals have as stiff and hence strong materials (27).
Improvements in the moduli of polydiacetylene crystals will be gained
by preparing good single crystals of new derivatives with smaller
side-groups.

Creep. One of the most remarkable aspects of the deformation of polydiacetylenes is that it is not possible to measure any time-dependent deformation or creep when crystals are deformed in tension parallel to the chain direction (14,24). This behviour is demonstrated in Figure 3 for a polyDCHD crystal held at constant stress at room temperature and the indications are that creep does not take place at temperatures of up to at least 100 °C (24). Creep and time-dependent deformation are normally a serious draw-back in the use of conventional high-modulus polymer fibres such as polyethylenes (28). Defects such as loops and chain-ends allow the translation of molecules parallel to the chain direction in polyethylene fibres. In contrast since polydiacetylene single crystal fibres contain perfectly-aligned long polymer molecules (cf Figure 1b) there is no mechanism whereby creep can take place even at high temperatures.

Fracture. The most interesting aspect of the fracture behaviour of polydiacetylenes is the high strength that single crystal fibres can exhibit when deformed parallel to the chain direction. It is found that the fracture strength of the fibres decreases as the fibre diameter increases (14,24,25). It has been shown (24,25) that this is due to the presence of surface defects on the fibres and the 'theoretical strength' (i.e. the strengh of a defect-free crystal) of polyDCHD fibres has been shown (24) to be 3±1GPa. This corresponds to a force required to break individual molecules of about 3 nN. Kelly (29) has estimated the strength of a polyethylene molecule as 6 nN but this is now thought to be rather high (30). Kausch (31) has shown that a covalently-bonded molecule should be broken by a force of the order of 3 nN-identical to the value determined experimentally for polyDCHD. Hence it can be seen that these high levels of strength measured for the polydiacetylene fibres are consistent with the predictions of Frank (27) in 1970.

Composites

It is well-established (32) that composites produced by incorporating high-modulus fibres in a brittle matrix such as an epoxy resin can have outstanding mechanical properties. Recent examples have included composites produced with high-modulus polyethylene fibres (33) and aromatic polyamide fibres (34). Polydiacetylene single crystal fibres also offer considerable promise as reinforcing fibres because they have high stiffness and strength, low creep, good thermal stability and low density (24). Recent investigations (35-37) into the behaviour of polydiacetylene single crystal fibres in epoxy resin matrices have shown that not only do such composites have promising mechanical properties but that fundamental details of the mechanisms of fibre reinforcement can also be revealed from their study.

Micromechanisms of reinforcement. It was pointed out earlier that the vibrational frequencies of certain main-chain Raman active modes are found to change with the level of applied strain (26). The biggest change is found for the C≡C triple bond stretching frequency which is of the order of 20 cm^{-1}/%. This property can be used to determine the strain in any polydiacetylene fibre subjected to any
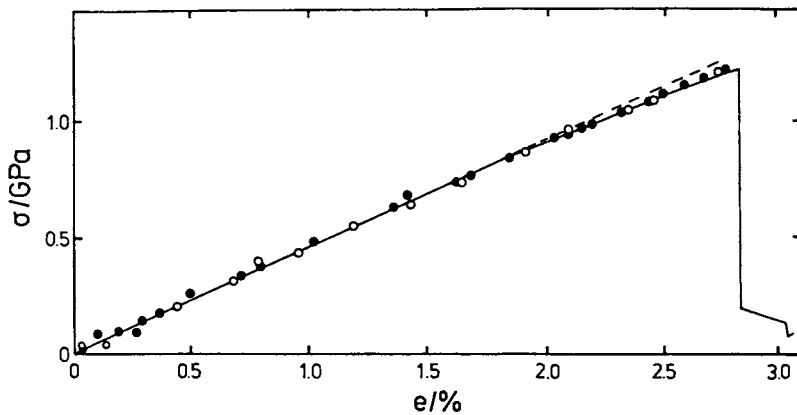
Figure 2. Stress/strain curve for a poly DCHD fibre.
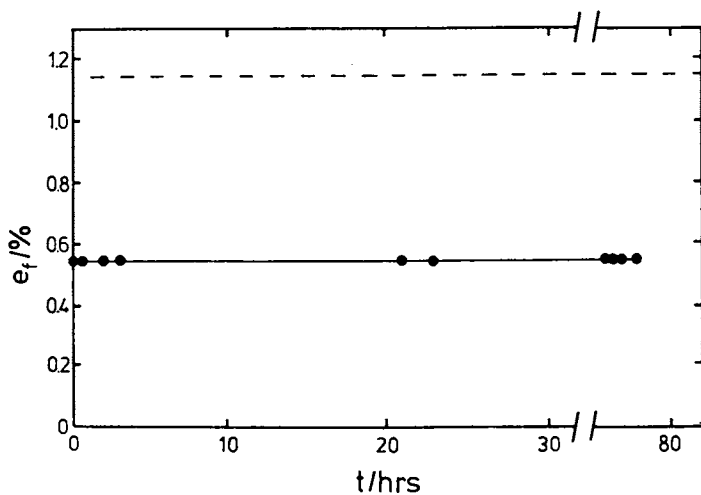
Figure 3. Variation of strain with time for a poly DCHD fibre held at constant load.

general state of stress. The fibres behave as though they have an
internal molecular strain gauge and the Raman technique has been
recently employed to monitor the point-to-point variation in strain
in polydiacetylene fibres in epoxy composites (35,36) to a high
degree of accuracy and precision. It has proved possible to measure
the dependence of critical lengths (32) of individual fibres as a
function of fibre diameter, confirming theoretical predictions (32).
In addition, it is also possible to follow interactions between the
fibres and matrix such as fibre twinning and kinking caused by resin
shrinkage (36).

Mechanical properties. Some preliminary measurements have been made
of the mechanical properties of composites consisting of aligned
polyDCHD single crystal fibres (~ 10 mm long) in an epoxy resin
matrix (37). Figure 4 shows a stress/strain curve for a sample with
fibre volume fraction, V_f, of 55.5%. The deformation is linear up
to the fracture strain of ~ 0.8% reflecting the linearity of the
stress/strain curves for individual fibres at low strains (Figure 2).
It is found that the mechanical properties of polyDCHD/epoxy
composites depend strongly upon the fibre volume fraction and this is
demonstrated in Figure 5. It can be seen that the Young's modulus,
E, of the composite increases as the volume fraction of fibres
increases. The experimental points fall between the Voigt (uniform
strain) and Reuss (uniform stress) lines (32). For a uniaxially-
aligned composite sample it would be expected that the data should
fall close to the Voigt line and it is thought (37) that the short-
fall in modulus is due to a combination of fibre misalignment and
fibre-twinning due to resin shrinkage.
     It is also found that there is a general increase in strength of
the composites with increasing fibre volume fraction. However, at
low values of V_f the strength is below that of the pure resin until
sufficient fibres are present to produce reinforcement (29) and at
high values of V_f (> 60%) the strength falls off because there is
not enough resin to wet the fibres (37).

Conclusions

It has been demonstrated that polydiacetylene single crystal fibres
are relatively perfect and have excellent molecular alignment. In
consequence they display high values of stiffness and strength and
are very resistant to creep. It has been shown that such fibres have
considerable promise as reinforcing fibres in an epoxy resin matrix
and the study of such composite systems has enabled considerable
fundamental information to be obtained concerning the mechanisms of
fibre reinforcement.
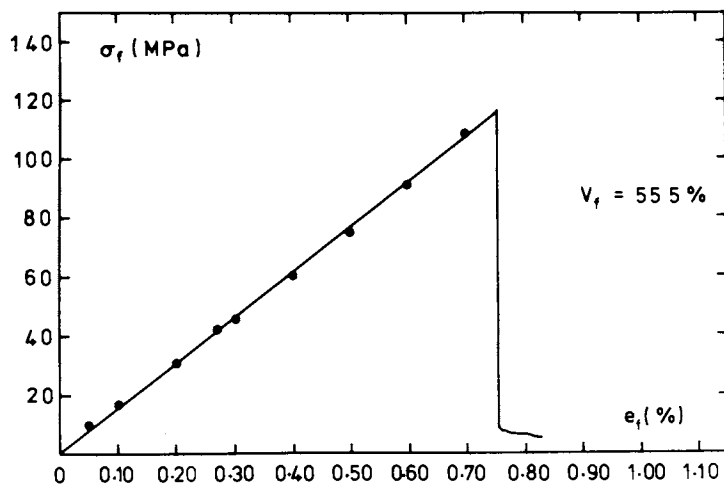
Figure 4. Stress/strain curve for an aligned poly DCHD/epoxy composite.
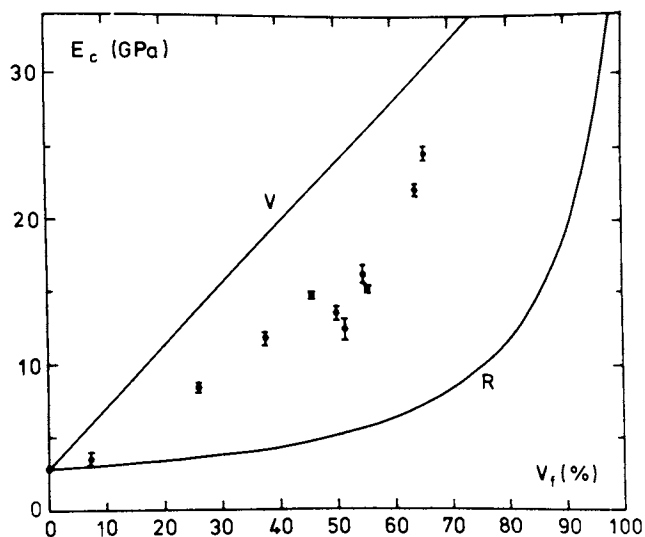
Figure 5. Variation of Youngs modulus, E with V_f for poly DCHD/ epoxy composites. The lines V and R denote the Voigt and Reuss bounds respectively.

Literature Cited

1. Wegner, G. Pure Appl. Chem. 1977, 49, 443.
2. Bloor, D.; Chance, R. R. "Polydiacetylenes" (NATO ASI); Martinus
    Nijhoff Publishers: Dordrecht, Holland, 1985.
3. Bloor, D.; Koski, L.; Stevens, G. C.; Preston, F. H.; Ando, D.J.
    J. Mater. Sci. 1975, 10, 1678.
4. Yee, K. C.; Chance, R. R. J. Polym. Sci., Polym. Phys. Ed.
    1978, 16, 431.
5. Young, R. J. "Introduction to Polymers"; Chapman and Hall:
    London, 1981.
6. Gell, P. H. "Polymer Single Crystals"; Interscience: New York,
    1963.
7. Kelly, A.; Groves, G. W. "Crystallography and Crystal Defects";
    Longman: London, 1970; Chap. 11.
8. Young, R. J.; Bowden, P. B. J. Mater. Sci. 1973, 8, 1177.
9. Bowden, P. B.; Young, R. J. J. Mater. Sci. 1974, 9, 2034.
10. Allan, P.; Bevis, M. Proc. Roy. Soc. 1974, A34, 75.
11. Allan, P.; Crellin E. B.; Bevis, M. Phil. Mag. 1973, 27, 127.
12. Andrews, E. H.; Martin, G. E. J. Mater. Sci. 1973, 8, 1315.
13. Galiotis, C.; Young, R. J.; Ando, D. J.; Bloor, D. Makromol.
    Chem. 1983, 194, 1083.
14. Galiotis, C.; Young, R. J. Polymer 1983, 24, 1923.
15. Kobelt, D.; Paulus, E. F. Acta Cryst. 1974, B30, 232.
16. Hädicke, E.; Mez, H. C.; Krauch, C. H.; Wegner, G.; Kaiser, J.
    Angew. Chem. 1971, 83, 253.
17. Apgar, P. A.; Yee, K. C. Acta Cryst. 1970, B34, 957.
18. Read, R. T.; Young, R. J. J. Mater. Sci. 1979, 14, 1968.
19. Read, R. T.; Young, R. J. J. Mater. Sci. 1984, 19, 327.
20. Read, R. T.; Young, R. J. J. Mater. Sci. Lett. 1981, 16, 2922.
21. Read, R. T.; Young, R. J. Phil. Mag. A. 1980, 42, 629.
22. Young, R. J.; Petermann, J. J. Polym. Sci., Polym. Phys. Ed.
    1982, 20, 961.
23. Young, R. J.; Read, R. T.; Petermann, J. J. Mater. Sci. 1981,
    16, 1835.
24. Galiotis, C.; Read, R. T.; Yeung, P. H. J.; Young, R. J.;
    Chalmers, I. F.; Bloor, D. J. Polym. Sci., Polym. Phys. Ed.
    1984, 22, 1589.
25. Baughman, R. H.; Gleiter, H.; Sendfeld, N. J. Polym. Sci.,
    Polym. Phys. Ed. 1975, 13, 1871.
26. Galiotis, C.; Young, R. J.; Batchelder, D. N. J. Polym. Sci.,
    Polym. Phys. Ed. 1983, 21, 2483.
27. Frank, F. C. Proc. Roy. Soc. 1970, A319, 127.
28. Capaccio, G.; Gibson, G.; Ward, I. M. In "Ultra-High Modulus
    Polymers"; Eds. Ciferri, A.; Ward, I. M.; Applied Science:
    London, 1979, p. 1.

29. Kelly, A. "Strong Solids"; Clarendon Press: Oxford, 1966.
30. Kinloch, A. J.; Young, R. J. "Fracture Behaviour of Polymers";
     Applied Science: London, 1983.
31. Kausch, H. H. "Polymer Fracture"; Springer-Verlag: Berlin, 1978.
32. Hull, D. "An Introduction to Composite Materials"; Cambridge
     University Press, 1981.
33. Ladizersky, N. H.; Ward, I. M. J. Mater. Sci. 1983, 18, 533.
34. Piggott, M. R.; Harris, B. J. Mater. Sci. 1980, 15, 2533.
35. Galiotis, C.; Young, R. J.; Yeung, P. H. J.; Batchleder, D. N.
     J. Mater. Sci. 1984, 19, 3640.
36. Robinson, I. M.; Yeung, P. H. J.; Galiotis, C.; Young, R. J.;
     Batchelder, D. N. J. Mater. Sci. submitted.
37. Galiotis, C.; Young, R. J.; Batchelder, D. N. to be published.

Author Index

Bassler, H., 218
Bloor, D., 128
Blum, T., 218
Booth, C. A., 95
Boudreaux, D. S., 140
Butera, R. J., 25
Cai, Y. M., 177
Carter, Gary M., 168
Chance, R. R., 140
Chapuis, G., 61
Chen, Yung Jui, 168
Di Silvestro, Giuseppe, 79
Donovan, K. J., 204
Eckert, Hellmut, 230
Eckhardt, C. J., 154
Eckhardt, H., 140
Elman, B. S., 118
Farina, Mario, 79
Federici, R. R., 140
Foxman, Bruce M., 95
Garito, A. F., 177
Grasso, R. P., 25
Hamill, G. P., 118
Harashina, H., 44
Hasegawa, M., 44
Hefter, J., 118
Hryniewicz, John V., 168
Jaufmann, J. D., 95

Jones, M. T., 253
Kato, S., 44
Kuwajima, S., 190
Lando, J. B., 25
Man, H. T., 177
Mazumdar, S., 190
Meyler, Stephen E., 168
Morrow, M., 154
Müller, H., 154
Prasad, Paras N., 106
Roble, J., 253
Saigo, K., 44
Sandman, Daniel J., 1,118,230,253
Sartwell, J., 154
Schott, M., 140
Sixl, Hans, 12
Soos, Z. G., 190
Sozzani, Piero, 79
Swerdloff, M., 140
Szobota, J. S., 140
Thakur, Mrinal K., 25,168
Tieke, B., 61
Turi, E. A., 140
Velazquez, Christopher S., 118,230
Wilson, E. G., 204
Yesinowski, James P., 230
Young, R. J., 266
Zamani-Khamiri, O., 177

Affiliation Index

Allied-Signal Corporation, 140
Brandeis University, 95
California Institute of Technology, 230
Case Western Reserve University, 25
GTE Laboratories, 1,118,168,190,230,253
Philipps-Universität, 218
Physikalisches Institut, 12
Princeton University, 190
Queen Mary College, 128,204
State University of New York at
    Buffalo, 106

Università di Milano, 79
Universität Freiburg, 61
Université de Lausanne, 61
University of Manchester, 266
University of Missouri--St. Louis, 253
University of Nebraska, 154
University of Paris VII, 140
University of Pennsylvania, 177
The University of Tokyo, 44

Subject Index

A

Absorption and emission spectra,
    DVDA1, 179-180,181-182f
Acetanilide, IR absorptions, 209
Acetylenes
  bonding, π-type, 191

Acetylenes—Continued
  carbon-carbon bond length, 197
  polymerization, 6f
  solid-state reactions, 96
  See also Diacetylenes, Mono-
        acetylenes, Polyacetylenes,
        Polydiacetylenes

277

Author Index

Bassler, H., 218
Bloor, D., 128
Blum, T., 218
Booth, C. A., 95
Boudreaux, D. S., 140
Butera, R. J., 25
Cai, Y. M., 177
Carter, Gary M., 168
Chance, R. R., 140
Chapuis, G., 61
Chen, Yung Jui, 168
Di Silvestro, Giuseppe, 79
Donovan, K. J., 204
Eckert, Hellmut, 230
Eckhardt, C. J., 154
Eckhardt, H., 140
Elman, B. S., 118
Farina, Mario, 79
Federici, R. R., 140
Foxman, Bruce M., 95
Garito, A. F., 177
Grasso, R. P., 25
Hamill, G. P., 118
Harashina, H., 44
Hasegawa, M., 44
Hefter, J., 118
Hryniewicz, John V., 168
Jaufmann, J. D., 95

Jones, M. T., 253
Kato, S., 44
Kuwajima, S., 190
Lando, J. B., 25
Man, H. T., 177
Mazumdar, S., 190
Meyler, Stephen E., 168
Morrow, M., 154
Müller, H., 154
Prasad, Paras N., 106
Roble, J., 253
Saigo, K., 44
Sandman, Daniel J., 1,118,230,253
Sartwell, J., 154
Schott, M., 140
Sixl, Hans, 12
Soos, Z. G., 190
Sozzani, Piero, 79
Swerdloff, M., 140
Szobota, J. S., 140
Thakur, Mrinal K., 25,168
Tieke, B., 61
Turi, E. A., 140
Velazquez, Christopher S., 118,230
Wilson, E. G., 204
Yesinowski, James P., 230
Young, R. J., 266
Zamani-Khamiri, O., 177

Affiliation Index

Allied-Signal Corporation, 140
Brandeis University, 95
California Institute of Technology, 230
Case Western Reserve University, 25
GTE Laboratories, 1,118,168,190,230,253
Philipps-Universität, 218
Physikalisches Institut, 12
Princeton University, 190
Queen Mary College, 128,204
State University of New York at
    Buffalo, 106

Università di Milano, 79
Universität Freiburg, 61
Université de Lausanne, 61
University of Manchester, 266
University of Missouri--St. Louis, 253
University of Nebraska, 154
University of Paris VII, 140
University of Pennsylvania, 177
The University of Tokyo, 44

Subject Index

A

Absorption and emission spectra,
    DVDA1, 179-180,181-182f
Acetanilide, IR absorptions, 209
Acetylenes
  bonding, π-type, 191

Acetylenes—Continued
  carbon-carbon bond length, 197
  polymerization, 6f
  solid-state reactions, 96
  See also Diacetylenes, Mono-
      acetylenes, Polyacetylenes,
      Polydiacetylenes

277